

JSCSEN 88(4)355–465(2023)

ISSN 1820-7421(Online)

# Journal of the Serbian Chemical Society

ersion  
lectronic

**VOLUME 88**

**No 4**

**BELGRADE 2023**

Available on line at



[www.shd.org.rs/JSCS/](http://www.shd.org.rs/JSCS/)

The full search of JSCS  
is available through

**DOAJ** DIRECTORY OF  
OPEN ACCESS  
JOURNALS  
[www.doaj.org](http://www.doaj.org)

The **Journal of the Serbian Chemical Society** (formerly Glasnik Hemijskog društva Beograd), one volume (12 issues) per year, publishes articles from the fields of chemistry. The **Journal** is financially supported by the **Ministry of Education, Science and Technological Development of the Republic of Serbia**.

Articles published in the **Journal** are indexed in **Clarivate Analytics products: Science Citation Index-Expanded<sup>TM</sup>** – accessed via **Web of Science<sup>®</sup>** and **Journal Citation Reports<sup>®</sup>**.

**Impact Factor** announced 2022: **1.100**; **5-year Impact Factor**: **1.175**.

Articles appearing in the **Journal** are also abstracted by: **Scopus**, **Chemical Abstracts Plus (CAplus<sup>SM</sup>)**, **Directory of Open Access Journals**, **Referativnii Zhurnal (VINITI)**, **RSC Analytical Abstracts**, **EuroPub**, **Pro Quest** and **Asian Digital Library**.

**Publisher:**

**Serbian Chemical Society**, Karnegijeva 4/III, P. O. Box 36, 1120 Belgrade 35, Serbia  
tel./fax: +381–11–3370–467, E-mails: **Society** – shd@shd.org.rs; **Journal** – jscs@shd.org.rs  
Home Pages: **Society** – <http://www.shd.org.rs/>; **Journal** – <http://www.shd.org.rs/JSCS/>  
Contents, Abstracts and full papers (from Vol 64, No. 1, 1999) are available in the electronic form at the Web Site of the **Journal** (<http://www.shd.org.rs/JSCS/>).

**Internet Service:**

**Former Editors:**

**Nikola A. Pušin** (1930–1947), **Aleksandar M. Leko** (1948–1954),  
**Panta S. Tutundžić** (1955–1961), **Miloš K. Mladenović** (1962–1964),  
**Đorđe M. Dimitrijević** (1965–1969), **Aleksandar R. Despić** (1969–1975),  
**Slobodan V. Ribnikar** (1975–1985), **Dragutin M. Dražić** (1986–2006).

**Editor-in-Chief:**

BRANISLAV Ž. NIKOLIĆ, Serbian Chemical Society (E-mail: jscs-ed@shd.org.rs)

**Deputy Editor:**

DUŠAN SLADIĆ, Faculty of Chemistry, University of Belgrade

**Sub editors:**

*Organic Chemistry*

DEJAN OPSENICA, Institute of Chemistry, Technology and Metallurgy, University of Belgrade

*Biochemistry and*

*Biotechnology*

JÁNOS CSANÁDI, Faculty of Science, University of Novi Sad

*Inorganic Chemistry*

OLGICA NEDIĆ, INEP – Institute for the Application of Nuclear Energy, University of Belgrade

*Theoretical Chemistry*

MILOŠ ĐURAN, Serbian Chemical Society

*Physical Chemistry*

IVAN JURANIĆ, Serbian Chemical Society

*Electrochemistry*

LJILJANA DAMJANOVIĆ-VASILJIĆ, Faculty of Physical Chemistry, University of Belgrade

*Analytical Chemistry*

SNEŽANA GOJKOVIĆ, Faculty of Technology and Metallurgy, University of Belgrade

*Polymers*

SLAVICA RAŽIĆ, Faculty of Pharmacy, University of Belgrade

*Thermodynamics*

BRANKO DUNJIĆ, Faculty of Technology and Metallurgy, University of Belgrade

*Chemical Engineering*

MIRJANA KIJEVCANIN, Faculty of Technology and Metallurgy, University of Belgrade

*Materials*

TATJANA KALUĐEROVIĆ RADOIČIĆ, Faculty of Technology and Metallurgy, University of Belgrade

*Metallic Materials and*

*Metallurgy*

RADA PETROVIĆ, Faculty of Technology and Metallurgy, University of Belgrade

*Environmental and*

*Geochemistry*

ANA KOSTOV, Mining and Metallurgy Institute Bor, University of Belgrade

*History of and*

*Education in Chemistry*

VESNA ANTIĆ, Faculty of Agriculture, University of Belgrade

DRAGICA TRIVIĆ, Faculty of Chemistry, University of Belgrade

**English Language**

LYNNE KATSIKAS, Serbian Chemical Society

**Editors:**

VLATKA VAJS, Serbian Chemical Society

JASMINA NIKOLIĆ, Faculty of Technology and Metallurgy, University of Belgrade

**Technical Editors:**

VLADIMIR PANIĆ, Institute of Chemistry, Technology and Metallurgy, University of Belgrade

MARIO ZLATOVIĆ, Faculty of Chemistry, University of Belgrade

**Journal Manager &**

**Web Master:**

MARIO ZLATOVIĆ, Faculty of Chemistry, University of Belgrade

**Office:**

VERA ČUŠIĆ, Serbian Chemical Society

**Editorial Board**

**From abroad:** **R. Adžić**, Brookhaven National Laboratory (USA); **A. Casini**, University of Groningen (The Netherlands); **G. Cobb**, Baylor University (USA); **D. Douglas**, University of British Columbia (Canada); **G. Inzelt**, Etvos Lorand University (Hungary); **J. Kenny**, University of Perugia (Italy); **Ya. I. Korenman**, Voronezh Academy of Technology (Russian Federation); **M. D. Lechner**, University of Osnabrueck (Germany); **S. Macura**, Mayo Clinic (USA); **M. Spiteller**, INFU, Technical University Dortmund (Germany); **M. Stratakis**, University of Crete (Greece); **M. Swart**, University de Girona (Cataluna, Spain); **G. Vunjak-Novaković**, Columbia University (USA); **P. Worsfold**, University of Plymouth (UK); **J. Zagal**, Universidad de Santiago de Chile (Chile).

**From Serbia:** **B. Abramović**, **V. Antić**, **V. Beškoski**, **J. Csanadi**, **Lj. Damjanović-Vasilić**, **A. Dekanski**, **V. Dondur**, **B. Dunjić**, **M. Đuran**, **S. Gojković**, **I. Gutman**, **B. Jovančičević**, **I. Juranić**, **T. Kaluđerović Radiočić**, **L. Katsikas**, **M. Kijevčanin**, **A. Kostov**, **V. Leovac**, **S. Milonjić**, **V.B. Mišković-Stanković**, **O. Nedić**, **B. Nikolić**, **J. Nikolić**, **D. Opsenica**, **V. Panić**, **M. Petkovska**, **R. Petrović**, **I. Popović**, **B. Radak**, **S. Ražić**, **D. Sladić**, **S. Sovilj**, **S. Šerbanović**, **B. Šolaja**, **Ž. Tešić**, **D. Trivić**, **V. Vajs**, **M. Zlatović**.

**Subscription:** The annual subscription rate is **150.00 €** including postage (surface mail) and handling. For Society members from abroad rate is **50.00 €**. For the proforma invoice with the instruction for bank payment contact the Society Office (E-mail: shd@shd.org.rs) or see JSCS Web Site: <http://www.shd.org.rs/JSCS/>, option Subscription.

**Godišnja pretplata:** Za članove SHD: **2.500,00 RSD**, za penzionere i studente: **1000,00 RSD**, a za ostale: **3.500,00 RSD**; za organizacije i ustanove: **16.000,00 RSD**. Uplate se vrše na tekući račun Društva: **205-13815-62**, poziv na broj **320**, sa naznakom "pretplata za JSCS".

**Nota:** Radovi čiji su svi autori članovi SHD prioritarno se publikuju.

Odlukom Odbora za hemiju Republičkog fonda za nauku Srbije, br. 66788/1 od 22.11.1990. godine, koja je kasnije potvrđena odlukom Saveta Fonda, časopis je uvršten u kategoriju međunarodnih časopisa (**M-23**). Takođe, aktom Ministarstva za nauku i tehnologiju Republike Srbije, 413-00-247/2000-01 od 15.06.2000. godine, ovaj časopis je proglašen za publikaciju od posebnog interesa za nauku. **Impact Factor** časopisa objavljen 2022. godini iznosi **1,100**, a petogodišnji **Impact Factor** **1,175**.



CONTENTS\*

**Organic Chemistry**

- M. D. Altintop, H. E. Temel and A. Özdemir:* Microwave-assisted synthesis of a series of 4,5-dihydro-1*H*-pyrazoles endowed with selective COX-1 inhibitory potency ..... 355

**Biochemistry and Biotechnology**

- A. M. Toader, I. Dascalu, E. I. Neacsu and M. Enache:* Binding interactions of actinomycin D anticancer drug with bile salts micelles ..... 367

**Theoretical Chemistry**

- S. Kumar:* Curcumin as a potential multiple-target inhibitor against SARS-CoV-2 infection: A detailed interaction study using quantum chemical calculations ..... 381

**Physical Chemistry**

- P. T. B. Campos, M. de Rezende Bonesio, A. L. D. Lima, A. C. da Silva, D. T. Mancini and T. C. Ramalho:* Xylose dehydration to furfural using niobium doped  $\delta$ -FeOOH as catalyst ..... 395

**Polymers**

- R. R. Vlasov, D. I. Ryabova, S. Z. Zeynalova, D. V. Sokolov and S. A. Ryabov:* The influence of nanoclays on the mechanical and thermal properties of rigid PIR and PUR foams ..... 409

**Materials**

- N. B. Nguyen, T. Q. P. Phan, C. T. T. Pham, H. N. Nguyen, S. N. Pham, Q. K. A. Nguyen and D. T. Nguyen:* Performance of carbon-coated magnetic nanocomposite in methylene blue and arsenate treatment from aqueous solution ..... 423

**Environmental**

- N. Boulahia, D. Hank, S. Meridja and A. Chergui:* Full factorial design methodology approach to optimize the elimination of gallic acid from water by coagulation using activated acorns barks as coagulant-aid ..... 437

**History of and Education in Chemistry**

- I. Nuić and S. A. Glažar:* The effects of E-learning units on 13–14-year-old students' misconceptions regarding some elementary chemical concepts ..... 451

Published by the Serbian Chemical Society  
Karnegijeva 4/III, P.O. Box 36, 11120 Belgrade, Serbia  
Printed by the Faculty of Technology and Metallurgy  
Karnegijeva 4, P.O. Box 35-03, 11120 Belgrade, Serbia

\* For colored figures in this issue please see electronic version at the Journal Home Page:  
<http://www.shd.org.rs/JSCS/>



*J. Serb. Chem. Soc.* 88 (4) 355–365 (2023)  
JSCS–5631

## Microwave-assisted synthesis of a series of 4,5-dihydro-1*H*-pyrazoles endowed with selective COX-1 inhibitory potency

MEHLİKA DİLEK ALTINTOP<sup>1</sup>, HALİDE EDİP TEMEL<sup>2</sup> and AHMET ÖZDEMİR<sup>1\*</sup>

<sup>1</sup>Department of Pharmaceutical Chemistry, Faculty of Pharmacy, Anadolu University, 26470 Eskişehir, Turkey and <sup>2</sup>Department of Biochemistry, Faculty of Pharmacy, Anadolu University, 26470 Eskişehir, Turkey

(Received 7 September, revised 22 November, accepted 30 December 2022)

**Abstract:** Considerable efforts have been directed towards the discovery of selective cyclooxygenase isozyme 1 (COX-1) inhibitors due to the recent work highlighting the involvement of COX-1 in the pathogenesis of pain, neuroinflammation, cancer and cardiovascular disorders. In this context, this paper aims to describe 2-pyrazolines endowed with selective COX-1 inhibitory potency. An efficient microwave-assisted synthetic method was applied for the preparation of a series of pyrazolines, which were tested for their COX-1 and cyclooxygenase isozyme 2 (COX-2) inhibitory effects using a colorimetric assay. The cytotoxic properties of the most potent derivatives on NIH/3T3 fibroblast cells were determined using MTT method. 1-(3-Fluorophenyl)-5-(3,4-methylenedioxyphenyl)-3-(2-thienyl)-4,5-dihydro-1*H*-pyrazole (**2g**) and 1-(3-bromophenyl)-5-(3,4-methylenedioxyphenyl)-3-(2-thienyl)-4,5-dihydro-1*H*-pyrazole (**2h**) were determined as selective COX-1 inhibitors. According to the *in silico* data obtained from Schrödinger's QikProp module, both compounds are estimated to possess favourable oral bioavailability and drug-likeness. This work could be a rational guideline for further modifications at different sites on 2-pyrazoline motif to bring out a new class of selective COX-1 inhibitors.

**Keywords:** pyrazoline; microwave heating; cyclooxygenase-1 inhibition.

### INTRODUCTION

Prostanoids (prostaglandins (PGs), thromboxane and prostacyclin) belong to the eicosanoid family of lipid mediators generated from arachidonic acid (AA).<sup>1,2</sup> Prostanoids play a central role in numerous physiological (*e.g.*, gastrointestinal (GI) integrity) and pathological (*e.g.* inflammation) processes.<sup>2,3</sup>

Cyclooxygenase (COX) is a rate-limiting enzyme implicated in the conversion of AA into prostanoids. There are two COX isozymes, namely the constitutive COX-1 and the inducible COX-2.<sup>2</sup> Both COXs possess similar structures, catalytic

\* Corresponding author. E-mail: ahmeto@anadolu.edu.tr  
<https://doi.org/10.2298/JSC220907001A>



features, and subcellular localizations<sup>2</sup> and yield the same product, prostaglandin H<sub>2</sub>. However, COX isozymes differ in terms of expression, tissue distribution, and biological tasks.<sup>4</sup> COX-1 contributes to homeostasis in most tissues (*e.g.*, platelets, GI tract, kidney, brain, lung, liver and spleen) where it is expressed under normal physiological conditions for the synthesis of PGs and exerts cytoprotective action along with the regulation of platelet activity, gastric and renal functions.<sup>4,5</sup> In general, non-steroidal anti-inflammatory drugs (NSAIDs), which inhibit both COX isoforms, cause GI damage through COX-1 inhibition.<sup>6</sup> In order to avoid GI toxicity, many researchers have focused on the discovery of selective COX-2 inhibitors based on the hypothesis that PGs beneficial for GI protection were generated solely by means of COX-1 activity, whilst PGs responsible for inflammation and pain were produced exclusively through COX-2 activity.<sup>6,7</sup> However, this assumption has lost its actuality since it is understood that COX-2 is constitutively expressed in some tissues and COX-1-derived PGs are also involved in inflammation and therefore COX-1 sparing is not adequate to prevent GI toxicity.<sup>7,8</sup>

Recent studies have revealed that COX-1 participates in the pathogenesis of many diseases (*e.g.*, cancer, neuroinflammation, cardiovascular diseases and pain).<sup>4,9</sup> It is noteworthy that low-dose aspirin is beneficial in the prevention of cardiovascular disorders through the inhibition of platelet COX-1. In addition, mounting evidence has also shown that long-term use of aspirin reduces the risk of some types of cancer and other diseases such as Alzheimer's disease.<sup>9</sup>

Despite all efforts devoted to the discovery of selective COX-1 inhibitors, there is only one selective COX-1 inhibitor (mofezolac) currently prescribed as a non-steroidal anti-inflammatory drug (NSAID) just in Japan for the management of pain/inflammation after surgery, trauma, or tooth extraction; lumbago, cervicobrachial syndrome and scapulohumeral periarthritis.<sup>9,10</sup> SC-560 and FR122047, selective COX-1 inhibitors commonly applied as reference agents in experimental studies, could not be introduced to the market as therapeutic agents because of their pharmacodynamic and pharmacokinetic drawbacks.<sup>6,9</sup>

From a chemical structural point of view, selective COX 1 inhibitors (mofezolac, SC-560 and FR122047, Fig. 1) possess a five-membered heteroaromatic central ring in common (isoxazole in mofezolac, pyrazole in SC-560, and thiazole in FR122047). Moreover, two aromatic rings linked to adjacent atoms of the five-membered heteroaromatic nucleus are found to be determinant.<sup>6,9</sup>

2-Pyrazoline (4,5-dihydro-1*H*-pyrazole), the partially reduced form of pyrazole, is a privileged member of the nitrogen-containing heterocycles due to its indispensable role in the discovery of new therapeutic drugs with improved potency and less toxicity along with favourable pharmacokinetic profiles.<sup>11,12</sup> 2-Pyrazolines have been reported to possess a broad range of biological activities (analgesic, anti-inflammatory, antitumor, antidepressant, antimicrobial, *etc.*)

known for their ability to interact with pivotal biological targets involved in diverse biochemical pathways.<sup>11–27</sup> There are many pyrazoline-based marketed agents as well as therapeutic candidates undergoing preclinical and clinical trials.<sup>12</sup> Some of them exert potent analgesic and anti-inflammatory action through the inhibition of COXs. Phenazone was the first pyrazoline-based agent used for the management of pain and inflammation. Dipyrone (metamizole, Fig. 2), was introduced to the market nearly a century ago and it is still used an analgesic and antipyretic drug in many countries worldwide.<sup>27</sup>

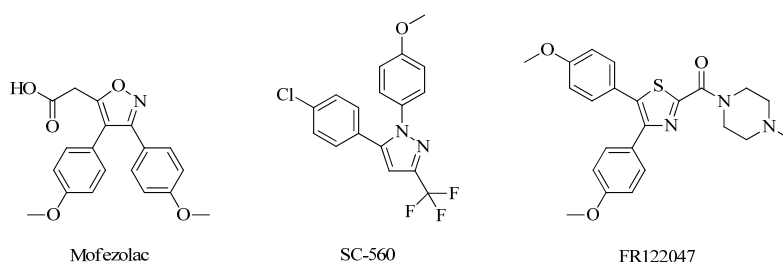


Fig. 1. Selective COX-1 inhibitors.

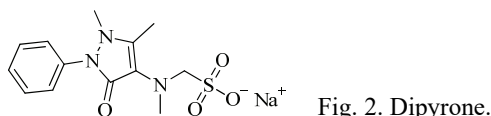


Fig. 2. Dipyrone.

A vast number of scientific reports related to 2-pyrazolines exerting marked COX inhibitory potency<sup>17–27</sup> prompted us to design a series of pyrazoline-based selective COX-1 inhibitors. With the given aim, the microwave (MW)-assisted synthesis of eight 2-pyrazolines was carried out expeditiously and afterwards *in vitro* experiments were performed to evaluate their potency as selective COX-1 inhibitors.

## EXPERIMENTAL

### General procedure

The chemicals used without further purification were obtained from commercial vendors (Sigma-Aldrich (St. Louis, MO, USA), Merck (Darmstadt, Almanyia), Acros Organics (Geel, Belgium), and Alfa Aesar (Karlsruhe, Germany)). The reactions were performed in Monowave 400 MW reactor (Anton Paar, Graz, Austria) in sealed reaction vessels, power supply voltage: AC 230 V ( $\pm 10\%$ ), 50 Hz/60 Hz, installed microwave power: 850 W, power consumption: 1600 V A, operating frequency: 2455 MHz. Compressed air cooling: 5.5 to 6 bar (80 to 87 psi). The reaction conditions are optimized by changing different temperatures and time under solvent medium. Melting points (M.p.) were detected by means of a digital melting point apparatus (Electrothermal, Staffordshire, UK) and are uncorrected. Thin layer chromatography (TLC) was performed on TLC silica gel 60 F254 aluminium sheets (Merck, Darmstadt, Germany) using petroleum ether-ethyl acetate solvent systems (3:1 and 1:1). IR spectra were recorded on a Fourier-transform IR spectrophotometer (Shimadzu, Tokyo, Japan). <sup>1</sup>H-

and  $^{13}\text{C}$ -NMR spectra were acquired using a NMR spectrometer (at 300 and 75 MHz, respectively). (Bruker, Billerica, MA, USA). Chemical shifts were expressed in parts per million (ppm). HRMS spectra were recorded on a LCMS-IT-TOF system (Shimadzu, Kyoto, Japan). The spectral data of the compounds are given in Supplementary material to this paper.

#### *Synthetic procedures*

##### *General procedure for the preparation of 1-(2-thienyl)-3-(3,4-methylenedioxyphenyl)-2-propen-1-one (1)*

2-Acetylthiophene (0.02 mol) was reacted with piperonal (0.02 mol) in the presence of 40 % aqueous NaOH (5 mL) in absolute ethanol (30 mL) at room temperature (rt) for 24 h. Upon the completion of the reaction, the reaction mixture was poured into crushed ice. The precipitate was filtered, and washed with water. After drying, the product was recrystallized from ethanol.<sup>28</sup>

##### *General procedure for the preparation of 1-aryl-3-(2-thienyl)-5-(3,4-methylenedioxyphenyl)-2-pyrazolines (2a–h)*

A mixture of compound **1** (1 mmol) and arylhydrazine hydrochloride (1.5 mmol) in absolute ethanol (8 mL) was heated to 180 °C within 15 min and kept at this temperature for 18 min under MW irradiation in a reaction vial with magnetic stirring at 500 rpm in a Mono-wave 400 MW reactor equipped with a ruby thermometer. Upon the completion of the reaction, the reaction mixture was cooled to room temperature. The precipitate was collected by filtration and dried. The product was crystallized from ethanol.

#### *Biochemistry*

*Determination of COX inhibitory activity.* COX inhibitor screening assay (catalog No.: 701050) was performed to determine the inhibitory activities of compounds **2a–h** (at 100  $\mu\text{M}$ ) towards COX-1 and COX-2 according to the manufacturer's guideline (Cayman, Ann Arbor, MI, USA). All measurements were performed in triplicate and the results were expressed as mean  $\pm$  SD. SC-560 (at 1  $\mu\text{M}$ ) was used as a selective COX-1 inhibitor, whereas drug rofecoxib (at 10  $\mu\text{M}$ ) was used as a selective COX-2 inhibitor.

*Cell culture and drug treatment.* NIH/3T3 mouse embryonic fibroblast cells (ATCC<sup>®</sup> CRL-1658<sup>™</sup>) were cultured and drug treatments were performed as reported previously.<sup>29</sup>

*3-[4,5-Dimethylthiazol-2-yl]-2,5-diphenyl tetrazolium bromide (MTT) test.* The level of cellular MTT (Sigma–Aldrich, St. Louis, MO, USA) reduction was quantified as explained earlier<sup>30</sup> with minor modifications.<sup>29</sup>

*In silico pharmacokinetic studies.* QikProp, an *in silico* absorption, distribution, metabolism, elimination (ADME) module within the Maestro suite produced by Schrödinger (Schrödinger Release 2022-2, LLC, New York, USA), was used to predict the crucial physicochemical parameters of compounds **2g** and **2h** for the assessment of their ADME profiles.

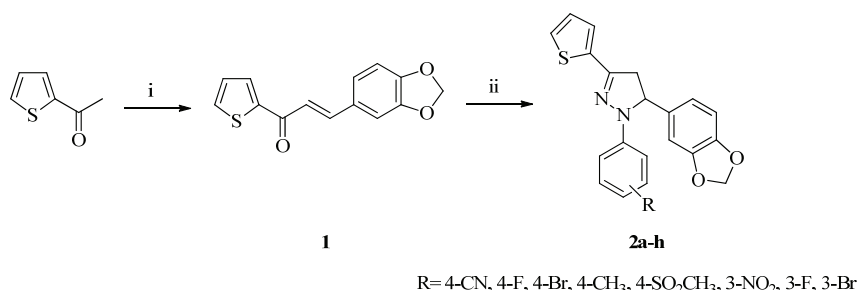
## RESULTS AND DISCUSSION

### *Chemistry*

The preparation of 2-pyrazolines (**2a–h**) followed the general pathway depicted in Scheme 1. The chalcone (**1**) was obtained *via* the Claisen–Schmidt condensation of 2-acetylthiophene with piperonal.

MW-assisted synthesis is recognized as an advantageous and eco-friendly technique for the rapid and efficient preparation of heterocyclic compounds inc-

cluding nitrogen-containing heterocycles.<sup>31–33</sup> The employment of this technique in dedicated MW reactors provides efficient and controlled heating along with excellent parameter control and therefore MW heating has several advantages over conventional heating such as shortening reaction time and obtaining products with high purity and yield.<sup>31–35</sup> In this work, an efficient MW-assisted protocol was applied for the preparation of compounds **2a–h**. Compounds **2a–e** were previously synthesized by our research group using a conventional method.<sup>28</sup> The comparison between MW and conventional techniques was made by comparing yield and total reaction time (Table I). MW technique led to a reduction in reaction time (from 480 min to 18 min) and an increase in product yields.



Scheme 1. The synthetic route for the preparation of compounds **2a–h**. Reagents and conditions: i) piperonal, 40 % NaOH, absolute ethanol, rt, 24 h; ii) arylhydrazine hydrochloride, absolute ethanol, MW, 180 °C, 18 min.

TABLE I. MW technique vs conventional method for the preparation of the compounds

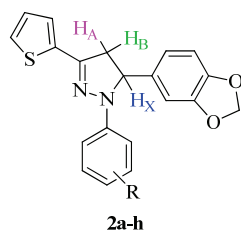
Compound	R	MW Irradiation		Conventional <sup>a</sup>	
		Yield, %	Time, min	Yield, %	Time, min
<b>2a</b>	4-CN	95	18	93	480
<b>2b</b>	4-F	82	18	76	480
<b>2c</b>	4-Br	91	18	90	480
<b>2d</b>	4-CH <sub>3</sub>	73	18	47	480
<b>2e</b>	4-SO <sub>2</sub> CH <sub>3</sub>	94	18	63	480
<b>2f</b>	3-NO <sub>2</sub>	84	18	–	–
<b>2g</b>	3-F	81	18	–	–
<b>2h</b>	3-Br	80	18	–	–

<sup>a</sup>Compounds **2a–e** were previously synthesized by our research team using a conventional method.<sup>28</sup> Compounds **2f, g** and **h** are reported for the first time in this work



The structures of compounds **2a–h** were confirmed by infrared (IR), nuclear magnetic resonance (NMR,  $^1\text{H}$  and  $^{13}\text{C}$ ) and high resolution mass spectrometry (HRMS).

In the IR spectra of compounds **2a–h**, Fig. 3, the absence of a band at  $1643.55\text{ cm}^{-1}$  due to the C=O stretching<sup>28</sup> confirmed that the formation of the 2-pyrazoline scaffold occurred efficiently. The C=N, C=C and C–N stretching bands appeared in the region 1612–1419 and  $1396\text{--}1107\text{ cm}^{-1}$ , respectively. In the  $^1\text{H}$ -NMR spectra of compounds **2a–h**, the  $\text{CH}_2$  protons of the 2-pyrazoline scaffold resonated as a pair of doublet of doublets at 3.08–3.26 ppm ( $\text{C}_4\text{-H}_\text{A}$ ) ( $J_{\text{AB}} = 17.28$  to  $17.64\text{ Hz}$ ,  $J_{\text{AX}} 4.95\text{--}6.81\text{ Hz}$ ) and 3.84–4.00 ppm ( $\text{C}_4\text{-H}_\text{B}$ ) ( $J_{\text{BA}} 17.25\text{--}17.70\text{ Hz}$ ,  $J_{\text{BX}} 11.91\text{--}12.06\text{ Hz}$ ).



R = 4-CN, 4-F, 4-Br, 4-CH<sub>3</sub>, 4-SO<sub>2</sub>CH<sub>3</sub>, 3-NO<sub>2</sub>, 3-F, 3-Br

Fig. 3. The ABX system of the pyrazoline scaffold belonging to compounds **2a–h**.

The CH proton appeared as a doublet of doublets at 5.36–5.63 ppm ( $\text{C}_5\text{-H}_\text{X}$ ) ( $J_{\text{BX}} 11.85\text{--}12.06\text{ Hz}$ ,  $J_{\text{AX}} 4.95\text{--}6.81\text{ Hz}$ ). The O–CH<sub>2</sub>–O protons gave rise to a singlet or a doublet in the region 5.97–6.04 ppm. The  $^{13}\text{C}$ -NMR chemical shift values of the carbons at 44.14–44.63 ppm ( $\text{C}_4$ ), 62.53–64.11 ppm ( $\text{C}_5$ ) and 144.46–154.85 ppm ( $\text{C}_3$ ) supported the  $^1\text{H}$ -NMR data confirming the formation of the pyrazoline motif. The HRMS data of compounds **2a–h** were also consistent with other spectral data.

### Biochemistry

A colorimetric test was conducted to assess the inhibitory effects of compounds **2a–h** on COX-1 and COX-2 (Table II). Among compounds **2a–h**, compounds **2g** and **h** were found to selective COX-1 inhibitors as compared to SC-560. The inhibition of compounds **2g** and **h** at 100  $\mu\text{M}$  for COX-1 were found as  $50.92 \pm 2.80$  and  $57.70 \pm 2.64\%$ , respectively as compared to SC-560 ( $97.36 \pm 2.62\%$  at 1  $\mu\text{M}$ ), a selective COX-1 inhibitor. *m*-Fluoro and *m*-bromo substituents enhanced COX-1 inhibitory potency.

The replacement of the halogen atom with the nitro group (compound **2f**) led to the loss of COX-1 inhibitory potency. However, *m*-nitro substitution gave rise to selective COX-2 inhibitory activity ( $36.48 \pm 2.18\%$ ). *p*-fluoro substitution (compound **2b**) caused the loss of inhibitory potency towards both COXs, whereas *p*-bromo substitution (compound **2c**) resulted in selective COX-2 inhi-

bitory potency ( $26.30 \pm 3.46$  %). The inhibition of compounds **2c** and **f** at  $100 \mu\text{M}$  were detected as  $26.30 \pm 3.46$  and  $36.48 \pm 2.18$  %, respectively in comparison with rofecoxib ( $98.36 \pm 1.86$  % at  $10 \mu\text{M}$ ), which is a selective COX-2 inhibitor. Compounds **2a**, **b** and **e** did not show any inhibitory activity towards COXs. According to the results, *p*-cyano, *p*-fluoro and *p*-methylsulfonyl groups led to the loss of COX inhibitory activity.

TABLE II. The inhibitory effects of compounds **2a–h**, SC-560 and rofecoxib on COXs

Compound ( $100 \mu\text{M}$ )	Inhibition, %	
	COX-1	COX-2
<b>2a</b>	–	–
<b>2b</b>	–	–
<b>2c</b>	–	$26.30 \pm 3.46$
<b>2d</b>	$9.65 \pm 1.56$	–
<b>2e</b>	–	–
<b>2f</b>	–	$36.48 \pm 2.18$
<b>2g</b>	$50.92 \pm 2.80$	–
<b>2h</b>	$57.70 \pm 2.64$	–
SC-560 ( $1 \mu\text{M}$ )	$97.36 \pm 2.62$	–
Rofecoxib ( $10 \mu\text{M}$ )	–	$98.36 \pm 1.86$

Compounds **2g** and **h**, the most potent COX-1 inhibitors in this series, were subjected to MTT assay for the evaluation of their cytotoxicity towards NIH/3T3 (normal) cells. Both compounds did not exhibit any cytotoxicity towards NIH/3T3 cell line at the tested concentrations ( $IC_{50} > 500 \mu\text{M}$ ).

*In silico ADME prediction.* *In silico* approaches are frequently used to assess pharmacokinetic profiles of drug candidates in drug development process since ADME experiments are not only costly and time-consuming for a vast number of chemicals, but also require a large number of animal tests and the corresponding ethical procedures.<sup>36</sup> In this context, a computational study for the prediction of the pharmacokinetic features of compounds **2g** and **h** was performed (Table III). The predicted values for total solvent accessible surface area (*SASA*), van der Waals surface area of polar nitrogen and oxygen atoms (*PSA*), octanol/water partition coefficient (*QPlog Po/w*) and binding to human serum albumin (*QPlog K<sub>hsa</sub>*) values were detected within the optimum range.

The predicted apparent Caco-2 cell permeability (*QPPCaco*) values of compounds **2g** and **2h** were found to be higher than 500 and therefore both compounds are estimated to possess good intestinal permeability. Compounds **2g** and **h** are also predicted to possess 100.000% human oral absorption. Furthermore, both compounds violated only one parameter of Lipinski's and Jorgensen's rules, making them drug-like molecules endowed with favourable oral bioavailability.

The capability of a drug to penetrate the blood-brain barrier (BBB) is required for its use in the treatment of central nervous system (CNS) dis-

orders.<sup>38,39</sup> Predicted brain/blood partition coefficient ( $QPlog\ BB$ ) was used to estimate the BBB permeability of each compound. The  $QPlog\ BB$  values of both compounds were detected within the recommended values. Moreover, Madin–Darby canine kidney (MDCK) cell permeability is an additional criterion which is widely used for the assessment of BBB penetration.<sup>40,41</sup> The estimated apparent MDCK cell permeability ( $QPPMDCK$ ) values of both compounds were found to be higher than 500. Based on the *in silico* data, compounds **2g** and **h** are predicted to possess the ability to cross BBB.

TABLE III. Predicted pharmacokinetic features of compounds **2g** and **h**

Property or descriptor	Compound <b>2g</b>	Compound <b>2h</b>	Range or recommended values
<i>SASA</i>	589.893	605.657	300.0–1000.0
<i>PSA</i>	32.674	32.687	7.0–200.0
$QPlog\ Po/w$	5.704	6.041	–2.0–6.5
$QPPCaco$	8585.887	8883.859	<25 poor, >500 great
$QPlog\ BB$	0.730	0.813	–3.0–1.2
$QPPMDCK$	10000.000	10000.000	<25 poor, >500 great
$QPlog\ Khsa$	1.009	1.112	–1.5–1.5
Human oral absorption, %	100.000	100.000	>80 % is high, <25 % is poor
Rule of Five <sup>a</sup>	1	1	Maximum is 4
Rule of Three <sup>b</sup>	1	1	Maximum is 3

<sup>a</sup>Rule of Five: number of violations of Lipinski's rule of five. The rules are: molecular weight of the compound < 500,  $QPlog\ Po/w$  < 5, hydrogen-bond donor atoms  $\leq 5$ , hydrogen-bond acceptor atoms  $\leq 10$ . Compounds that provide these rules are considered as drug-like molecules; <sup>b</sup>Rule of Three: number of violations of Jorgensen's rule of three. The three rules are: predicted aqueous solubility ( $QPlog\ S$ ) > –5.7,  $QPPCaco$  > 22 nm s<sup>–1</sup>, primary metabolites < 7. Compounds with fewer (and preferably no) violations of these rules are more likely to be orally available agents<sup>37</sup>

## CONCLUSION

In this paper was described an efficient MW-assisted protocol for the preparation of a series of pyrazolines (**2a–h**), which were investigated for their inhibitory effects on COXs at 100  $\mu$ M using an *in vitro* colorimetric assay. According to *in vitro* experimental data, compounds **2g** and **h** were determined as selective COX-1 inhibitors in this series, as compared to SC-560. MTT test was applied to assess their cytotoxic effects on NIH/3T3 cells. None of the compounds displayed any cytotoxicity towards NIH/3T3 cell line at the tested concentrations. *In silico* ADME prediction was performed for the assessment of their pharmacokinetic features. Compounds **2g** and **h** are predicted to have favourable oral bioavailability and drug-likeness. Based on this work, a new generation of pyrazolines could be designed through the molecular modification of compounds **2g** and **h** for the treatment of many diseases in which selective COX-1 inhibition is required.

## SUPPLEMENTARY MATERIAL

Additional data and information are available electronically at the pages of journal website: <https://www.shd-pub.org.rs/index.php/JSCS/article/view/12058>, or from the corresponding author on request.

## ИЗВОД

## МИКРОТАЛАСНА СИНТЕЗА СЕРИЈЕ ДЕРИВАТА 4,5-ДИХИДРО-1H-ПИРАЗОЛА КОЈИ ПОСЕДУЈУ ИЗРАЖЕНУ ИНХИБИТОРНУ АКТИВНОСТ ПРЕМА СОХ-1

МЕНЛИКА DILEK ALTINTOP<sup>1</sup>, HALIDE EDIP TEMEL<sup>2</sup> и АНМЕТ ÖZDEMİR<sup>1</sup>

<sup>1</sup>Department of Pharmaceutical Chemistry, Faculty of Pharmacy, Anadolu University, 26470 Eskişehir, Turkey и <sup>2</sup>Department of Biochemistry, Faculty of Pharmacy, Anadolu University, 26470 Eskişehir, Turkey

Учињен је значајан покушају проналажењу селективних СОХ-1 инхибитора током скорјих истраживања о значају инхибитора изозима 1 циклооксигеназе (СОХ-1) у патогенези бола, упале неурона, канцеру, и кардио-васкуларним поремећајима. У том правцу, у овом раду описани су деривати 2-пиразолина који поседују способност селективне инхибиције СОХ-1. Примењена је ефикасна метода микроталасне синтезе за добијање серије пиразолина који су тестирани као инхибитори СОХ-1 и инхибитора изоксима 2-циклооксигеназе (СОХ-2) применом колориметријске методе. Цитотоксична активност најактивнијих деривата је одређена на НИН/ЗТЗ ћелијама фибропласта применом МТТ метода. Показано је да су деривати 1-(3-флуорфенил)-5-(3,4-метиледиоксифенил)-3-(2-тиенил)-4,5-дихидро-1H-пиразол (**2g**) и 1-(3-бромфенил)-5-(3,4-метиледиоксифенил)-3-(2-тиенил)-4,5-дихидро-1H-пиразол (**2h**) селективни СОХ-1 инхибитори. На основу података добијених *in silico* прорачунима помоћу Schrödinger QikProp модула, процењено је да оба једињења имају повољну оралну биодоступност и повољне особине за примену као лек (drug-likeness). Овај рад би могао да буде основа за истраживање даљих модификација на различитим позицијама 2-пиразолинског језгра у циљу синтезе нове класе селективних СОХ-1 инхибитора.

(Примљено 7. септембра, ревидирано 22. новембра, прихваћено 30. децембра 2022)

## REFERENCES

1. T. Schmid, B. Brüne *Front. Immunol.* **12** (2021) 714042 (<https://dx.doi.org/10.3389/fimmu.2021.714042>)
2. L. L. Mazaleuskaya, E. Ricciotti, *Adv. Exp. Med. Biol.* **1274** (2020) 29 ([https://dx.doi.org/10.1007/978-3-030-50621-6\\_3](https://dx.doi.org/10.1007/978-3-030-50621-6_3))
3. C. S. Williams, M. Mann, R. N. DuBois, *Oncogene* **18** (1999) 7908 (<https://dx.doi.org/10.1038/sj.onc.1203286>)
4. A. Pannunzio, M. Coluccia, *Pharmaceuticals* **11** (2018) 101 (<https://dx.doi.org/10.3390/ph11040101>)
5. V. Sharma, P. Bhatia, O. Alam, M. Javed Naim, F. Nawaz, A. Ahmad Sheikh, M. Jha *Bioorg. Chem.* **89** (2019) 103007 (<https://dx.doi.org/10.1016/j.bioorg.2019.103007>)
6. M. G. Perrone, A. Scilimati, L. Simone, P. Vitale, *Curr. Med. Chem.* **17** (2010) 3769 (<https://dx.doi.org/10.2174/092986710793205408>)
7. E. Caiazzo, A. Ialenti, L. Cicala, C. Vitale, *Eur. J. Pharmacol.* **848** (2019) 105 (<https://dx.doi.org/10.1016/j.ejphar.2019.01.044>)
8. P. Vitale, A. Panella, A. Scilimati, M. G. Perrone, *Med. Res. Rev.* **36** (2016) 641 (<https://dx.doi.org/10.1002/med.21389>)

9. P. Vitale, A. Scilimati, M. G. Perrone, *Curr. Med. Chem.* **22** (2015) 4271 (<https://dx.doi.org/10.2174/0929867322666151029104717>)
10. K. Goto, H. Ochi, Y. Yasunaga, H. Matsuyuki, T. Imayoshi, H. Kusuhara, T. Okumoto, *Prostaglandins Other Lipid Mediat.* **56** (1998) 245 ([https://dx.doi.org/10.1016/s0090-6980\(98\)00054-9](https://dx.doi.org/10.1016/s0090-6980(98)00054-9))
11. J.M. Alex, R. Kumar, *J. Enzyme Inhib. Med. Chem.* **29** (2014) 427 (<https://dx.doi.org/10.3109/14756366.2013.795956>)
12. B. Nehra, S. Rulhania, S. Jaswal, B. Kumar, G. Singh, V. Monga, *Eur. J. Med. Chem.* **205** (2020) 112666 (<https://dx.doi.org/10.1016/j.ejmech.2020.112666>)
13. S. Kumar, S. Bawa, S. Drabu, R. Kumar, H. Gupta, *Recent Pat. Anti-Infect. Drug Discov.* **4** (2009) 154 (<https://dx.doi.org/10.2174/157489109789318569>)
14. M. R. Shaaban, A. S. Mayhoub, A. M. Farag, *Expert Opin. Ther. Pat.* **22** (2012), 253 (<https://dx.doi.org/10.1517/13543776.2012.667403>)
15. A. Marella, R. Ali, T. Alam, R. Saha, O. Tanwar, M. Akhter, M. Shaquiquzzaman, M. M. Mini-Rev. *Med. Chem.* **13** (2013) 921 (<https://dx.doi.org/10.2174/1389557511313060012>)
16. D. Matiadis, M. Sagnou, *Int. J. Mol. Sci.* **21** (2020) 5507 (<https://dx.doi.org/10.3390/ijms21155507>)
17. C. Cusan, G. Spalluto, M. Prato, M. Adams, A. Bodensieck, R. Bauer, A. Tubaro, P. Bernardi, T. Da Ros, *Farmaco* **60** (2005) 327 (<https://dx.doi.org/10.1016/J.FARMAC.2004.09.002>)
18. M. V. R. Reddy, V. K. Billa, V. R. Pallela, M. R. Mallireddigari, R. Boominathan, J.L. Gabriel, E. P. Reddy, *Bioorg. Med. Chem.* **16** (2008) 3907 (<https://dx.doi.org/10.1016/j.bmc.2008.01.047>)
19. R. Fioravanti, A. Bolasco, F. Manna, F. Rossi, F. Orallo, F. Ortuso, S. Alcaro, R. Cirilli, *Eur. J. Med. Chem.* **45** (2010) 6135 (<https://dx.doi.org/10.1016/j.ejmech.2010.10.005>)
20. S. Carradori, D. Secci, A. Bolasco, C. De Monte, M. Yáñez, *Arch. Pharm. Chem. Life Sci.* **345** (2012) 973 (<https://dx.doi.org/10.1002/ardp.201200249>)
21. M. A. El-Sayed, N. I. Abdel-Aziz, A. A. Abdel-Aziz, A. S. El-Azab, K. E. ElTahir, *Bioorg. Med. Chem.* **20** (2012) 3306 (<https://dx.doi.org/10.1016/j.bmc.2012.03.044>)
22. M. Yu, H. Yang, K. Wu, Y. Ji, L. Ju, X. Lu, *Bioorg. Med. Chem.* **22** (2014) 4109 (<https://dx.doi.org/10.1016/j.bmc.2014.05.059>)
23. K. R. A. Abdellatif, M. A. Abdelgawad, M. B. Labib, T. H. Zidan, *Bioorg. Med. Chem. Lett.* **25** (2015) 5787 (<https://dx.doi.org/10.1016/j.bmcl.2015.10.047>)
24. K. R. A. Abdellatif, H. A. H. Elshemy, A. A. Azoz, *Bioorg. Chem.* **63** (2015) 13 (<https://dx.doi.org/10.1016/j.bioorg.2015.09.002>)
25. M. A. Abdel-Sayed, S. M. Bayomi, M. A. El-Sherbeny, N. I. Abdel-Aziz, K. E. ElTahir, G. S. Shehatou, A. A. Abdel-Aziz, *Bioorg. Med. Chem.* **24** (2016) 2032 (<https://dx.doi.org/10.1016/j.bmc.2016.03.032>)
26. K. R. A. Abdellatif, M. T. Elsaady, S. A. Abdel-Aziz, A. H. Abusabaa, *J. Enzyme Inhib. Med. Chem.* **31** (2016) 1545 (<https://dx.doi.org/10.3109/14756366.2016.1158168>)
27. M. Lutz, *J. Clin. Pharmacol.* **59** (2019) 1433 (<https://dx.doi.org/10.1002/jcph.1512>)
28. A. Özdemir, B. Sever, M. D. Altıntop, E. Kaya Tilki, M. Dikmen, *Molecules* **23** (2018) 2151 (<https://dx.doi.org/10.3390/molecules23092151>)
29. A. Özdemir, M. D. Altıntop, Z. A. Kaplancıklı, G. Turan-Zitouni, G. Akalın Çiftçi, Ş. Ulusoylar Yıldırım, *J. Enzyme Inhib. Med. Chem.* **28** (2013) 1221 (<https://dx.doi.org/10.3109/14756366.2012.724682>)
30. T. Mosmann, *J. Immunol. Methods* **16** (1983) 55 ([https://dx.doi.org/10.1016/0022-1759\(83\)90303-4](https://dx.doi.org/10.1016/0022-1759(83)90303-4))

31. E. Berrino, C. T. Supuran, *Expert Opin. Drug Discov.* **13** (2018) 861 (<https://dx.doi.org/10.1080/17460441.2018.1494721>)
32. T. L. Lambat, P. K. P. G. Chopra, S. H. Mahmood, *Curr. Org. Chem.* **24** (2020) 2527 (<https://dx.doi.org/10.2174/1385272824999200622114919>)
33. M. Henary, C. Kananda, L. Rotolo, B. Savino, E. A. Owens, G. Cravotto, *RSC Adv.* **10** (2020) 14170 (<https://dx.doi.org/10.1039/D0RA01378A>)
34. M. B. Gawande, S. N. Shelke, R. Zboril, R. S. Varma, *Acc. Chem. Res.* **47** (2014) 1338 (<https://dx.doi.org/10.1021/ar400309b>)
35. J. M. Kremsner, A. Stadler, *A Chemist's Guide to Microwave Synthesis*, 3<sup>rd</sup> ed., Anton Paar GmbH, Graz, 2018, p. 300
36. Y. Wang, J. Xing, Y. Xu, N. Zhou, J. Peng, Z. Xiong, X. Liu, X. Luo, C. Luo, K. Chen, M. Zheng, H. Jiang, *Q. Rev. Biophys.* **48** (2015) 488 (<https://dx.doi.org/10.1017/S0033583515000190>)
37. *Schrödinger Release 2022-2*, Schrödinger, LLC, New York (<https://www.schrodinger.com/>)
38. C. Lohmann, S. Hüwel, H. J. Galla, *J. Drug Target.* **10** (2002) 263 (<https://dx.doi.org/10.1080/10611860290031903>)
39. T. J. Hou, X. J. Xu, *J. Chem. Inf. Comput. Sci.* **43** (2003) 2137 (<https://dx.doi.org/10.1021/ci034134i>)
40. S. Shahbazi, T. R. Sahrawat, M. Ray, S. Dash, D. Kar, S. Singh, *PLoS ONE* **11** (2016) e0156156 (<https://dx.doi.org/10.1371/journal.pone.0156156>)
41. F. Neumaier, B. D. Zlatopolskiy, B. Neumaier, *Pharmaceutics* **13** (2021) 1542 (<https://dx.doi.org/10.3390/pharmaceutics13101542>).

SUPPLEMENTARY MATERIAL TO  
**Microwave-assisted synthesis of a series of 4,5-dihydro-1H-  
-pyrazoles endowed with selective COX-1 inhibitory potency**

MEHLİKA DİLEK ALTINTOP<sup>1</sup>, HALİDE EDİP TEMEL<sup>2</sup> and AHMET ÖZDEMİR<sup>1\*</sup>

<sup>1</sup>Department of Pharmaceutical Chemistry, Faculty of Pharmacy, Anadolu University, 26470 Eskişehir, Turkey and <sup>2</sup>Department of Biochemistry, Faculty of Pharmacy, Anadolu University, 26470 Eskişehir, Turkey

*J. Serb. Chem. Soc.* 88 (4) (2023) 355–365

*1-(4-Cyanophenyl)-5-(3,4-methylenedioxyphenyl)-3-(2-thienyl)-4,5-dihydro-1H-pyrazole (2a)*<sup>28</sup>

Beige powder. M.P.: 156-158 °C. IR  $\nu_{\max}$  (cm<sup>-1</sup>): 3103, 3076, 2976, 2899, 2208, 1600, 1521, 1510, 1481, 1440, 1396, 1325, 1311, 1242, 1193, 1174, 1151, 1132, 1118, 1095, 1056, 1035, 993, 958, 933, 900, 860, 840, 821, 802, 734, 727, 665. <sup>1</sup>H NMR (300 MHz, DMSO-*d*<sub>6</sub>)  $\delta$  / ppm: 3.26 (dd,  $J_{AB} = 17.64$  Hz,  $J_{AX} = 4.95$  Hz, 1H, C<sub>4</sub>-H<sub>A</sub> pyrazoline), 4.00 (dd,  $J_{BA} = 17.70$  Hz,  $J_{BX} = 11.97$  Hz, 1H, C<sub>4</sub>-H<sub>B</sub> pyrazoline), 5.63 (dd,  $J_{BX} = 11.85$  Hz,  $J_{AX} = 4.95$  Hz, 1H, C<sub>5</sub>-H<sub>X</sub> pyrazoline), 6.04 (d,  $J = 2.40$  Hz, 2H), 6.78-6.81 (m, 2H), 6.93 (d,  $J = 7.92$  Hz, 1H), 7.07 (d,  $J = 8.82$  Hz, 2H), 7.18-7.21 (m, 1H), 7.42 (d,  $J = 3.57$  Hz, 1H), 7.63 (d,  $J = 8.85$  Hz, 2H), 7.74-7.76 (m, 1H). <sup>13</sup>C NMR (75 MHz, DMSO-*d*<sub>6</sub>)  $\delta$  / ppm: 44.3 (CH<sub>2</sub>), 62.5 (CH), 99.5 (C), 101.6 (CH<sub>2</sub>), 106.4 (CH), 109.2 (CH), 113.2 (2CH), 119.4 (CH), 120.4 (C), 128.5 (CH), 129.2 (CH), 129.5 (CH), 133.8 (2CH), 135.4 (d,  $J = 17.26$  Hz, 2C), 146.8 (C), 147.2 (C), 147.5 (C), 148.3 (C). HRMS (*m/z*): [M+H]<sup>+</sup> calcd. for C<sub>21</sub>H<sub>15</sub>N<sub>3</sub>O<sub>2</sub>S: 374.0958. Found: 374.0964.

*1-(4-Fluorophenyl)-5-(3,4-methylenedioxyphenyl)-3-(2-thienyl)-4,5-dihydro-1H-pyrazole (2b)*<sup>28</sup>

Brown powder. M.P.: 138-139 °C. IR  $\nu_{\max}$  (cm<sup>-1</sup>): 3082, 2960, 2885, 1604, 1504, 1496, 1481, 1442, 1373, 1361, 1315, 1288, 1247, 1224, 1180, 1153, 1109, 1078, 1033, 993, 927, 910, 866, 813, 802, 746, 707, 661. <sup>1</sup>H NMR (300 MHz, DMSO-*d*<sub>6</sub>)  $\delta$  / ppm: 3.17 (dd,  $J_{AB} = 17.31$  Hz,  $J_{AX} = 6.81$  Hz, 1H, C<sub>4</sub>-H<sub>A</sub> pyrazoline), 3.93 (dd,  $J_{BA} = 17.31$  Hz,  $J_{BX} = 11.94$  Hz, 1H, C<sub>4</sub>-H<sub>B</sub> pyrazoline), 5.42 (dd,  $J_{BX} = 11.94$  Hz,  $J_{AX} = 6.81$  Hz, 1H, C<sub>5</sub>-H<sub>X</sub> pyrazoline), 6.04 (s, 2H), 6.83-6.86 (m, 2H), 6.94-6.97 (m, 1H), 6.98-7.00 (m, 2H), 7.05-7.11 (m, 2H), 7.14-7.17 (m, 1H), 7.31 (d,  $J = 3.48$  Hz, 1H), 7.66 (d,  $J = 4.98$  Hz, 1H). <sup>13</sup>C NMR (75 MHz, DMSO-*d*<sub>6</sub>)  $\delta$  / ppm: 44.4 (CH<sub>2</sub>), 64.1 (CH), 101.6 (CH<sub>2</sub>), 106.6 (CH), 109.1 (CH), 114.7 (d,  $J = 7.49$  Hz, 2CH), 115.9 (d,  $J = 22.18$  Hz, 2CH), 119.7 (CH), 123.2 (C), 128.1 (d,  $J = 22.19$  Hz, 2CH), 136.2 (d,  $J = 20.52$  Hz, CH), 141.5 (C), 144.5 (C), 147.1 (C), 148.2 (C), 154.9 (C), 157.9 (C). HRMS (*m/z*): [M+H]<sup>+</sup> calcd. for C<sub>20</sub>H<sub>15</sub>FN<sub>2</sub>O<sub>2</sub>S: 367.0911. Found: 367.0917.

\* Corresponding author. E-mail: ahmeto@anadolu.edu.tr

*1-(4-Bromophenyl)-5-(3,4-methylenedioxyphenyl)-3-(2-thienyl)-4,5-dihydro-1H-pyrazole (2c)*<sup>28</sup>

Dark beige powder. M.P.: 107-108 °C. IR  $\nu_{\max}$  (cm<sup>-1</sup>): 3105, 3070, 2962, 2899, 1589, 1481, 1442, 1381, 1319, 1240, 1193, 1128, 1118, 1107, 1093, 1072, 1035, 997, 958, 937, 898, 854, 813, 802, 748, 721, 705, 690. <sup>1</sup>H NMR (300 MHz, DMSO-*d*<sub>6</sub>)  $\delta$  / ppm: 3.18 (dd,  $J_{AB}$  = 17.43 Hz,  $J_{AX}$  = 6.21 Hz, 1H, C<sub>4</sub>-H<sub>A</sub> pyrazoline), 3.94 (dd,  $J_{BA}$  = 17.25 Hz,  $J_{BX}$  = 12.03 Hz, 1H, C<sub>4</sub>-H<sub>B</sub> pyrazoline), 5.47 (dd,  $J_{BX}$  = 12.06 Hz,  $J_{AX}$  = 5.91 Hz, 1H, C<sub>5</sub>-H<sub>X</sub> pyrazoline), 6.03 (s, 2H), 6.82-6.85 (m, 2H), 6.91-6.96 (m, 2H), 7.01 (d,  $J$  = 8.70 Hz, 1H), 7.15-7.21 (m, 2H), 7.32-7.38 (m, 2H), 7.68 (d,  $J$  = 5.04 Hz, 1H). <sup>13</sup>C NMR (75 MHz, DMSO-*d*<sub>6</sub>)  $\delta$  / ppm: 44.3 (CH<sub>2</sub>), 63.3 (CH), 101.6 (CH<sub>2</sub>), 106.5 (CH), 109.1 (CH), 110.3 (C), 113.5 (CH), 115.3 (2CH), 119.4 (d,  $J$  = 30.54 Hz, CH), 128.1 (d,  $J$  = 28.02 Hz, CH), 129.4 (CH), 131.9 (2CH), 136.3 (d,  $J$  = 43.55 Hz, 2C), 143.6 (C), 145.1 (C), 147.1 (C), 148.2 (C). HRMS ( $m/z$ ): [M+H]<sup>+</sup> calcd. for C<sub>20</sub>H<sub>15</sub>BrN<sub>2</sub>O<sub>2</sub>S: 427.0110. Found: 427.0111.

*1-(4-Methylphenyl)-5-(3,4-methylenedioxyphenyl)-3-(2-thienyl)-4,5-dihydro-1H-pyrazole (2d)*<sup>28</sup>

Dark brown powder. M.P.: 152-154 °C. IR  $\nu_{\max}$  (cm<sup>-1</sup>): 3107, 3070, 2916, 2860, 1606, 1556, 1514, 1504, 1483, 1442, 1377, 1321, 1311, 1240, 1193, 1130, 1114, 1099, 1037, 995, 939, 898, 854, 817, 804, 721, 702, 665. <sup>1</sup>H NMR (300 MHz, DMSO-*d*<sub>6</sub>)  $\delta$  / ppm: 2.16 (s, 3H), 3.08 (dd,  $J_{AB}$  = 17.28 Hz,  $J_{AX}$  = 6.54 Hz, 1H, C<sub>4</sub>-H<sub>A</sub> pyrazoline), 3.84 (dd,  $J_{BA}$  = 17.28 Hz,  $J_{BX}$  = 12.06 Hz, 1H, C<sub>4</sub>-H<sub>B</sub> pyrazoline), 5.36 (dd,  $J_{BX}$  = 11.97 Hz,  $J_{AX}$  = 6.54 Hz, 1H, C<sub>5</sub>-H<sub>X</sub> pyrazoline), 5.97 (s, 2H), 6.77 (s, 2H), 6.85 (d,  $J$  = 8.37 Hz, 2H), 6.95-6.98 (m, 3H), 7.07-7.10 (m, 1H), 7.21-7.22 (m, 1H), 7.58 (d,  $J$  = 4.86 Hz, 1H). <sup>13</sup>C NMR (75 MHz, DMSO-*d*<sub>6</sub>)  $\delta$  / ppm: 20.6 (CH<sub>3</sub>), 44.1 (CH<sub>2</sub>), 63.8 (CH), 101.5 (CH<sub>2</sub>), 106.6 (CH), 109.0 (CH), 113.7 (2CH), 119.6 (CH), 123.1 (C), 125.6 (CH), 127.8 (d,  $J$  = 19.81 Hz, CH), 128.2 (CH), 129.9 (d,  $J$  = 16.17 Hz, 2CH), 136.6 (2C), 142.4 (C), 143.7 (C), 146.9 (C), 148.1 (C). HRMS ( $m/z$ ): [M+H]<sup>+</sup> calcd. for C<sub>21</sub>H<sub>18</sub>N<sub>2</sub>O<sub>2</sub>S: 363.1162. Found: 363.1167.

*1-(4-Methylsulfonylphenyl)-5-(3,4-methylenedioxyphenyl)-3-(2-thienyl)-4,5-dihydro-1H-pyrazole (2e)*<sup>28</sup>

Yellow powder. M.P.: 170-171 °C. IR  $\nu_{\max}$  (cm<sup>-1</sup>): 3099, 3001, 2924, 2823, 1589, 1502, 1483, 1442, 1419, 1388, 1315, 1298, 1246, 1139, 1089, 1029, 948, 921, 900, 821, 769, 717. <sup>1</sup>H NMR (300 MHz, DMSO-*d*<sub>6</sub>)  $\delta$  / ppm: 3.07 (s, 3H), 3.19 (dd,  $J_{AB}$  = 17.58 Hz,  $J_{AX}$  = 5.01 Hz, 1H, C<sub>4</sub>-H<sub>A</sub> pyrazoline), 3.96 (dd,  $J_{BA}$  = 17.61 Hz,  $J_{BX}$  = 11.91 Hz, 1H, C<sub>4</sub>-H<sub>B</sub> pyrazoline), 5.58 (dd,  $J_{BX}$  = 11.88 Hz,  $J_{AX}$  = 5.01 Hz, 1H, C<sub>5</sub>-H<sub>X</sub> pyrazoline), 5.99 (d,  $J$  = 1.74 Hz, 2H), 6.74-6.79 (m, 2H), 6.88 (d,  $J$  = 7.92 Hz, 1H), 7.07 (d,  $J$  = 8.88 Hz, 2H), 7.14 (dd,  $J$  = 4.98 Hz,  $J$  = 3.69 Hz, 1H), 7.36 (d,  $J$  = 3.51 Hz, 1H), 7.65-7.69 (m, 3H). <sup>13</sup>C NMR (75 MHz, DMSO-*d*<sub>6</sub>)  $\delta$  / ppm: 44.3 (CH<sub>3</sub>), 44.6 (CH<sub>2</sub>), 62.6 (CH), 101.6 (CH<sub>2</sub>), 106.4 (CH), 109.2 (CH), 112.6 (2CH), 119.4 (CH), 128.5 (CH), 129.1 (2CH), 129.4 (CH), 129.6 (CH), 135.3 (C), 135.6 (2C), 147.3 (3C), 148.3 (C). HRMS ( $m/z$ ): [M+H]<sup>+</sup> calcd. for C<sub>21</sub>H<sub>18</sub>N<sub>2</sub>O<sub>4</sub>S<sub>2</sub>: 427.0781. Found: 427.0781.

*1-(3-Nitrophenyl)-5-(3,4-methylenedioxyphenyl)-3-(2-thienyl)-4,5-dihydro-1H-pyrazole (2f)*

Orange powder. M.P.: 179-181 °C. IR  $\nu_{\max}$  (cm<sup>-1</sup>): 3113, 2914, 2887, 1612, 1570, 1519, 1498, 1481, 1438, 1379, 1344, 1319, 1242, 1205, 1186, 1111, 1099, 1033, 1008, 966, 929, 887, 856, 848, 827, 804, 786, 734, 709, 663. <sup>1</sup>H NMR (300 MHz, DMSO-*d*<sub>6</sub>)  $\delta$  / ppm: 3.22



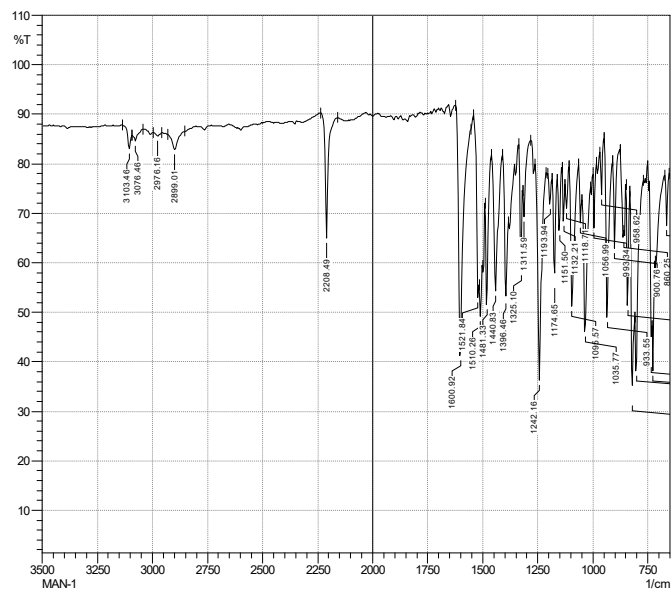
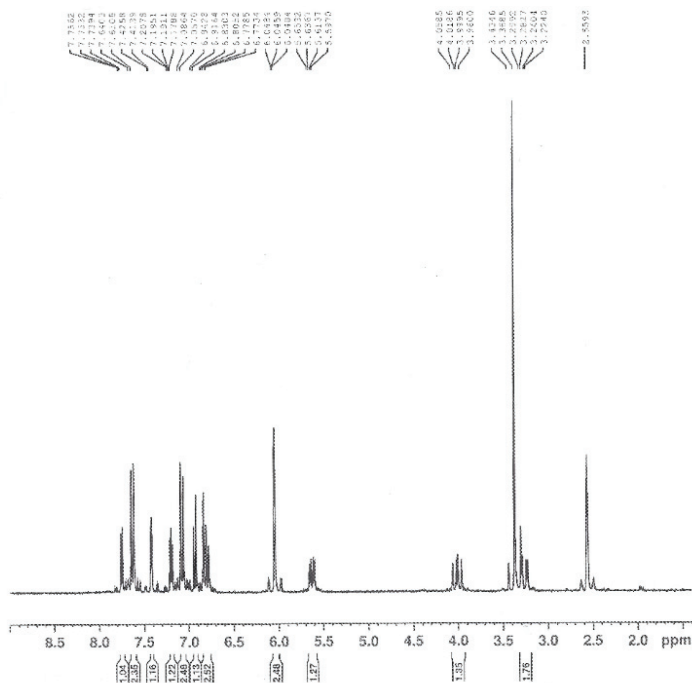
(dd,  $J_{AB}$  = 17.58 Hz,  $J_{AX}$  = 5.58 Hz, 1H, C<sub>4</sub>-H<sub>A</sub> pyrazoline), 3.96 (dd,  $J_{BA}$  = 17.55 Hz,  $J_{BX}$  = 11.94 Hz, 1H, C<sub>4</sub>-H<sub>B</sub> pyrazoline), 5.56 (dd,  $J_{BX}$  = 11.88 Hz,  $J_{AX}$  = 5.70 Hz, 1H, C<sub>5</sub>-H<sub>X</sub> pyrazoline), 5.99 (d,  $J$  = 2.46 Hz, 2H), 6.78-6.83 (m, 2H), 6.89 (d,  $J$  = 7.83 Hz, 1H), 7.14 (dd,  $J$  = 3.63 Hz,  $J$  = 5.01 Hz, 1H), 7.25 (dd,  $J$  = 8.22 Hz and  $J$  = 2.31 Hz, 1H), 7.35 (d,  $J$  = 3.60 Hz, 1H), 7.43 (t,  $J$  = 8.16 Hz, 8.10 Hz, 16.26 Hz, 1H), 7.54 (dd,  $J$  = 8.04 Hz,  $J$  = 2.22 Hz, 1H), 7.68 (d,  $J$  = 5.04 Hz, 1H), 7.76-7.78 (m, 1H). <sup>13</sup>C NMR (75 MHz, DMSO-*d*<sub>6</sub>)  $\delta$  / ppm: 44.4 (CH<sub>2</sub>), 63.2 (CH), 101.6 (CH<sub>2</sub>), 106.5 (CH), 107.1 (CH), 109.2 (CH), 113.1 (CH), 119.1 (CH), 119.7 (CH), 128.4 (CH), 128.9 (CH), 129.1 (CH), 130.8 (CH), 135.5 (2C), 145.0 (C), 146.6 (C), 147.3 (C), 148.4 (C), 149.0 (C). HRMS (*m/z*): [M+H]<sup>+</sup> calcd. for C<sub>20</sub>H<sub>15</sub>N<sub>3</sub>O<sub>4</sub>S: 394.0856. Found: 394.0862.

*1-(3-Fluorophenyl)-5-(3,4-methylenedioxyphenyl)-3-(2-thienyl)-4,5-dihydro-1H-pyrazole (2g)*

Yellow powder. M.P.: 130-131 °C. IR  $\nu_{\max}$  (cm<sup>-1</sup>): 3105, 3072, 2904, 1604, 1571, 1490, 1483, 1442, 1382, 1323, 1269, 1242, 1230, 1186, 1155, 1130, 1112, 1037, 1006, 960, 939, 891, 840, 819, 802, 761, 719, 680, 669. <sup>1</sup>H NMR (300 MHz, DMSO-*d*<sub>6</sub>)  $\delta$  / ppm: 3.14 (dd,  $J_{AB}$  = 17.46 Hz,  $J_{AX}$  = 5.91 Hz, 1H, C<sub>4</sub>-H<sub>A</sub> pyrazoline), 3.90 (dd,  $J_{BA}$  = 17.46 Hz,  $J_{BX}$  = 12.00 Hz, 1H, C<sub>4</sub>-H<sub>B</sub> pyrazoline), 5.44 (dd,  $J_{BX}$  = 11.94 Hz,  $J_{AX}$  = 5.88 Hz, 1H, C<sub>5</sub>-H<sub>X</sub> pyrazoline), 5.98 (s, 2H), 6.47-6.54 (m, 1H), 6.69-6.79 (m, 4H), 6.88 (d,  $J$  = 7.68 Hz, 1H), 7.10-7.13 (m, 1H), 7.17 (d,  $J$  = 7.23 Hz, 1H), 7.29 (d,  $J$  = 3.57 Hz, 1H), 7.63 (d,  $J$  = 5.04 Hz, 1H). <sup>13</sup>C NMR (75 MHz, DMSO-*d*<sub>6</sub>)  $\delta$  / ppm: 44.3 (CH<sub>2</sub>), 63.3 (CH), 99.9 (CH), 100.3 (CH), 101.6 (CH<sub>2</sub>), 105.1 (CH), 105.4 (CH), 106.5 (CH), 109.2 (d,  $J$  = 17.66 Hz, 2CH), 119.6 (CH), 128.4 (d,  $J$  = 14.67 Hz, 2CH), 131.1 (C), 135.7 (C), 136.1 (C), 145.4 (C), 147.1 (C), 148.3 (C), 161.8 and 164.9 (C). HRMS (*m/z*): [M+H]<sup>+</sup> calcd. for C<sub>20</sub>H<sub>15</sub>FN<sub>2</sub>O<sub>2</sub>S: 367.0911. Found: 367.0911.

*1-(3-Bromophenyl)-5-(3,4-methylenedioxyphenyl)-3-(2-thienyl)-4,5-dihydro-1H-pyrazole (2h)*

Beige powder. M.P.: 125-126 °C. IR  $\nu_{\max}$  (cm<sup>-1</sup>): 3107, 3070, 2914, 2872, 1589, 1579, 1556, 1500, 1475, 1444, 1373, 1346, 1317, 1238, 1203, 1184, 1118, 1099, 1078, 1035, 1001, 985, 933, 910, 858, 837, 817, 758, 715, 705, 675. <sup>1</sup>H NMR (300 MHz, DMSO-*d*<sub>6</sub>)  $\delta$  / ppm: 3.14 (dd,  $J_{AB}$  = 17.49 Hz,  $J_{AX}$  = 5.82 Hz, 1H, C<sub>4</sub>-H<sub>A</sub> pyrazoline), 3.89 (dd,  $J_{BA}$  = 17.52 Hz,  $J_{BX}$  = 12.03 Hz, 1H, C<sub>4</sub>-H<sub>B</sub> pyrazoline), 5.45 (dd,  $J_{BX}$  = 11.94 Hz,  $J_{AX}$  = 5.82 Hz, 1H, C<sub>5</sub>-H<sub>X</sub> pyrazoline), 5.98 (s, 2H), 6.75-6.78 (m, 2H), 6.83-6.89 (m, 3H), 7.07-7.15 (m, 3H), 7.30 (dd,  $J$  = 3.57 Hz,  $J$  = 0.93 Hz, 1H), 7.64 (dd,  $J$  = 5.04 Hz,  $J$  = 0.93 Hz, 1H). <sup>13</sup>C NMR (75 MHz, DMSO-*d*<sub>6</sub>)  $\delta$  / ppm: 44.3 (CH<sub>2</sub>), 63.1 (CH), 101.6 (CH<sub>2</sub>), 106.5 (CH), 109.1 (CH), 112.2 (CH), 115.6 (CH), 119.6 (CH), 121.4 (CH), 122.7 (C), 128.4 (d,  $J$  = 7.41 Hz, 2CH), 128.6 (CH), 131.3 (CH), 135.8 (d,  $J$  = 22.81 Hz, 2C), 145.7 (d,  $J$  = 5.97 Hz, 2C), 147.1 (C), 148.3 (C). HRMS (*m/z*): [M+H]<sup>+</sup> calcd. for C<sub>20</sub>H<sub>15</sub>BrN<sub>2</sub>O<sub>2</sub>S: 427.0110. Found: 427.0119.

IR,  $^1\text{H}$  AND  $^{13}\text{C}$  NMR, HRMS SPECTRA OF COMPOUNDS **2a-h**Figure S-1. IR spectrum of compound **2a**Figure S-2.  $^1\text{H}$  NMR spectrum of compound **2a**

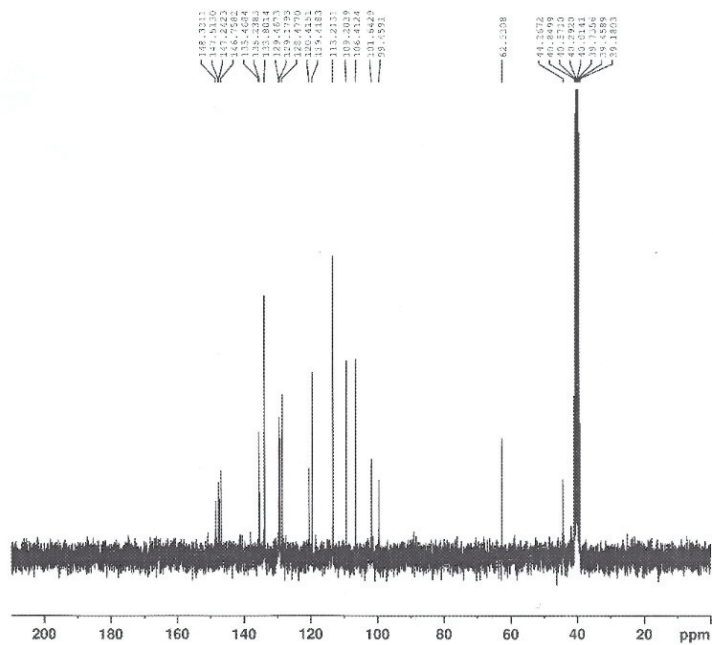


Figure S-3.  $^{13}\text{C}$  NMR spectrum of compound **2a**

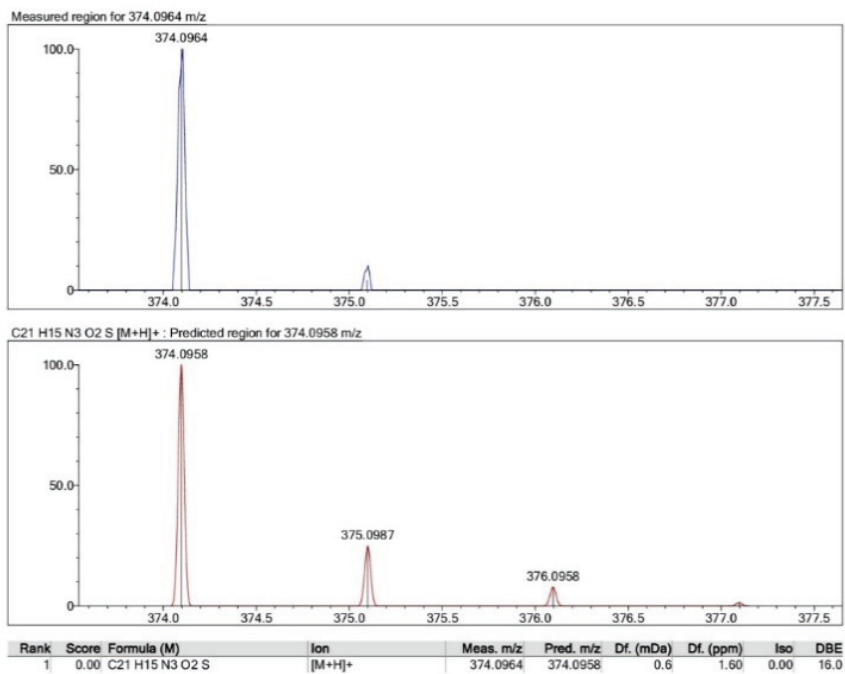
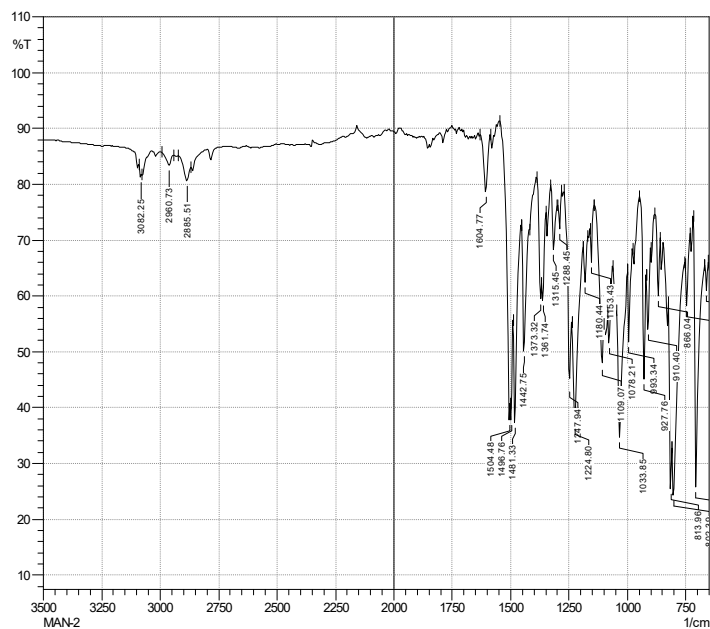
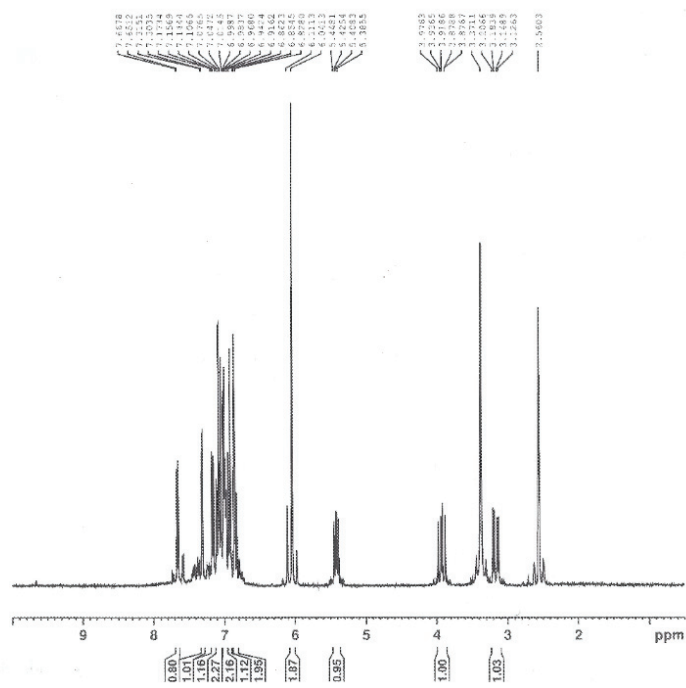


Figure S-4. HRMS spectrum of compound **2a**

Figure S-5. IR spectrum of compound **2b**Figure S-6. <sup>1</sup>H NMR spectrum of compound **2b**

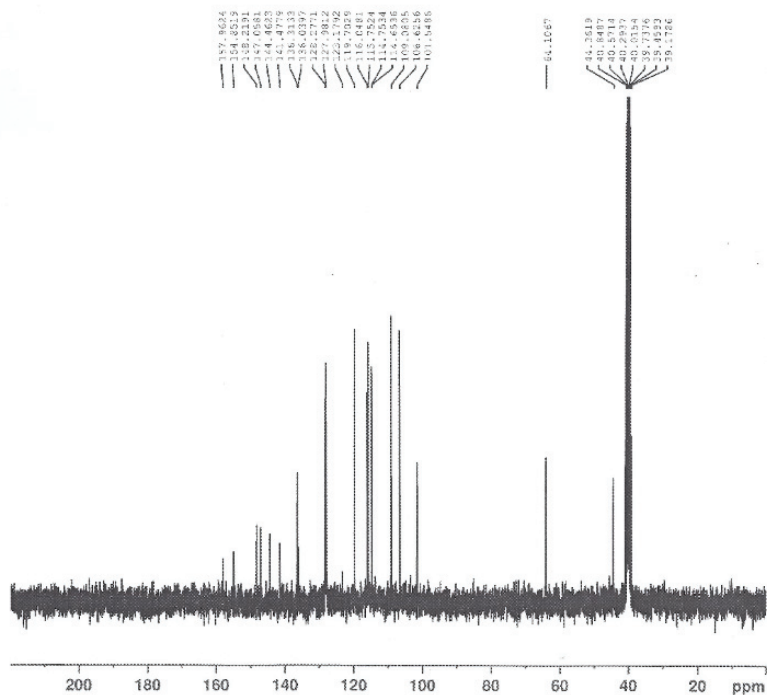


Figure S-7. <sup>13</sup>C NMR spectrum of compound **2b**

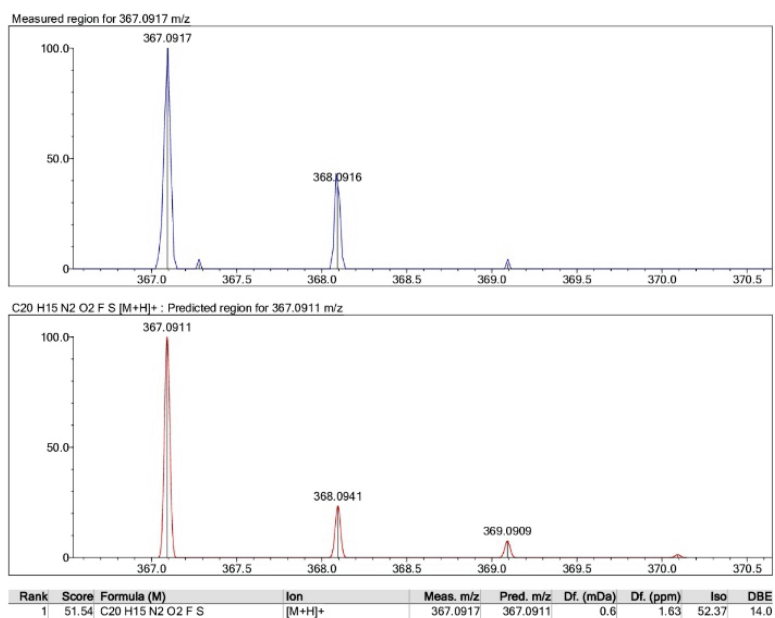
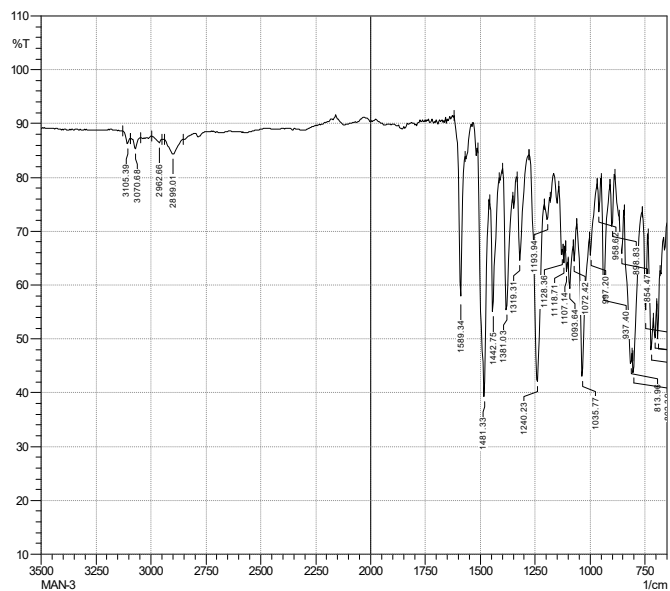
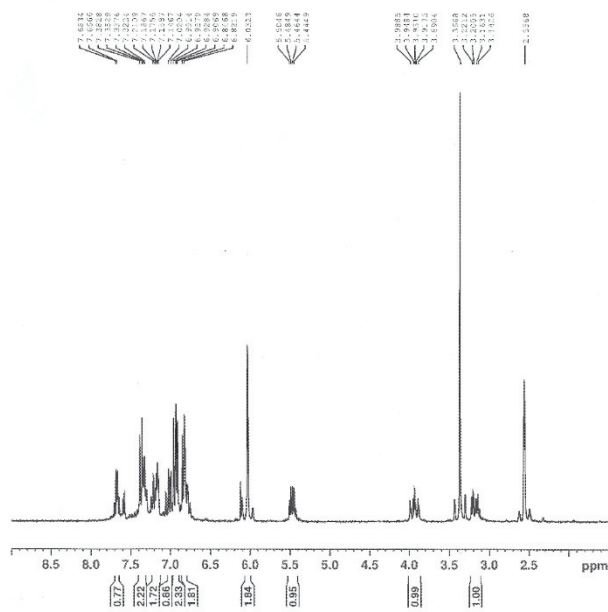


Figure S-8. HRMS spectrum of compound **2b**

Figure S-9. IR spectrum of compound **2c**Figure S-10.  $^1\text{H}$  NMR spectrum of compound **2c**

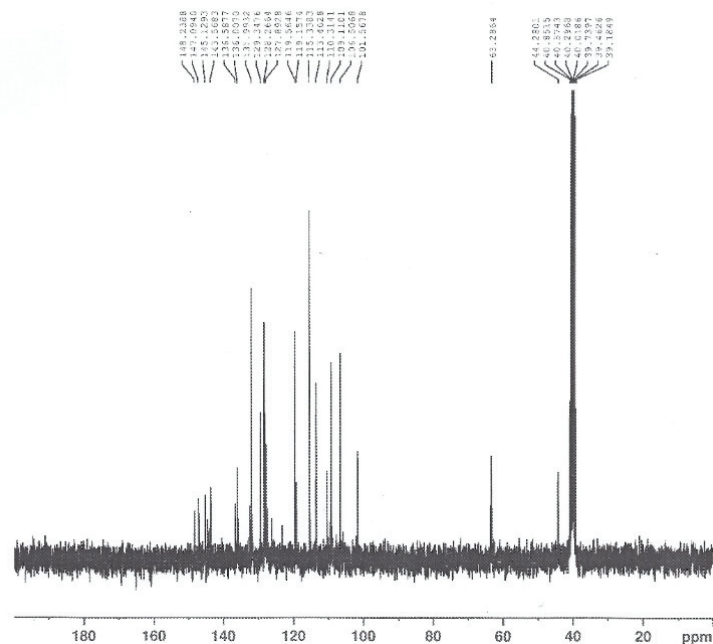


Figure S-11. <sup>13</sup>C NMR spectrum of compound **2c**

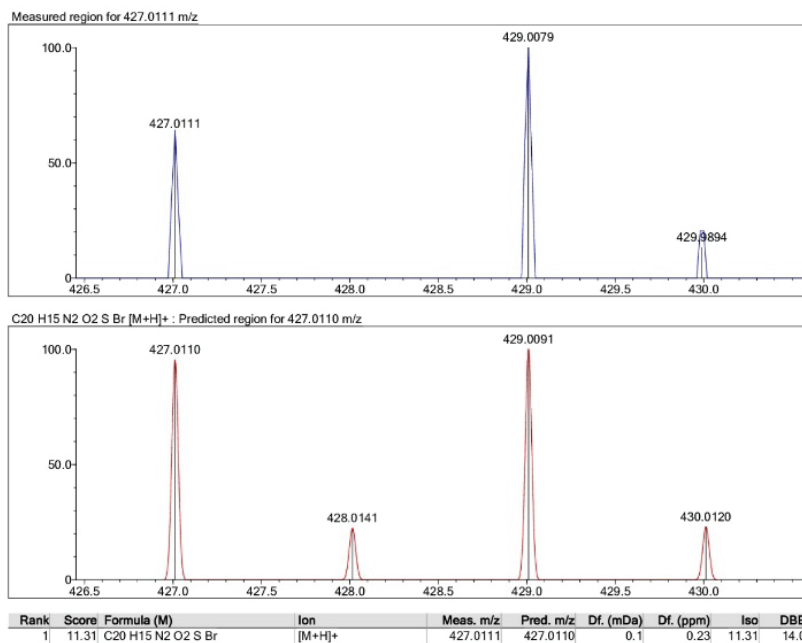


Figure S-12. HRMS spectrum of compound **2c**

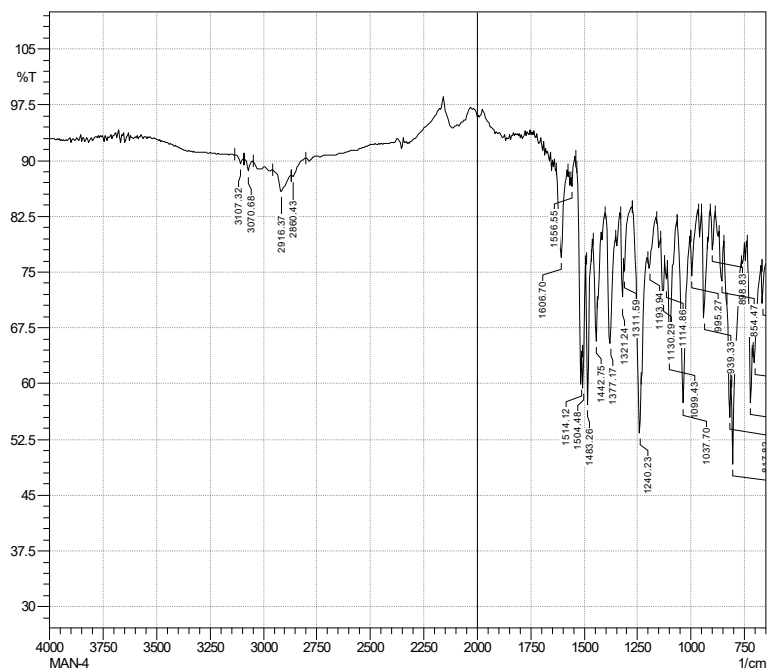
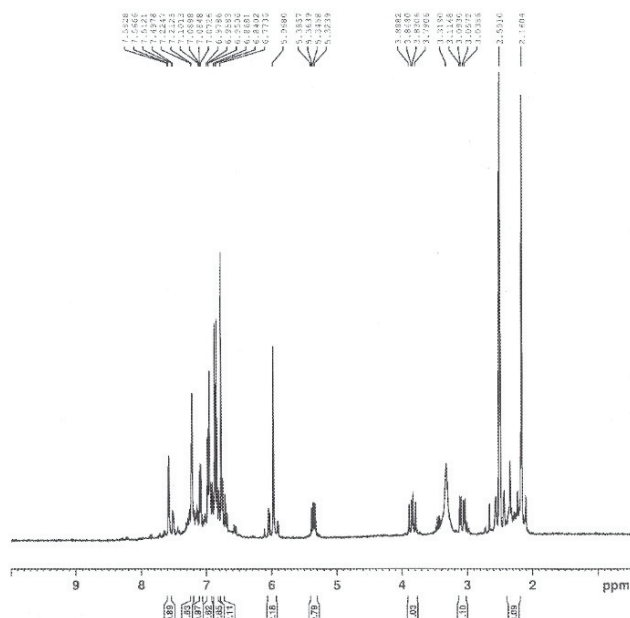


Figure S-13. IR spectrum of compound 2d

Figure S-14. <sup>1</sup>H NMR spectrum of compound 2d



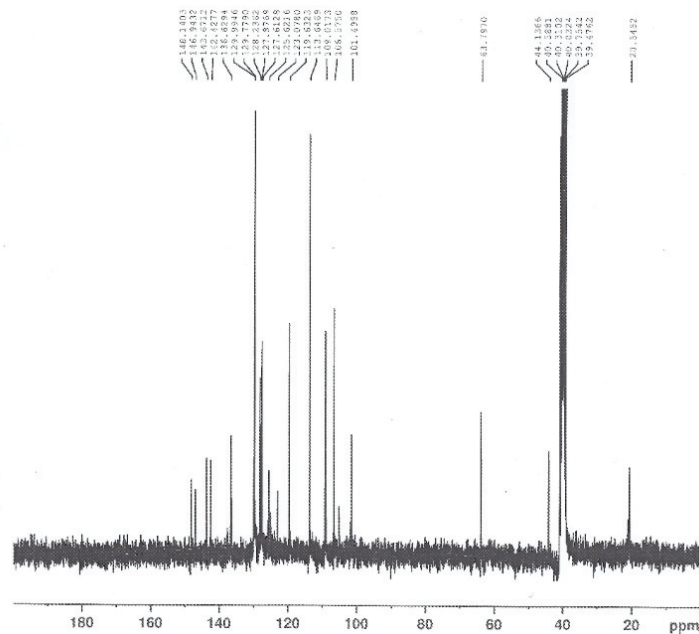


Figure S-15. <sup>13</sup>C NMR spectrum of compound **2d**

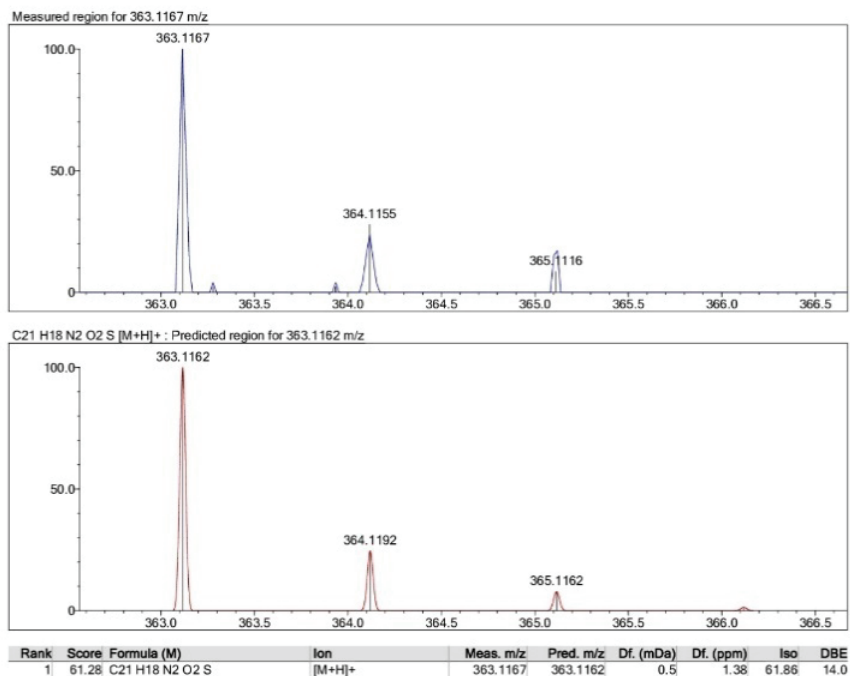


Figure S-16. HRMS spectrum of compound **2d**



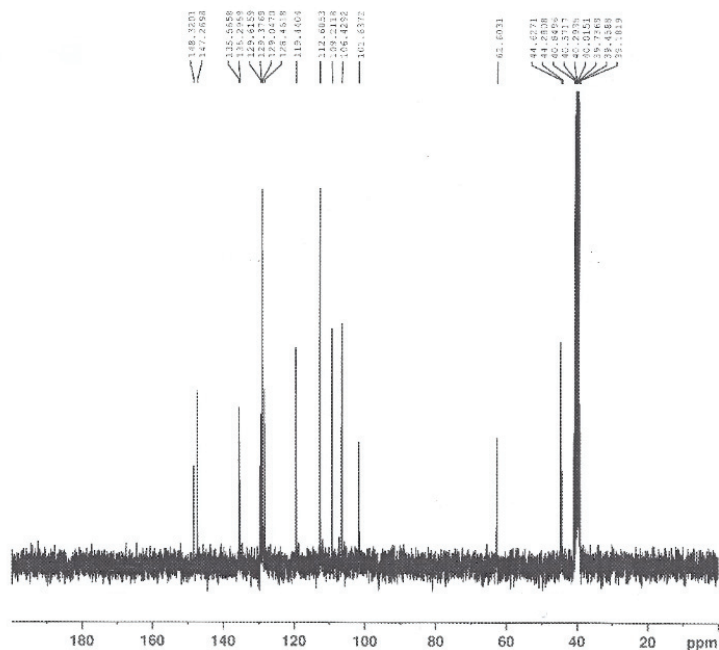


Figure S-19. <sup>13</sup>C NMR spectrum of compound **2e**

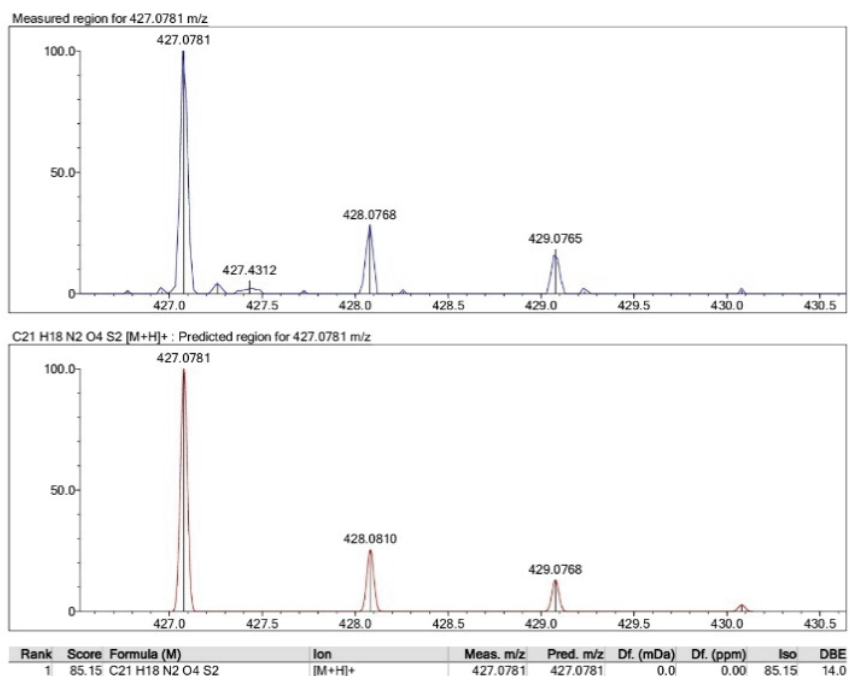
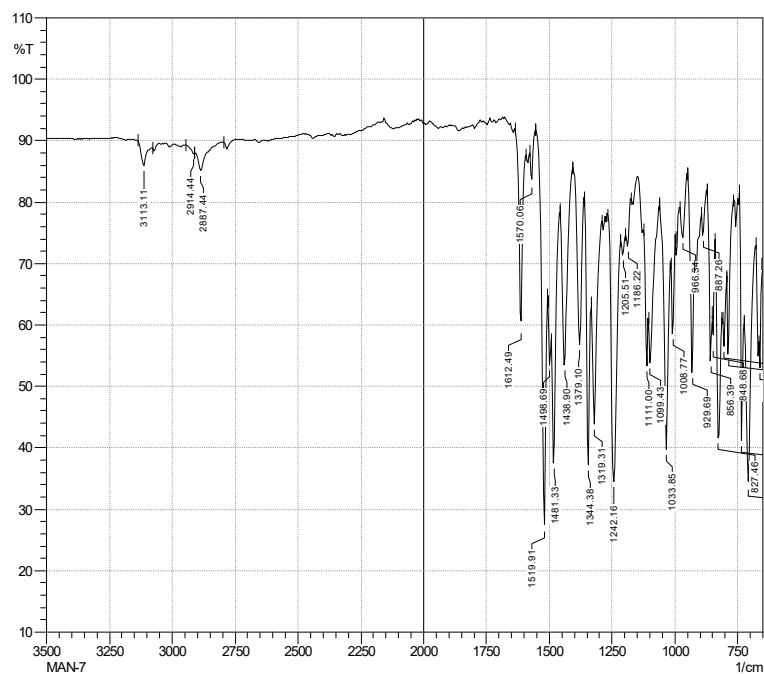
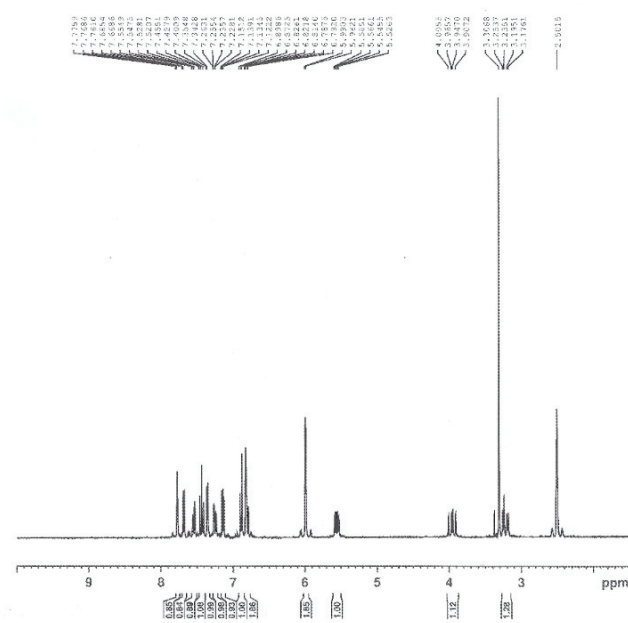


Figure S-20. HRMS spectrum of compound **2e**

Figure S-21. IR spectrum of compound **2f**Figure S-22. <sup>1</sup>H NMR spectrum of compound **2f**

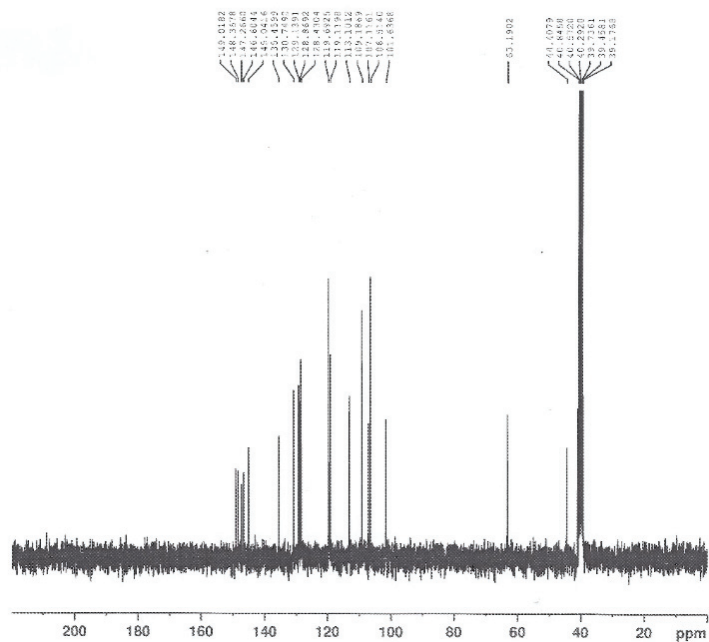


Figure S-23. <sup>13</sup>C NMR spectrum of compound **2f**

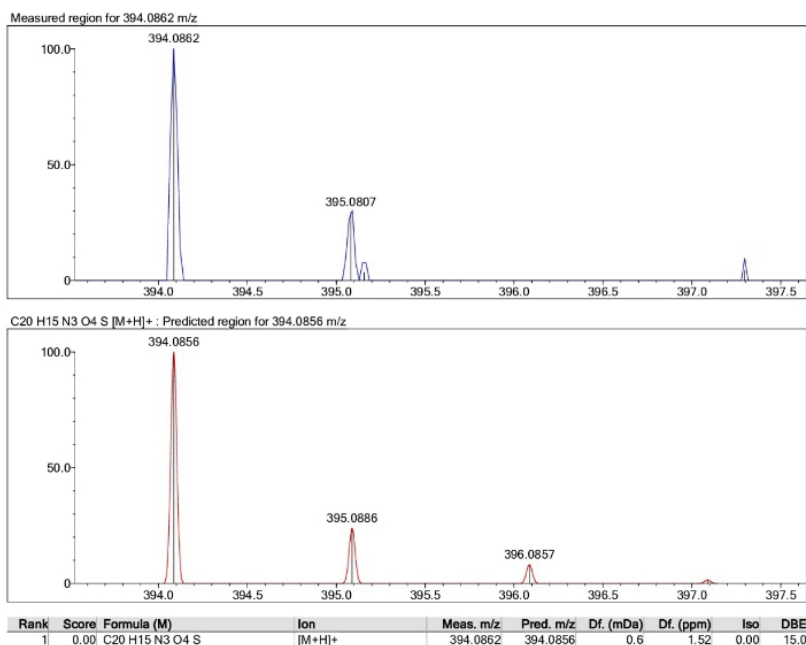


Figure S-24. HRMS spectrum of compound **2f**



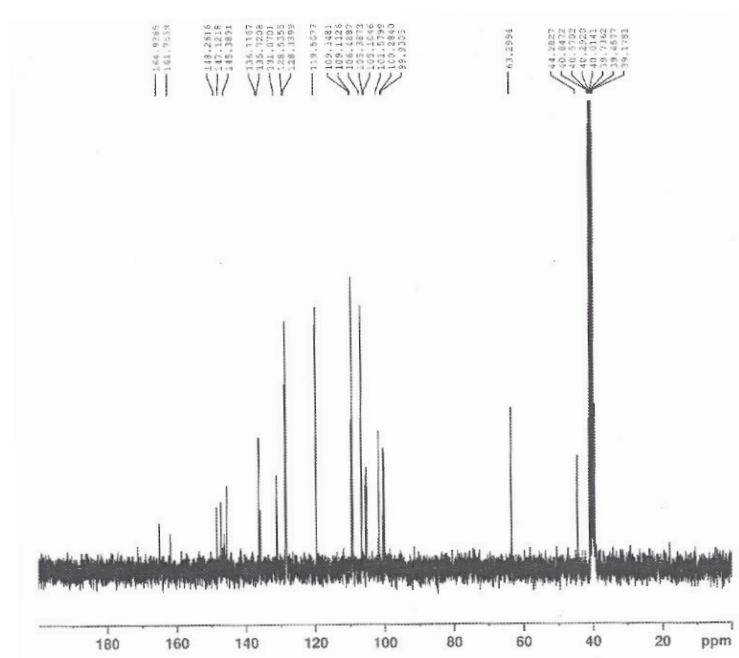


Figure S-27.  $^{13}\text{C}$  NMR spectrum of compound **2g**

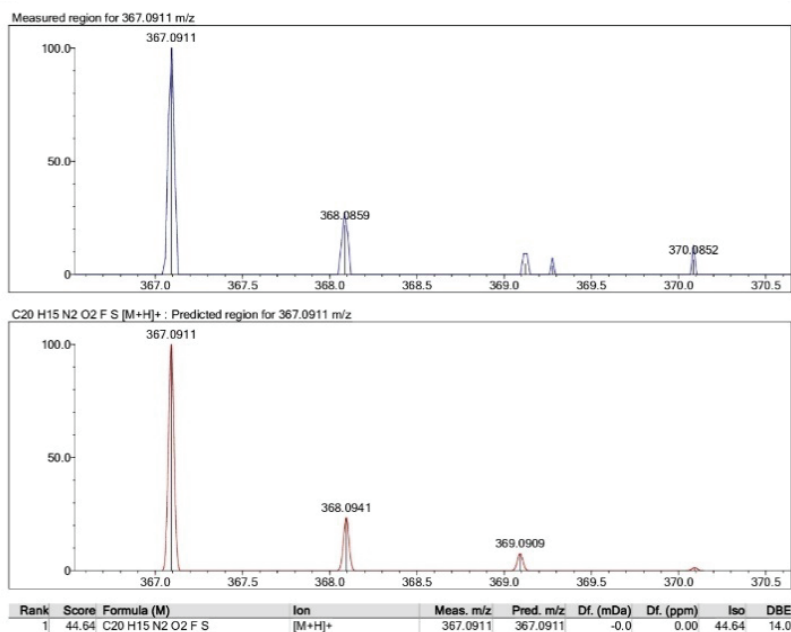
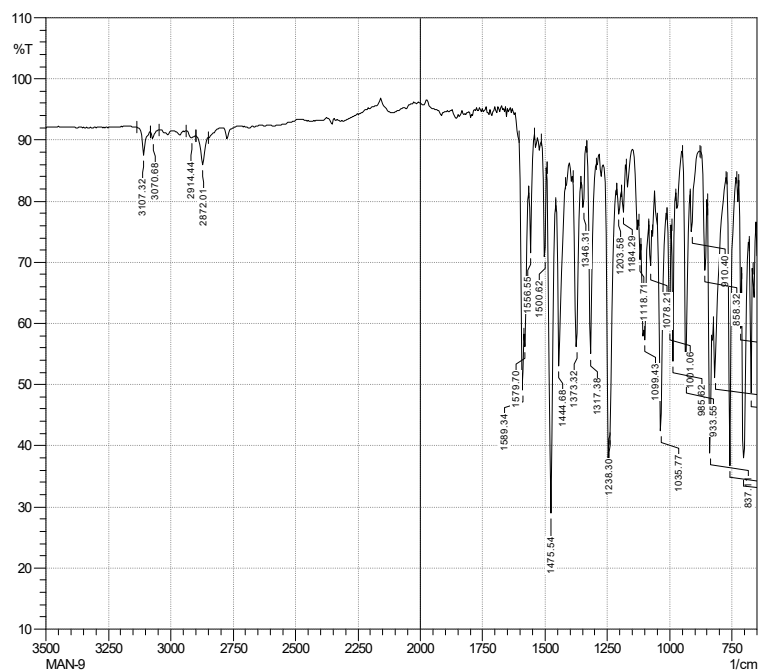
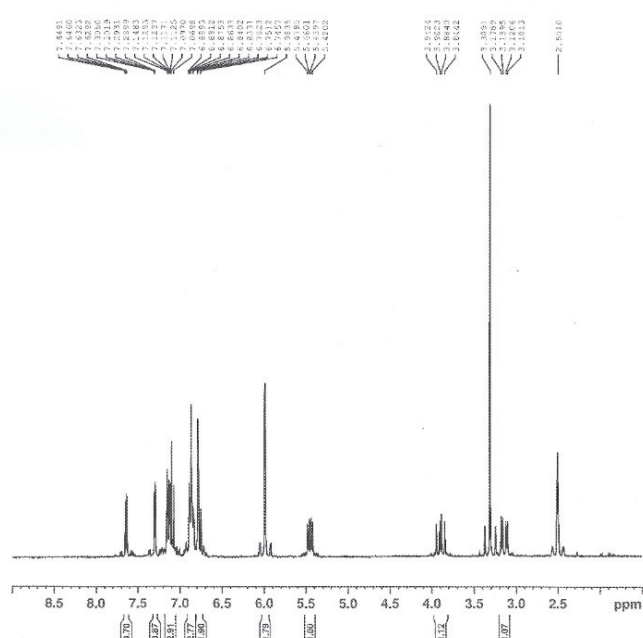


Figure S-28. HRMS spectrum of compound **2g**

Figure S-29. IR spectrum of compound **2h**Figure S-30. <sup>1</sup>H NMR spectrum of compound **2h**



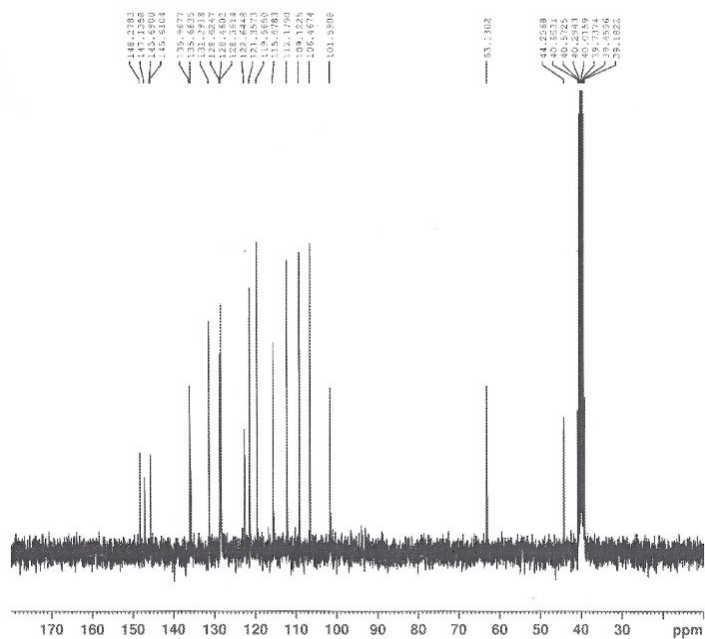


Figure S-31.  $^{13}\text{C}$  NMR spectrum of compound **2h**

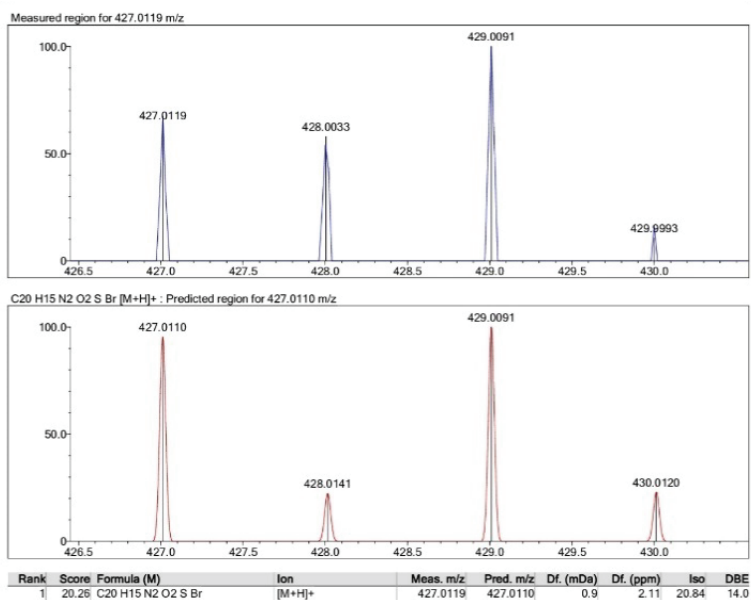


Figure S-32. HRMS spectrum of compound **2h**.





*J. Serb. Chem. Soc.* 88 (4) 367–379 (2023)  
JSCS–5632

## Binding interactions of actinomycin D anticancer drug with bile salts micelles

ANA MARIA TOADER, IZABELLA DASCALU, ELENA IONELA NEACSU  
and MIRELA ENACHE\*

*Institute of Physical Chemistry “Ilie Murgulescu”, Romanian Academy,  
Splaiul Independentei 202, Bucharest 060021, Romania*

(Received 2 November 2022, revised 17 January, accepted 25 January 2023)

**Abstract:** The interactions of actinomycin D (ActD) anticancer drug with two bile salts of different hydrophobicity (sodium cholate (NaC) and sodium deoxycholate (NaDC) and the influence of these bile salts aggregates on the ActD–DNA complex was investigated in 10 mM phosphate buffer (pH 7.4) by UV–Vis spectroscopy (absorption and thermal denaturation). The binding strength of ActD to NaDC is higher than for NaC, and this difference attests stronger hydrophobic interactions between ActD and NaDC micelles. Also, the partition coefficient is significantly higher for NaDC micelles than for NaC micelles, in line with larger aggregates formed by NaDC. The spectral profile of ActD molecules in NaC and NaDC micelles, in comparison with different solvents, implies that ActD molecule experiences a hydrophobic environment in bile salts aggregates. Regarding the influence of NaC and NaDC aggregates on the ActD–DNA complex, it was shown that the presence of both bile salts micelles do not induce the deintercalation of ActD molecules from DNA duplex.

**Keywords:** binding constant; partition coefficient; deintercalation.

### INTRODUCTION

Actinomycin D or dactinomycin (ActD), isolated from *Streptomyces* species, is a well-known antibiotic that exhibits high antitumor and antibacterial activity. ActD is used alone, or in combination with other drugs to treat many tumors, such as Wilms and Ewing tumors, testicular cancer, sarcomas and choriocarcinoma.<sup>1–3</sup> Structurally, ActD contains a 2-aminophenoxazin-3-one chromophore and two identical cyclic pentapeptide lactones (Fig. 1).

ActD exerts its biological activity *via* the inhibition of transcription by binding DNA at the transcription initiation complex and *via* the prevention of elongation of RNA chain by RNA polymerase.<sup>4</sup>

\* Corresponding author. E-mail: enachemir@yahoo.com  
<https://doi.org/10.2298/JSC221102004T>

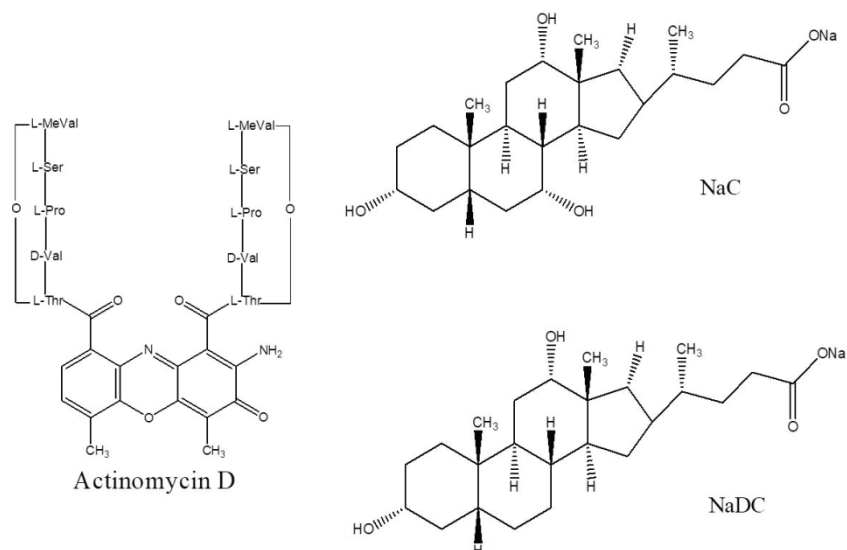


Fig. 1. Molecular structures of ActD, sodium cholate (NaC) and sodium deoxycholate (NaDC).

Bile salts are naturally occurring amphiphilic molecules, synthesized from cholesterol in the liver, deposited in the gall bladder, and then secreted into the small intestine. Unlike conventional surfactants, bile salts have a rigid nonplanar steroidal skeleton with a convex side of hydrophobic groups and a concave side which is made up of hydrophilic polar groups (typically two or three hydroxyl groups). Beside the physiological functions like solubilization and digestion of fats and lipids, hydrolysis of triglycerides, cholesterol elimination from the body,<sup>5,6</sup> bile salts aggregates play a significant role in pharmaceutical, biochemical and cosmetic fields.<sup>7,8</sup> Due to their biocompatible and biodegradable nature, there has been a growing interest in using bile salts aggregates as drug carrier vehicles to increase drug transport across various biological barriers such as the blood-brain, nasal, pulmonary and intestinal membranes.<sup>9</sup> As a result of their particular structure and the rigidity of molecules, bile salts exhibit distinct properties of aggregation in comparison with those of traditional surfactants.<sup>10</sup> Various models have been proposed to explain the uncommon aggregation behaviour of bile salts. The primary and secondary aggregate model proposed by Small *et al.* is the most widely accepted one.<sup>11–16</sup> According to this model, in the first step the small primary aggregates containing 2 to 10 monomers are formed around the critical micellar concentration (CMC) by the hydrophobic interaction between the convex hydrophobic surfaces of monomers. In the second step at higher concentration of bile salts, the larger secondary aggregates are formed by

the interaction of the primary aggregates *via* the formation of hydrogen bonds between the hydroxyl groups.

Due to the presence of different binding sites, bile salt aggregates are interesting host systems capable to bind both hydrophobic and hydrophilic guest molecules depending on the structure and size of the guests.<sup>17–20</sup>

Taking into account the intracellular damage caused by reactive oxygen species or reactive radical intermediates generated by the bioreduction of the quinone–imine structure of ActD,<sup>21</sup> a possible way to overcome these toxic side effects is to use the bile salts aggregates as drug carrier systems. Bearing this in mind and in continuation of our interest in the study of the interaction of drugs with biomimicking assemblies (surfactant and bile salts micelles), in this work we have investigated the interaction of ActD with two different bile salts, sodium cholate (NaC) and sodium deoxycholate (NaDC). NaC and NaDC bile salts contain the same head group ( $-\text{CH}_2-\text{CH}_2-\text{COO}^-$ ) but NaC contains one hydroxyl group more in the hydrophilic surface making NaC more hydrophilic than NaDC. The present paper is divided into two parts: the first part describes the interaction of ActD with NaC and NaDC micelles, and the second part deals with the influence of these bile salts micelles on the ActD–DNA complexes. Spectral (absorption and thermal denaturation) measurements were used to accomplish the proposed aims.

## EXPERIMENTAL

### *Materials*

Actinomycin D (98 % purity, ActD), sodium cholate (99 % purity, NaC), sodium deoxycholate (97 % purity, NaDC), deoxyribonucleic acid (DNA) sodium salt from calf thymus, pyrene and other chemicals were purchased from Sigma–Aldrich and employed as received. Experiments were performed in 10 mM phosphate buffer (pH 7.4) and deionized water (Mili-Q water purification system) was used for the preparation of solutions. The concentration of ActD solution was determined using its molar absorption coefficient,  $\epsilon = 24450 \text{ M}^{-1} \text{ cm}^{-1}$  at 440 nm.<sup>22</sup> DNA stock solution was prepared by dissolving solid DNA in 10 mM phosphate buffer and the exact concentration of DNA solutions was determined by measuring the absorbance at 260 nm and using the molar absorption coefficient  $\epsilon = 6600 \text{ M}^{-1} \text{ cm}^{-1}$ .

### *Apparatus and methods*

Spectrophotometric measurements were made on a Jasco V-630 spectrophotometer equipped with a Peltier-controlled ETCR-762 model accessory (Jasco Corporation, Tokyo, Japan) using a matched pair of quartz cuvettes with a path length of 1 cm. The absorption spectra of ActD in 10 mM phosphate buffer (pH 7.4) and in the presence of different concentrations of NaC and NaDC were recorded in the wavelength range of 300–600 nm.

For thermal denaturation experiments, the absorbance at 260 nm of DNA solution, ActD–DNA complex and ActD–DNA complex in the presence of bile salts aggregates was measured in the temperature range 20 to 95 °C with heating speed of 1 °C/min. The melting temperature ( $T_m$ ) was taken as the midpoint of the melting curve. All measurements of  $T_m$  were repeated three times and the data presented are average values.

The hyperchromicity ( $H$ ) of DNA was calculated as:<sup>23</sup>

$$H = 100 \frac{A_U - A_L}{A_L} \quad (1)$$

where  $A_U$  and  $A_L$  are the absorbance of the upper baseline and the absorbance of the lower baseline, respectively.

## RESULTS AND DISCUSSION

### *Binding interaction of actinomycin D with NaC and NaDC micelles*

Fig. 2 displays the absorption spectra of ActD in the presence of different increasing NaC (Fig. 2a) and NaDC concentrations (Fig. 2b). In 10 mM phosphate buffer (pH 7.4) ActD presents a broad absorption maxima around 440 nm, including at least three different electronic transitions: one is centred at about 372 nm is localized to a large degree on the benzenoid part of the phenoxazone chromophore; the second one located at about 490 nm is predominantly centred on the quinoid ring and the third transition occurs in the range 425–445 nm is extensively delocalized across the entire chromophore.<sup>24</sup> The incremental addition of NaC and NaDC leads to the following spectral behaviour: for bile salts concentrations less than *CMC*, a minor influence on the absorption spectra of ActD is noticed (data not shown), while for micellar bile salts concentrations a decrease of absorbance of ActD coupled with a splitting of the absorption maxima into two peaks and a bathochromic shift of these new absorption peaks (insets in Fig. 2) are observed. It can be observed that the addition of bile salts yields an isosbestic point at about 370 nm in the case of the interaction with NaC and at about 355 nm in the case of the interaction with NaDC. These spectral changes confirm the occurrence of interaction of ActD molecules with NaC and NaDC bile salts, which further indicates the new complex formation between drug molecules and bile salts. Also, the red shifts in the absorption maximum (insets in Fig. 2a and b) imply the transfer of ActD molecules from the aqueous solution into the bile salt assemblies with lower polarity.

The changes in the absorption maximum of ActD at 440 nm in the presence of varying bile salts concentrations were used to calculate the binding constant ( $K_b$ ) and the partition coefficient ( $K_x$ ), and the respective thermodynamic parameters, thus obtaining a quantitative characterization of the interaction between ActD and bile salt micelles.

The binding constant was determined using the Benesi–Hildebrand equation:<sup>25</sup>

$$\frac{1}{A_0 - A} = \frac{1}{K_b(A_0 - A_1)c_{BS}} + \frac{1}{A_0 - A_1} \quad (2)$$

where  $c_{BS}$  is the concentration of bile salts,  $A_0$  is the absorbance value in the absence of bile salts,  $A$  is the absorbance value in the presence of bile salts and  $A_1$  is the absorbance value at infinite concentration of bile salts.

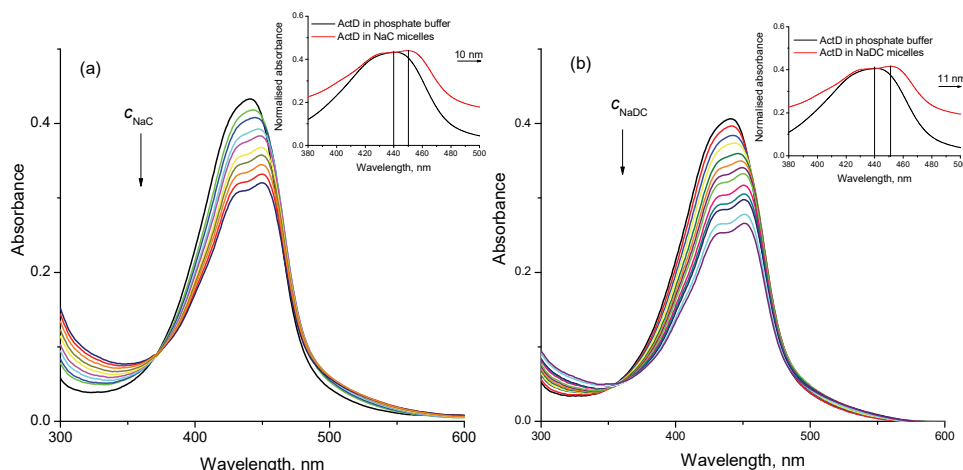


Fig. 2. Absorption spectra of ActD ( $17.7 \mu\text{M}$ ) in 10 mM phosphate buffer (pH 7.4) with increasing concentration of bile salts: a) NaC (0–19.29 mM), b) NaDC (0–31 mM). Insets show the normalised absorption spectra of ActD in NaC and NaDC micelles.

The Benesi–Hildebrand plots of  $1/(A_0 - A)$  versus  $1/c_{\text{BS}}$  are shown in Fig. 3a and indicate a straight line for both bile salts which attest a 1:1 stoichiometric complexation between ActD and bile salts. The obtained binding constant values are listed in Table I and illustrate a stronger interaction of ActD with NaDC micelles than NaC micelles. The head groups of NaDC and NaC are the same ( $-\text{COONa}$ ) but NaC contains one more hydroxyl group in its hydrophilic surface, making NaC less hydrophobic as compared to NaDC. The hydrophobicity index of NaDC and NaC are 0.72 and 0.13, respectively. Therefore, this difference in the hydrophobicity of NaC and NaDC leads to their distinct binding abilities and

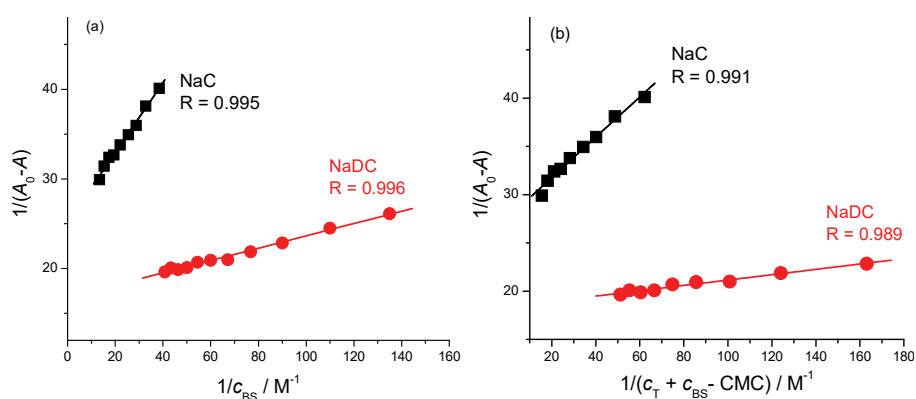


Fig. 3. a) Benesi–Hildebrand plots and b) Relation between  $1/(A_0 - A)$  and  $1/(c_T + c_{\text{BS}} - \text{CMC})$  for the interaction of ActD with NaC and NaDC micelles.  $R$  is the correlation coefficient.

prove that the hydrophobic interactions between ActD and NaDC micelles are much stronger compared to that between ActD and NaC micelles. The hydrophobic interactions between the planar aromatic chromophore of neutral ActD and the hydrophobic surface of bile salts are the main interaction forces responsible for the formation of ActD–bile salts complexes. Also, hydrogen bonds can be formed between the carbonyl oxygen atoms of the L-threonine residues of the pentapeptides chains of ActD and the hydroxyl groups of bile salts.

TABLE I. Binding constant ( $K_b$ ), change in free energy of binding ( $\Delta G_b^0$ ), partition coefficient ( $K_x$ ) and change in free energy of partition ( $\Delta G_x^0$ ) for the interaction of ActD with NaC and NaDC micelles

System	$K_b \pm SD^a / M^{-1}$	$\Delta G_b^0 / \text{kJ mol}^{-1}$	$K_x \pm SD^a$	$\Delta G_x^0 / \text{kJ mol}^{-1}$
ActD + NaC	68±5	-10.28	7294±187	-21.67
ActD + NaDC	281±12	-13.74	37822±2147	-25.68

<sup>a</sup>Standard deviation of the mean of three determinations

The partition coefficient ( $K_x$ ) was determined according to the pseudo-phase model:<sup>26,27</sup>

$$\frac{1}{A_0 - A} = \frac{1}{A_0 - A_1} + \frac{n_w}{K_x(A_0 - A_1)(c_{BS} + c_T - CMC)} \quad (3)$$

In Eq. (3),  $c_T$  is the total ActD concentration and  $n_w = 55.5 \text{ M}$  is the molarity of water.

The magnitude of partition coefficient (Table I) is very high for both bile salts and this result clearly suggests that the drug molecule resides into the hydrophobic environment of micelles rather than the aqueous medium. The partition coefficients value is significantly higher for NaDC micelles than NaC micelles, suggesting a larger affinity of ActD towards the more hydrophobic environment of NaDC. A larger degree of partitioning implies a greater number of ActD molecules accommodated into the hydrophobic core of NaDC micelles. Moreover, NaDC aggregates are known to be larger than the aggregates formed by NaC, as a consequence of the larger hydrophobic surface area<sup>28</sup> which supports the higher extent of partitioning of ActD molecules into NaDC aggregates. Both binding constant and partition coefficient parameters indicate that neutral ActD molecules are entrapped more efficiently into more hydrophobic core of NaDC aggregates than that of NaC aggregates. Studies performed by Thakur *et al.*<sup>17</sup> showed that the neutral ellipticine is entrapped in the hydrophobic pocket of micellar aggregates of bile salts, while the cationic species are solubilized in the hydrophilic surface. The difference in the strength of binding and the partitioning of ActD molecules into NaC and NaDC aggregates can be explained by the differences in the micellar structures between dihydroxy and trihydroxy bile salts. Theoretical studies indicated that NaDC aggregates have a spherical structure



whereas NaC aggregates were disklike, oblate or flattened in shape and this difference is due to the various distributions in the hydrophilic moieties: for trihydroxyl bile salt NaC, the three hydroxyl groups and the headgroup form a plane of hydrophilic moieties whereas in the case of dihydroxyl bile salt NaDC, the hydrophilic groups are lined on the edge of the monomer.<sup>28,29</sup>

From the values of  $K_b$  and  $K_x$ , change in free energy of interaction ( $\Delta G_b^0$ ) and change in free energy of the transfer of drug from bulk aqueous phase to micellar phase ( $\Delta G_x^0$ ) were calculated employing the following equation:

$$\Delta G^0 = -RT \ln K \quad (4)$$

The negative values of  $\Delta G^0$  for both binding and partitioning of ActD to NaC and NaDC micelles indicate the spontaneity and thermodynamic feasibility of both processes.

In order to obtain information about the possible positioning of ActD molecules into bile salts micelles we compared the absorption spectrum of the drug in surfactant micelles with the adsorption spectra in solvents with different polarities, which mimic the polarity of different parts of the micelles. Fig. 4 shows that the absorption spectra of ActD in 10 mM phosphate buffer present a broad maximum around 440 nm. In NaC and NaDC micelles, the absorption maximum of the drug is split into two peaks and these peaks are shifted to higher wavelength with about 10–11 nm. Also, it can be observed that the shape of ActD spectrum in solvents with different polarities is similar to the absorption spectrum in bile salts micelles, but the cleavage of the absorption maximum is more evident and the shift of the two newly appeared peaks towards longer wavelengths increases as the polarity of the solvents decreases. The absorption spectrum of ActD in NaC and NaDC micelles presents quite similar characteristics with the spectra in

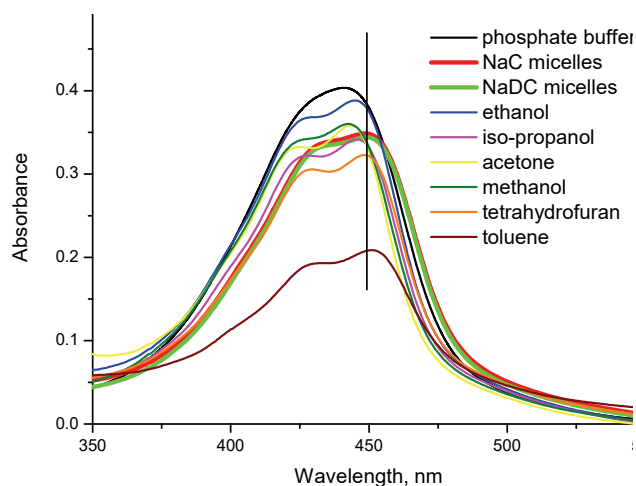


Fig. 4. Absorption spectra of ActD in different solvents and NaC and NaDC micelles.

non-polar solvents with dielectric constants smaller than 10 (tetrahydrofuran and toluene), thus we can say that ActD molecules are located in a hydrophobic microenvironment meaning that ActD molecules are more probable solubilized in the hydrophobic region, rather than in the hydrophilic region of micelles.

*Determination of critical micellar concentration (CMC) of bile salts using pyrene probe*

The UV spectral characteristics of pyrene in aqueous surfactant solutions are used for the estimation of *CMC* of cationic, ionic and nonionic surfactants.<sup>30,31</sup> The absorption spectrum of pyrene in 10 mM phosphate buffer shows eight strong and weak peaks at 232, 240, 252, 260, 272, 308, 320 and 335 nm, as depicted in Figs. 5a and 6a. As the concentration of bile salts increases, pyrene molecules are incorporated in micelles and the absorption peaks of pyrene are shifted towards longer wavelengths and their intensities change. Plot of the sum of absorbances of all four major pyrene peaks ( $A_T$ ) against the bile salts concentration is presented in Figs. 5b and 6b. The profiles show a sigmoidal increase and fitting them to the Sigmoidal–Boltzmann equation was used for *CMC* evaluation. Also, the absorbances of each major peak were also plotted separately and were all sigmoidal in nature. The obtained *CMC* values in 10 mM phosphate buffer (pH 7.4) are 0.0154 M for NaC and 0.0056 M for NaDC, respectively. These values are in the range of *CMC* values reported in literature and determined in water or in the presence of salt using other methods.<sup>32,33</sup> The presence of ActD leads to the decrease of the *CMC* of NaC and NaDC bile salts. This decrease in *CMC* could be explained by the hydrophobic interactions between ActD

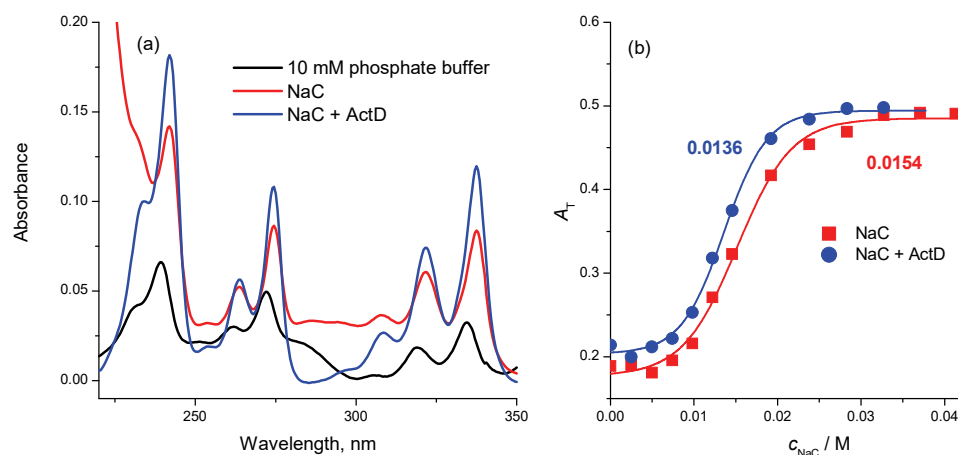


Fig. 5. a) Absorbance spectrum of pyrene (2.0 μM) in 10 mM phosphate buffer (pH 7.4), NaC micelles and NaC micelles in the presence of ActD. b) Plots of  $A_T$  vs. concentration of NaC. The values indicated on the graph are *CMC* of NaC and NaC in the presence of ActD.

and bile salts which further strengthen the hydrophobicity of studied bile salts and make their micellization process easier thereby lowering the  $CMC$  values.<sup>34</sup>

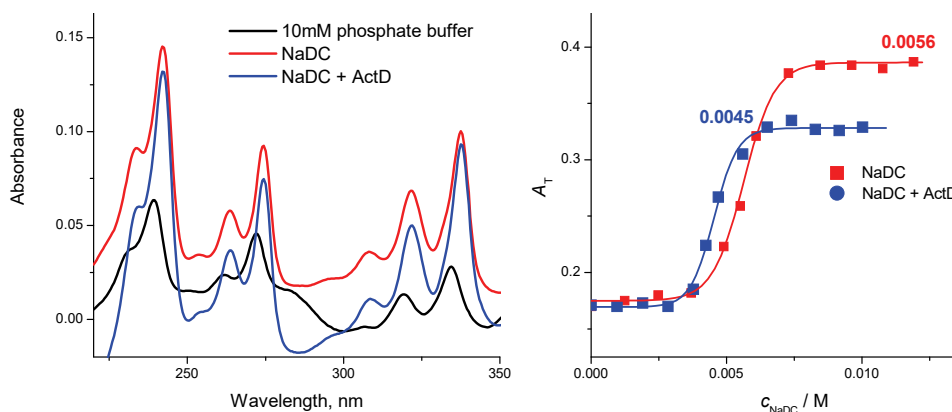


Fig. 6. a) Absorbance spectrum of pyrene (2.0  $\mu$ M) in 10 mM phosphate buffer (pH 7.4), NaDC micelles and NaDC micelles in the presence of ActD. b) Plots of  $A_T$  vs.  $c_{NaDC}$ . The values indicated on the graph are  $CMC$  of NaDC and NaDC in the presence of ActD.

#### Effect of NaC and NaDC micelles on ActD–DNA complex

Differing surfactant micelles,<sup>35–39</sup> liposomes<sup>40,41</sup> or surface active ionic liquids<sup>42</sup> were studied for the effective sequestration of drugs after their deintercalation from DNA double helix. The binding of to DNA leads to an increase of melting temperature ( $T_m$ ) of DNA of about 10 °C and this high positive value proves the intercalation binding mode of ActD to DNA. Also, the amplitude of the melting curve, which measures the hyperchromism of the system decreases (Fig. 7). When NaC and NaDC micelles are added to a pre-formed ActD–DNA

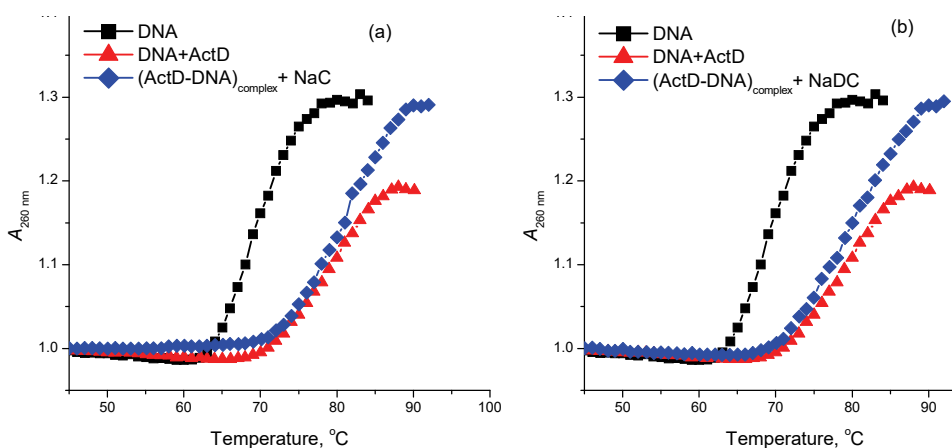


Fig. 7. Thermal melting profile of DNA, ActD–DNA complex and ActD–DNA complex in the presence of: a) NaC and b) NaDC micelles.

complex, the melting temperature does not change significantly (80.56 °C for NaC and 80.15 °C for NaDC as against 79.25 °C for ActD–DNA system), while the hyperchromicity increases almost up to the value corresponding to DNA alone (Table II). Also, the addition of NaC and NaDC micelles to ActD–DNA system induce minor changes (a small increase in absorbance in the case of NaDC micelles) in the absorption spectra (Fig. 8).

TABLE II. DNA melting temperature ( $T_m$ ) and hyperchromicity ( $H$ ) for DNA, ActD–DNA complex and ActD–DNA complex in the presence of NaC and NaDC micelles

System	$T_m / ^\circ\text{C}$	$H / \%$
DNA	69.58	23.04
ActD + DNA	79.25	15.97
ActD–DNA complex + NaC	80.56	22.94
ActD–DNA complex + NaDC	80.15	22.83

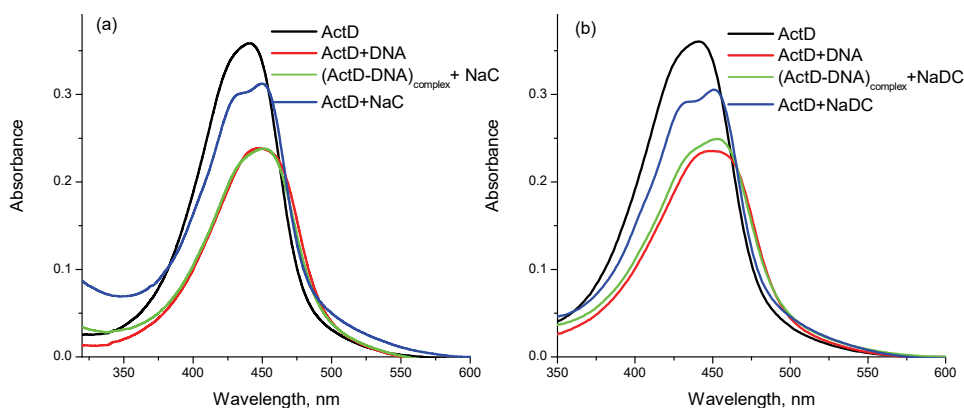


Fig. 8. Absorption spectra of ActD, ActD–DNA complex and ActD and ActD–DNA complex in the presence of: a) NaC and b) NaDC micelles.

These results show that the presence of NaC and NaDC micelles does not induce the deintercalation of ActD molecules from DNA duplex, probable due to the strong binding of ActD to DNA. In comparison with these results, the presence of SDS micelles induce the dissociation of the intercalated ActD molecules from DNA and their relocation in SDS micelles as was evidenced from spectral and thermal denaturation experiments.<sup>39</sup>

#### CONCLUSIONS

The prominent changes observed in the absorption spectra (the decrease in absorbance, the red shift) of ActD in the presence of NaC and NaDC bile salts are clear statement of the interaction between drug molecules and bile salts, and the encapsulation of ActD molecules into the more hydrophobic environment provided by the bile salt aggregates. The results indicate that the binding cons-

tants and the partition coefficients are higher for NaDC aggregates and this difference can be explained by the difference in the micellar structure as well as the hydrophobicity of two bile salts. Regarding the position of ActD molecules into NaC and NaDC micelles, the spectral signatures of the drug in different solvents suggest that ActD molecule experiences the hydrophobic environment of bile salts micelles, rather than the hydrophilic medium. Considering the influence of NaC and NaDC micelles on the ActD–DNA complex, it was shown that the presence of both bile salts micelles does not induce the deintercalation of ActD molecules from DNA duplex.

## ИЗВОД

## ИНТЕРАКЦИЈЕ ВЕЗИВАЊА ЛЕКА АКТИНОМИЦИНА Д ПРОТИВ РАКА СА МИЦЕЛАМА ЖУЧНИХ СОЛИ

ANA MARIA TOADER, IZABELLA DASCALU, ELENA IONELA NEACSU и MIRELA ENACHE  
*Institute of Physical Chemistry "Ilie Murgulescu", Romanian Academy, Splaiul Independentei 202,  
Bucharest 060021, Romania*

Испитивана је интеракција лека актиномицина Д (ActD) против рака са две жучне соли различите хидрофобности: натријум-холат (NaC) и натријум-деоксихолат (NaDC), као и утицај агрегата ових жучних соли на комплекс између ActD и ДНК у 10 mM фосфатном пуферу (pH 7,4), користећи UV–Vis спектроскопске методе (апсорпције и термалне денатурације). Јаче је везивање ActD за NaDC него за NaC, што указује на јаче хидрофобне интеракције између ActD и NaDC мицела. Такође, коефицијент расподеле је значајно већи за NaDC него за NaC мицеле, што је у складу са формирањем већих агрегата NaDC. Профил спектра молекула ActD у NaC и NaDC мицелама, у поређењу са спектром у различитим растварачима, указује да је окружење ActD у мицелама жучних соли хидрофобно. Показано је и да мицеле ових жучне соли не изазивају деинтеркалацију молекула ActD из ДНК двоструког ланца, када се налази у комплексу ActD–ДНК.

(Примљено 2. новембра 2022, ревидирано 17. јануара, прихваћено 25. јануара 2023)

## REFERENCES

1. J. C. Schink, D. K. Singh, A. W. Rademaker, D. S. Miller, J. R. Lurain, *Obstet. Gynecol.* **80** (1992) 817 ([https://doi.org/10.1016/0020-7292\(93\)90503-O](https://doi.org/10.1016/0020-7292(93)90503-O))
2. H. Hosoi, *Pediatr. Int.* **58** (2016) 81 (<https://doi.org/10.1111/ped.12867>)
3. R. D. Jenkin, R. D. Jeffs, C. A. Stephens, M. J. Sonley, *Can. Med. Assoc. J.* **115** (1976) 136 (<https://www.ncbi.nlm.nih.gov/pmc/articles/PMC1878570/pdf/canmedaj01484-0048.pdf>)
4. H. M. Sobell, *Proc. Natl. Acad. Sci. U.S.A.* **82** (1985) 5328 (<https://doi.org/10.1073/pnas.82.16.5328>)
5. A. F. Hofmann, L. R. Hagey, *Cell Mol. Life Sci.* **65** (2008) 2461 (<https://doi.org/10.1007/s00018-008-7568-6>)
6. J. Maldonado-Valderrama, P. Wilde, A. Macierzanka, A. Mackie, *Adv. Colloid Interface Sci.* **165** (2011) 36 (<https://doi.org/10.1016/j.cis.2010.12.002>)
7. Y. S. R. Elnaggar, *Int. J. Nanomedicine* **10** (2015) 3955 (<https://doi.org/10.2147/IJN.S82558>)

8. M. Stojancevic, N. Pavlovic, S. Golocorbin-Kon, M. Mikov, *Front. Life Sci.* **7** (2013) 112 (<https://doi.org/10.1080/21553769.2013.879925>)
9. C. Faustino, C. Serafim, P. Rijo, C. Pinto Reis, *Expert Opin. Drug Deliv.* **13** (2016) 1133 (<https://doi.org/10.1080/17425247.2016.1178233>)
10. D. Madenci, S. U. Egelhaaf, *Curr. Opin. Colloid Interface Sci.* **15** (2010) 109 (<https://doi.org/10.1016/j.cocis.2009.11.010>)
11. D. M. Small, S. A. Penkett, D. Chapman, *Biochim. Biophys. Acta* **176** (1969) 178 ([https://doi.org/10.1016/0005-2760\(69\)90086-1](https://doi.org/10.1016/0005-2760(69)90086-1))
12. D. M. Small, *Advances in Chemistry Series*, E. D. Goddard, Ed., Plenum Press, New York, 1968, p. 31 (<https://doi.org/10.1021/ba-1968-0084.ch004>)
13. S. Gouin, X. X. Zhu, *Langmuir* **14** (1998) 4025 (<https://doi.org/10.1021/la971155w>)
14. M. Posa, A. Sebenji, *Biochim. Biophys. Acta - Gen. Subj.* **1840** (2014) 1072 (<https://doi.org/10.1016/j.bbagen.2013.11.008>)
15. M. Haustein, P. Schiller, M. Wahab, H.-J. Mögel, *J. Sol. Chem.* **43** (2014) 1755
16. (<https://doi.org/10.1007/s10953-014-0239-3>)
17. M. Posa, A. Pilipovic, *J. Mol. Liq.* **238** (2017) 48 (<https://doi.org/10.1016/j.molliq.2017.04.109>)
18. R. Thakur, A. Das, C. Adhikari, A. Chakraborty, *Phys. Chem. Chem. Phys.* **16** (2014) 15681 (<https://doi.org/10.1039/C4CP01308E>)
19. S. Mandal, S. Ghosh, H. H. K. Aggala, C. Banerjee, V. G. Rao, N. Sarkar, *Langmuir* **29** (2013) 133 (<https://doi.org/10.1021/la304319r>)
20. S. Mandal, S. Ghosh, C. Banerjee, V. G. Rao, N. Sarkar, *J. Phys. Chem., B* **116** (2012) 8780 (<https://doi.org/10.1021/jp302435h>)
21. M. Gomez-Mendoza, E. Nuin, I. Andreu, M. Luisa Marin, M. A. Miranda, *J. Phys. Chem., B* **116** (2012) 10213 (<https://doi.org/10.1021/jp304708y>)
22. H. Nakazawa, N. R. Bachur, F. E. Chou, M. M. Mossoba, P. L. Gutierrez, *Biophys. Chem.* **21** (1985) 137 ([https://doi.org/10.1016/0301-4622\(85\)85015-8](https://doi.org/10.1016/0301-4622(85)85015-8))
23. R. Bittman, L. Blau, *Biochemistry* **14** (1975) 2138 (<https://doi.org/10.1021/bi00681a015>)
24. H. K. S. Souza, *Thermochim. Acta* **501** (2010) 1 (<https://doi.org/10.1016/j.tca.2009.12.012>)
25. H. E. Auer, *FEBS Lett.* **73** (1977) 167 ([https://doi.org/10.1016/0014-5793\(77\)80973-3](https://doi.org/10.1016/0014-5793(77)80973-3))
26. H. A. Benesi, J. H. Hildebrand, *J. Am. Chem. Soc.* **71** (1949) 2703 (<https://doi.org/10.1021/ja01176a030>)
27. L. Sepulveda, E. Lissi, F. Quina, *Adv. Colloid Int. Sci.* **25** (1986) 1 ([https://doi.org/10.1016/0001-8686\(86\)80001-X](https://doi.org/10.1016/0001-8686(86)80001-X))
28. H. Kawamura, M. Manabe, Y. Miyamoto, Y. Fujita, S. Tokunaga, *J. Phys. Chem.* **93** (1989) 5536 (<https://doi.org/10.1021/j100351a042>)
29. R. Li, E. Carpentier, E. D. Newell, L. M. Olague, E. Heafey, C. Yihwa, C. Bohne, *Langmuir* **25** (2009) 13800 (<https://doi.org/10.1021/la901826y>)
30. L. B. Partay, M. Sega. P. Jedlovszky, *Langmuir* **23** (2007) 12322 (<https://doi.org/10.1021/la701749u>)
31. G. B. Ray, I. Chakraborty, S. P. Moulik, *J. Colloid Interface Sci.* **294** (2006) 248 (<https://doi.org/10.1016/j.jcis.2005.07.006>)
32. L. Stopkova, J. Galisinova, Z. Suchtova, J. Cizmarik, F. Andriamainty, *Molecules* **23** (2018) (<https://doi.org/10.3390/molecules23051064>)
33. B. Natalini, R. Sardella, A. Gioiello, F. Ianni, A. Di Michele, M. Marinozzi, *J. Pharm. Biomed. Anal.* **87** (2014) 62 (<https://doi.org/10.1016/j.jpba.2013.06.029>)

34. T. S. Wiedmann, L. Kamel, *J. Pharm. Sci.* **91** (2002) 1743 (<https://doi.org/10.1002/jps.10158>)
35. K. Kumar, B. S. Patial, S. Chauhan, *J. Chem. Thermodyn.* **82** (2015) 25 (<http://dx.doi.org/10.1016/j.jct.2014.10.014>)
36. A. Mukherjee, S. Ghosh, M. Pal, B. Singh, *J. Mol. Liq.* **289** (2019) 111116 (<https://doi.org/10.1016/j.molliq.2019.111116>)
37. F. Westerlund, M. Wilhelmsson, B. Norden, P. Lincoln, *J. Am. Chem. Soc.* **125** (2003) 3773 (<https://doi.org/10.1021/ja029243c>)
38. A. Patra, S. Hazra, G. S. Kumar, R. K. Mitra, *J. Phys. Chem., B* **118** (2014) 901 (<https://doi.org/10.1021/jp4091816>)
39. M. Enache, S. Ionescu, E. Volanschi, *J. Mol. Liq.* **208** (2015) 333 (<https://doi.org/10.1016/j.molliq.2015.05.006>)
40. A. M. Toader, I. Dascalu, M. Enache, *Acta Chim. Slov.* **69** (2022) 331 (<https://dx.doi.org/10.17344/acsi.2021.7189>)
41. A. Das, C. Adhikari, D. Nayak, A. Chakraborty, *Langmuir* **32** (2016) 159 (<https://doi.org/10.1021/acs.langmuir.5b03702>)
42. A. Das, C. Adhikari, A. Chakraborty, *Langmuir* **32** (2016) 8889 (<https://doi.org/10.1021/acs.langmuir.6b01860>)
43. N. Maurya, Z. A. Parray, J. K. Maurya, A. Islam, R. Patel, *ACS Omega* **4** (2019) 21005 (<https://doi.org/10.1021/acsomega.9b02246>).







*J. Serb. Chem. Soc.* 88 (4) 381–394 (2023)  
JSCS–5633

## Curcumin as a potential multiple-target inhibitor against SARS-CoV-2 infection: A detailed interaction study using quantum chemical calculations

SUMIT KUMAR\*

*Department of Chemistry, Magadh University, Bodh Gaya-824234, Bihar, India*

(Received 21 September, revised 21 November, accepted 9 December 2022)

**Abstract:** Curcumin is one of the important naturally occurring compounds having several medicinal properties such as: antiviral, antioxidant, antifibrotic, antineoplastic as well as anti-inflammatory. SARS-CoV-2 has emerged as infectious virus, which severely infected a large number of people all over the world. Many efforts have been made to prepare novel antiviral compound, but it is still challenging. Naturally occurring compound, curcumin, can be used as an alternative to antiviral compound against SARS-CoV-2. Its effect against SARS-CoV-2 is already highlighted in the literature. But the quantitative study of its interaction with various precursors of SARS-CoV-2 is not reported till date. This paper reports the interaction of curcumin with angiotensin-converting enzyme2, transmembrane serine protease 2, 3-chymotrypsin-like protease and papain-like protease through molecular docking and quantum chemistry calculations to achieve quantitative understanding of underlying interactions. Here the conformational flexibility of curcumin is also highlighted, which helps it to accommodate in the four different docking sites. The study has been performed using calculations of geometrical parameter, atomic charge, electron density, Laplacian of electron density, dipole moment and the energy gap between highest occupied and lowest unoccupied molecular orbitals. The non-covalent interaction (NCI) analysis is performed to visualize the weak interaction present in the active sites. Combinedly molecular docking and detailed quantum chemistry calculations revealed that curcumin can be adopted as a potential multiple-target inhibitor against SARS-CoV-2.

**Keywords:** antiviral drug; non-covalent interaction; charge density analysis; atom-in-molecule calculation; angiotensin-converting enzyme2; transmembrane serine protease 2.

\* E-mail: [sumitkrmgr@gmail.com](mailto:sumitkrmgr@gmail.com)  
<https://doi.org/10.2298/JSC220921087K>

## INTRODUCTION

In the last couple of years, coronavirus 2 (SARS-CoV-2) widely spread and affected over more than 600 million population of the world and 6.5 million people died according to world health organization (<https://www.who.int/>). Considering this situation world health organization already characterized it as pandemic in 2020. In comparison to middle east respiratory syndrome coronavirus (MERS-CoV), SARS-CoV-2 has been found more contagious and therefore spread fast through population.<sup>1</sup> The development of novel antivirals against SARS-CoV-2 is a matter of great interest as well as a challenge ahead of the scientific community. A great effort has been made to validate antiviral compounds. Some naturally occurring compounds already have antiviral properties, thus can be used as an alternative to antiviral complex compounds evolved during the development of novel antivirals.<sup>2,3</sup> Curcumin, a yellow pigmented polyphenolic compound, majorly found in turmeric and used as a food additive.<sup>4</sup> Its antiviral activity against SARS-CoV-2 along with other viral infections are already reported in the literature.<sup>5-9</sup> It is an interesting naturally occurring substance, which has antioxidant, antifibrotic, antineoplastic as well as anti-inflammatory properties.<sup>4,10</sup>

SARS-CoV-2 belongs to fusion protein containing two major subunits (S1 and S2).<sup>11</sup> For the spread of SARS-CoV-2, angiotensin-converting enzyme2 plays a major role determining its entry through interaction with viral spike protein.<sup>11,12</sup> Further transmembrane serine protease 2 (TMPRSS2) cleaves the spike protein into smaller subunits, which leads to subsequent cellular entry of infectious viral RNA.<sup>13-16</sup> Upon entry to the cell, two SARS-CoV-2 proteases 3-chymotrypsin-like protease (3CLpro, also known as main protease, Mpro) and papain-like protease (PLpro) cleaves the proteins.<sup>13-16</sup> Both 3CLpro and PLpro are essential for the release of 16 non-structural proteins (nsps) on breaking down polyprotein.<sup>13-16</sup> Further the replication and transcription occur to produce viral genomes by accumulation of infectious replicase on the host membrane.<sup>17</sup> Later the four major proteins: the spike (S) protein, membrane (M) protein, nucleocapsid (N) protein, and the envelope (E) protein form and leads to the formation of viral particle. Some viral particle of CoVs is also reported, without using full ensemble of all four proteins, by encoding extra protein having similar or compensatory ability.<sup>18-20</sup> Till date there is no report available in the literature providing in-depth molecular level study, of interaction of curcumin along with TMPRSS2, ACE2, PLpro and 3CLpro, to understand its ability to encounter with SARS-CoV-2. Therefore, the study of curcumin along with precursors of SARS-CoV-2 has been reported here to provide necessary information, which may be helpful to understand the applicability of curcumin in the treatment against SARS-CoV-2.

In the present study, not only the interaction of the curcumin with precursors of SARS-CoV-2 but also its conformational flexibility has been monitored to get the in-depth understanding related to the protein-ligand interaction. The study has been performed to monitor the distribution of electron density, dipole moment, atomic charge and atom-in-molecule (AIM) properties of curcumin in the gas phase as well as in the active sites of four different precursors related to SARS-CoV-2. The non-covalent interaction (NCI) analysis is performed for the visualization of weak interactions in the active sites. The NCI plot allows to study the macromolecular system effectively.

#### COMPUTATIONAL DETAILS

Molecular docking is the most famous tool to monitor the interaction of ligand and receptor.<sup>21</sup> It provides the useful information about the binding site of the protein used by the ligand to accommodate through various non-covalent interactions. The docking studies has been performed using computational software. AutoDock4 together with AutoGrid4 python programming-based tool has been used to study the molecular docking of curcumin with TMPRSS2, ACE2, PLpro and 3CLpro.<sup>22,23</sup> The docking uses the grid driven method to prepare grids around the protein and the lookup table for the simulation by calculating the energy keeping an atom as a probe on each of the grid points. The lookup table helps the simulation to effectively measure the binding energy of the conformers with the target protein. Further Lamarckian genetic algorithm has been used to search the lowest binding energy conformer associated in the local minima position close to the protein. AutoDock4 uses the semiempirical method to obtain the binding energies for the suitable conformers at the docking site of the protein in bound as well as unbound states. The study therefore provides interesting information about the reliable docking pose prediction for ligand protein interactions. PyMOL, LigPlot+ and Protein-ligand interaction profiler (PLIP) tools are used to draw the informative pictures of docking studies.<sup>24-26</sup> PLIP tool is also used here to identify the non-covalent interaction of curcumin with TMPRSS2, ACE2, PLpro and 3CLpro.

The efficacy of curcumin against the SARS-CoV-2 virus has been realized by studying the interaction of curcumin with TMPRSS2, ACE2, 3CLpro and PLpro. This interaction has been monitored using the docking studies. For these docking studies, crystal structures of TMPRSS2 (PDB ID: 1Z8A), ACE2 (PDB ID: 3D0G), PLpro (PDB: 3E9S), and 3CLpro (PDB ID: 3AW0) are used. These PDBs are obtained from Protein Data Bank (<https://www.rcsb.org/>).<sup>27</sup>

To understand the conformational flexibility of the curcumin, its diketone form in the gas phase is compared with the same obtained from the active sites of TMPRSS2, ACE2, PLpro and 3CLpro. Single point calculations are performed for curcumin obtained from active sites of TMPRSS2, ACE2, PLpro and 3CLpro whereas optimization has been performed to obtain the most stable geometry of curcumin in the gas phase at B3LYP/def2-TZVP level of theory. B3LYP is Becke's three-parameter exchange functional with the Lee–Yang–Parr correlation functional, which provides good result with reasonable error.<sup>28</sup> The def2-TZVP proposed by Ahlrichs–Weigend is triple-zeta valence with polarization basis set.<sup>29</sup> It provides better result than 6–311G\*\*.<sup>30,31</sup> Furthermore, def2 basis sets are designed to deliver consistent accuracy for nearly all atoms up to radon.<sup>30,32</sup> These calculations are performed using Turbo mole version 7.6 *ab initio* quantum-chemical calculation software package.<sup>33,34</sup> The comparison has also been made based on the geometrical parameter, atomic charge, electron density, Laplacian of electron density, dipole moment and the energy gap between highest occupied and

lowest unoccupied molecular orbitals. NCI and AIM analysis are performed using NCI Plot and Turbomole version 7.6 software, respectively.<sup>33-35</sup>

## RESULTS AND DISCUSSION

The docking studies of curcumin have been performed with TMPRSS2, ACE2, PLpro and 3CLpro, which are related to coronavirus 2 (SARS-CoV-2). For these docking studies, ten rotatable bonds of curcumin are used. The lowest binding energy docking pose of curcumin with TMPRSS2, ACE2, PLpro and 3CLpro are shown in Fig. 1.

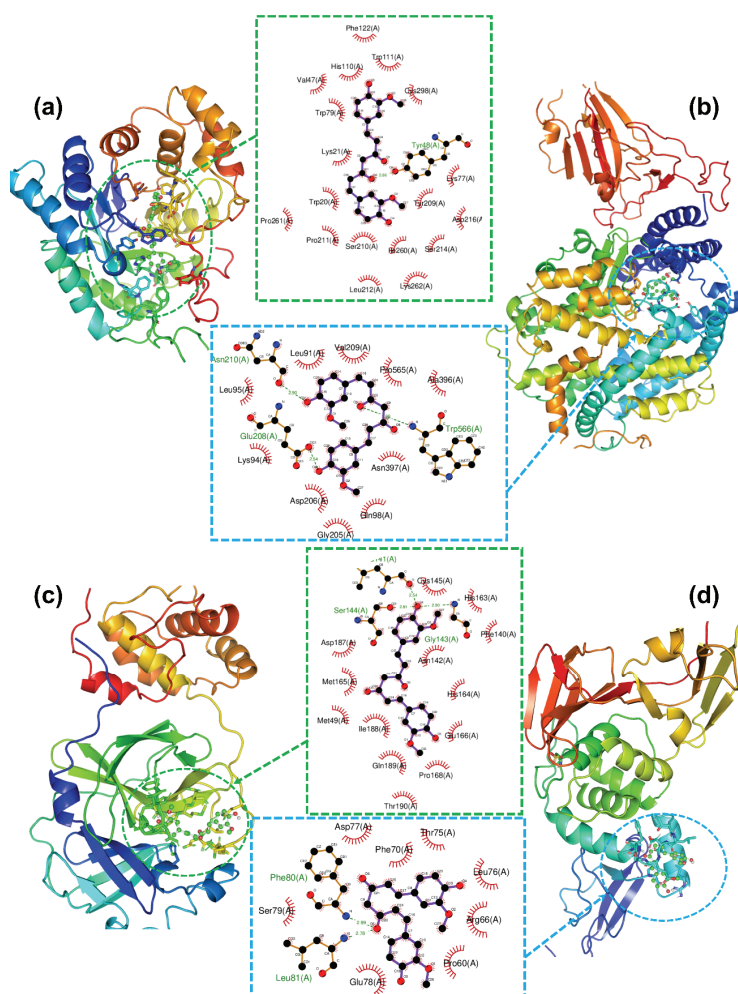


Fig. 1. Lowest binding energy docking pose of curcumin in: a) the transmembrane serine protease 2 (TMPRSS2) PDB ID: 1Z8A, b) angiotensin-converting enzyme 2 (ACE2) PDB ID: 3D0G, c) 3-chymotrypsin-like protease (3CLpro) PDB ID: 3AW0 and d) papain-like protease (PLpro) PDB ID: 3E9S.

The lowest binding energy of curcumin with TMPRSS2, ACE2, PLpro and 3CLpro are  $-42.34$ ,  $-28.53$ ,  $-33.85$  and  $-31.33$  kJ/mol, respectively. Interestingly, the most stable docking pose of curcumin has been observed with TMPRSS2. The detailed study of the four most stable docking poses of curcumin in TMPRSS2, ACE2, PLpro and 3CLpro has been reported in the supporting information. The ligand efficiency and the intermolecular energy of curcumin with TMPRSS2 are measured the highest, whereas the torsional free energy is found the same for all four complexes formed after docking. At the same time, the inhibition efficiency of curcumin with TMPRSS2 (38.37 nM) is found the lowest compared to that with ACE2 (10.0  $\mu$ M), PLpro (1.18  $\mu$ M) and 3CLpro (3.22  $\mu$ M).

Furthermore, the docking studies show that curcumin interacts with TMPRSS2 through both hydrogen bonding (H-bonding) and dispersion interactions. Amino acids LYS21, TYR48, TRP111 and LEU212 of Chain A interacts through H-bonding and the corresponding H-bonding distance is found 4.01, 3.15, 3.72 and 3.86 Å, respectively. Interestingly, the aromatic rings of amino acid TRP21 of chain A of TMPRSS2 and curcumin interact through  $\pi$ - $\pi$  stacking interaction with an interplanar distance of 5.49 Å, the interaction is shown in Fig. 1a. Several other amino acids interact through hydrophobic interactions. These interactions are shown in Fig. 1a. Amino acids LYS94, GLN98, TYR196, GLU208 and TRP566 of chain A of ACE2 interact with curcumin through H-bonding and the corresponding H-bonding distances are 3.92, 3.84, 3.79, 2.54 and 2.99 Å, respectively whereas other interactions have been shown in Fig. 1b. Interestingly, GLY143, SER144 and GLU189 of chain A of PLpro and ARG66, PHE80 and LEU81 of Chain A of 3CLpro interacts with curcumin through hydrogen bonding. The detailed chart of interactions in the lowest binding energy docking poses of curcumin with TMPRSS2, ACE2, PLpro and 3CLpro is shown in the supporting information. The adaptive Poisson-Boltzmann solver (ABPS), which provides the Poisson-Boltzmann electrostatic calculation, are also depicted in the Supplementary material to this paper, which shows the electrostatic interaction of curcumin with TMPRSS2, ACE2, 3CLpro and PLpro.

Amino acids GLY143, SER144 and GLN189 of chain A of PLpro interacts to curcumin through H-bonding with distance of 2.90, 2.58 and 2.56 Å, respectively. 2D and 3D representation of docking poses of curcumin with PLpro are shown in Fig. 1c. Amino acids ARG66, PHE80 and LEU81 of chain A of 3CLpro interacts to curcumin through H-bonding with distance of 3.43, 2.99 and 2.78 Å, respectively (Fig. 1d).

#### *Structural analysis*

The optimized geometry of curcumin in the gas phase (I) at B3LYP/def2-TZVP level of theory and geometries of curcumin lifted from the lowest binding energy active sites of TMPRSS2 (IIa), ACE2 (IIb), 3CLpro (IIc) and PLpro (IId)

are depicted in Fig. 2, whereas the corresponding geometrical parameters are tabulated in the Supporting material to this paper. Curcumin is an interesting molecule connected through a long chain of multiple conjugated double bonds, which provides structural flexibility to adjust in the active sites. Fig. 2 shows a surprising glimpse of this structural flexibility of curcumin in various active sites. The geometry of curcumin bends a lot in the active site of ACE2 and PLpro, in comparison to the gas phase geometry, and acquires U-shape. Interestingly, the study of geometrical parameters provides in-depth understanding about this.

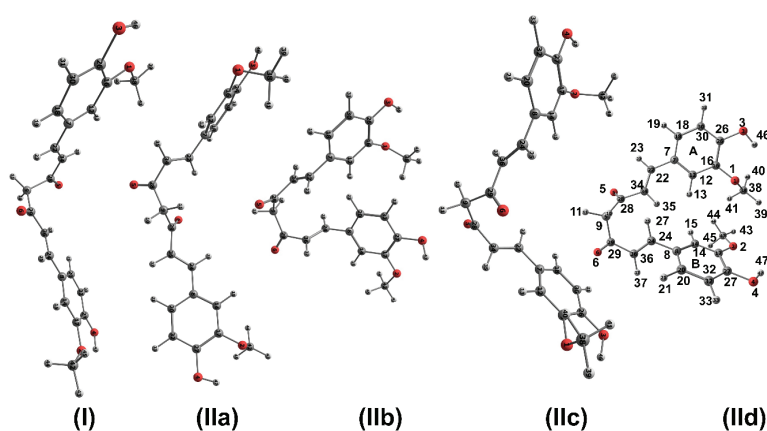


Fig. 2. Optimized geometry (I) of curcumin in gas phase at B3LYP/def2-TZVP level of theory. Geometries of curcumin lifted from the active site of TMPRSS2 (IIa), ACE2 (IIb), 3CLpro (IIc) and PLpro (IId).

The bond length of ring  $C(sp^2)-C(sp^2)$  carbon bonds in curcumin in gas phase (I) and the same lifted from active sites (IIa, IIb, IIc, IId) are measured between 1.38–1.41 Å, whereas the bond angles inside the rings are found between 118.3–121.5°. A small change is reported in the geometrical parameters inside ring. The bond lengths of chain carbon bonds C8–C24, C36–C29, C28–C34 and C7–C22 are found to be increased by 0.02 Å in the active sites compared to that in the gas phase. The increase in bond length is attributed to intermolecular interaction with the amino acids in the active sites.

Interestingly, the major change is observed in the dihedral angles along the chain length in different forms of curcumin. Dihedral angles  $\angle C22-C34-C28-C9$ ,  $\angle C34-C28-C9-C29$ ,  $\angle C28-C9-C29-C36$  and  $\angle C9-C29-C36-C24$  in the form (I) are measured 5.2°, –80.3°, –67.5° and –177.3°, respectively. The same in the form (IIb) are –135.7°, 104.3°, –39.1° and –66.7°, respectively, whereas the same in the form (IId) are –141.1°, –93.1°, 79.3° and –5.4°, respectively. The changes in the dihedral angles are mainly responsible for the geometrical change to U-shape in IIb and IId forms, which can be observed in Fig. 2.

### Atomic charge

Mulliken population analysis (MPA) charges of curcumin in the gas phase and that lifted from the active site of TMPRSS2 (IIb), ACE2 (IIb), 3CLpro (IIc) and PLpro (IId) calculated at B3LYP/def2-TZVP level of theory are reported in Fig. 3. The corresponding plot of natural population analysis (NPA) charge along with detailed data is reported in the Supplementary material. The study depicts that MPA charges of hydroxyl oxygens O3 are  $-0.38681e$ ,  $-0.39929e$ ,  $-0.39646e$ ,  $-0.40884e$  and  $-0.38819e$  for I, IIa, IIb, IIc and IId, respectively. Similarly, MPA charges of hydroxyl oxygens O4 are  $-0.38775e$ ,  $-0.38995e$ ,  $-0.42946e$ ,  $-0.39773e$  and  $-0.39995e$  for I, IIa, IIb, IIc and IId, respectively. It shows that MPA charge of hydroxy oxygen increases on binding with amino acids in the active site of receptor in comparison to that in the gas phase (I). Interestingly, the MPA charges of hydroxyl oxygen O3 and O4 are found lower than carbonyl oxygens, O5 and O6. At the same time the carbon atom attached to the electronegative oxygens O3, O4, O5 and O6 are C26, C27, C28 and C29, respectively, and the MPA charges of these carbons are found higher. This is prominently reported in case of NPA charges (see Fig. S7 of the Supplementary material). NPA charges for hydroxyl oxygen O3 and O4 are less than that for carbonyl oxygen O5 and O6 for all forms of curcumin, whereas an increase in NPA charges is also reported for O3, O4, O5 and O6 in case of curcumin lifted from the active sites. Overall, the comparison of atomic charges (MPA and NPA) nicely helps to understand the interaction of curcumin with TMPRSS2, ACE2, 3CLpro and PLpro.

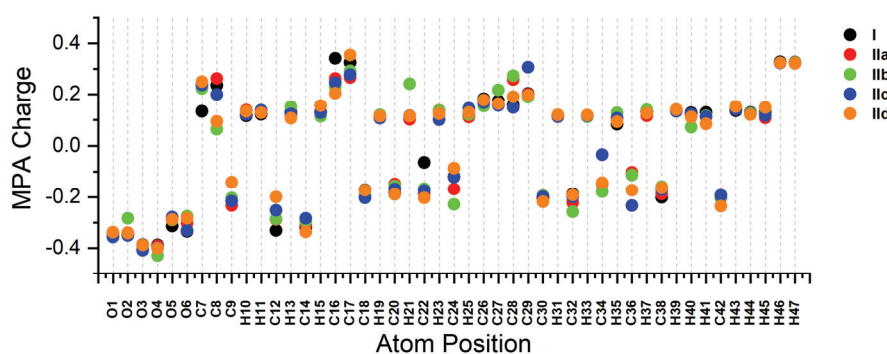


Fig. 3. Mulliken population analysis (MPA) charges of curcumin in the gas phase and that lifted from the active site of TMPRSS2 (IIb), ACE2 (IIb), 3CLpro (IIc) and PLpro (IId).

### AIM analysis

Electron density  $\rho_{\text{bcp}}(r)$  and Laplacian of electron density  $\nabla^2\rho_{\text{bcp}}(r)$  of curcumin in the gas phase (I) and that lifted from the active site of TMPRSS2 (IIa), ACE2 (IIb), 3CLpro (IIc) and PLpro (IId) are studied at B3LYP/def2-TZVP level

of theory and graphically represented in Fig. 4. The corresponding detailed report and figure have been added in the supporting information. An average of  $\rho_{\text{bcp}}(r)$  at the bond critical points (BCP) of carbon bonds in the two aromatic rings of curcumin (I) are 0.3191/0.3190 a.u., whereas the same of curcumin in the form IIa, IIb, IIc and IId are 0.3213/0.3214, 0.3207/0.3207, 0.3215/0.3210 and 0.3219/0.3202 a.u., respectively. Interestingly, the  $\rho_{\text{bcp}}(r)$  at ring critical points (RCPs) of two aromatic rings of curcumin in I form are 0.0229/0.0230 a.u., whereas the same for curcumin in IIa, IIc, IIc and IId are 0.0233/0.0232, 0.0231/0.0232, 0.0231/0.0232 and 0.0233/0.0231 a.u., respectively. It shows that the electron densities at the curcumin in the forms IIa, IIb, IIc and IId increase in comparison to that in gas phase, *i.e.*, isolated form (I) due to interaction with amino acids present in the docking site.

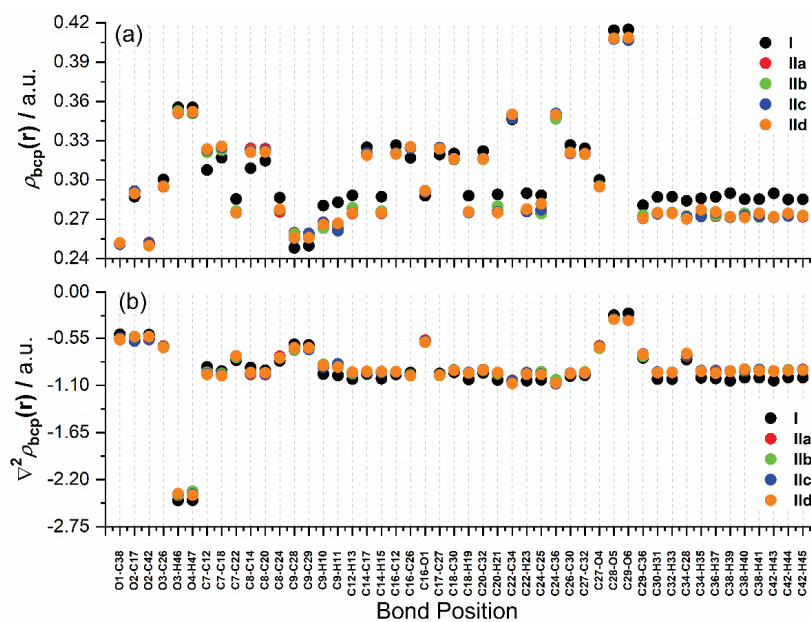


Fig. 4. Plots of: a) electron density  $\rho_{\text{bcp}}(r)$  and b) Laplacian of electron density  $\nabla^2\rho_{\text{bcp}}(r)$  of curcumin in the gas phase and the same lifted from the active site of TMPRSS2 (IIa), ACE2 (IIb), 3CLpro (IIc) and PLpro (IId).

The  $\rho_{\text{bcp}}(r)$  of alcoholic bonds O3–H46 and O4–H47 are measured 0.3555/0.3555 a.u. in form (I), whereas that are in curcumin in the form IIa, IIb, IIc and IId are 0.3523/0.3520, 0.3525/0.3507, 0.3510/0.3516 and 0.3514/0.3521 a.u., respectively. A jump in  $\rho_{\text{bcp}}(r)$  of ketonic bond C28–O5 and C29–O6 are measured 0.4143/0.415 a.u. in form (I), whereas the same in curcumin lifted from the form IIa, IIb, IIc and IId are 0.4078/0.4075, 0.4078/0.4076, 0.4077/0.4068 and 0.4082/0.4087 a.u., respectively. Thus, the  $\rho_{\text{bcp}}(r)$  of alcoholic and ketonic bonds of



curcumin decreases in the active site compared to that in gas phase by 0.003 and 0.007 a.u. The H-bonding interaction is found responsible for this difference.

Sometime  $\nabla^2\rho_{\text{bc}}(r)$  for the hydroxyl groups of curcumin in the forms IIa, IIb, IIc and IId are higher than that in the gas phase (I). The difference is attributed to H-bonding interaction. The comparison of  $\rho_{\text{bc}}(r)$  and  $\nabla^2\rho_{\text{bc}}(r)$  of the ketonic groups (C29–O6 and C28–O5) in the four different forms of curcumin defines its interaction with amino acids in the docking site.

#### *HOMO–LUMO band gap and dipole moment measurements*

The geometries of curcumin in gas phase are optimized at B3LYP/def2-TZVP level of theory while single point calculations are performed for IIa, IIb, IIc and IId at same level of theory. HOMO energy gives the impression of ionization potential relating the ability to donate an electron while LUMO energy directly correlates with electron affinity relating the ability to accept an electron. Thus HOMO–LUMO energy gap provides the information about the molecular stability. As HOMO–LUMO energy gap for a molecule decreases the polarizability and the reactivity of the molecule increases. The HOMO–LUMO calculations are performed and reported 3.699 eV in the gas phase, whereas the same obtained for IIa, IIb, IIc and IId are 4.367, 4.392, 3.714 and 4.058 eV, respectively. The band gap is found lowest at the gas phase and the band gap for IIc is measured close to gas phase but high value of band gap is measured for IIa and IIb.

Dipole moments ( $\mu$ ) has also calculated for all the forms of curcumin at B3LYP/def2-TZVP level of theory and reported in the supporting information. The dipole moment of curcumin in the gas phase (I) is calculated 3.26 D\*, whereas dipole moments of IIa, IIb, IIc and IId are 7.022, 4.147, 4.429 and 6.8 D, respectively. The dipole moments of IIa, IIb, IIc and IId are greater than that of I, which is attributed to intermolecular interaction as well as charge distribution present close to curcumin in the active sites. Interestingly, the dipole moment of IIa is found higher than that of IIb, IIc and IId. Interestingly, the binding energy for the most preferable docking pose of curcumin with TMPRSS2 (–42.34 kJ/mol) is found lower than that in case of ACE2, PLpro and 3CLpro.

#### *Non-covalent interaction (NCI) plot*

NCI plot is helpful to understand the various non-covalent interactions present in the macromolecule. Yang and coworkers implemented reduced density gradient ( $\text{RDG} = |\nabla\rho|/2(3\pi^2)^{1/3}\rho^{4/3}$ ) to measure the parameters related to the non-covalent interactions in NCI plot.<sup>35</sup> Therefore, NCI plot is used to monitor the interaction of curcumin in the active site of TMPRSS2, ACE2, PLpro and 3CLpro. The lowest binding energy docking sites are chosen for this purpose. The closest interaction within 3.5 Å was selected using Pymol software. The

\* 1 D =  $3.34 \times 10^{-30}$  C m

selected residues from TMPRSS2, ACE2, PLpro and 3CLpro along with curcumin are used for NCI plot. Fig. 5 shows the NCI plot and underlying interactions for curcumin with the TMPRSS2, ACE2, PLpro and 3CLpro.

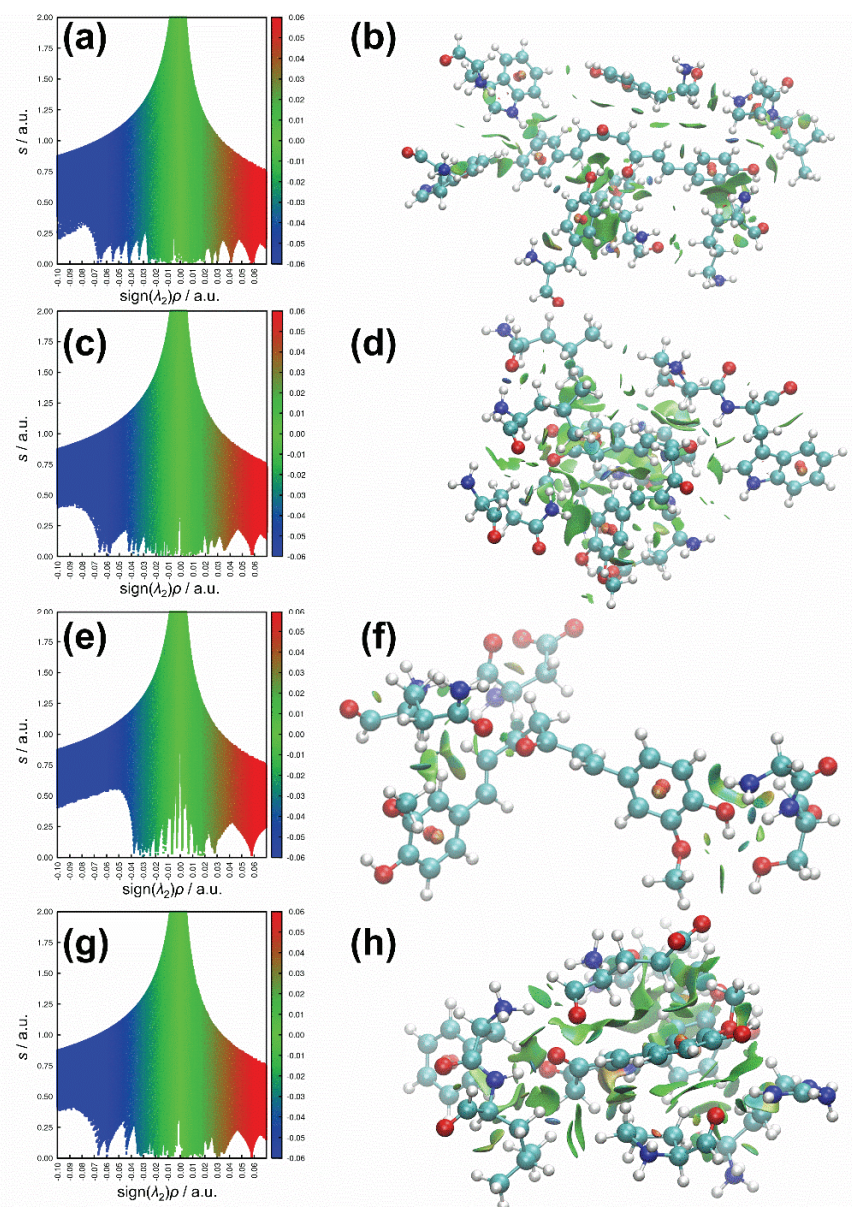


Fig. 5. RDG plot of NCI analysis for docking poses of curcumin with TMPRSS2, ACE2, 3CLpro and PLpro are plotted (a, c, e and g, respectively) along corresponding isosurface extractions of RDG plots of NCI analysis (b, d, f and h, respectively).

The coloring scheme used to discuss the isosurfaces is as follows. The blue colour indicates the strong attractive interaction. The green color indicates the interactions having intermediate strength such as H-bonding,  $\pi$ - $\pi$  and van der Waals interactions (vdW). The red colour represents the repulsive forces. A mixture of green and blue has been mostly seen in the NCI plot, which also represents electrostatic as well as dispersion interactions. Fig. 5 (a, c, e and f) depict RDG plots of NCI analysis of docking poses of curcumin with TMPRSS2, ACE2, PLpro and 3CLpro. These plots show mostly blue and green colours indicating that the main contribution to the binding strength is originated from H-bonding and vdW interactions. The same is also confirmed through PLIP analysis.<sup>26</sup> The extended plots are separately shown in the supporting information for clear visibility.

Fig. 5b shows the isosurface extraction of NCI analysis showing H-bonding interaction between C=O and O-H groups of curcumin with O-H group of tyrosine and N-H group of leucine, respectively. At the same time curcumin also interacts with TRP20, TRP79, TRP111 and TYR209 through hydrogen bonding interaction in the active site of TMPRSS2P. The study support the interactions shown in Fig. 1. Fig. 5c and d shows the NCI plot and its isosurface extractions of the intermolecular interactions between curcumin and amino acids present in the active site of ACE2. Fig. 5f shows that the C=O group of curcumin interacts with N-H groups of LEU81 and PHE80 of chain A. Thus, NCI plots provided in-depth understanding of intermolecular interaction present between ligand and receptor.

#### CONCLUSIONS

The study of curcumin interactions with transmembrane serine protease 2 (TMPRSS2), angiotensin-converting enzyme 2 (ACE2), 3-chymotrypsin-like protease (3CLpro) and papain-like protease (PLpro) are performed using molecular docking and detailed quantum chemistry calculation. Quantum chemistry calculation provides in-depth quantitative information regarding the underlying interactions. Curcumin has multiple single bonds providing it freedom to adjust into the lowest binding energy pockets after geometrical rearrangements. The study of curcumin in the active sites has been performed through calculation of geometrical parameters, atomic charges, electron density, Laplacian of electron density, dipole moments, energy gap between highest occupied and lowest unoccupied molecular orbitals as well as NCI analysis. The study revealed that curcumin can act as a potential multiple-target inhibitor against SARS-CoV-2.

#### SUPPLEMENTARY MATERIAL

Additional data and information are available electronically at the pages of journal website: <https://www.shd-pub.org.rs/index.php/JSCS/article/view/12081>, or from the corresponding author on request.

*Acknowledgements.* I would like to thank Magadh University, Bodh Gaya-824234, Bihar, India, for providing lab facility to perform research. Science and Engineering Research Board, Department of Science and Technology (DST), Ministry of Science and Technology, India (Grant No. SRG/2019/002284) has been acknowledged for financial support.

## ИЗВОД

КУРКУМИН КАО ПОТЕНЦИЈАЛНИ ИНХИБИТОР ВИШЕСТРУКИХ МЕТА ПРОТИВ SARS-COV-2 ИНФЕКЦИЈЕ: ДЕТАЉНО ПРОУЧАВАЊЕ ИНТЕРАКЦИЈЕ КОРИШЋЕЊЕМ КВАНТНО-ХЕМИЈСКИХ ИЗРАЧУНАВАЊА

SUMIT KUMAR

*Department of Chemistry, Magadh University, Bodh Gaya-824234, Bihar, India*

Куркумин је једно од значајних природних једињења са особинама као што су: антивирусне, антиоксидантне и противупалне. SARS-CoV-2 се појавио као заразни вирус који озбиљно угрожава велике групе становништва у свету. Било је више покушаја да се направе нова антивирусна једињења, али то је остао изазов чак и након озбиљних истраживања. Природни производ куркумин, може се користити као алтернатива антивирусним једињењима за SARS-CoV-2. Његово дејство против SARS-CoV-2 већ је истакнуто у литератури. До данас нема радова о квантитативном проучавању његове интеракције са различитим прекурсорима SARS-CoV-2. Овај чланак саопштава о интеракцији куркумина са ангиотензин-конвертујућим ензимом 2, трансмембранском серин протеазом 2, на 3-химотрипсин-налик протеазом и на папаин-налик протеазом, помоћу молекулског докинга и квантно-хемијских израчунавања, да би постигли квантитативно разумевање основа интеракција. Овде је постигнуто да и конформациона флексибилност куркумина буде расветљена, што помаже да га се смести у четири различита места за доковање. Студија је изведена коришћењем израчунавања геометријских параметара, атомских наелектрисања, густине електрона, Лапласијана електронске густине, диполног момента и енергетског процепа између највише попуњене и најниже незаузете молекулске орбитале. Урађена је анализа не-ковалентних интеракција (NCI) да би се визуализовале слабе интеракције присутне у активним местима. Комбиновање молекулског докинга и детаљних квантно-хемијских израчунавања показује да куркумин може бити прихваћен као потенцијални инхибитор вишеструких мета против SARS-CoV-2.

(Примљено 21. септембра, ревидирано 21. новембра, прихваћено 9. децембра 2022)

## REFERENCES

1. M. Cevik, M. Tate, O. Lloyd Maraolo, J. Schafers, A. Ho, *Lancet Microbe* **2** (2021) e13 ([http://dx.doi.org/10.1016/S2666-5247\(20\)30172-5](http://dx.doi.org/10.1016/S2666-5247(20)30172-5))
2. L. M. Mattio, G. Catinella, A. Pinto, S. Dallavalle, *Eur. J. Med. Chem.* **202** (2020) 112541 (<http://dx.doi.org/10.1016/j.ejmech.2020.112541>)
3. L. T. Lin, W. C. Hsu, C. C. Lin, *J. Tradit. Complement. Med.* **4** (2014) 24 (<http://dx.doi.org/10.4103/2225-4110.124335>)
4. F. A. C. Rocha, M. R. de Assis, *Phytother. Res.* **34** (2020) 2085 (<http://dx.doi.org/10.1002/ptr.6745>)
5. F. Zahedipour, S. A. Hosseini, T. Sathyapalan, M. Majeed, T. Jamialahmadi, K. Al-Rasadi, M. Banach, A. Sahebkar, *Phytother. Res.* **34** (2020) 2911 (<http://dx.doi.org/10.1002/ptr.6738>)

6. V. K. Soni, A. Mehta, Y. K. Ratre, A. K. Tiwari, A. Amit, R. P. Singh, S. C. Sonkar, N. Chaturvedi, D. Shukla, N. K. Vishvakarma, *Eur. J. Pharmacol.* **886** (2020) 173551 (<http://dx.doi.org/10.1016/j.ejphar.2020.173551>)
7. F. Babaei, M. Nassiri-Asl, H. Hosseinzadeh, *Food Sci. Nutr.* **8** (2020) 5215 (<http://dx.doi.org/10.1002/fsn3.1858>)
8. R. K. Thimmulappa, K. K. Mudnakudu-Nagaraju, C. Shivamallu, K. J. T. Subramaniam, A. Radhakrishnan, S. Bhojraj, G. Kuppusamy, *Heliyon* **7** (2021) e06350 (<http://dx.doi.org/10.1016/j.heliyon.2021.e06350>)
9. A. Saeedi-Boroujeni, M. R. Mahmoudian-Sani, M. Bahadoram, A. Alghasi, *Basic Clin. Pharmacol. Toxicol.* **128** (2021) 37 (<http://dx.doi.org/10.1111/bcpt.13503>)
10. N. Chainani-Wu, *J. Altern. Complement. Med.* **9** (2003) 161 (<http://dx.doi.org/10.1089/107555303321223035>)
11. Y. Huang, C. Yang, X. F. Xu, W. Xu, S. W. Liu, *Acta Pharmacol. Sin.* **41** (2020) 1141 (<http://dx.doi.org/10.1038/s41401-020-0485-4>)
12. H. Zhang, J. M. Penninger, Y. Li, N. Zhong, A. S. Slutsky, *Intensive Care Med.* **46** (2020) 586 (<http://dx.doi.org/10.1007/s00134-020-05985-9>)
13. A. Domling, L. Gao, *Chem* **6** (2020) 1283 (<http://dx.doi.org/10.1016/j.chempr.2020.04.023>)
14. M. Hoffmann, H. Kleine-Weber, S. Schroeder, N. Kruger, T. Herrler, S. Erichsen, T. S. Schiergens, G. Herrler, N. H. Wu, A. Nitsche, M. A. Muller, C. Drosten, S. Pohlmann, *Cell* **181** (2020) 271 (<http://dx.doi.org/10.1016/j.cell.2020.02.052>)
15. A. B. Jena, N. Kanungo, V. Nayak, G. B. N. Chainy, J. Dandapat, *Sci. Rep.* **11** (2021) 2043 (<http://dx.doi.org/10.1038/s41598-021-81462-7>)
16. A. C. Walls, Y. J. Park, M. A. Tortorici, A. Wall, A. T. McGuire, D. Veesele, *Cell* **181** (2020) 281 (<http://dx.doi.org/10.1016/j.cell.2020.02.058>)
17. N. Barretto, D. Jukneliene, K. Ratia, Z. Chen, A. D. Mesecar, S. C. Baker, *J. Virol.* **79** (2005) 15189 (<http://dx.doi.org/10.1128/jvi.79.24.15189-15198.2005>)
18. M. L. DeDiego, E. Alvarez, F. Almazán, M. T. Rejas, E. Lamirande, A. Roberts, W.-J. Shieh, S. R. Zaki, K. Subbarao, L. Enjuanes, *J. Virol.* **81** (2007) 1701 (<http://dx.doi.org/10.1128/JVI.01467-06>)
19. L. Kuo, P. S. Masters, *J. Virol.* **77** (2003) 4597 (<http://dx.doi.org/10.1128/JVI.77.8.4597-4608.2003>)
20. J. Ortego, J. E. Ceriani, C. Patino, J. Plana, L. Enjuanes, *Virology* **368** (2007) 296 (<http://dx.doi.org/10.1016/j.virol.2007.05.032>)
21. X. Y. Meng, H. X. Zhang, M. Mezei, M. Cui, *Curr. Comput. Aided Drug Des.* **7** (2011) 146 (<http://dx.doi.org/10.2174/157340911795677602>)
22. G. M. Morris, R. Huey, W. Lindstrom, M. F. Sanner, R. K. Belew, D. S. Goodsell, A. J. Olson, *J. Comput. Chem.* **30** (2009) 2785 (<http://dx.doi.org/10.1002/jcc.21256>)
23. M. F. Sanner, *J. Mol. Graph. Model.* **17** (1999) 57 ([http://dx.doi.org/10.1016/S1093-3263\(99\)99999-0](http://dx.doi.org/10.1016/S1093-3263(99)99999-0))
24. R. A. Laskowski, M. B. Swindells, *J. Chem. Inf. Model.* **51** (2011) 2778 (<http://dx.doi.org/10.1021/ci200227u>)
25. A. C. Wallace, R. A. Laskowski, J. M. Thornton, *Protein Eng.* **8** (1995) 127 (<http://dx.doi.org/10.1093/protein/8.2.127>)
26. M. F. Adasme, K. L. Linnemann, S. N. Bolz, F. Kaiser, S. Salentin, V. J. Haupt, M. Schroeder, *Nucleic Acids Res.* **49** (2021) W530 (<http://dx.doi.org/10.1093/nar/gkab294>)

27. H. M. Berman, J. Westbrook, Z. Feng, G. Gilliland, T. N. Bhat, H. Weissig, I. N. Shindyalov, P. E. Bourne, *Nucleic Acids Res.* **28** (2000) 235 (<http://dx.doi.org/10.1093/nar/28.1.235>)
28. M. D. Wodrich, C. Corminboeuf, P. v. R. Schleyer, *Org. Lett.* **8** (2006) 3631 (<http://dx.doi.org/10.1021/ol061016i>)
29. F. Weigend, R. Ahlrichs, *Phys. Chem. Chem. Phys.* **7** (2005) 3297 (<http://dx.doi.org/10.1039/B508541A>)
30. F. Weigend, *Phys. Chem. Chem. Phys.* **8** (2006) 1057 (<http://dx.doi.org/10.1039/B515623H>)
31. X. Xu, D. G. Truhlar, *J. Chem. Theory Comput.* **7** (2011) 2766 (<http://dx.doi.org/10.1021/ct200234r>)
32. J. Zheng, X. Xu, D. G. Truhlar, *Theor. Chem. Acc.* **128** (2011) 295 (<http://dx.doi.org/10.1007/s00214-010-0846-z>)
33. F. Furche, R. Ahlrichs, C. Hättig, W. Klopper, M. Sierka, F. Weigend, *Wiley Interdiscip. Rev. Comput. Mol. Sci.* **4** (2014) 91 (<http://dx.doi.org/10.1002/wcms.1162>)
34. C. Steffen, K. Thomas, U. Huniar, A. Hellweg, O. Rubner, A. Schroer, *J. Comput. Chem.* **31** (2010) 2967 (<http://dx.doi.org/10.1002/jcc.21576>)
35. E. R. Johnson, S. Keinan, P. Mori-Sanchez, J. Contreras-Garcia, A. J. Cohen, W. Yang, *J. Am. Chem. Soc.* **132** (2010) 6498 (<http://dx.doi.org/10.1021/ja100936w>).

SUPPLEMENTARY MATERIAL TO  
**Curcumin as a potential multiple-target inhibitor against  
SARS-CoV-2 infection: A detailed interaction study using  
quantum chemical calculations**

SUMIT KUMAR\*

*Department of Chemistry, Magadh University, Bodh Gaya-824234, Bihar, India*

*J. Serb. Chem. Soc.* 88 (4) (2023) 381–394

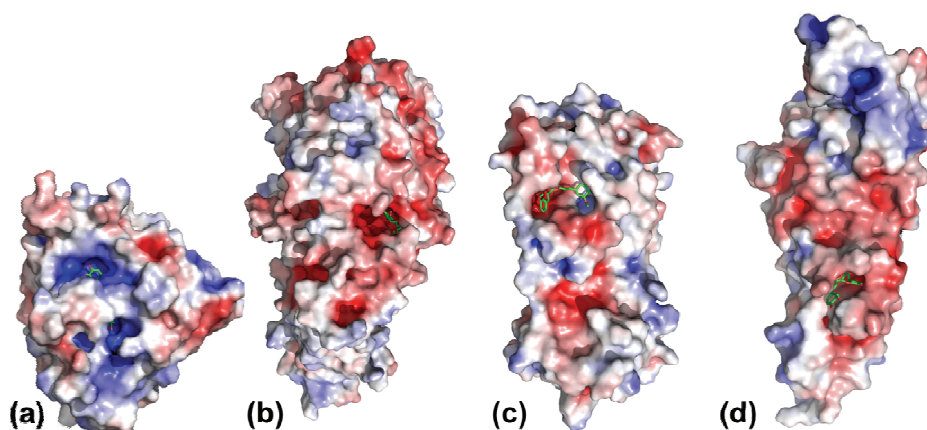


Figure S-1. Adaptive Poisson-Boltzmann Solver (ABPS) plots of the lowest binding energy docking site for the electrostatic interaction of curcumin with (a) TMPRSS2, (b) ACE2, (c) 3CLpro and (d) PLpro.

\* E-mail: [sumitkrmgr@gmail.com](mailto:sumitkrmgr@gmail.com)

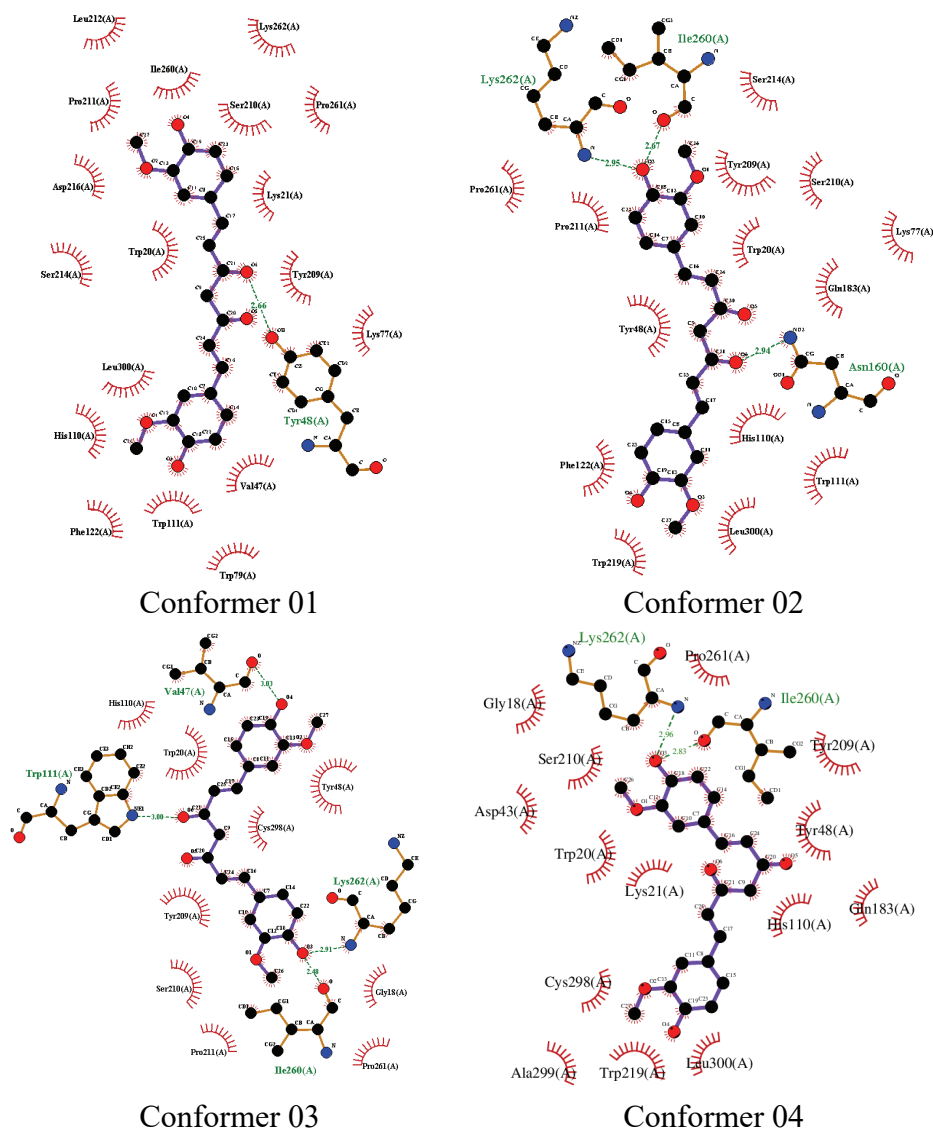


Figure S-2. The four most preferred docking poses of curcumin in the transmembrane serine protease 2 (TMRSS2) PDB ID: 1Z8A.



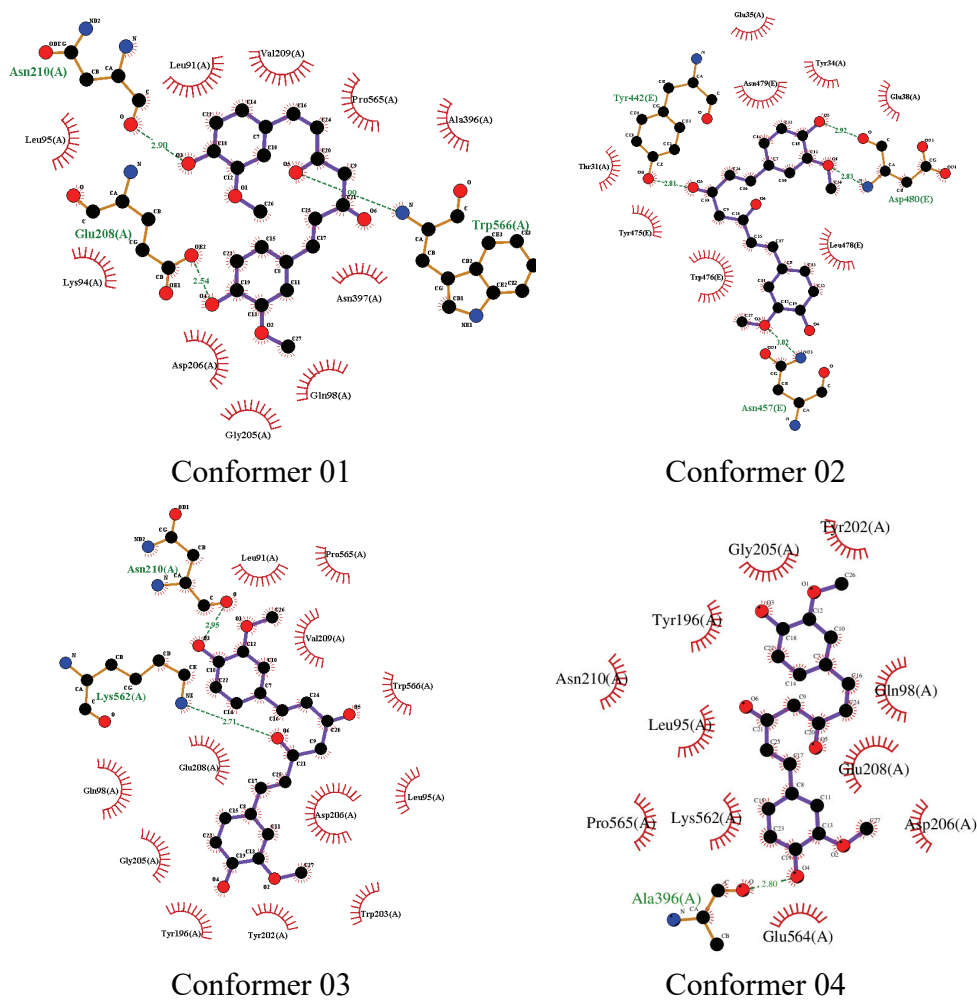


Figure S-3. The four most preferred docking poses of curcumin in the angiotensin-converting enzyme 2 (ACE2) PDB ID: 3D0G.

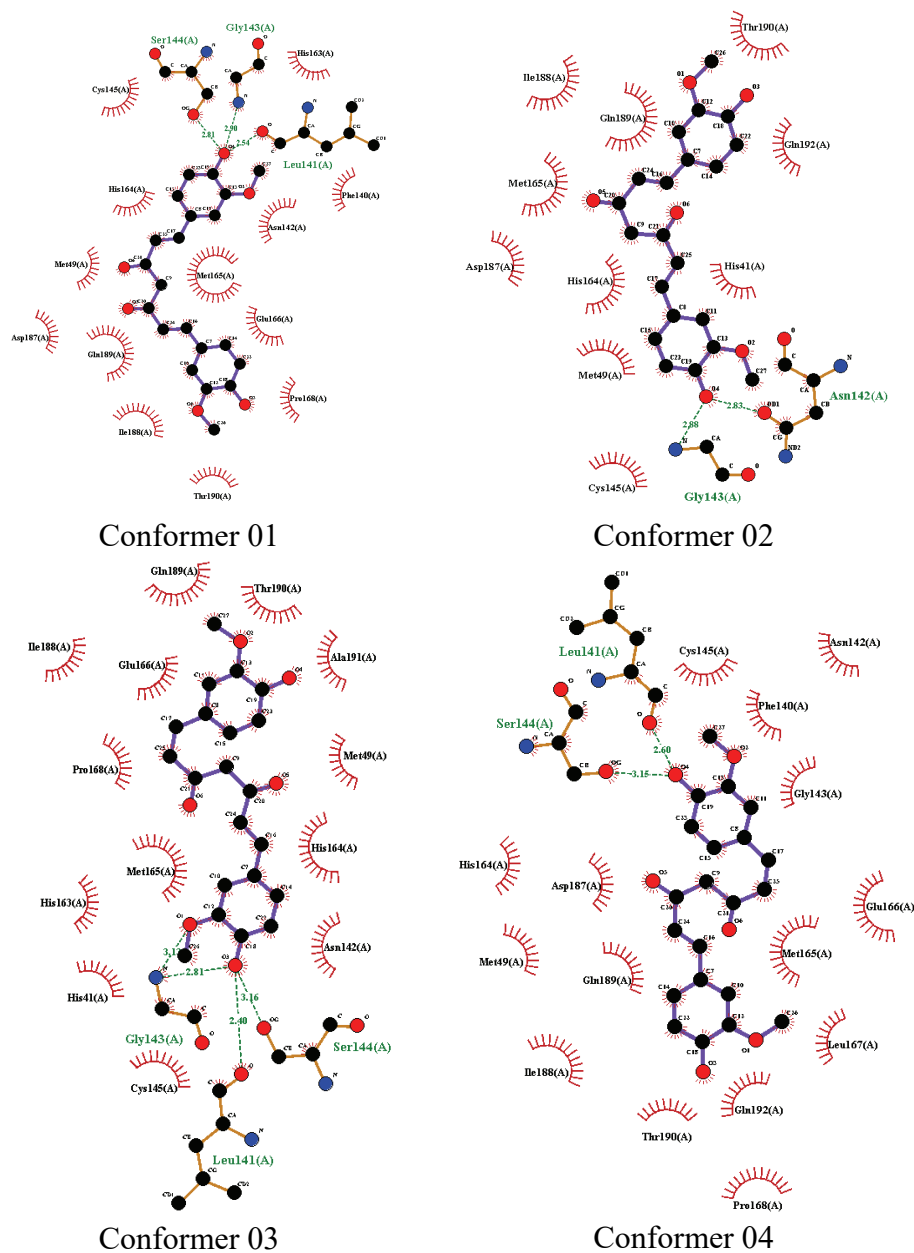


Figure S-4. The four most preferred docking poses of curcumin in the 3-chymotrypsin-like protease (3CLpro) PDB ID: 3AW0.

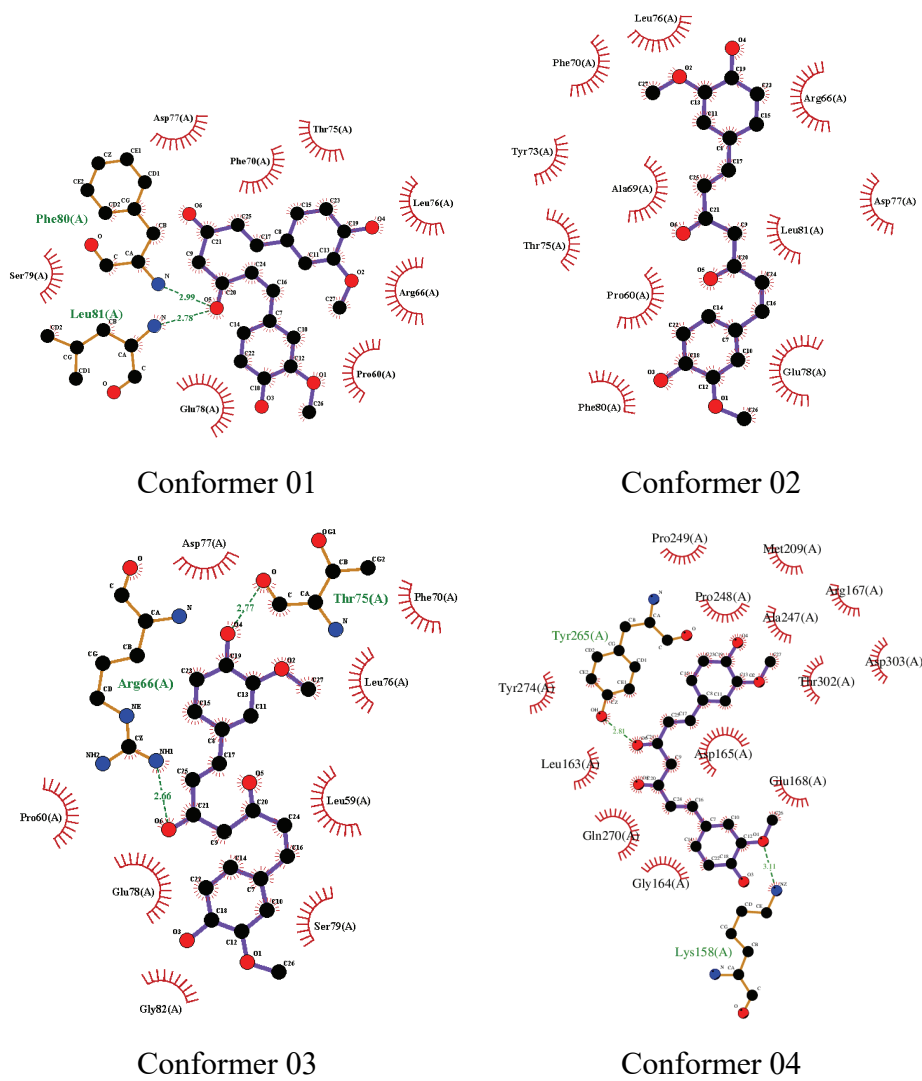


Figure S-5. The four most preferred docking poses of curcumin in the papain-like protease (PLpro) PDB ID: 3E9S.

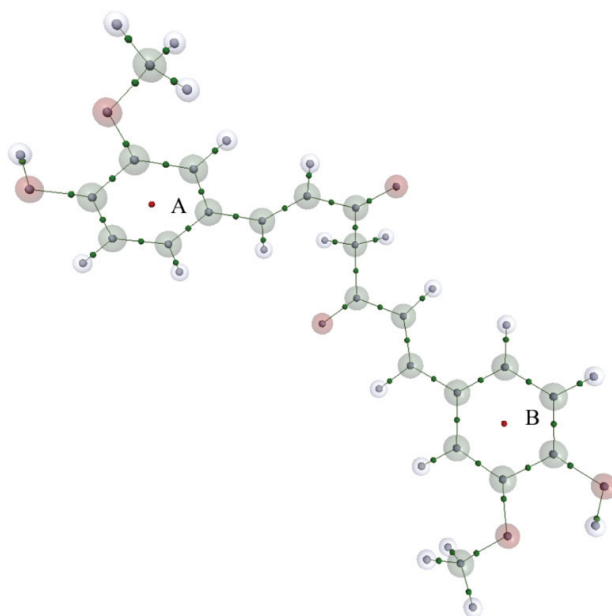


Figure S-6. Bond critical points (BCP) and ring critical points (RCPs) for curcumin in the gas phase obtained from AIM analysis at B3LYP/def2-TZVP level of theory.

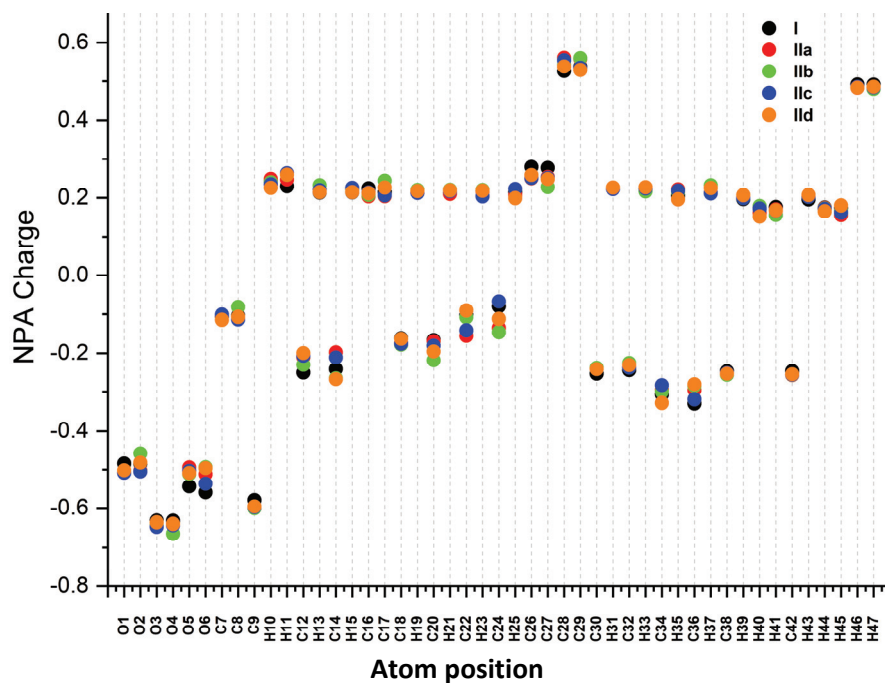


Figure S-7. Natural population analysis (NPA) charges of curcumin in the gas phase and that lifted from the active site of TMPRSS2 (IIb), ACE2 (IIb), 3CLpro (IIc) and PLpro (IIId).

Table S-I. Estimated free energy of binding along with its subsidiary components and estimated inhibition constants for the four most preferred docking sites of curcumin in the transmembrane serine protease 2 (TMPRSS2) PDB ID: 1Z8A.

Receptor	Conformer 01	Conformer 02	Conformer 03	Conformer 04
Binding energy, kJ/mol	-42.34	-42.09	-41.97	-41.92
Inhibition constant, nM	38.37	42.32	44.57	45.47
Total intermolecular energy, kJ/mol	-54.43	-54.56	-54.43	-54.39
Total internal energy, kJ/mol	-8.74	-6.40	-5.52	-6.32
Torsional free energy, kJ/mol	12.47	12.47	12.47	12.47
Unbound system's energy, kJ/mol	-8.74	-6.40	-5.52	-6.32
Cluster RMSD, Å	0.00	1.29	0.00	0.79
Reference RMSD, Å	24.81	23.14	23.80	23.34

Table S-II. Estimated free energy of binding along with its subsidiary components and estimated inhibition constants for the four most preferred docking sites of curcumin in the angiotensin-converting enzyme 2 (ACE2) PDB ID: 3D0G.

Receptor	Conformer 01	Conformer 02	Conformer 03	Conformer 04
Binding energy, kJ/mol	-28.53	-27.24	-26.65	-25.65
Inhibition constant, $\mu$ M	10.00	16.87	21.43	32.23
Total intermolecular energy, kJ/mol	-41.00	-39.71	-39.12	-38.12
Total internal energy, kJ/mol	-10.08	-10.88	-8.37	-9.00
Torsional free energy, kJ/mol	12.47	12.47	12.47	12.47
Unbound system's energy, kJ/mol	-10.08	-10.88	-8.37	-9.00
Cluster RMSD, Å	0.00	0.00	0.00	0.00
Reference RMSD, Å	102.60	127.25	104.15	104.66

Table S-III. Estimated free energy of binding along with its subsidiary components and estimated inhibition constants for the four most preferred docking sites of curcumin in the 3-chymotrypsin-like protease (3CLpro) PDB ID: 3AW0

Receptor	Conformer 01	Conformer 02	Conformer 03	Conformer 04
Binding energy, kJ/mol	-33.85	-32.05	-30.12	-29.71
Inhibition constant, $\mu$ M	1.18	2.41	5.27	6.21
Total intermolecular energy, kJ/mol	-46.32	-44.56	-42.59	-42.22
Total internal energy, kJ/mol	-9.16	-9.50	-6.53	-9.62
Torsional free energy, kJ/mol	12.47	12.47	12.47	12.47
Unbound system's energy, kJ/mol	-9.16	-9.50	-6.53	-9.62
Cluster RMSD, Å	0.00	1.73	1.65	1.95
Reference RMSD, Å	42.05	42.92	42.20	41.44

Table S-IV. Estimated free energy of binding along with its subsidiary components and estimated inhibition constants for the four most preferred docking sites of curcumin in the papain-like protease (PLpro) PDB ID: 3E9S.

Receptor	Conformer 01	Conformer 02	Conformer 03	Conformer 04
Binding energy, kJ/mol	-31.33	-30.33	-29.71	-27.36
Inhibition constant, $\mu\text{M}$	3.22	4.84	6.26	16.02
Total intermolecular energy, kJ/mol	-43.81	-42.84	-42.17	-39.87
Total internal energy, kJ/mol	-10.92	-10.71	-9.41	-8.62
Torsional free energy, kJ/mol	12.47	12.47	12.47	12.47
Unbound system's energy, kJ/mol	-10.92	-10.71	-9.41	-8.62
Cluster RMSD, $\text{\AA}$	0.00	0.00	0.00	0.00
Reference RMSD, $\text{\AA}$	31.12	30.86	29.67	43.00

Table S-V. List of interactions present in the lowest binding energy active site of curcumin with TMPRSS2 (PDB ID: 1Z8A), ACE2 (PDB ID: 3D0G), 3CLpro (PDB ID: 3AW0) and PLpro (PDB ID: 3E9S). These interactions are obtained from PLIP analysis

Receptor	Residues number	Residue	Curcumin	Distance, $\text{\AA}$	Angle, $^\circ$	Types
TMPRSS2P	21A	LYS	O2	4.01	133	H-bond
	48A	TYR	O5	3.15	109	H-bond
	111A	TRP	O1	3.72	112	H-bond
	212A	LEU	O4	3.86	126	H-bond
	20A	TRP	-	5.49	-	$\pi$ -stack
ACE2	94A	LYS	O3	3.92	143	H-bond
	98A	GLN	O1	3.84	135	H-bond
	196A	TYR	O2	3.79	120	H-bond
	208A	GLU	O4	2.54	126	H-bond
	566A	TRP	O5	2.99	162	H-bond
PLpro	143A	GLY	O4	2.9	122	H-bond
	144A	SER	O4	2.58	122	H-bond
	144A	SER	O4	2.81	146	H-bond
	189A	GLN	O6	2.56	162	H-bond
3CLpro	66A	ARG	O1	3.43	116	H-bond
	80A	PHE	O5	2.99	115	H-bond
	81A	LEU	O5	2.78	168	H-bond

Table S-VI. Coordinate of the curcumin in the gas phase optimized at def2-TZVP level of theory

O	14.5117	-6.7691	16.0957
O	20.4987	-6.8693	28.2342
O	15.7944	-8.9503	15.3302
O	19.3112	-4.6659	29.1076
O	18.3812	-2.2935	20.5274
O	21.0747	-5.7176	20.9155
C	17.8078	-6.1900	17.7049
C	20.1320	-4.9955	25.0412
C	20.3892	-3.5407	20.1988
H	20.8293	-2.6088	20.5558
H	20.8837	-3.8494	19.2796
C	16.4706	-5.9625	17.3217
H	15.9673	-5.0634	17.6452
C	20.4781	-6.0331	25.9287
H	20.9616	-6.9160	25.5335
C	15.8034	-6.8770	16.5336
C	20.2089	-5.9300	27.2810
C	18.4350	-7.3600	17.2656
H	19.4610	-7.5502	17.5553
C	19.5054	-3.8566	25.5628
H	19.2215	-3.0457	24.9060
C	18.5578	-5.2635	18.5379
H	19.5838	-5.5629	18.7249
C	20.4412	-5.1645	23.6322
H	20.8962	-6.1125	23.3567
C	16.4525	-8.0535	16.1029
C	19.5803	-4.7777	27.7844
C	18.9021	-3.2475	19.9717
C	20.6134	-4.6378	21.2432
C	17.7663	-8.2846	16.4738
H	18.2508	-9.1912	16.1360
C	19.2332	-3.7501	26.9168
H	18.7475	-2.8728	27.3237
C	18.1124	-4.1254	19.1037
H	17.0884	-3.7908	18.9807
C	20.2382	-4.2962	22.6251
H	19.7949	-3.3212	22.7849
C	13.7576	-5.6251	16.4727
H	12.7751	-5.7499	16.0238
H	14.2176	-4.7084	16.0937
H	13.6566	-5.5615	17.5596
C	21.1405	-8.0712	27.8315
H	21.2731	-8.6603	28.7359
H	22.1172	-7.8654	27.3846
H	20.5237	-8.6284	27.1210

H	14.8986	-8.6158	15.1794
H	19.6223	-5.4710	29.5460

Table S-VII. Coordinate of the curcumin lifted from the active site of transmembrane serine protease 2 (TMPRSS2) PDB ID: 1Z8A

O	17.5840	-6.0610	14.7080
O	23.1110	-6.7400	26.5750
O	15.7480	-8.1100	14.3190
O	23.0290	-4.5390	28.2700
O	15.2930	-2.7810	21.1560
O	16.3560	-5.2890	23.0120
C	15.9100	-6.1260	17.9410
C	20.1520	-5.0140	25.3410
C	17.4680	-3.7490	21.5280
H	18.0140	-2.7930	21.7060
H	18.2130	-4.2860	20.8960
C	16.7810	-5.7550	16.9280
H	17.5070	-4.9400	17.0880
C	21.1520	-5.9640	25.4640
H	21.1790	-6.8350	24.7880
C	16.7290	-6.4230	15.7050
C	22.1250	-5.8080	26.4520
C	14.9890	-7.1450	17.7620
H	14.3030	-7.4260	18.5790
C	20.0970	-3.9110	26.1790
H	19.2930	-3.1650	26.0660
C	15.9640	-5.4210	19.2340
H	15.8380	-6.0210	20.1510
C	19.1240	-5.1780	24.2990
H	19.0380	-6.1660	23.8160
C	15.8070	-7.4510	15.5100
C	22.0840	-4.7040	27.3030
C	16.2050	-3.4860	20.7330
C	17.2700	-4.4870	22.8380
C	14.9370	-7.8130	16.5380
H	14.2080	-8.6270	16.3840
C	21.0700	-3.7550	27.1670
H	21.0380	-2.8820	27.8400
C	16.1550	-4.1020	19.3730
H	16.2760	-3.4680	18.4790
C	18.2860	-4.2130	23.8960
H	18.3480	-3.2090	24.3490
C	18.8180	-6.7710	14.6200
H	19.5180	-6.4750	13.8040
H	18.6130	-7.8650	14.5540
H	19.3470	-6.7180	15.6000
C	22.9350	-7.7430	27.5740
H	23.7420	-8.5060	27.6750
H	21.9570	-8.2550	27.4180



S102

KUMAR

H	22.7580	-7.2570	28.5620
H	16.3880	-7.7030	13.7110
H	23.6110	-5.3180	28.2800

Table S-VIII. Coordinate of the curcumin lifted from the active site of angiotensin-converting enzyme 2 (ACE2) PDB ID: 3D0G.

O	42.8250	-16.3020	95.6150
O	50.0770	-15.7900	95.8640
O	40.8640	-16.5800	93.6670
O	48.2690	-17.2730	94.3620
O	44.9740	-9.1740	93.7350
O	47.6670	-8.9640	96.8100
C	43.1640	-13.1510	93.8230
C	47.2450	-13.5070	95.7220
C	45.4010	-9.3750	96.0980
H	44.8310	-9.8140	96.9500
H	45.2330	-8.2890	96.2880
C	43.3860	-14.1540	94.7530
H	44.1660	-14.0370	95.5240
C	48.4970	-14.0160	96.0240
H	49.2100	-13.4230	96.6200
C	42.6110	-15.3130	94.7030
C	48.8470	-15.2860	95.5670
C	42.1910	-13.2740	92.8450
H	42.0300	-12.4650	92.1130
C	46.3320	-14.2340	94.9740
H	45.3390	-13.8120	94.7430
C	43.9830	-11.9260	93.8750
H	44.7220	-11.7690	93.0710
C	46.8750	-12.1650	96.2040
H	46.1990	-12.1010	97.0740
C	41.6270	-15.4530	93.7240
C	47.9400	-16.0300	94.8130
C	44.7630	-9.7780	94.7830
C	46.8750	-9.7050	96.2330
C	41.4160	-14.4340	92.7960
H	40.6370	-14.5440	92.0230
C	46.6820	-15.5040	94.5160
H	45.9650	-16.0920	93.9190
C	43.8930	-10.9900	94.8300
H	43.1720	-11.1160	95.6550
C	47.3010	-11.0160	95.6610
H	47.9710	-11.0400	94.7850
C	43.7440	-17.3310	95.2530
H	43.9190	-18.1410	95.9990
H	44.7190	-16.8740	94.9650
H	43.4330	-17.7820	94.2820
C	50.8690	-15.0590	96.7990
H	51.8760	-15.4720	97.0420

H	50.2910	-14.9110	97.7410
H	50.9730	-14.0040	96.4530
H	41.1590	-17.1860	94.3670
H	49.0740	-17.2110	93.8210

Table S-IX. Coordinate of the curcumin lifted from the active site of 3-chymotrypsin-like protease (3CLpro) PDB ID: 3AW0

O	-28.1110	-35.0320	5.3490
O	-18.9650	-41.3030	2.1840
O	-26.3900	-32.8820	5.7220
O	-19.2640	-43.4760	0.4770
O	-24.5710	-40.5870	8.9140
O	-25.7900	-40.3060	4.7770
C	-25.2220	-36.6910	6.8200
C	-22.5060	-42.0400	2.5990
C	-25.2360	-41.5120	6.7900
H	-24.5480	-42.3530	7.0400
H	-26.2200	-42.0250	6.8970
C	-26.4790	-36.5040	6.2660
H	-27.1580	-37.3610	6.1210
C	-21.2750	-41.4240	2.7510
H	-21.1630	-40.5620	3.4300
C	-26.8760	-35.2200	5.8940
C	-20.1780	-41.9050	2.0360
C	-24.3530	-35.6300	7.0120
H	-23.3570	-35.7990	7.4540
C	-22.6720	-43.1240	1.7520
H	-23.6600	-43.6020	1.6440
C	-24.8010	-38.0480	7.2130
H	-23.7220	-38.2310	7.3500
C	-23.6650	-41.5320	3.3540
H	-24.4750	-41.0460	2.7840
C	-26.0120	-34.1410	6.0810
C	-20.3280	-42.9950	1.1790
C	-25.1080	-40.4100	7.8240
C	-25.0280	-41.0800	5.3520
C	-24.7510	-34.3450	6.6400
H	-24.0680	-33.4910	6.7880
C	-21.5750	-43.6040	1.0370
H	-21.6930	-44.4660	0.3590
C	-25.6380	-39.0750	7.4160
H	-26.7240	-38.9330	7.2810
C	-23.8060	-41.6180	4.6840
H	-23.0140	-42.0900	5.2890
C	-28.3040	-35.4820	4.0100
H	-29.3140	-35.3280	3.5640
H	-28.0250	-36.5590	3.9360
H	-27.5320	-35.0230	3.3490
C	-18.6590	-40.2320	1.2930

S104

KUMAR

H	-17.6660	-39.7390	1.4140
H	-19.4640	-39.4630	1.3460
H	-18.7750	-40.5800	0.2400
H	-27.3610	-32.8560	5.6720
H	-18.4710	-42.9660	0.7150

Table S-X. Coordinate of the curcumin lifted from the active site of papain-like protease (PLpro) PDB ID: 3E9S

O	-1.0210	30.1960	14.9090
O	-4.1630	32.2480	14.0690
O	1.2650	29.3220	16.2260
O	-4.0660	32.8400	11.3550
O	-5.8730	24.7800	16.2730
O	-8.5190	25.6350	13.7490
C	-2.0800	26.9030	16.0450
C	-5.2980	29.1040	12.6250
C	-6.1760	25.0910	13.9020
H	-5.4210	25.1480	13.0830
H	-6.4780	24.0210	13.8170
C	-2.1170	28.1500	15.4420
H	-3.0280	28.4910	14.9210
C	-4.9360	30.0520	13.5680
H	-4.9750	29.8110	14.6440
C	-0.9890	28.9690	15.5010
C	-4.5210	31.3150	13.1440
C	-0.9490	26.4530	16.7040
H	-0.9390	25.4570	17.1780
C	-5.2550	29.3840	11.2680
H	-5.5460	28.6160	10.5310
C	-3.2710	26.0360	15.9830
H	-3.2750	25.1250	16.6050
C	-5.7370	27.7720	13.0720
H	-4.9620	27.0620	13.4050
C	0.1580	28.5300	16.1610
C	-4.4720	31.6110	11.7820
C	-5.5100	25.3390	15.2420
C	-7.3550	25.9900	13.5860
C	0.1790	27.2730	16.7630
H	1.0860	26.9270	17.2860
C	-4.8400	30.6470	10.8440
H	-4.8030	30.8830	9.7670
C	-4.3490	26.2770	15.2240
H	-4.3780	27.1740	14.5820
C	-7.0130	27.3610	13.1030
H	-7.8150	28.0400	12.7690
C	-1.4140	31.2990	15.7230
H	-1.4400	32.3030	15.2390
H	-0.7670	31.3410	16.6300
H	-2.4050	31.0840	16.1860

C	-4.4920	31.9720	15.4300
H	-4.1990	32.7360	16.1870
H	-4.0720	30.9810	15.7200
H	-5.5850	31.7660	15.5140
H	1.0130	30.2220	15.9550
H	-3.8470	33.3870	12.1280

Table S-XI. Geometrical parameters of curcumin in the gas phase and the same lifted from the active sites of TMPRSS2 (IIa), ACE2 (IIb), 3CLpro (IIc) and PLpro (IId).

Group	I	IIa	IIb	IIc	IId
Aromatic ring 1					
	Bond distance, Å				
C7-C18	1.39830	1.3852	1.3850	1.3848	1.3842
C18-C30	1.38888	1.3954	1.3959	1.3957	1.3958
C30-C26	1.38457	1.3945	1.3943	1.3944	1.3939
C26-C16	1.41102	1.3946	1.3951	1.3949	1.3942
C16-C12	1.37934	1.3945	1.3951	1.3945	1.3952
C12-C7	1.40950	1.3865	1.3857	1.3863	1.3856
Aromatic ring 2					
	Bond distance, Å				
C8-C20	1.40064	1.3863	1.3862	1.3856	1.3863
C20-C32	1.38519	1.3954	1.3947	1.3946	1.3954
C32-C27	1.38895	1.3955	1.3955	1.395	1.3945
C27-C17	1.40583	1.3945	1.3945	1.3947	1.3947
C17-C14	1.38268	1.3954	1.3944	1.395	1.3954
C14-C8	1.40856	1.3848	1.3848	1.3849	1.3853
Aromatic ring 1					
	Bond angles, °				
C7-C18-C30	121.3	119.4	119.3	119.3	119.3
C18-C30-C26	119.9	119.9	120.0	120.0	120.0
C30-C26-C16	119.6	120.1	120.0	120.1	120.1
C26-C16-C12	120.3	120.0	120.0	120.0	120.0
C16-C12-C7	120.5	119.3	119.2	119.3	119.2
C12-C7-C18	118.4	121.3	121.5	121.4	121.4
Aromatic ring 2					
	Bond angles, °				
C8-C20-C32	121.0	119.3	119.3	119.2	119.3
C20-C32-C27	120.3	120.0	120.0	120.1	120.0
C32-C27-C17	119.6	120.0	120.0	120.0	120.1
C27-C17-C14	119.9	120.0	120.0	120.0	120.0
C17-C14-C8	120.9	119.3	119.4	119.3	119.4
C14-C8-C20	118.3	121.4	121.4	121.4	121.3
Chain					
	Dihedral angles, °				
C7-C22-C34-C28	178.0	-179.5	-179.5	-179.5	-179.5
C22-C34-C28-C9	5.2	73.8	-135.7	-111.7	-141.1
C34-C28-C9-C29	-80.3	-119.1	104.3	36.9	-93.1
C28-C9-C29-C36	-67.5	-152.4	-39.1	112.5	79.3
C9-C29-C36-C24	-177.3	-113.4	-66.7	166.2	-5.4
C29-C36-C24-C8	-179.9	-179.5	-179.5	-179.5	-179.5
Chain					
	Bond distance, Å				
C8-C24	1.45239	1.47290	1.47316	1.47356	1.47199
C24-C36	1.34514	1.34010	1.34035	1.34022	1.34092
C36-C29	1.47211	1.49221	1.49244	1.49297	1.49328
C29-C9	1.53123	1.51656	1.51651	1.51583	1.51595
C9-C28	1.53265	1.51538	1.51614	1.51656	1.51679
C28-C34	1.46552	1.49384	1.49267	1.49318	1.49268
C34-C22	1.34677	1.33999	1.34023	1.34034	1.34024
C22-C7	1.45423	1.47370	1.47448	1.47416	1.47445

C29-O6	1.21908	1.22836	1.22853	1.22896	1.22780
C28-O5	1.22076	1.22788	1.22786	1.22792	1.22769
C27-O4	1.35491	1.36211	1.36260	1.36245	1.36294
C17-O2	1.36925	1.36233	1.36260	1.36223	1.36172
C26-O3	1.35440	1.36244	1.36218	1.36266	1.36270
C16-O1	1.36817	1.36238	1.36223	1.36294	1.36272

Table S-XII. Detailed summary of Mulliken population analysis (MPA) and natural population analysis (NPA) charges of curcumin in gas phase (I) and curcumin lifted from the active site of (b) transmembrane serine protease 2 (TMPRSS2) PDB ID: 1Z8A (IIa), (c) angiotensin-converting enzyme 2 (ACE2) PDB ID: 3D0G (IIb), (d) 3-chymotrypsin-like protease (3CLpro) PDB ID: 3AW0 (IIc) and (e) papain-like protease (PLpro) PDB ID: 3E9S (IId). The calculation is performed at B3LYP/def2-TZVP level of theory.

Sequence Number	Atom Symbol	I		IIa		IIb		IIc		IId	
		MPA, e	NPA, e	MPA, e	NPA, e	MPA, e	NPA, e	MPA, e	NPA, e	MPA, e	NPA, e
1	O	-0.34563	-0.48409	-0.35051	-0.50581	-0.34798	-0.50634	-0.35644	-0.50833	-0.33756	-0.50172
2	O	-0.34552	-0.48398	-0.34018	-0.50261	-0.2836	-0.45772	-0.35045	-0.50514	-0.34102	-0.48199
3	O	-0.38681	-0.63191	-0.39929	-0.64285	-0.39646	-0.64221	-0.40884	-0.64768	-0.38819	-0.63608
4	O	-0.38775	-0.63212	-0.38995	-0.64007	-0.42946	-0.66471	-0.39773	-0.6432	-0.39995	-0.64037
5	O	-0.31345	-0.54325	-0.28097	-0.49423	-0.29018	-0.51148	-0.27884	-0.50347	-0.28818	-0.50889
6	O	-0.33479	-0.559	-0.30249	-0.51179	-0.27549	-0.49379	-0.33061	-0.53663	-0.283	-0.49625
7	C	0.13326	-0.1051	0.24018	-0.10286	0.22315	-0.11405	0.23682	-0.10156	0.24939	-0.11455
8	C	0.23511	-0.10494	0.26268	-0.10899	0.06402	-0.08182	0.19978	-0.113	0.09404	-0.10695
9	C	-0.14137	-0.57914	-0.23387	-0.59987	-0.20352	-0.60048	-0.21577	-0.59736	-0.14111	-0.59554
10	H	0.1165	0.24062	0.13782	0.24843	0.12723	0.23957	0.12073	0.23431	0.13364	0.225
11	H	0.12212	0.22952	0.13569	0.24653	0.1383	0.25891	0.13711	0.26319	0.12805	0.25944
12	C	-0.33067	-0.24997	-0.28759	-0.20999	-0.28569	-0.23003	-0.25196	-0.20657	-0.19996	-0.19958
13	H	0.12873	0.21338	0.11896	0.21897	0.15095	0.23174	0.1225	0.21922	0.10724	0.21413
14	C	-0.3196	-0.24068	-0.30899	-0.19752	-0.29467	-0.26476	-0.28309	-0.21102	-0.33625	-0.26737
15	H	0.13047	0.21368	0.11406	0.21986	0.11399	0.22101	0.12789	0.22514	0.1555	0.21427
16	C	0.34123	0.22379	0.26257	0.20379	0.22971	0.20741	0.24608	0.21316	0.20376	0.21147
17	C	0.32459	0.21373	0.26533	0.2041	0.29276	0.24351	0.27688	0.20609	0.35394	0.22617
18	C	-0.17153	-0.16122	-0.19352	-0.17354	-0.19417	-0.17784	-0.20341	-0.17568	-0.17304	-0.16262
19	H	0.11884	0.21364	0.11744	0.21723	0.11913	0.21952	0.10688	0.2125	0.11549	0.21723
20	C	-0.18438	-0.16599	-0.14899	-0.16894	-0.15615	-0.21804	-0.16854	-0.18008	-0.1893	-0.19542
21	H	0.11428	0.21231	0.10164	0.20996	0.24189	0.22004	0.11612	0.21656	0.11467	0.21891
22	C	-0.06459	-0.1032	-0.18668	-0.15483	-0.16767	-0.10785	-0.17416	-0.14112	-0.20351	-0.0909
23	H	0.13719	0.21665	0.13677	0.21552	0.13531	0.2197	0.10102	0.20383	0.12365	0.21794
24	C	-0.11913	-0.07977	-0.16874	-0.13451	-0.22839	-0.14582	-0.12144	-0.06783	-0.08674	-0.11201
25	H	0.11747	0.21388	0.11177	0.20656	0.12025	0.19909	0.14488	0.22229	0.12859	0.19898
26	C	0.18269	0.27931	0.1669	0.24971	0.15455	0.25076	0.16694	0.25042	0.17703	0.25822
27	C	0.17419	0.27689	0.16268	0.25325	0.21694	0.22745	0.15689	0.2507	0.16409	0.24794
28	C	0.15692	0.52655	0.25821	0.56067	0.273	0.5418	0.14805	0.55414	0.19004	0.53778
29	C	0.20286	0.53703	0.20127	0.55782	0.18926	0.55985	0.30592	0.53452	0.19593	0.52913
30	C	-0.20365	-0.25309	-0.20859	-0.23992	-0.19409	-0.23775	-0.19799	-0.24143	-0.21829	-0.24124
31	H	0.11323	0.22326	0.11442	0.22325	0.11736	0.22427	0.11248	0.222	0.11899	0.22579
32	C	-0.18847	-0.24377	-0.22177	-0.23601	-0.25726	-0.22518	-0.19986	-0.23754	-0.19101	-0.23078
33	H	0.11533	0.22317	0.11721	0.22387	0.11222	0.21626	0.11599	0.22396	0.11858	0.22702
34	C	-0.14545	-0.30723	-0.14817	-0.29466	-0.17835	-0.3	-0.03469	-0.28283	-0.14413	-0.32849
35	H	0.08325	0.20485	0.12793	0.22155	0.1276	0.21434	0.1064	0.2181	0.09229	0.19591
36	C	-0.23364	-0.32978	-0.10318	-0.29563	-0.11374	-0.2844	-0.23287	-0.31913	-0.17246	-0.28048
37	H	0.13062	0.21134	0.11573	0.2124	0.13883	0.23168	0.12708	0.21135	0.12622	0.22473
38	C	-0.20067	-0.24674	-0.18784	-0.25576	-0.15926	-0.25625	-0.1702	-0.25155	-0.16392	-0.25306
39	H	0.13627	0.19673	0.13876	0.20143	0.13864	0.20353	0.13291	0.19903	0.1404	0.20649
40	H	0.12737	0.17574	0.11664	0.16248	0.07241	0.17893	0.12261	0.17241	0.11142	0.15256

41	H	0.12904	0.17617	0.11514	0.17056	0.11663	0.1567	0.11249	0.16767	0.08497	0.16837
42	C	-0.20035	-0.24622	-0.19482	-0.25703	-0.19847	-0.25598	-0.19225	-0.25542	-0.23597	-0.25451
43	H	0.13558	0.19621	0.14146	0.20359	0.14336	0.20698	0.14039	0.20256	0.15155	0.20683
44	H	0.12839	0.17516	0.12184	0.17401	0.12611	0.17248	0.12153	0.17156	0.12053	0.16569
45	H	0.12841	0.1752	0.10756	0.15653	0.12195	0.16789	0.1168	0.16266	0.14804	0.18028
46	H	0.3268	0.49129	0.32349	0.48239	0.3237	0.48365	0.32285	0.4853	0.32344	0.48294
47	H	0.32671	0.49106	0.32198	0.48298	0.32533	0.47945	0.32314	0.4839	0.32212	0.48556

Table S-XIII. Detailed summary of electron density,  $\rho_{\text{bcp}}(r)$  and Laplacian of electron density,  $\nabla^2\rho_{\text{bcp}}(r)$  of curcumin in gas phase (I) and curcumin lifted from the active site of (b) transmembrane serine protease 2 (TMPRSS2) PDB ID: 1Z8A (IIa), (c) angiotensin-converting enzyme 2 (ACE2) PDB ID: 3D0G (IIb), (d) 3-chymotrypsin-like protease (3CLpro) PDB ID: 3AW0 (IIc) and (e) papain-like protease (PLpro) PDB ID: 3E9S (IId). The calculation is performed at B3-LYP/def2-TZVP level of theory

Curcumin Bond	I		IIa		IIb		IIc		IId	
	$\rho_{\text{bcp}}(r)$ , a.u.	$\nabla^2\rho_{\text{bcp}}(r)$ , a.u.	$\rho_{\text{bcp}}(r)$ , a.u.	$\nabla^2\rho_{\text{bcp}}(r)$ , a.u.	$\rho_{\text{bcp}}(r)$ , a.u.	$\nabla^2\rho_{\text{bcp}}(r)$ , a.u.	$\rho_{\text{bcp}}(r)$ , a.u.	$\nabla^2\rho_{\text{bcp}}(r)$ , a.u.	$\rho_{\text{bcp}}(r)$ , a.u.	$\nabla^2\rho_{\text{bcp}}(r)$ , a.u.
O1-C38	0.2511	-0.5045	0.2519	-0.5639	0.2509	-0.5516	0.2509	-0.5504	0.2519	-0.5608
O2-C17	0.2872	-0.5830	0.2914	-0.5827	0.2915	-0.5761	0.2915	-0.5833	0.2897	-0.5296
O2-C42	0.2515	-0.5078	0.2521	-0.5655	0.2510	-0.5435	0.2515	-0.5601	0.2497	-0.5301
O3-C26	0.3003	-0.6409	0.2947	-0.6446	0.2952	-0.6502	0.2950	-0.6562	0.2952	-0.6576
O3-H46	0.3555	-2.4420	0.3523	-2.3750	0.3525	-2.3810	0.3510	-2.3690	0.3514	-2.3630
O4-H47	0.3555	-2.4410	0.3520	-2.3710	0.3507	-2.3370	0.3516	-2.3720	0.3521	-2.3810
O6-C29	0.4150	-0.2481	0.4075	-0.3306	0.4076	-0.3334	0.4068	-0.3333	0.4087	-0.3393
C7-C12	0.3076	-0.8863	0.3220	-0.9593	0.3211	-0.9469	0.3227	-0.9647	0.3235	-0.9724
C7-C18	0.3169	-0.9326	0.3243	-0.9754	0.3227	-0.9619	0.3248	-0.9793	0.3257	-0.9864
C7-C22	0.2854	-0.8065	0.2755	-0.7637	0.2761	-0.7736	0.2749	-0.7571	0.2750	-0.7554
C8-C14	0.3090	-0.8925	0.3241	-0.9733	0.3223	-0.9571	0.3220	-0.9558	0.3212	-0.9497
C8-C20	0.3147	-0.9232	0.3239	-0.9745	0.3217	-0.9530	0.3226	-0.9628	0.3214	-0.9514
C8-C24	0.2865	-0.8135	0.2756	-0.7598	0.2769	-0.7812	0.2771	-0.7794	0.2775	-0.7815
C9-C28	0.2481	-0.6202	0.2597	-0.6867	0.2589	-0.6802	0.2556	-0.6600	0.2560	-0.6624
C9-C29	0.2497	-0.6283	0.2568	-0.6674	0.2562	-0.6641	0.2591	-0.6804	0.2559	-0.6619
C9-H10	0.2804	-0.9676	0.2637	-0.8617	0.2631	-0.8554	0.2676	-0.8849	0.2659	-0.8670
C9-H11	0.2829	-0.9839	0.2648	-0.8686	0.2658	-0.8792	0.2613	-0.8491	0.2669	-0.8860
C12-H13	0.2882	-1.0260	0.2743	-0.9451	0.2787	-0.9638	0.2750	-0.9485	0.2749	-0.9459
C14-C17	0.3249	-0.9672	0.3201	-0.9461	0.3204	-0.9498	0.3203	-0.9482	0.3189	-0.9362
C14-H15	0.2872	-1.0210	0.2744	-0.9471	0.2762	-0.9490	0.2748	-0.9497	0.2749	-0.9381
C16-C12	0.3266	-0.9719	0.3205	-0.9471	0.3198	-0.9438	0.3206	-0.9449	0.3198	-0.9400
C16-C26	0.3168	-0.9510	0.3246	-0.9791	0.3243	-0.9758	0.3246	-0.9816	0.3253	-0.9875
C16-O1	0.2879	-0.5817	0.2909	-0.5741	0.2918	-0.5893	0.2913	-0.5904	0.2917	-0.5967
C17-C27	0.3194	-0.9619	0.3247	-0.9787	0.3244	-0.9857	0.3246	-0.9779	0.3238	-0.9810
C18-C30	0.3201	-0.9487	0.3161	-0.9223	0.3155	-0.9191	0.3160	-0.9220	0.3161	-0.9233
C18-H19	0.2879	-1.0310	0.2754	-0.9532	0.2757	-0.9553	0.2752	-0.9509	0.2756	-0.9547
C20-C32	0.3220	-0.9551	0.3158	-0.9179	0.3158	-0.9224	0.3163	-0.9236	0.3159	-0.9242
C20-H21	0.2889	-1.0370	0.2761	-0.9544	0.2800	-0.9646	0.2755	-0.9533	0.2750	-0.9497

Curcumin Bond	I		IIa		IIb		IIc		IIId	
	$\rho_{\text{bcp}}(\text{f})$ , a.u.	$\nabla^2\rho_{\text{bcp}}(\text{f})$ , a.u.	$\rho_{\text{bcp}}(\text{f})$ , a.u.	$\nabla^2\rho_{\text{bcp}}(\text{f})$ , a.u.	$\rho_{\text{bcp}}(\text{f})$ , a.u.	$\nabla^2\rho_{\text{bcp}}(\text{f})$ , a.u.	$\rho_{\text{bcp}}(\text{f})$ , a.u.	$\nabla^2\rho_{\text{bcp}}(\text{f})$ , a.u.	$\rho_{\text{bcp}}(\text{f})$ , a.u.	$\nabla^2\rho_{\text{bcp}}(\text{f})$ , a.u.
C22-C34	0.3463	-1.0660	0.3472	-1.0420	0.3489	-1.0600	0.3474	-1.0470	0.3501	-1.0770
C22-H23	0.2899	-1.0460	0.2762	-0.9562	0.2764	-0.9596	0.2758	-0.9524	0.2776	-0.9694
C24-C25	0.2883	-1.0360	0.2762	-0.9565	0.2742	-0.9388	0.2772	-0.9677	0.2818	-0.9713
C24-C36	0.3473	-1.0710	0.3482	-1.0560	0.3467	-1.0350	0.3507	-1.0810	0.3498	-1.0700
C26-C30	0.3267	-0.9919	0.3203	-0.9586	0.3206	-0.9601	0.3205	-0.9583	0.3209	-0.9619
C27-C32	0.3242	-0.9815	0.3200	-0.9594	0.3196	-0.9440	0.3201	-0.9576	0.3197	-0.9510
C27-O4	0.3000	-0.6394	0.2948	-0.6432	0.2953	-0.6663	0.2948	-0.6489	0.2948	-0.6559
C28-O5	0.4143	-0.2675	0.4078	-0.3170	0.4078	-0.3187	0.4077	-0.3235	0.4082	-0.3262
C29-C36	0.2806	-0.7786	0.2721	-0.7501	0.2731	-0.7611	0.2706	-0.7328	0.2708	-0.7366
C30-H31	0.2870	-1.0260	0.2742	-0.9451	0.2746	-0.9477	0.2741	-0.9441	0.2749	-0.9502
C32-H33	0.2872	-1.0280	0.2748	-0.9495	0.2751	-0.9472	0.2745	-0.9475	0.2745	-0.9483
C34-C28	0.2841	-0.7991	0.2723	-0.7556	0.2722	-0.7478	0.2717	-0.7469	0.2703	-0.7293
C34-H35	0.2859	-1.0120	0.2720	-0.9279	0.2733	-0.9361	0.2722	-0.9279	0.2772	-0.9367
C36-H37	0.2871	-1.0200	0.2721	-0.9254	0.2729	-0.9386	0.2748	-0.9445	0.2756	-0.9575
C38-H39	0.2899	-1.0470	0.2714	-0.9331	0.2714	-0.9326	0.2715	-0.9334	0.2719	-0.9362
C38-H40	0.2853	-1.0100	0.2721	-0.9180	0.2745	-0.9301	0.2728	-0.9238	0.2714	-0.9115
C38-H41	0.2853	-1.0100	0.2724	-0.9217	0.2717	-0.9135	0.2722	-0.9195	0.2745	-0.9279
C42-H43	0.2898	-1.0460	0.2715	-0.9338	0.2715	-0.9343	0.2714	-0.9332	0.2718	-0.9352
C42-H44	0.2851	-1.0090	0.2726	-0.9228	0.2723	-0.9195	0.2727	-0.9231	0.2745	-0.9259
C42-H45	0.2852	-1.0090	0.2718	-0.9148	0.2729	-0.9206	0.2721	-0.9179	0.2725	-0.9213

Table S-XIV. HUMO-LUMO band gap and dipole moments of curcumin in the gas phase and that lifted from the active site of TMPRSS2 (IIa), ACE2 (IIb), 3CLpro (IIc) and PLpro (IIId)

Structure	I	IIa	IIb	IIc	IIId
HOMO-LUMO band gap, eV	3.699	4.367	4.392	3.714	4.058
$\mu_x, \text{D}$	-0.632	2.574	0.317	0.328	1.725
$\mu_y, \text{D}$	-1.058	-1.003	-1.547	-0.036	2.033
$\mu_z, \text{D}$	0.355	-0.044	0.412	-1.711	0.218
$\mu, \text{D}$	3.26	7.022	4.147	4.429	6.8

$\mu_x, \mu_y$  and  $\mu_z$  are the dipole moments in  $x, y,$  and  $z$ -directions whereas  $\mu$  represents the resultant dipole moment



*J. Serb. Chem. Soc.* 88 (4) 395–408 (2023)  
JSCS–5634

## Xylose dehydration to furfural using niobium doped $\delta$ -FeOOH as catalyst

PAULO TADASHI BANNAI CAMPOS<sup>1</sup>, MARIANA DE REZENDE BONESIO<sup>1</sup>,  
ANDRÉ LUIZ DIAS LIMA<sup>2</sup>, ADILSON CÂNDIDO DA SILVA<sup>2</sup>,  
DAIANA TEIXEIRA MANCINI<sup>1\*</sup> and TEODORICO CASTRO RAMALHO<sup>1\*\*</sup>

<sup>1</sup>Department of Chemistry, Federal University of Lavras 37200-900, Lavras – MG, Brazil and

<sup>2</sup>Department of Chemistry, Federal University of Ouro Preto, 35400-000,  
Ouro Preto – MG, Brazil

(Received 16 March, revised 22 November, accepted 9 December 2022)

**Abstract:** The effect of modification of  $\delta$ -FeOOH with niobium, applied to dehydration reaction of xylose, was evaluated by experimental and theoretical methods. The experimental data confirmed, namely the characteristic peaks in the X-ray diffractometer analysis, that the materials were obtained. Inductively coupled plasma mass spectrometry analysis defined the percentage of Nb as 0 for pure  $\delta$ -FeOOH and 9.5 wt. % ( $\delta$ -FeOOH/Nb) for doped. In relation to obtaining furfural, the doped material presents a conversion improvement of 290 % when compared to pure catalyst. Theoretical calculations were useful in understanding the preferential route of the mechanisms proposed by the obtained potential energy values. To understand the preferred routes, the most favorable position of xylose in relation to  $\delta$ -FeOOH was initially calculated. From this, the conditions favoring furfural formation were calculated based on the routes of the proposed mechanisms and the energy values indicated that the furfural formation is more likely to happen on the doped material.

**Keywords:** feroxyhyte; xylose; furfural; niobium.

### INTRODUCTION

The fossil raw materials dependency can be problematic in the long term, because of scarcity perspective.<sup>1</sup> In this context, the study of renewable raw materials may solve the scarcity issues, also decreases the environmental impacts as the emission of greenhouse gases and the contamination of effluents.<sup>2,3</sup>

Herewith, the vegetable residues generated from agriculture are considered as a renewable material; however, they are used as energy source, through combustion. Nowadays, new forms to increase the added values of these products are being studied using lignin, pentoses and hexoses in the material.<sup>4,5</sup> For example,

\* Corresponding authors. E-mail: (\*)daianateixeira60@yahoo.com.br; (\*\*)teo@ufla.br  
<https://doi.org/10.2298/JSC220316085B>



furfural is produced from pentoses processing, to be more specific, from xylose. This compound owns numerous applications, as a fungicide, an extracting agent of aromatic compounds for lubricating oils and as diesel.<sup>6</sup> Besides that, furfural would be the basis to produce important compounds as furfuryl alcohol, furan, furoic acid, levulinic acid and tetrahydrofuran.<sup>7</sup>

Currently, homogeneous catalysts are mostly used for the furfural production since these materials own corrosive and dangerous characteristics that damage the production reactors. Associate with this, there is a difficulty of reuse and need for extra steps to catalyst separation, making the process more expensive.<sup>8,9</sup>

Herewith, the study and research of heterogeneous catalysts to the reaction are encouraged. The iron oxides and oxyhydroxides are of great interest since they have natural abundance, chemical stability, corrosion resistance, own attractive physicochemical properties, are easy to obtain and low cost.<sup>10</sup>

Among the iron oxides and oxyhydroxides, feroxyhyte ( $\delta$ -FeOOH) stands out due to important catalyst characteristics as: ease of obtaining, high surface area, large amount of hydroxyl groups on its surface, and bifunctional catalytic activity. In fact, the superficial groups Fe–OH and its conjugated base Fe–O– act as Brønsted acid and base, respectively,<sup>11</sup> however, the  $\delta$ -FeOOH has low acid character. Thus, the catalyst modification with other metals may be an alternative to improve these properties.

The modifications of ferric catalyst with niobium are substantially present in the literature, evidencing the modification effectiveness and thus, the study of  $\delta$ -FeOOH modified with Nb becomes relevant.<sup>12–14</sup> The catalyst modification may increase the catalytic efficiency and material stability. Understanding behavior of these materials as a catalyst is crucial to keep the reaction yield to desirable levels.

The purpose of this work was to evaluate pure and Nb modified  $\delta$ -FeOOH, as a catalyst, applied to xylose dehydration reaction to furfural employing theoretical and experimental methods.

## EXPERIMENTAL

General procedure for synthesis of pure and doped material.  $\delta$ -FeOOH nanoparticles were obtained according to the modified procedure described in the literature.<sup>15,16</sup> The method consists mainly of precipitation of an alcoholic solution of Fe<sup>2+</sup> with NaOH followed by an oxidation with H<sub>2</sub>O<sub>2</sub>, leading directly to the product. The sample was set as Nb 0 wt. %. The Nb doped  $\delta$ -FeOOH nanoparticles were similarly obtained, however an alcoholic solution of NbCl<sub>5</sub> was added before the precipitation step with NaOH, so the final material would have 10 % in Nb mass. The sample was set as Nb 10 wt. %.

The present iron and niobium in the material were determined by the inductively coupled plasma mass spectrometry technique (ICP-MS) monitoring the <sup>57</sup>Fe and <sup>93</sup>Nb isotopes. An ELAN DRC II (Perkin Elmer Life and Analytical Sciences, USA) equipment was used. The spectrometry was conducted using platinum sampled and Skimmer cones, both from Perkin Elmer, and argon 99.999 % (White Martins, São Paulo, Brazil). The surface areas were deter-

mined by Brunauer, Emmett and Teller (BET) technique by  $N_2$  adsorption/desorption procedure of 22 points in a gas sorption analyzer AUTOSORB Quantachrome. Crystalline phases were got using a X-ray diffractometer (XRD), Rigaku Geigerflex model, equipped with a graphite diffracted beam monochromator. Silicon was used as external standard; the scan was made in the interval  $10$ – $80^\circ$  ( $2\theta$ ) with  $CuK\alpha$  radiation ( $\lambda = 0.154056$  nm).

The xylose dehydration reaction to furfural was investigated using a stainless-steel tubular reactor of 15 mL keeping the temperature controlled at  $140^\circ C$  in a glycerol bath thermostat (Marconi model MA159/30Glic). 10 mg of catalyst and 10 mL of xylose  $20\text{ g L}^{-1}$  solution were added to the reactor. After the pre-stipulated reaction intervals of 15, 30 and 60 min, the process was immediately interrupted by cooling the reactor in an ice bath. Then, the reaction medium was subjected to centrifugation (FANEM excels II model) by 15 min (250 rpm) and the catalyst was recovered by the supernatant collection.

The quantification of xylose and furfural in the liquid phase, after the reaction was carried out, was performed by HPLC (Agilent, model 1260 infinity II). The chromatography system was equipped with an Aminex HPX-87H column ( $300 \times 7.8\text{ mm}^2$ , Bio-Rad) maintained at  $55^\circ C$  by an oven with forced air circulation, a refractive index detector for detection of xylose, and an ultraviolet-visible (UV-Vis) detector set at 274 nm for detection of 2-furfuraldehyde. An aqueous sulfuric acid ( $5\text{ mmol L}^{-1}$ ) solution was used as the eluent at a constant flow rate of  $0.6\text{ mL min}^{-1}$ .

The conversion and formation of products from xylose were quantified, using an external calibration curve acquired by the injection of the pure product with known concentrations. Xylose conversion ( $X_c$ ) was calculated as:

$$X_c = 100 \frac{\text{Final xylose content, mol}}{\text{Initial xylose content, mol}} \quad (1)$$

In order to better understand the role of  $\delta$ -FeOOH pure and Nb doped applied to the xylose conversion, a theoretical study was made, evaluating the adsorption sites of xylose and the different mechanism reactions.

All calculations are made in Gaussian09 software.<sup>17</sup> The system total energy was calculated using the hybrid method of our own  $n$ -layered integrated molecular orbital and molecular mechanics (ONIOM).<sup>18,19</sup> The region treated as high level was calculated by the density functional theory (DFT) using 6-31G basis set for carbon, oxygen and hydrogen atoms<sup>20–23</sup> and for iron<sup>24</sup> and niobium atoms,<sup>25</sup> the LanL2DZ basis set was chosen. Generalized gradient approximation Perdew–Burke–Ernzerhof (GGA-PBE)<sup>26</sup> was chosen to describe the exchange and correlation term as a function of spin density. The region treated as low level was calculated by molecular mechanical using universal force field (UFF).

For our calculations, we have used a cluster model based on structure previously built and optimized by Lacerda *et al.*,<sup>27</sup> in which, the Nb 0 wt. % was done as described by Drits *et al.*,<sup>28</sup> using DFT under periodic boundary conditions, the functional for the exchange and correlation term was the GGA-PBE,<sup>26</sup> and the projector augmented-wave method, PAW<sup>29</sup>, was used with a cutting energy equal to 500 eV. The Nb 10 wt. % structure was made at the same conditions, but due to the similarity in the size of the Fe and Nb atoms, the doping was performed by substitute Fe atoms by Nb atoms of the upper layer of the surface, to produce the material with approximately 10 wt. % ( $\delta$ -FeOOH/Nb). The substitutions were made in order to leave the dopants equally distributed in surface.

The surface model for both catalysts was generated using a  $3 \times 3 \times 2$  super cell on the (001) plane, totalizing 288 atoms, in which 72 are iron atoms (6 atoms of Fe were replaced by Nb

atoms in Nb 10 wt. %). The size of surfaces cluster models is sufficient to see the interactions between xylose and  $\delta$ -FeOOH in QM/MM methods.<sup>30,31</sup>

The xylose has three reaction sites that possibly lead to furfural<sup>32</sup> (marked red in Fig. 1), and, considering these sites, three arbitrary positions for each reaction site were elaborated, totalizing nine different spatial positions. For the input files, VESTA software was used, as it is presented in the Supplementary material to this paper.

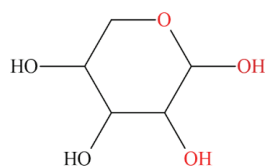


Fig. 1. Xylose reaction sites to furfural.

To evaluate the materials as catalysts, initially we made an adsorption study, combining the different xylose spatial positions and surfaces of Nb 0 and 10 wt. %. For this, the distances between xylose and surfaces ranged from 0.17 to 0.35 nm, with intervals of 0.01 nm, and then we evaluated the most stable combinations of xylose/surfaces. For thermodynamic study the positions and distances, with the minimum energy for each reaction site, were considered.

The xylose dehydration reaction to furfural was thermodynamically studied, optimizing the reaction intermediaries in the presence of Nb 0 and 10 wt. %. The reaction mechanisms used have been proposed in the previous experimental work.<sup>32</sup> The adsorbed/released energy of each step was obtained by applying the equation.

$$\Delta E_{(n)} = (E_{\text{ONIOM/intermediary}(n)} - mE_{\text{ONIOM/H}_2\text{O}}) - E_{\text{ONIOM/xylose}} \quad (2)$$

In which  $\Delta E_{(n)}$  is the relative energy to the intermediary formation,  $n$  is the identification of the associated intermediary,  $m$  is the number of free water molecules present in the system,  $E_{\text{ONIOM/H}_2\text{O}}$  is the energy of free water molecule and  $E_{\text{ONIOM/xylose}}$  is the xylose potential energy on the catalyst.

## RESULTS AND DISCUSSION

ICP–MS technique was used to quantify niobium as the catalyst. Thus, it was determined that the materials Nb 0 and 10 wt. % have 0.00 and 9.50 wt. % of Nb, respectively. On the other hand, the amount of iron present decreased from 63.4 in Nb 0 to 55.1 % in Nb 10 wt. %, respectively. The adsorption  $\text{N}_2$  isotherms for both catalysts are IV type, showing interparticle mesoporosity. The total pore volume of Nb 0 and 10 wt. % was 0.27 and 0.16  $\text{cm}^3 \text{g}^{-1}$ , respectively. The estimated specific surface area of Nb 0 and 10 wt. % were 99 and 73  $\text{m}^2 \text{g}^{-1}$ , respectively, according to the literature (20–300  $\text{m}^2 \text{g}^{-1}$ ).<sup>33</sup>

The X-ray patterns of synthesized compounds are presented in Fig. 2. In both diffractograms ferrosite were identified, based on its own characteristics reflection planes, according to the Joint Committee on Powder Diffraction Standards – JCPDS card 13-87. The planes are (100), (101), (102) and (110). In the interval from  $2\theta$  25 to 35°, some shoulders can be observed, and they are assigned to ultrafine iron oxides present in all  $\delta$ -FeOOH phases.<sup>34</sup> The amorphous contribution rises the Nb incorporation to the material, as seen on Nb 10 wt. % diffractogram.

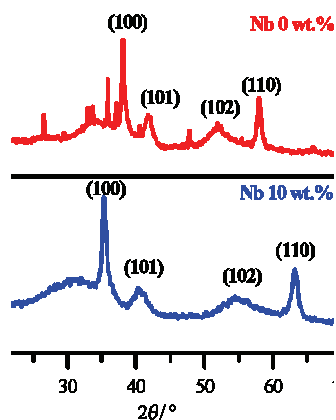


Fig. 2. XRD diffratograms for Nb 0 and 10 wt. %.

To the reflection plane (001), the ratio of relative area from amorphous/ reflection contribution of  $\delta$ -FeOOH was estimated at 0.93 and 1.81 for Nb 0 and 10 wt. %, respectively. This fact suggests that the increase from amorphous contribution might be related to a small amount of  $\text{Nb}^{5+}$  oxyhydroxides formed during the synthesis (JCPDS No 31-928). Both catalysts had particles formed in size 15 nm.

The pure and Nb doped ferroxhyte performances as catalysts were evaluated using the xylose dehydration reaction to furfural as most likely reaction. After one hour of reaction conversion results were obtained as presented in Fig. 3. For Nb 0 wt. % catalyst the conversion rate was about 2.0 %, while for Nb 10 wt. % the conversion was about 7.8 %. Although the conversion rates were relatively low, the catalyst Nb modification presents a conversion improvement of 290 % when compared to pure catalyst. Niobium and its oxides possess Brønsted and Lewis acidity so their higher acidity, when compared to iron oxides, favor heterogeneous catalytic reactions.<sup>13</sup> However, for a superior investigation of the studied material as a catalyst to this reaction, a theoretical approach may contribute to its comprehension.

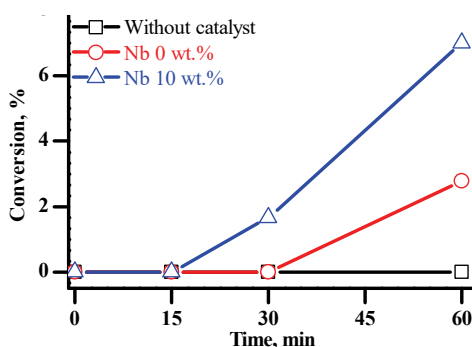


Fig. 3. Xylose conversion kinetic at 140 °C using water as solvent.

In order to understand the reaction mechanism, the ONIOM approach (DFT/UFF) was chosen. With this is possible to see the local structure and better evaluate the regions of interest at low computational demand. Similar structures have shown satisfactory results with this approach.<sup>12,35</sup>

Regarding the computational analysis, Nb 0 and 10 wt. % models were built for a more detailed investigation of xylose dehydration reaction to furfural. To inquire  $\delta$ -FeOOH catalytic properties the plane (001) was chosen, Fig. 4, corresponding to the one of the most stable catalyst geometry, according to Lacerda.<sup>27</sup>

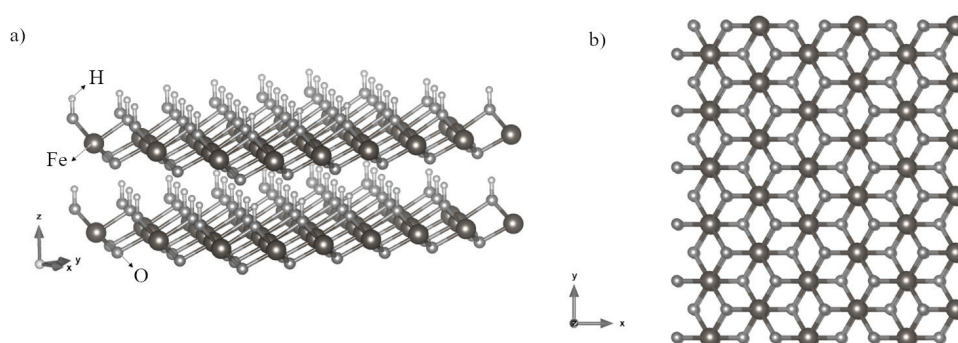


Fig. 4. Nb 0 wt. % system model. The Fe, O and H atoms are pointed out.

The Nb isomorphic substitution in ferrosyhyte crystal is due to the similarity in the size of the Fe and Nb atoms. Furthermore, Silva *et al.*,<sup>36</sup> evidenced that the presence of Nb stabilizes the iron oxides structure. There is also the remote possibility of niobium oxide formation on the catalyst surface,<sup>14</sup> but for computational studies only the atoms substitution was considered in super cell building, as shown in Fig. 5.

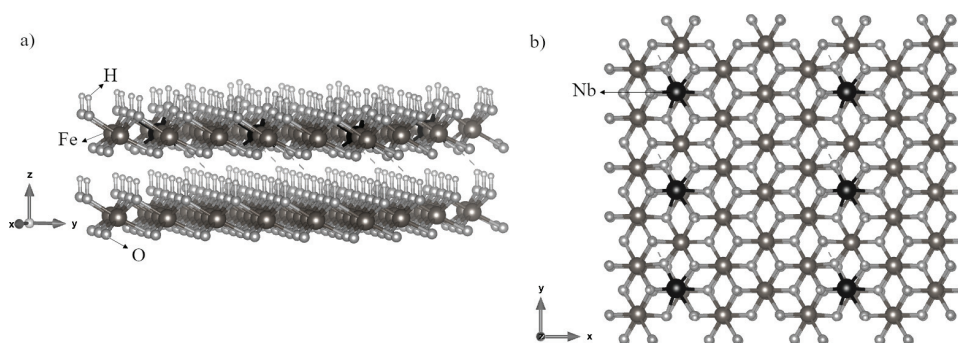


Fig. 5. Nb 10 wt. % system model. The Fe, Nb, O and H atoms are pointed out and Nb atoms are marked black.

The first step to a better understanding dehydration reaction is to know how the catalyst surface interacts with xylose by adsorption tests. Xylose has 3 pos-

sible reaction sites that lead to furfural conversion, Fig. 6, each site leads to a different route reaction, namely routes 1, 2 and 3.

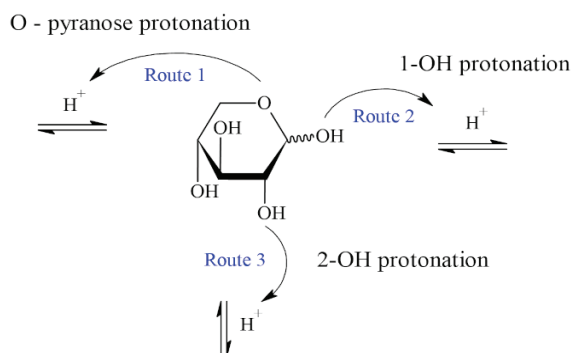


Fig. 6. Possible xylose reaction sites for dehydration reaction to furfural.

Three arbitrary positions for each reaction site were elaborated for adsorption tests (as seen in supplementary material), namely position I, II or III for routes 1, 2 or 3. Combining the possibilities, in total there are 9 different systems for each catalyst.

Fig. 7 shows the best positions and distances chosen after the study of different spatial positions and distances between the catalyst and the sugar. For a superior presentation of the results, potential energy values for distances less than 0.25 nm were omitted, once they were too high. Comparing the results among pure and doped catalyst the resemblance on preference of xylose above feroyxhyte is remarkable. Besides that, the distances are the same or minimally distinct. Fig. 8 shows the most stable positions of xylose on the catalyst for routes 1; 2 and 3, respectively. Table I summarizes all these results.

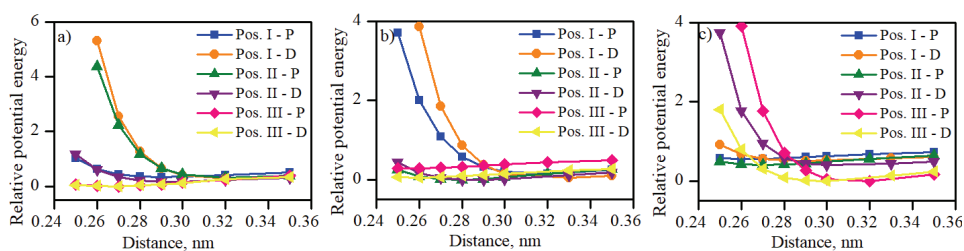


Fig. 7. Calculated potential energy curve for xylose adsorption favoring route: a) 1, b) 2 and c) 3 at different positions. P and D refer to Nb 0 and 10 wt. %, respectively.

The three mechanisms for xylose dehydration to furfural, supported by experimental evidence,<sup>32</sup> are proposed as an acyclic mechanism by the ring opening and two cyclic mechanisms. The difference between them is in the oxygen atom that will be protonated: the ring oxygen (*O*-pyranose), the hydroxyl oxygen in

position 1 (1-OH) or the hydroxyl oxygen in position 2 (2-OH) respectively to the routes 1, 2 and 3, Fig. 8.

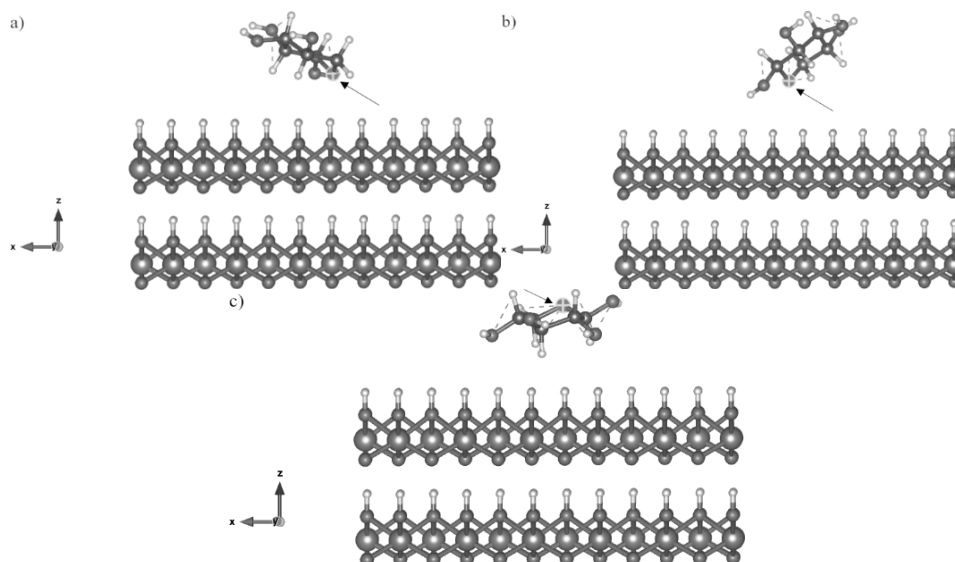


Fig. 8. a), b) and c) refer to routes 1, 2 and 3, respectively. The pointed atom refers to the oxygen belonging to the ring.

TABLE I. Summary of selected positions and distances

Parameter	Route 1		Route 2		Route 3	
	Nb content, wt. %					
	0	10	0	10	0	10
Position	III	III	II	II	III	III
Distance, nm	0.27	0.27	0.28	0.28	0.32	0.30

Route 1, Fig. 9a, would occur with the xylose carbonic chain opening resulting in the intermediates reaction formation.

The process finishes with furfural production and three water molecules loss. Routes 2 and 3, Fig. 9b and c, respectively, would occur without breaking of the xylose carbonic chain. The reaction would happen upon three water molecules loss until the furfural formation.<sup>37</sup>

To thermodynamic analysis, reactants, reaction intermediaries and products from xylose dehydration to furfural were optimized, respecting the preferred positions previously determined, for the respective reaction routes described. Fig. 10a shows the relative results of the reaction mechanism thermodynamic analysis in the presence of Nb 0 wt. % catalyst.

The theoretical results do not show the favoring of furfural formation using the pure catalyst, agreeing with experimental results. To xylose protonation in all

routes, an average energy about 77.82 kJ/mol is necessary. By the reaction mechanism to the three routes, it is possible to observe that only in the 2C intermediary formation an expressive decrease on the system energy occurs, equivalent to  $\Delta E = -355.14$  kJ/mol, but shortly thereafter there is the energy of adsorption in the other reaction steps.

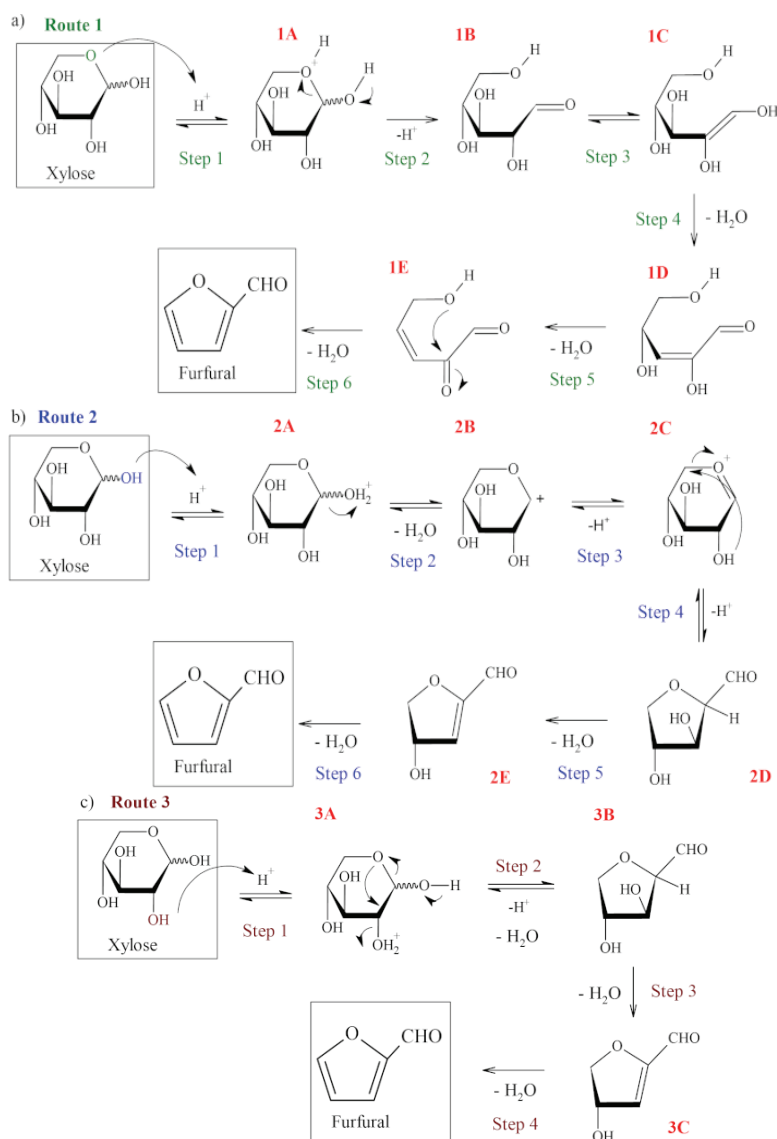


Fig. 9. a) Acyclic reaction mechanism from the *O*-pyranose protonation, route 1; b) cyclic reaction mechanism from the 1-OH protonation, route 2; c) cyclic reaction mechanism from the 2-OH protonation, route 3.



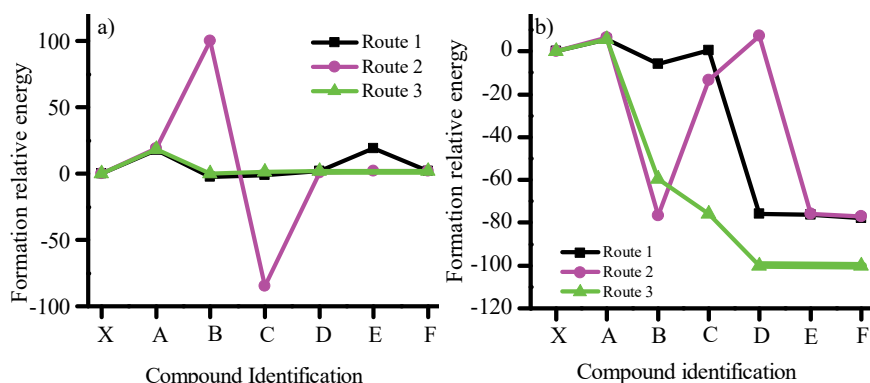
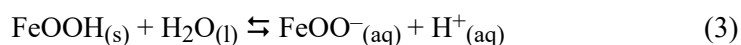


Fig. 10. Relative energy values between reaction steps by: a) Nb 0 and b) 10 wt. % catalyst.

Analyzing the furfural formation in the last step of each route, there is no significant energy difference compared to the other steps, showing that the formation of the product is unlikely. However, the results for Nb 10 wt. % presented in Fig. 10b demonstrate the favoring of furfural production, especially the route 3. For xylose protonation to occur, a 25.10 kJ/mol energy difference is required. Considering B formation, all routes correspond to an exothermic reaction and observing the values to routes 1, 2 and 3 of  $\Delta E$  -25.15, -321.46 and -248.32 kJ/mol, respectively, the last two values being high.

Routes 1 and 2 have the furfural production  $\Delta E$  of -322.80 kJ/mol, although route 2 is the least likely to happen since between the intermediaries B and D there is a difference of 351.92 kJ/mol. In energetic terms, route 3 is the one thermodynamically favorable, because after xylose protonation the reaction runs an exothermic path until a minimal energetic level through a release of 418.40 kJ/mol.

It is important to keep in mind that iron oxyhydroxides exist in equilibrium with its conjugated basis, but the low acid character of iron compounds limits its use as a catalyst for dehydration reaction:<sup>38</sup>



The modification of iron oxides with niobium might rise the catalytic activity and stability as related by Oliveira and collaborators<sup>12</sup> using computational and experimental studies for iron oxide  $\alpha$  phase. Studies conducted by Lacerda<sup>27</sup> had shown that the bond distance between hydrogen and oxygen on ferroxhyte surface to pure and doped systems is slightly distinct. In case of pure catalyst the distance is of 0.097 nm, but for the doped is 0.098 nm and this favor the  $\text{H}^+$  release, implying the Brønsted acidity rise.

According to Pholjaroen,<sup>39</sup> there is evidence that the xylose dehydration reaction to furfural, using a heterogeneous catalyst, may be favored by one active site, especially the cyclic routes. The Lewis acid sites favor the first conversion

step from xylose to xylulose by isomerization, whereas the Brønsted active sites favor the following dehydration steps.<sup>40</sup> Fig. 11 presents a scheme.

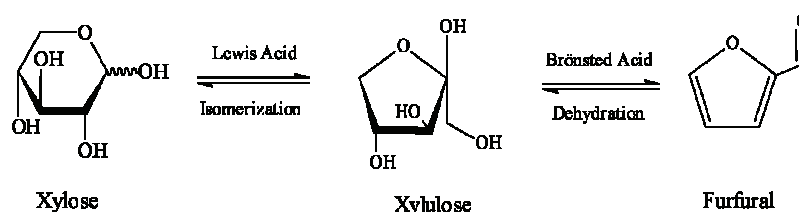


Fig. 11. Xylose Isomerization and dehydration to furfural.

Niobium and its oxides feature Brønsted and Lewis acidity,<sup>13,14,41</sup> that justifies the superior conversion rate of xylose to furfural for the experimental results and a greater thermodynamic stability presented by the calculations.

#### CONCLUSION

Synthesis and characterization of pure  $\delta$ -FeOOH (Nb 0 wt. %) and doped (Nb 10 wt. %) nanoparticles had proved satisfactory. The doping went close to theoretical value (Nb 9.50 wt. %) and the surface areas are in the literature range.

By conversion rate results, the Nb doped material proved to be more efficient than the pure catalyst, showing a xylose conversion rise of 290 %.

Furthermore, the computational studies indicated that thermodynamic favor use of Nb doped catalyst, related to the pure, when applied to the xylose dehydration reaction to furfural. Hence, route 3 is the most likely reaction route.

The Nb atoms incorporation to  $\delta$ -FeOOH raises the  $-OOH$  groups Brønsted acidity, because it facilitates the  $H^+$  release, and the Lewis acid sites formation. Thus, the use of Nb doped materials  $\delta$ -FeOOH based may be promising in the heterogeneous catalysis field. This paper has supplementary material.

#### SUPPLEMENTARY MATERIAL

Additional data and information are available electronically at the pages of journal website: <https://www.shd-pub.org.rs/index.php/JSCS/article/view/11693>, or from the corresponding author on request.

*Acknowledgements.* The authors would like to thank the Brazilian agencies CNPq (Conselho Nacional de Desenvolvimento Científico e Tecnológico, 409723/2018-5) and FAPEMIG (Fundação de Amparo à Pesquisa do Estado de Minas Gerais, APQ-03226-18), for financial support. Also, this study was financed in part by the Coordenação de Aperfeiçoamento de Pessoal de Nível Superior – Brasil (CAPES) – Finance Code 001, and part of the project involving the Programa de Pós-Graduação da Rede Mineira de Química de Minas Gerais (PPGMQ-MG). This work was supported by University of Hradec Kralove (Faculty of Science, VT2019-2021).

ИЗВОД  
ДОБИЈАЊЕ ФУРФУРАЛА ДЕХИДРАТАЦИЈОМ КСИЛОЗЕ У ПРИСУСТВУ  
КАТАЛИЗАТОРА  $\delta$ -FeOОН ДОПИРАНОГ НИОБИЈУМОМ

PAULO TADASHI BANNAI CAMPOS<sup>1</sup>, MARIANA DE REZENDE BONESIO<sup>1</sup>, ANDRÉ LUIZ DIAS LIMA<sup>2</sup>,  
ADILSON CÂNDIDO DA SILVA<sup>2</sup>, DAIANA TEIXEIRA MANCINI<sup>1</sup> и TEODORICO CASTRO RAMALHO<sup>1</sup>

<sup>1</sup>Department of Chemistry, Federal University of Lavras 37200-900, Lavras – MG, Brazil u <sup>2</sup>Department of  
Chemistry, Federal University of Ouro Preto, 35400-000, Ouro Preto – MG, Brazil

Ефекат модификације  $\delta$ -FeOОН ниобијумом, примењен на реакцију дехидратације ксилозе, испитиван је експерименталним и теоријским методама. Експериментално је потврђено да су материјали добијени на основу карактеристичних рефлексција при меном дифракције X-зрачења на праху. Масеном спектрометријом са индуктивно спрегнутом плазмом је одређен садржај Nb и то 0 за чист  $\delta$ -FeOОН и 9,5 мас. % ( $\delta$ -FeOОН/ Nb) за допиран. Када се прати добијање фурфурала, допирани материјал показује побољшање конверзије од 290 % у поређењу са чистим катализатором. Теоријски прорачуни су омогућили разумевање најповољнијег реакционог пута за механизме предложене на основу вредности потенцијалне енергије. Да би се објаснили најповољнији реакциони путеви, најпре је израчуната најповољнија позиција ксилозе у односу на  $\delta$ -FeOОН. Затим је на основу реакционих путева предложених механизма израчунато када је фаворизовано формирање фурфурала и добијене енергетске вредности указују на то да је већа вероватноћа формирања фурфурала на допираном материјалу.

(Примљено 16. марта, ревидирано 22. новембра, прихваћено 9. децембра 2022)

REFERENCES

1. D. Kumar, B. Singh, J. Korstad, *Renew. Sust. Energ. Rev.* **73** (2017) 654 (<https://doi.org/10.1016/j.rser.2017.01.022>)
2. G. Toscano, G. Riva, E. Foppa Pedretti, D. Duca, *Biomass Bioenergy* **35** (2011) 3139 (<https://doi.org/10.1016/j.biombioe.2011.04.010>)
3. L. Kuznetsova, L. Zabodalova, N. Yakovchenko, M. Domoroshchenkova, *Energy Procedia* **95** (2016) 230 (<https://doi.org/10.1016/j.egypro.2016.09.057>)
4. T. Forster-Carneiro, M. D. Berni, I. L. Dorileo, M. A. Rostagno, *Resour. Conserv. Recycl.* **77** (2013) 78 (<https://doi.org/10.1016/j.resconrec.2013.05.007>)
5. P. L. de Hoyos-Martínez, X. Erdocia, F. Charrier-El Bouhtoury, R. Prado, J. Labidi, *Waste Manage.* **80** (2018) 40 (<https://doi.org/10.1016/j.wasman.2018.08.051>)
6. P. Kubelka, F. Munk, *Zeitsch. Tech. Phys.* **12** (1931) 593 (<http://www.graphics.cornell.edu/~westin/pubs/kubelka.pdf>)
7. G. Machado, S. Leon, F. Santos, R. Lourega, J. Dullius, M. Mollmann, P. Eichler, *Nat. Resour.* **07** (2016) 115 (<http://dx.doi.org/10.4236/nr.2016.73012>)
8. A. Chatterjee, X. HU, F. L. Y. Lam, *Fuel* **239** (2019) 726 (<https://doi.org/10.1016/j.fuel.2018.10.138>)
9. C. Garcia-Sancho, I. Agirrezabal-Telleria, M. B. Guemez, P. Maireles-Torres, *Appl. Catal., B* **152** (2014) 1 (<https://doi.org/10.1016/j.apcatb.2014.01.013>)
10. R. K. Pal, S. Pradhan, L. Narayanan, V. K. Yadavalli, *Sensors Actuators, B* **259** (2018) 498 (<http://dx.doi.org/10.1016/j.snb.2017.12.082>)
11. P. Chen, K. Xu, X. Li, Y. Guo, D. Zhou, J. Zhao, X. Wu, C. Wu, Y. Xie, *Chem. Sci.* **5** (2014) 2251 (<https://doi.org/10.1039/C3SC53303D>)
12. L. C. A. Oliveira, F. Zaera, I. Lee, D. Q. Lima, T. C. Ramalho, A. C. Silva, E. M. B. Fonseca, *Appl. Catal., A* **368** (2009) 17 (<https://doi.org/10.1016/j.apcata.2009.08.001>)

13. H. S. Oliveira, L. D. Almeida, V. A. A. De Freitas, F. C. C. Moura, P. P. Souza, L. C. A. Oliveira, *Catal. Today* **240** (2015) 176 (<http://dx.doi.org/10.1016/j.cattod.2014.07.016>)
14. A. L. D. Lima, D. C. Batalha, H. V. Fajardo, J. L. Rodrigues, M. C. Pereira, A. C. Silva, *Catal. Today* **344** (2020) 118 (<https://doi.org/10.1016/j.cattod.2018.10.035>)
15. L. V. C. Lima, M. Rodriguez, V. A. A. Freitas, T. E. Souza, A. E. H. Machado, A. O. T. Patrocínio, J. D. Fabris, L. C. A. Oliveira, M. C. Pereira, *Appl. Catal., B* **165** (2015) 579 (<http://dx.doi.org/10.1016/j.apcatb.2014.10.066>)
16. M. C. Pereira, E. M. Garcia, A. Cândido da Silva, E. Lorençon, J. D. Ardisson, E. Murad, J. D. Fabris, T. Matencio, T. de Castro Ramalho, M. V. J. Rocha, *J. Mater. Chem.* **21** (2011) 10280 (<https://doi.org/10.1039/C1JM11736J>)
17. *Gaussian 16, revision C.01*, Gaussian, Inc., Wallingford, CT, 2016 (<https://gaussian.com/gaussian16/>)
18. L. W. Chung, W. M. C. Sameera, R. Ramozzi, A. J. Page, M. Hatanaka, G. P. Petrova, T. V. Harris, X. Li, Z. Ke, F. Liu, H. B. Li, L. Ding, K. Morokuma, *Chem. Rev.* **115** (2015) 5678 (<https://doi.org/10.1021/cr5004419>)
19. E. F. F. da Cunha, W. Sippl, T. de Castro Ramalho, O. A. Ceva Antunes, R. B. de Alencastro, M. G. Albuquerque, *Eur. J. Med. Chem.* **44** (2009) 4344 ([10.1016/j.ejmech.2009.05.016](https://doi.org/10.1016/j.ejmech.2009.05.016))
20. T. Costa Martins, T. Ramalho, J. Figueroa-Villar, A. Flores, C. Pereira, *Magn. Reson. Chem.* **41** (2003) 983 (<https://doi.org/10.1002/mrc.1299>)
21. T. C. Ramalho, M. Bühl, *Magn. Reson. Chem.* **43** (2005) 139 (<https://doi.org/10.1002/mrc.1514>)
22. A. P. Guimarães, A. A. Oliveira, E. F. F. da Cunha, T. C. Ramalho, T. C. C. França, *J. Biomol. Struct. Dyn.* **28** (2011) 455 (<https://doi.org/10.1080/07391102.2011.10508588>)
23. T. C. C. França, P. G. Pascutti, T. C. Ramalho, J. D. Figueroa-Villar, *Biophys. Chem.* **115** (2005) 1 (<https://doi.org/10.1016/j.bpc.2004.12.002>)
24. L. E. Roy, P. J. Hay, R. L. Martin, *J. Chem. Theory Comput.* **4** (2008) 1029 (<https://doi.org/10.1021/ct8000409>)
25. T. Jian, L. F. Cheung, T.-T. Chen, G. V Lopez, W.-L. Li, L.-S. Wang, *Int. J. Mass Spectrom.* **434** (2018) 7 (<https://doi.org/10.1016/j.ijms.2018.08.013>)
26. J. P. Perdew, K. Burke, M. Ernzerhof, *Phys. Rev. Lett.* **77** (1996) 3865 (<https://doi.org/10.1103/PhysRevLett.77.3865>)
27. L. C. T. Lacerda, M. S. Pires, I. S. S. Oliveira, T. C. Telles, A. A. de Castro, S. Corrêa, V. S. Vaiss, T. C. Ramalho, *J. Mol. Model.* **27** (2021) 249 (<https://doi.org/10.1007/s00894-021-04864-4>)
28. V. A. Drits, B. A. Sakharov, A. Manceau, *Clay Miner.* **28** (1993) 209 (<https://doi.org/10.1180/claymin.1993.028.2.03>)
29. P. E. Blöchl, *Phys. Rev., B* **50** (1994) 17953 (<https://doi.org/10.1103/PhysRevB.50.17953>)
30. I. Kumari, N. Kaur, S. Gupta, N. Goel, *J. Mol. Model.* **25** (2019) (10.1007/s00894-018-3899-x)
31. M. Casarin, D. Falcomer, A. Glisenti, M. M. Natile, F. Poli, A. Vittadini, *Chem. Phys. Lett.* **405** (2005) 459 (<https://doi.org/10.1016/j.cplett.2005.02.076>)
32. H. Rasmussen, H. Sørensen, A. Meyer, *Carbohydr. Res., C* **385** (2013) 45 (<https://doi.org/10.1016/j.carres.2013.08.029>)
33. R. M. Cornell, U. Schwertmann, *The Iron Oxides: Structure, Properties, Reactions, Occurrences and Uses*, 2<sup>nd</sup> ed., Wiley-VCH, Weinheim, 2003 (<https://doi.org/10.1002/3527602097>)

34. C. B. Koch, C. A. Oxborrow, S. Mørup, M. B. Madsen, A. J. Quinn, J. M. D. Coey, *Phys. Chem. Miner.* **22** (1995) 333 (<https://doi.org/10.1007/BF00202774>)
35. J. B. Lopes Martins, E. Longo, O. D. Rodríguez Salmon, V. A. A. Espinoza, C. A. Taft, *Chem. Phys. Lett.* **400** (2004) 481 (<https://doi.org/10.1016/j.cplett.2004.10.150>)
36. A. C. Silva, R. M. Cepera, M. C. Pereira, D. Q. Lima, J. D. Fabris, L. C. A. Oliveira, *Appl. Catal., B* **107** (2011) 237 (<http://dx.doi.org/10.1016/j.apcatb.2011.07.017>)
37. M. J. Antal, T. Leesomboon, W. S. Mok, G. N. Richards, *Carbohydr. Res.* **217** (1991) 71 ([https://doi.org/10.1016/0008-6215\(91\)84118-X](https://doi.org/10.1016/0008-6215(91)84118-X))
38. M. Pires, L. Lacerda, S. Corrêa, T. Silva, A. Castro, T. Ramalho, in *Recent Advances in Complex Functional Materials*, Springer, Berlin, 2017, pp. 409–425 ([https://doi.org/10.1007/978-3-319-53898-3\\_16](https://doi.org/10.1007/978-3-319-53898-3_16))
39. B. Pholjaroen, N. Li, Z. Wang, A. Wang, T. Zhang, *J. Energy Chem.* **22** (2013) 826 ([https://doi.org/10.1016/S2095-4956\(14\)60260-6](https://doi.org/10.1016/S2095-4956(14)60260-6))
40. I. Agirrezabal-Telleria, C. García Sancho, P. Maireles-Torres, P. L. Arias, *Chinese J. Catal.* **34** (2013) 1402 ([https://doi.org/10.1016/S1872-2067\(12\)60599-3](https://doi.org/10.1016/S1872-2067(12)60599-3))
41. J. B. Gabriel, V. Oliveira, T. E. De Souza, I. Padula, L. C. A. Oliveira, L. V. A. Gurgel, B. E. L. Baêta, A. C. Silva, *ACS Omega* **5** (2020) 21392 (<https://doi.org/10.1021/acsomega.0c01547>).

SUPPLEMENTARY MATERIAL TO  
**Xylose dehydration to furfural using niobium doped  $\delta$ -FeOOH as catalyst**

PAULO TADASHI BANNAI CAMPOS<sup>1</sup>, MARIANA DE REZENDE BONESIO<sup>1</sup>,  
 ANDRÉ LUIZ DIAS LIMA<sup>2</sup>, ADILSON CÂNDIDO DA SILVA<sup>2</sup>,  
 DAIANA TEIXEIRA MANCINI<sup>1\*</sup> and TEODORICO CASTRO RAMALHO<sup>1\*\*</sup>

<sup>1</sup>Department of Chemistry, Federal University of Lavras 37200-900, Lavras – MG, Brazil and

<sup>2</sup>Department of Chemistry, Federal University of Ouro Preto, 35400-000, Ouro Preto – MG, Brazil

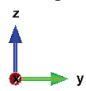
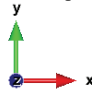
*J. Serb. Chem. Soc.* 88 (4) (2023) 395–408

TABLE S-I. Positions of xylose on materials for adsorption study

	View under plane X 	View under plane Z 	Xylose Coordinates (VESTA)
I Route 1			Positioning Place (x,y,z) of this layer at (x,y,z) of layer 0 : This layer: 0 0 0      Global coordinate system: 7.8 4.5 12.75 Orientation Align orientation of this layer with respect to layer 0 : This layer: [u v w] 1 0 0      Global coordinate system: [u v w] 1 0 5 (h k l) 0 0 1      (h k l) 0 0 3
II Route 1			Positioning Place (x,y,z) of this layer at (x,y,z) of layer 0 : This layer: 0 0 0      Global coordinate system: 8 8.5 13 Orientation Align orientation of this layer with respect to layer 0 : This layer: [u v w] 1 0 0      Global coordinate system: [u v w] 1 -2 5 (h k l) 1 0 -1      (h k l) 0 0 3

\* Corresponding authors. E-mail: (\*)daianateixeira60@yahoo.com.br; (\*\*)teo@ufla.br

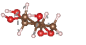
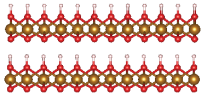
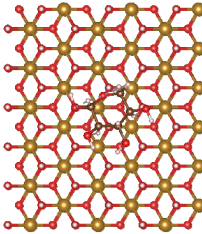
View under plane X      View under plane Z

Position  

Xylose Coordinates (VESTA)

---

**III Route 1**

Positioning  
Place (x,y,z) of this layer at (x,y,z) of layer 0


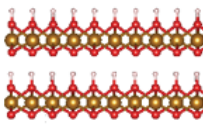
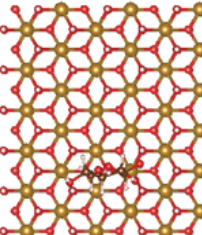
This layer	0	0	0
Global coordinate system	8	8.5	13

Orientation  
Align orientation of this layer with respect to layer 0

This layer	[u v w]	1	0	0
(h k l)		1	0	1
Global coordinate system	[u v w]	1	-19	5
(h k l)		0	0	3

---

**I Route 2**

Positioning  
Place (x,y,z) of this layer at (x,y,z) of layer 0

This layer	0	0	0
Global coordinate system	7.8	4.5	12.75

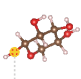
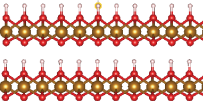
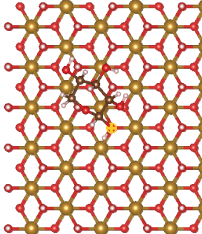
Orientation  
Align orientation of this layer with respect to layer 0

This layer	[u v w]	1	0	0
(h k l)		1	0	0
Global coordinate system	[u v w]	1	0	5
(h k l)		0	0	3

OK    Cancel    Apply

---

**II Route 2**

Positioning  
Place (x,y,z) of this layer at (x,y,z) of layer 0

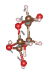
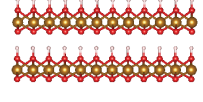
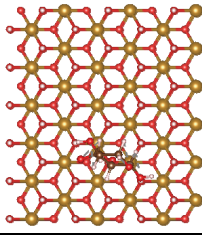
This layer	0	0	0
Global coordinate system	6.5	10	12.812

Orientation  
Align orientation of this layer with respect to layer 0

This layer	[u v w]	-1	2	-1
(h k l)		1	2	1
Global coordinate system	[u v w]	-1	1	-1
(h k l)		-1	2	2

---

**III Route 2**

Positioning  
Place (x,y,z) of this layer at (x,y,z) of layer 0


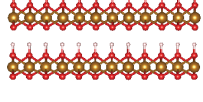
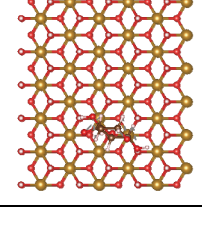
This layer	0	0	0
Global coordinate system	8	5	14

Orientation  
Align orientation of this layer with respect to layer 0

This layer	[u v w]	1	0	15
(h k l)		1	-1	0
Global coordinate system	[u v w]	1	7	-2
(h k l)		0	0	1

---

**I Route 3**

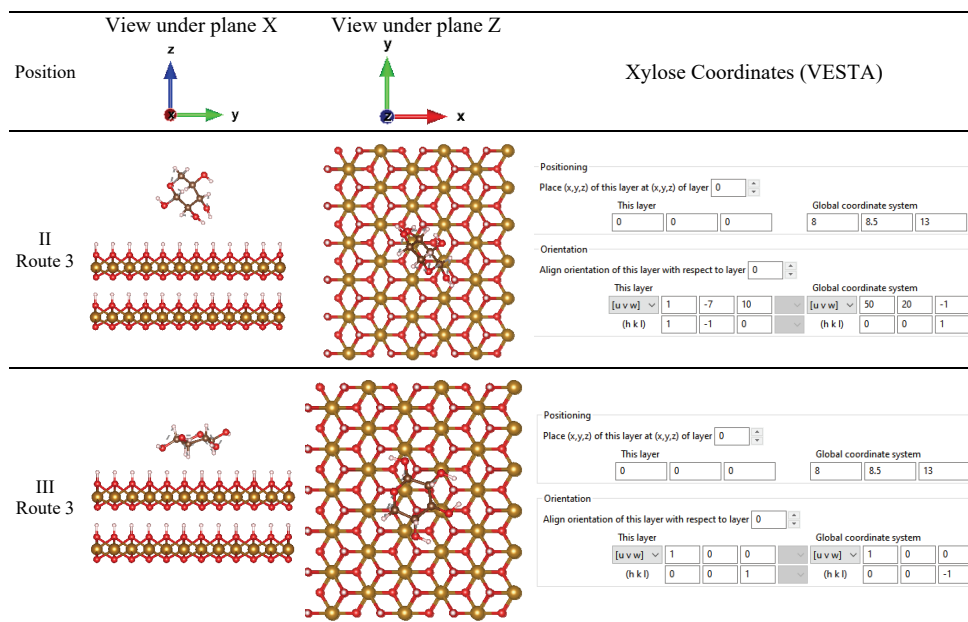




Positioning  
Place (x,y,z) of this layer at (x,y,z) of layer 0

This layer	0	0	0
Global coordinate system	8	5	14

Orientation  
Align orientation of this layer with respect to layer 0

This layer	[u v w]	1	0	15
(h k l)		1	-1	0
Global coordinate system	[u v w]	1	7	-2
(h k l)		0	0	1







## The influence of nanoclays on the mechanical and thermal properties of rigid PIR and PUR foams

RUSLAN R. VLASOV<sup>1\*</sup>, DARIA I. RYABOVA<sup>1</sup>, SAKINA Z. ZEYNALOVA<sup>2</sup>,  
DMITRY V. SOKOLOV<sup>1</sup> and SERGEI A. RYABOV<sup>1</sup>

<sup>1</sup>Lobachevsky State University – Faculty of Chemistry, Department of Macromolecular Compounds and Colloidal Chemistry, Gagarina av. 23, 603098 Nizhny Novgorod, Russia and <sup>2</sup>Tre Tau Engineering srl, Pietro Colletta 85, 10153 Torino, Italy

(Received 3 November, revised 8 December, accepted 21 December 2022)

**Abstract:** The effect of small amounts of chemically modified nanosized clays (from 0.05 to 1 %) on the morphological, physical-mechanical and thermo-physical characteristics of rigid polyurethane–polyisocyanurate (PIR) and polyurethane (PUR) foams has been studied. The effect of these additives on the structure of the resulting material, the change in its compressive strength, Young's modulus, mass loss during combustion, and thermal conductivity are evaluated. Based on the results obtained, it is noted that the addition of small amounts (up to 0.2 %) of chemically modified Cloisite 30B nanoclay effectively reduces the average cell size of nanocomposite foams, which leads to an improvement in their performance.

**Keywords:** polyurethane; polyurethane–polyisocyanurate foam; nanosized fillers; compressive strength; cell morphology; thermal conductivity.

### INTRODUCTION

Currently, one of the largest molar weight polymers is polyurethane – a polymeric material, traditionally obtained by polycondensation (polyaddition) of aromatic or aliphatic di- and polyisocyanates with polyol resins.<sup>1</sup> Due to the distinctive features of the material, such as insulation ability from high temperature and sound in the case of polyurethane foams, and exceptional mechanical properties, polyurethanes have now become an integral part of everyday life. One of the main industrially significant types of polyurethane is rigid polyurethane (PUR) and polyurethane–polyisocyanurate (PIR) foam. PIR foams are obtained using isocyanate trimerization catalysts as a result of technological processes similar to those in the case of PUR foams. It should be noted that PIR foams have improved thermal insulation properties and are less flammable than conventional

\* Corresponding author. E-mail: vlasovruslan.hs@yandex.ru  
<https://doi.org/10.2298/JSC221103089V>

polyurethane foams. Reactions of the formation of urethane and isocyanurate groups are shown in Fig. 1.<sup>2</sup> It is important to note that in the framework of the synthesis of both polyurethane and, mainly, polyurethane–polyisocyanurate foams, a number of secondary chemical processes occur, the consideration of which is beyond the scope of this publication.<sup>3,4</sup>

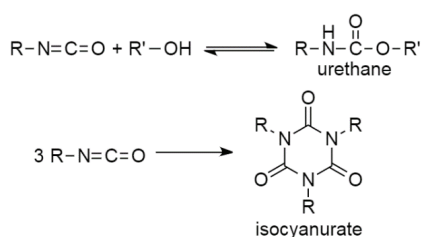


Fig. 1. Reactions of urethane and isocyanurate formation.

It is important to note that the annually growing demand for polymeric materials inevitably leads to ever greater requirements of functional (physical-mechanical, thermophysical, *etc.*) characteristics of the resulting polymers, which the existing ones, for a very wide range of applications, no longer meet. One of the most promising ways to solve this problem is the synthesis of composite materials based on these polymers. Today, the filled polyurethane systems are used everywhere, while the mass fraction of the filler in the formulation can traditionally vary from 1 to 50 % by weight of the composition. The most common fillers currently used in the polyurethane industry are chalk, carbon black,<sup>5</sup> sand,<sup>6</sup> expandable graphite,<sup>7</sup> titanium dioxide<sup>8</sup> and a wide range of other oxides and inorganic salts.

It should be noted that the introduction of such inorganic additives in acceptable amounts into systems for producing foams contributes to a decrease in the average cell size of the formed foam,<sup>9</sup> since fillers act as a nucleating agent, creating many smaller cells.<sup>10,11</sup> In addition, these additives prevent the additional growth of bubbles due to an increase in the viscosity of the reaction medium.<sup>12</sup> Thus, the use of nanosized fillers to a large extent contributes to the improvement of the morphological characteristics of foams and, as a result, to an increase in a number of performance characteristics, increasing strength indicators<sup>13,14</sup> to a significant extent and preventing a gradual increase in the thermal conductivity of foams during aging.<sup>15,16</sup>

The trend towards the addition of micro-sized clays (mainly montmorillonite and vermiculite) in polyurethane foam compositions arose about 20 years ago.<sup>17–19</sup> Nanoclays, on the other hand, are finely dispersed material, which improves the mechanical and thermal insulation properties of polyurethane composite foams due to a significantly increased specific surface area.<sup>20</sup>

It is extremely necessary to select the optimal amount of nanofiller, since at an excessively high content of these additives, a significant deterioration in the morphology of the material and degradation of performance characteristics are noted.<sup>21,22</sup> This deterioration in morphology can manifest itself both as an increase in the average cell size<sup>13</sup> and as a decrease in their density,<sup>23</sup> as well as an increase in the anisotropy coefficient of the foam.<sup>24,25</sup>

Thus, in the case of polyurethane and polyurethane–polyisocyanurate foams, nanoclays are of significant interest. In this regard, it is expedient to develop formulations of new nanocomposite materials based on polyurethane–polyisocyanurate and polyurethane foams, using the additives described above, which possess some improved performance characteristics.

## EXPERIMENTAL

### Materials

For the synthesis of polyurethane and polyurethane–polyisocyanurate foams, a mixture of polyether polyols (H6007 (HongBaoLi PU, China) and HF-310 (Zhejiang Hengfeng New Material, China)), tris(2-chloropropyl)phosphate (TCPP, Shijiazhuang Hejia Chemical Products, China) as a flame retardant, a mixture of 1,1,4,7,7-pentamethyldiethylenetriamine (PMDETA, Evonik, Germany) and dibenzylamine (Evonik, Germany) as catalysts for urethane and urea formation, a solution of potassium acetate in diethylene glycol in a ratio of 30:70 (Evonik, Germany) as trimerization catalyst, as well as water and *n*-pentane (for synthesis, Ekos-1, Russia) as blowing agents, were used. A highly functional polymeric MDI – Lupranat M50 (BASF, Germany) – with dynamic viscosity of 557 mPa s, determined at 25 °C in accordance with ISO 3219-2:2021,<sup>26</sup> and NCO content of 31.5 %, determined in accordance with ISO 148696:2009,<sup>27</sup> was used as the isocyanate component. The composition of the systems used is shown in Table I.

TABLE I. The composition (amount in g) of PIR/PUR foam systems

Component	Foam	
	PUR	PIR
Polyether polyols blend	50.0	50.0
TCPP	7.0	7.0
PMDETA	0.8	0.8
Dibenzylamine	2.1	2.1
Potassium acetate in diethylene glycol (30:70)	–	2.5
Water	2.4	2.4
<i>n</i> -Pentane	2.7	2.7
Polymeric MDI (Lupranat M 50)	62.3	155.8

Commercially available chemically modified organoclays Cloisite 30B (surface layer modified with a quaternary salt of bis-2-hydroxyethylmethylammonium, modifier content <90 meq/100 g) and Cloisite 25A (surface layer modified with a quaternary salt of diethylmethylammonium, content modifier <95 meq/100 g) manufactured by BYK Additives (Germany).

### *Nanoclay suspensions*

The insertion of fillers into the isocyanate component to obtain PUR and PIR foams was carried out by ultrasonic dispersion using an Inlab I100-6/4 unit equipped with an I10-2.0 ultrasonic generator at a frequency of 22.5 kHz with an output power of 2 kW.

### *Dynamic viscosity measurements*

The dynamic viscosity of the suspensions obtained was measured using a Lamy RM200 CP4000 Plus rotary rheometer using R-6 disc ( $\varnothing$ 14.62 mm) at shear rate of 60 rpm in accordance with ISO 3219-2:2021<sup>26</sup> at 25 °C. Further in the work, the average viscosity values determined by analyzing three samples are given.

### *PUR and PIR foams preparation*

The isocyanate and polyol components were thermostated at 20 °C. To obtain foam samples, the required weights of the blended polyether component were placed in plastic cylinders with a volume of 1000 cm<sup>3</sup>, the required amount of *n*-pentane was added, after which it was actively mixed with the component for 2 min. After adding the required weight of isocyanate (or nanoclay suspensions), the system was mixed for 5 s using an automatic mixer at a speed of 3000 rpm. Foaming was carried out in the above-described plastic containers or wooden cubes with a volume of 15625 cm<sup>3</sup>. Ten min after mixing the components, fragments were cut out from the core of the formed foams, which were subsequently used as analysed samples.

### *Gel time*

The so called “gel time” was tested as the time elapsed from the start of mixing polyol and isocyanate components to the point at which soft threads are formed when an ordinary wire yarn is touched to the surface of the foaming material and withdrawn.

### *Isocyanate group content measurements*

The content of isocyanate groups in the polyisocyanate used was determined using the potentiometric titration method on an 848 Titrino plus Metrohm automatic titrator in accordance with ISO 148696:2009.<sup>27</sup>

### *Apparent density*

The determination of the apparent density of the synthesized foams was carried out in accordance with ASTM D1622-20,<sup>28</sup> for which cubic samples of 50×50×mm<sup>2</sup> in size were cut from the obtained materials. Further in the work, the average apparent density values, determined by analysing five samples, are given.

### *Mechanical tests*

The determination of compressive strength and Young's modulus was carried out in the direction of foaming on Roell/Zwick Z005 universal testing machine at a strain rate of 10 mm min<sup>-1</sup> at 10 % linear strain in accordance with the EN 826:2013 method.<sup>29</sup> Within this work, only the relative compressive strength and Young's modulus are considered, numerically equal to the ratio of the compressive strength and Young's modulus to the square of the apparent density of the foam sample. The data shown in the work are averages calculated from analyses of five samples of each of the investigated formulations of polyurethane–polyisocyanurate and polyurethane foams.

### *Open cell content*

The content of open cells (OC / %) in the analysed polyurethane and polyurethane–polyisocyanurate foams was analysed using an AccuPyc II 1340 gas pycnometer in accordance

with ASTM D6226-05.<sup>30</sup> Further, the paper presents the average value of the content of open cells in the studied samples, determined from the results of three independent measurements.

#### *Thermal conductivity*

The thermal conductivity of the analysed polyurethane-polyisocyanurate and polyurethane foams was determined at 24 °C using LaserComp Fox600 HFM and Fox200 SN instruments in accordance with EN 12667:2001.<sup>31</sup> The size of each sample was 200 mm×200 mm×25 mm. Further, the paper presents the average values of thermal conductivity determined by analysing three samples.

#### *Morphological characteristics analysis*

The morphological characteristics of the closed-cell structure of the foam samples were studied using the method of scanning electron microscopy (SEM). A Hitachi TM4000 Plus II instrument was used as a scanning electron microscope. Using a blade, 0.5 mm thick layers of the analysed foam were cut out, and they were subsequently placed in the sample compartment of the above-described photomicrograph instrument.

The average cell size ( $\Phi$ ) and the anisotropy coefficient ( $A_{y/x}$ ) were estimated using the ImageJ software with the help of the intersection method, in accordance with the methods proposed by Brondi *et al.*<sup>32</sup> Each analysed micrograph was overlaid with a grid composed of equidistant perpendicular lines ( $m$  vertical lines of length  $h$  and  $l$  horizontal lines of length  $w$ ). For each of the lines, the number of crossed cells ( $n_i, n_j$ ) was counted. Dividing the length of each individual line by a certain number of intersections, we found the lengths of the chords of the cells ( $\Phi_i$  and  $\Phi_j$ , *i.e.*, one-dimensional values). This operation was carried out for each of the lines of the constructed grid, after which the average cell size was determined in accordance with the Eq. (1) and the anisotropy coefficient in accordance with the Eq. (2). Further in the paper, the averaged values of all these quantities, determined by analyzing five samples, are given:

$$\bar{\Phi} = \frac{\sum_{i,j=1}^{m,l} \Phi_{i,j}}{m+l} \quad (1)$$

where  $\Phi$  is average cell size,  $\Phi_{i,j}$  are the lengths of cell chords,  $m$  is the number of vertical grid lines,  $l$  is the number of horizontal grid lines.

$$A_{y/x} = \left( \left( \sum_{i=1}^m \Phi_i \right) / m \right) \left( \left( \sum_{j=1}^l \Phi_j \right) / l \right) \quad (2)$$

where  $A_{y/x}$  is the anisotropy coefficient,  $\Phi_{i,j}$  are the lengths of cell chords,  $m$  is the number of vertical grid lines,  $l$  is the number of horizontal grid lines.

Cell density was estimated using ImageJ software according to Kumar's theoretical approximation principle.<sup>33,34</sup> After opening the microphotograph in the ImageJ program, the area for analysis was selected. The number of cells and the square of the analysed area of the micrograph were determined. The density of cells in the volume was estimated in accordance with the Eq. (3) proposed by Kumar, which can be expressed in terms of the number of cells located per cubic centimetre of the analysed foam (cells cm<sup>-3</sup>). Further in the work, the average values of cell density determined by analysing five samples are given:

$$N_f = \left( \frac{n}{A} \right)^{3/2} \quad (3)$$

where  $N_f$  is the density of cells in the foam,  $n$  is the number of cells in the analysed area of the microphotograph,  $A$  is the square of the analysed area,  $\text{cm}^2$ .

#### Combustibility

In order to assess the change in the combustibility of the analysed polyurethane–polyisocyanurate foams, samples (30 mm×30 mm×15 mm) were vertically fixed in a tripod, after which the edge (30 mm×30 mm) was blown over for 30 s by the flame of a gas burner located at a distance of 5 cm from the sample, so that the entire surface of the facet was covered in flames. The gas flow rate was  $0.36 \text{ ml s}^{-1}$ . Further, the paper presents the average values of the degree of damage by mass ( $S_m$ ) determined by analysing five samples, calculated taking into account the change in the mass of the analysed samples before and after the test.

### RESULTS AND DISCUSSION

In accordance with the ISO 3219-2:2021 method,<sup>26</sup> the dynamic viscosity of the resulting organoclay suspensions in the polyisocyanate component used was determined. The trend in dynamic viscosity versus filler content is shown in Fig. 2.

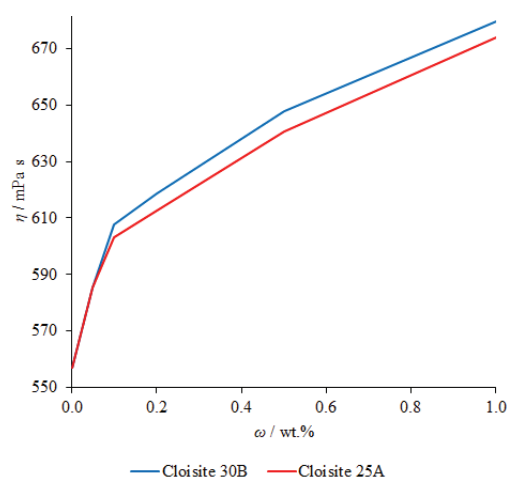


Fig. 2. Dependence of the dynamic viscosity of the isocyanate component on filler content.

Thus, there is a gradual increase in the dynamic viscosity of the isocyanate component as the content of the filler in it increases.

In order to study the effect of small additions of organoclays on the physical-mechanical, thermophysical and morphological properties, the samples of rigid closed-cell polyurethane and polyurethane–polyisocyanurate foams were obtained using the suspensions of the filler in polyisocyanate. It is noted that the addition of the considered fillers into the composition slightly shifted the parameters of the system, slowing down the so called “gel time” by 1–2 s in the case of organoclay concentration of 0.05 and 0.1 % and 2–3 s in the case of using these additives in higher concentrations. These minor changes in the technological parameters of the system are the result of a clear effect exerted by the additives on the physics of the foaming process.

The values of the physical-mechanical, morphological and thermophysical characteristics of the obtained composite foams were determined using the methods described above are presented in Tables II and III, and in a graphic form as the Supplementary material to this paper.

TABLE II. Physical and mechanical characteristics of PUR and PIR foams

Foam sample		$\omega$ wt. %	$\gamma$ kg m <sup>-3</sup>	$\sigma$ kPa	$\sigma_{rel.}$ kPa m <sup>6</sup> kg <sup>-2</sup>	$E$ kPa	$E_{rel.}$ kPa m <sup>6</sup> kg <sup>-2</sup>	
PUR	Standard	0.00	40.35	209.71	0.129	1974.10	1.21	
		Cloisite 30B	0.05	40.15	229.51	0.142	1981.01	1.23
			0.10	39.95	238.80	0.150	1990.68	1.25
			0.20	39.81	246.51	0.156	1993.45	1.26
			0.50	39.72	245.13	0.155	1979.59	1.25
			1.00	39.49	242.05	0.155	1976.67	1.27
	Cloisite 25A		0.05	40.17	224.79	0.139	1983.54	1.23
			0.10	40.02	231.46	0.145	1981.21	1.24
			0.20	39.79	235.02	0.148	1981.60	1.25
			0.50	39.71	234.58	0.149	1977.65	1.25
		1.00	39.54	232.07	0.148	1992.46	1.27	
PIR	Standard	0.00	40.32	266.09	0.164	3319.21	2.04	
		Cloisite 30B	0.05	40.12	295.49	0.184	3328.50	2.07
			0.10	39.92	309.30	0.194	3333.48	2.09
			0.20	39.78	320.13	0.202	3331.49	2.11
			0.50	39.69	318.70	0.202	3350.41	2.13
			1.00	39.51	316.05	0.202	3325.85	2.13
	Cloisite 25A		0.05	40.14	288.41	0.179	3374.97	2.09
			0.10	39.99	298.31	0.187	3360.37	2.10
			0.20	39.76	303.58	0.192	3328.50	2.11
			0.50	39.68	302.11	0.192	3339.46	2.12
		1.00	39.61	301.00	0.192	3334.81	2.13	

As a result of the introduction of the considered additives into the composition for the synthesis of PIR and PUR foams, there is a slight decrease in the apparent density of the resulting materials. Similar results, confirming the decrease in the foam density with the introduction of small amounts of carbon filler, were obtained by Pikhurov *et al.*<sup>35</sup> It is noted that the proven decrease in the apparent density of the materials under consideration can be explained by the increasing degree of stabilization of the three-dimensional polymer network.<sup>36</sup>

There is gradual increase in the compressive strength index of the obtained composite foams until the mass concentration of the additive is equal to 0.2 %, over that value this index slightly decreases. In the case of Young's modulus, no such trend is observed: this value remains almost unchanged when the fillers considered in this work are introduced, regardless of their concentration. This pattern was previously revealed by Gibson *et al.*,<sup>37</sup> who proved that Young's modulus does not change significantly even with a significant decrease or inc-

rease in the average size of the foam cells (the trends of parameter is described below). On the contrary, the compressive strength index is closely related to the morphology of the cellular structure, increasing with homogeneity of the spatially cross-linked polymer network.

TABLE III. Morphological and thermophysical characteristics of PUR and PIR foams

Foam sample		$\omega$ wt. %	$\bar{\phi}$ $\mu\text{m}$	$A_{y/x}$	$N_f \times 10^{-3}$ cell $\text{cm}^{-3}$	$\lambda$ $\text{mW m}^{-1} \text{K}^{-1}$	$OC$ %	$S_m$ %	
PUR	Standard	0.00	568.32	1.12	5.58	26.41	5.62	–	
		Cloisite 30B	0.05	528.54	1.04	16.13	25.58	5.97	
		0.10	500.12	1.00	20.26	25.34	6.01		
		0.20	454.66	0.97	33.87	25.13	6.13		
		0.50	471.71	0.92	30.79	25.13	6.24		
		1.00	511.49	0.88	29.46	25.19	6.41		
	Cloisite 25A	0.05	539.90	1.06	15.23	25.61	6.01		
		0.10	505.80	0.99	18.47	25.40	6.13		
		0.20	471.71	0.98	32.48	25.22	6.18		
		0.50	488.76	0.91	29.46	25.23	6.29		
		1.00	522.85	0.86	27.44	25.27	6.52		
		Standard	0.00	681.07	1.07	3.27	24.17	6.24	57.03
	PIR	Cloisite 30B	0.05	627.20	1.02	9.78	23.40	6.63	48.35
			0.10	588.72	0.95	12.36	23.17	6.68	46.22
0.20			527.15	0.93	20.79	22.96	6.81	42.03	
0.50			550.24	0.88	18.89	22.97	6.93	42.05	
1.00			604.11	0.85	18.06	23.03	7.12	44.78	
Cloisite 25A		0.05	642.59	1.03	9.25	23.41	6.68	49.35	
		0.10	596.41	0.94	11.23	23.23	6.81	47.01	
		0.20	550.24	0.93	19.93	23.07	6.87	44.27	
		0.50	573.32	0.88	18.06	23.06	6.99	44.61	
		1.00	619.50	0.82	16.82	23.11	7.24	47.04	

The observed difference between the relative strengths of composite foams obtained using Cloisite 30B and Cloisite 25A can be explained by the presence of hydroxyl groups on the surface of Cloisite 30B particles, which contribute to a better distribution of nanosized filler particles over the emerging polymer matrix.

It is known that the strength characteristics of both PIR and PUR foams largely depend on the morphology of the cellular structure of the material.<sup>38</sup> Within the framework of this research, the change in the morphological characteristics of the obtained foams was analysed using the method of scanning electron microscopy. SEM microphotographs examples are presented in Fig. 3: the standard (non-filled) polyurethane and polyurethane–polyisocyanurate foams are shown in Fig. 3A and C, respectively, and microphotographs of nanocomposite foam samples (comprising 0.2 % Cloisite 30B) are shown in Fig. 3B and D.



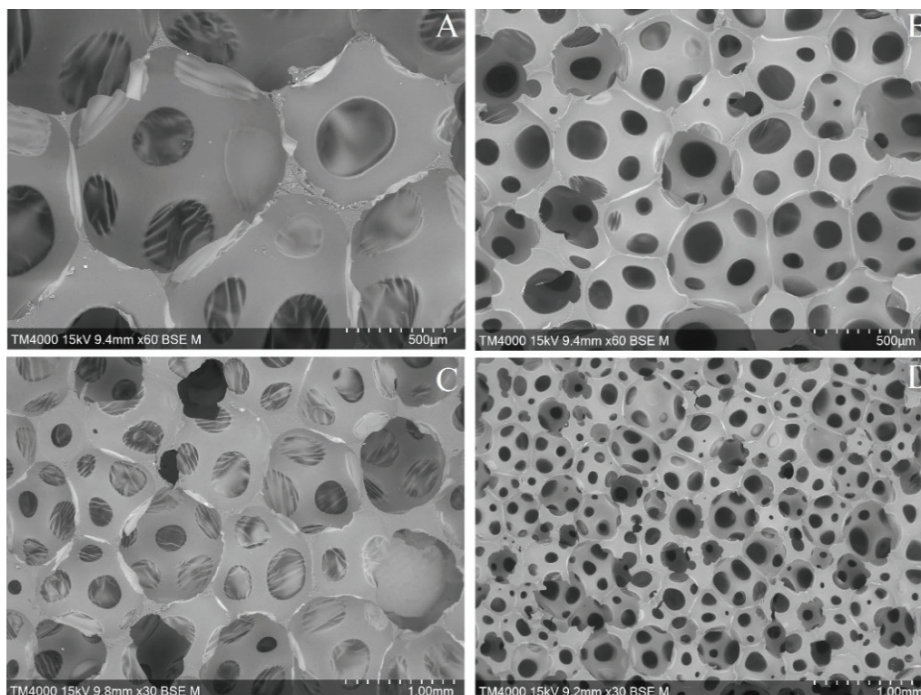


Fig. 3. Microphotographs of the obtained non-composite and composite PUR (A, B) and PIR (C, D) foams.

It should be noted that the introduction of the additives under consideration significantly affects the uniformity of the structure of the final polymer.

It is important to note that the introduction of a filler significantly affects both the average cell size and their density, contributing to the formation of the cells closest in size. It is assumed that such a modification of the cellular structure of the emerging foam makes a significant contribution to the identified increase in the functional characteristics of the foam.

Based on the information presented in Table III, we failed to identify a clear dependence of the anisotropy coefficient of PIR and PUR foams on the type and concentration of the introduced fillers. Nevertheless, it is known that the introduction of such additives can lead to an increase of the anisotropy coefficient of composite foams,<sup>39</sup> however, an increase or decrease in this index has only a slight effect on the performance characteristics of composite foams, which was proved in literature.<sup>35</sup>

It is important to note that in a number of studies, for example,<sup>13,35</sup> as a consequence of the introduction of a filler into the system, an increase in the average cell size is noted. Apparently, this trend is associated with an insufficient degree of dispersion of the solid phase during the preparation of the initial suspensions.

When small amounts of the considered additives are introduced into the composition, a noticeable decrease in their thermal conductivity index is noted. The most noticeable decrease in this characteristic was observed in the case of PIR foams, which may be due to the better distribution of the filler in the polymer matrix. Such an effect is quite natural, since when the filler was dispersed directly in the isocyanate component, the excess of it is shown during the synthesis of PIR foams.

Espadas-Escalante *et al.*<sup>40</sup> noted an increase in the thermal conductivity of composite foams, probably associated with an insufficient degree of homogeneity of the final suspension used for the synthesis of foams.

Since one of the most important characteristics of PIR foams is combustibility, the effect of fillers introduced into the composition on the stability of the final foams was evaluated by assessing the degree of damage by mass during combustion,  $S_m$ . The combustibility of the analysed PIR foams significantly decreases when small additives of the considered fillers are introduced into the composition.

The content of open cells,  $OC$ , in the analysed composite foam plastics naturally increases with the content of filler particles. However, there is an extremely low influence of this parameter on the other properties of PIR and PUR foams considered and described above. It is expected that such an increase in the content of open cells will primarily negatively affect the thermal conductivity of the synthesized foams, however, the thermal insulation properties of the obtained foams only increase, which leads to a conclusion that the degree of influence of such a small content of opened cells is negligible.

The relative compressive strength,  $\bar{\Phi}$ , directly depends on the average cell size of the foams, increasing with a decrease in average cell size of the resulting foamed material. We conclude that in order to improve the strength characteristics of foam plastics, it is extremely advisable to obtain foam plastics with the best morphology of the cellular structure, including the lowest average cell size.

#### CONCLUSION

Thus, when using small amounts of chemically modified nanoclays (Cloisite 30B, Cloisite 25A), two series of composite polyurethane and polyurethane–polyisocyanurate foams were obtained. The main physical-mechanical, thermo-physical and morphological characteristics of the synthesized materials have been studied. It is shown that the introduction of small additives of the considered fillers leads to an improvement in the main performance characteristics of PIR and PUR foams: an increase in relative compressive strength, a decrease in thermal conductivity and a damage of mass during combustion. Based on the data obtained, it is expected that the use of the nanosized fillers described in the

work will be appropriate in the development of new industrially used heat-insulating foams.

#### SUPPLEMENTARY MATERIAL

Additional data and information are available electronically at the pages of journal website: <https://www.shd-pub.org.rs/index.php/JSCS/article/view/12125>, or from the corresponding author on request.

#### ИЗВОД

#### УТИЦАЈ НАНОГЛИНЕ НА МЕХАНИЧКА И ТОПЛОТНА СВОЈСТВА КРУТИХ ПИР И PUR ПЕНА

RUSLAN R. VLASOV<sup>1</sup>, DARIA I. RYABOVA<sup>1</sup>, SAKINA Z. ZEYNALOVA<sup>2</sup>, DMITRY V. SOKOLOV<sup>1</sup>  
и SERGEI A. RYABOV<sup>1</sup>

<sup>1</sup>Lobachevsky State University – Faculty of Chemistry, Department of Macromolecular Compounds and Colloidal Chemistry, Gagarina av. 23, 603098 Nizhny Novgorod, Russia и <sup>2</sup>Tre Tau Engineering srl, Pietro Colletta 85, 10153 Torino, Italy

Проучаван је ефекат додавања малих количина (од 0,05 до 1 мас. %) наночестица глина на морфологију, физичко-механичке и термофизичке карактеристике крутих полиуретан–полиизоцијануратних (PIR) и полиуретанских (PUR) пена. Процењени су ефекти ових адитива на структуру добијеног материјала, промену његове компресивне чврстоће, Јангов моду еластичности, губитак масе током сагоревања и топлотну проводљивост. На основу добијених резултата закључено је да додавање малих количина (до 0,2 мас. %) хемијски модификоване Cloisite 30В наноглине ефикасно смањује просечну величину ћелија нанокомполитних пена, што доводи до побољшања својстава пена.

(Примљено 3. новембра, ревидирано 8. децембра, прихваћено 21. децембра 2022)

#### REFERENCES

1. U. Stirna, I. Beverte, V. Yakushin, U. Cabulis, *J. Cell. Plast.* **47** (2011) 337 (<https://doi.org/10.1177/0021955X1139838>)
2. H. Ulrich, *J. Cell. Plast.* **17** (1981) 31 (<https://doi.org/10.1177/0021955X8101700102>)
3. A. Al Nabulsi, D. Cozzula, T. Hagen, W. Leitner, T. E. Muller, *Polym. Chem.* **9** (2018) 4891 (<https://doi.org/10.1039/C8PY00637G>)
4. J. N. Gibb, J. M. Goodman, *Org. Biomol. Chem.* **11** (2013) 90 (<https://doi.org/10.1039/C2OB26547H>)
5. Bozyel, Y. I. Keser, D. Gokcen, *Sens. Actuators, A* **332** (2021) 113056 (<https://doi.org/10.1016/j.sna.2021.113056>)
6. G. Tao, J. Yuan, Q. Chen, W. Peng, R. Yu, S. Basack, *Constr. Build. Mater.* **295** (2021) 123609 (<https://doi.org/10.1016/j.conbuildmat.2021.123609>).
7. X. Zhang, S. Sun, B. Liu, Z. Wang, H. Xie, *Int. J. Polym. Anal. Charact.* **27** (2022) 302 (<https://doi.org/10.1080/1023666X.2022.2070694>)
8. A. M. Norouzi, M. E. Kojabad, M. Chapalaghi, A. Hosseinkhani, A. A. Nareh, E. N. Lay, *J. Mol. Liq.* **360** (2022) 119540 (<https://doi.org/10.1016/j.molliq.2022.119540>)
9. E. Ciecierska, M. Jurczyk-Kowalska, P. Bazarnik, M. Gloc, M. Kulesza, M. Kowalski, S. Krauze, M. Lewandowska, *Compos. Struct.* **140** (2016) 67 (<https://doi.org/10.1016/j.compstruct.2015.12.022>)

10. L. Madaleno, R. Pyrz, A. Crosky, L. R. Jensen, J. C. M. Rauhe, V. Dolomanova, A. M. M. V. B. Timmons, J. J. C. Pinto, J. Norman, *Composites, A* **44** (2013) 1 (<https://doi.org/10.1016/j.compositesa.2012.08.015>)
11. C. Caglayan, I. Gurkan, S. Gungor, H. Cebeci, *Composites, A* **115** (2018) 187 (<https://doi.org/10.1016/j.compositesa.2018.09.019>)
12. M. Modesti, A. Lorenzetti, S. Besco, *Polym. Eng. Sci.* **47** (2007) 1351 (<https://doi.org/10.1002/pen.20819>)
13. D. Yan, L. Xu, C. Chen, J. Tang, X. Ji, Z. Li, *Polym. Int.* **61** (2012) 1107 (<https://doi.org/10.1002/pi.4188>)
14. J. Espadas-Escalante, F. Aviles, *Mech. Mater.* **91** (2015) 167 (<https://doi.org/10.1016/j.mechmat.2015.07.006>)
15. S. Q. Tan, T. Abraham, D. Ference, C. W. Macosko, *Polymer* **52** (2011) 2840 (<https://doi.org/10.1016/j.polymer.2011.04.040>)
16. M. Modesti, A. Lorenzetti, C. Dall'Acqua, *Polym. Eng. Sci.* **45** (2005) 260 (<https://doi.org/10.1002/pen.20272>)
17. M. S. Han, Y. H. Kim, S. J. Han, S. J. Choi, S. B. Kim, W. N. Kim, *J. Appl. Polym. Sci.* **110** (2008) 376 (<https://doi.org/10.1002/app.28521>)
18. S. Semenzato, A. Lorenzetti, M. Modesti, E. Ugel, D. Hrelja, S. Besco, R. A. Michelin, A. Sassi, G. Facchin, F. Zorzi, R. Bertani, *Appl. Clay Sci.* **44** (2009) 35 (<https://doi.org/10.1016/j.clay.2009.01.003>)
19. T. U. Parto, G. Harikrishnan, A. Misra, D. V. Khakhar, *Polym. Eng. Sci.* **48** (2008) 1778 (<https://doi.org/10.1002/pen.21145>)
20. Xu, T. S. Fisher, *Int. J. Heat Mass Transfer* **49** (2006) 1658 (<https://doi.org/10.1016/j.ijheatmasstransfer.2005.09.039>)
21. C. C. Zeng, N. Hossieny, C. Zhang, B. Wang, *Polymer* **51** (2010) 655 (<https://doi.org/10.1016/j.polymer.2009.12.032>)
22. X. M. Han, C. C. Zeng, L. J. Lee, K. W. Koelling, D. L. Tomasko, *Polym. Eng. Sci.* **43** (2003) 1261 (<https://doi.org/10.1002/pen.10107>)
23. J. Bhinder, P. K. Agnihotri, *J. Cell. Plast.* **57** (2020) 287 (<https://doi.org/10.1177/0021955X20917280>)
24. D. X. Yan, K. Dai, Z. D. Xiang, Z. M. Li, X. Ji, W. Q. Zhang, *J. Appl. Polym. Sci.* **120** (2011) 3014 (<https://doi.org/10.1002/app.33437>)
25. J. Xiong, D. Zhou, Z. Zheng, X. Yang, X. Wang, *Polymer* **47** (2006) 1763 (<https://doi.org/10.1016/j.polymer.2006.01.083>)
26. ISO 3219-2:2021: *Rheology — Part 2: General principles of rotational and oscillatory rheometry* (2021)
27. ISO 148696:2009: *Plastics — Polyurethane raw materials — Determination of isocyanate content* (2009)
28. ASTM D1622-20: *Standard Test Method for Apparent Density of Rigid Cellular Plastics* (2020)
29. EN 826:2013: *Thermal insulating products for building applications - Determination of compression behaviour* (2013)
30. ASTM D6226-05: *Standard Test Method for Open Cell Content of Rigid Cellular Plastics* (2005)
31. EN 12667:2001: *Building materials and products of high and medium thermal resistance. Methods of determination of thermal resistance by means of guarded hot plate and heat flow meter* (2001)

32. C. Brondi, E. D. Maio, L. Bertucelli, V. Parenti, T. Mosciatti, *J. Cell. Plast.* **58** (2022) 121 (<https://doi.org/10.1177/0021955X2098715>)
33. V. Kumar, N. P. Suh, *Polym. Eng. Sci.* **30** (1990) 1323 (<https://doi.org/10.1002/pen.760302010>)
34. J. E. Weller, V. Kumar, *Polym. Eng. Sci.* **50** (2010) 2160 (<https://doi.org/10.1002/pen.21736>)
35. D. V. Pikhurov, *PhD thesis*, ITMO University, Saint-Petersburg, 2018, p. 128 ([https://technolog.edu.ru/cms\\_files/p\\_file/36678307961e2d694eac98](https://technolog.edu.ru/cms_files/p_file/36678307961e2d694eac98))
36. D. V. Pikhurov, A. S. Sakhatskii, V. V. Zuev, *Eur. Polym. J.* **99** (2018) 403 (<https://doi.org/10.1016/j.eurpolymj.2017.12.036>)
37. J. Gibson, M. F. Ashby, *Cellular Solids. Structure and properties*, 2<sup>nd</sup> ed., Cambridge University Press, Cambridge, 1997, pp. 175–279 (<https://doi.org/10.1017/CBO9781139878326>)
38. R. Yang, W. Hu, L. Xu, Y. Song, J. Li, *Polym. Degrad. Stab.* **112** (2015) 102 (<https://doi.org/10.1016/j.polymdegradstab.2015.10.007>)
39. Oliveira-Salmazo, A. Lopez-Gil, F. Silva-Bellucci, A. E. Job, M. A. Rodriguez-Perez, *Ind. Crops Prod.* **80** (2016) 26 (<https://doi.org/10.1016/j.indcrop.2015.10.050>).
40. J. J. Espadas-Escalante, F. Aviles, P. I. Gonzalez-Chi, A. Oliva, *J. Cell. Plast.* **53** (2016) 215 (<https://doi.org/10.1177/0021955X16644893>).

SUPPLEMENTARY MATERIAL TO  
**The influence of nanoclays on the mechanical and thermal  
properties of rigid PIR and PUR foams**

RUSLAN R. VLASOV<sup>1\*</sup>, DARIA I. RYABOVA<sup>1</sup>, SAKINA Z. ZEYNALOVA<sup>2</sup>,  
DMITRY V. SOKOLOV<sup>1</sup> and SERGEI A. RYABOV<sup>1</sup>

<sup>1</sup>Lobachevsky State University – Faculty of Chemistry, Department of Macromolecular  
Compounds and Colloidal Chemistry, Gagarina av. 23, 603098 Nizhny Novgorod, Russia  
and <sup>2</sup>Tre Tau Engineering srl, Pietro Colletta 85, 10153 Torino, Italy

*J. Serb. Chem. Soc.* 88 (4) (2023) 409–421

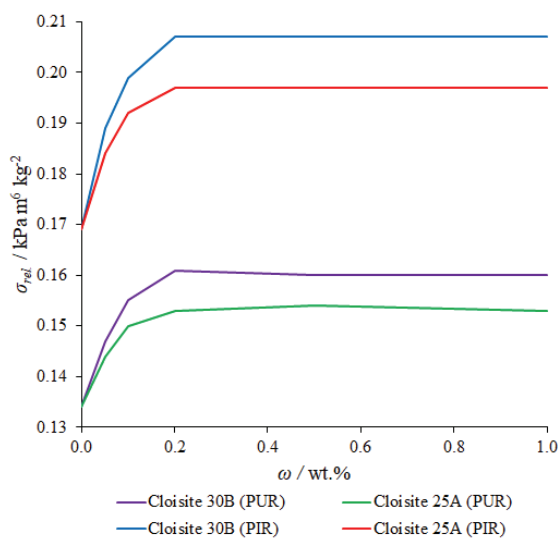


Fig. S-1. Dependence of relative compressive strength on filler content.

\* Corresponding author. E-mail: vlasovruslan.hs@yandex.ru

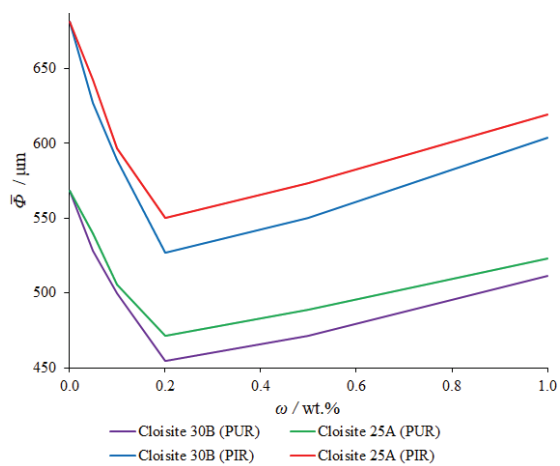


Fig. S-2. Dependence of the change in the average cell size of the composite foam on the content of the filler.

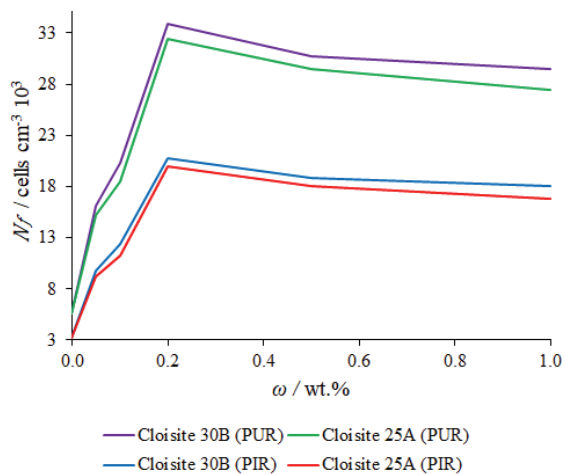


Fig. S-3. Dependence of cell density change in composite foams on filler content.

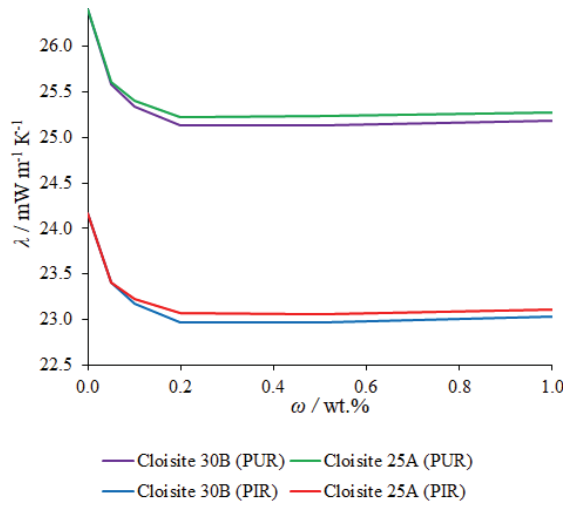


Fig. S-4. The dependence of thermal conductivity of composite foams from filler content.

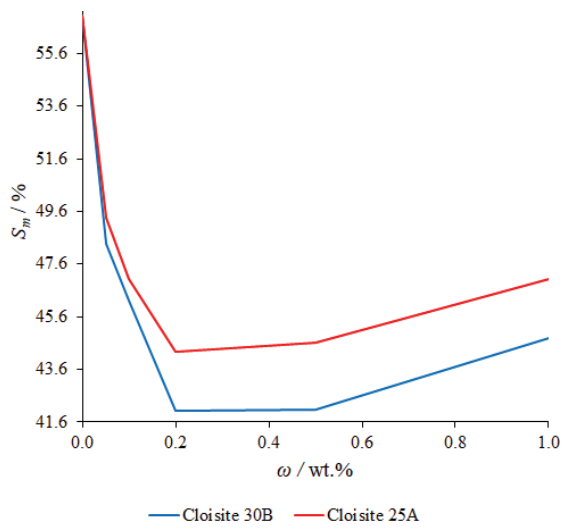


Fig. S-5. The dependence of damage by mass of composite foams from filler content.



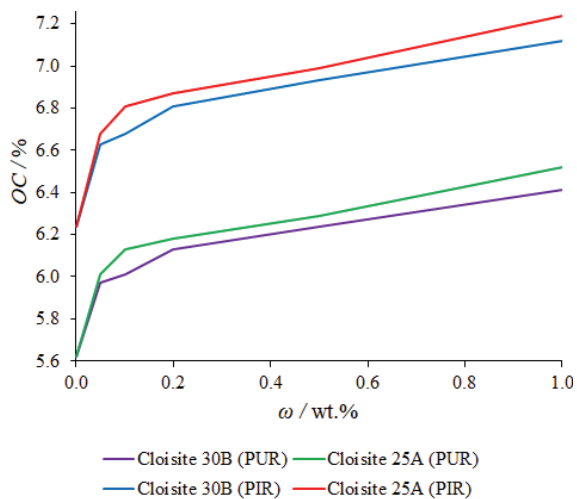
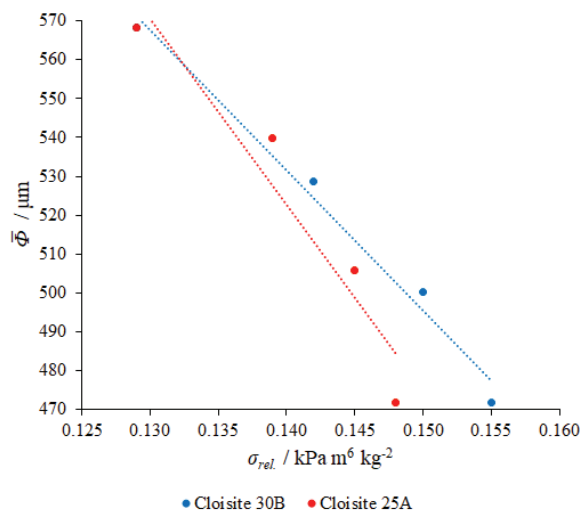


Fig. S-6. The dependence of the content of open cells in composite foams on the content of the filler.



Fig, S-7. Dependence of relative compressive strength from the average cell size of composite foams.





*J. Serb. Chem. Soc.* 88 (4) 423–435 (2023)  
JSCS–5636

## Performance of carbon-coated magnetic nanocomposite in methylene blue and arsenate treatment from aqueous solution

NGOC BICH NGUYEN<sup>1,2\*</sup>, THI QUE PHUONG PHAN<sup>3</sup>, CAO THANH TUNG PHAM<sup>1,4</sup>,  
HUU NGHI NGUYEN<sup>2</sup>, SY NGUYEN PHAM<sup>5</sup>, QUOC KHUONG ANH NGUYEN<sup>6\*\*\*</sup>  
and DINH THANH NGUYEN<sup>1,3\*\*\*</sup>

<sup>1</sup>Graduate University of Science and Technology, Viet Nam Academy of Science and Technology, Hanoi City, 100000, Vietnam, <sup>2</sup>Dong Thap University, Cao Lanh City, 870000, Vietnam, <sup>3</sup>Institute of Applied Materials Science, Viet Nam Academy of Science and Technology, Ho Chi Minh City, 700000, Vietnam, <sup>4</sup>Institute of Chemical Technology, Viet Nam Academy of Science and Technology, Ho Chi Minh City, 700000, Vietnam, <sup>5</sup>Ho Chi Minh City University of Natural Resources and Environment, Vietnam and <sup>6</sup>Institute of Applied Technology and Sustainable Development, Nguyen Tat Thanh University, Ho Chi Minh City, 70000, Vietnam

(Received 2 August, revised 5 October, accepted 3 November 2022)

**Abstract:** Herein, carbon-coated magnetic nanocomposite fabricated by a low-temperature hydrothermal method was used for methylene blue and arsenate treatment in aqueous solution. The Langmuir model fits the experimental data with a calculated maximum adsorption capacity of 110.63 and 2.31 mg g<sup>-1</sup> for methylene blue and arsenate adsorption, respectively. Furthermore, the adsorption mechanisms of methylene blue as well as arsenate are physical adsorption and a combination of physical adsorption and chemisorption, respectively. Gibbs energy change with negative values indicates that methylene blue and arsenate adsorption on magnetic materials occurs naturally. This research demonstrated a simple, efficient, and reliable method for removing methylene blue and arsenate.

**Keywords:** hydrothermal carbonization; rice straw; adsorption.

### INTRODUCTION

The rapid development of industries has posed many potentially serious issues in relation to ecosystems such as heavy metal and dye contamination.<sup>1</sup> Several technologies have been introduced for wastewater treatment, including oxidation, photocatalytic degradation, ultrafiltration, adsorption/precipitation process and coagulation.<sup>2</sup> Adsorption has been regarded as one of the most common

\* Corresponding authors. E-mail: (\*)nmbich@dthu.edu.vn; (\*\*)nqkanh@ntt.edu.vn; (\*\*\*)dinhthanhg53@gmail.com  
<https://doi.org/10.2298/JSC220802080N>

and effective techniques for contaminant removal from wastewater.<sup>3</sup> Recently, carbon material derived from low-cost biomass residuals such as rice straw has received a lot of attention due to its potential environmental benefits.<sup>4</sup> Moreover, magnetic modifications of the low-cost adsorbents can result in novel adsorbents that can be rapidly removed from the treated solution using a magnetic separator.<sup>5</sup>

Methylene blue (MB) is used in many fields, so a significant amount of MB ends up in wastewater, posing a risk to aquatic life. In addition, due to its high toxicity, arsenic can cause serious health problems such as lung, liver, kidney, and skin cancers.<sup>6–11</sup> As a result, it is critical to investigate efficient technologies for extracting MB and As(V) from aqueous solutions.<sup>12–16</sup> Rice straw (RS) is an inexpensive and abundant carbon-containing lignocellulose in Vietnam. In the paper industry, biomass is usually pre-alkali-treated to remove lignin. As a result, this process emits a large amount of black liquor containing lignin, which can be utilized for carbon-containing materials.<sup>17</sup>

In this study, we simultaneously carbonize and magnetize the lignin liquor obtained from rice straw to synthesize carbon-coated magnetic nanocomposite (CMC) by a hydrothermal method. The primary goal of this work is to study the potential adsorption of low-cost CMC for MB and As(V) from wastewater. Aside from that, another goal is to evaluate the effect of concentration, contact time, temperature and pH solution. This work also discusses the Langmuir and Freundlich adsorption isotherm models, as well as various thermodynamic parameters like change in heat of adsorption ( $\Delta H^\circ$ ), entropy change ( $\Delta S^\circ$ ) and Gibbs energy change ( $\Delta G^\circ$ ) in MB and As(V) adsorption.

## EXPERIMENTAL

### *Materials*

RS was collected in Vietnam and washed several times with distilled water before being milled into powder and filtered through a 250-mesh sieve.

Potassium hydroxide (KOH,  $\geq 85\%$ ), sodium hydroxide (NaOH,  $\geq 97\%$ ), hydrochloric acid (HCl, 37%), iron(III) nitrate nonahydrate ( $\text{Fe}(\text{NO}_3)_3 \cdot 9\text{H}_2\text{O}$ ,  $\geq 99\%$ ), sodium chloride (NaCl,  $\geq 99.5\%$ ),  $\text{H}_3\text{AsO}_4$  in  $\text{HNO}_3$  0.5 mol L<sup>-1</sup> 1000 mg L<sup>-1</sup> purchased from Merck. MB ( $\text{C}_{16}\text{H}_{18}\text{N}_3\text{SCl} \cdot \text{H}_2\text{O}$ , 99.5%), was obtained from Sigma–Aldrich. All chemicals used were of analytical grade and were used as received without any further purification.

### *Synthesis of carbon-coated magnetic nanocomposite*

Firstly, 15 g of RS was combined with 150 ml KOH 5%. The mixture was hydrothermally treated in an autoclave at 120 °C for 4 h. After slowly mixing 50 ml of 0.125 mol  $\text{Fe}(\text{NO}_3)_3$  into 125 ml of the above-solution for 2 h, hydrothermal treatment was carried out at 180 °C for 14 h. The CMC is then collected by filtration and rinsed several times with distilled water until the pH value reached neutral. Finally, the remaining solid was dried in an oven at 40 °C for 12 h. In comparison, a blank sample (BS) was fabricated under the same condition but without the addition of  $\text{Fe}(\text{NO}_3)_3$ .

### Characterization of CMC

X-ray diffraction (XRD) was carried out ON X D8 Advance Bruker with  $\text{CuK}_\alpha$  radiation ( $\lambda = 0,15418$  nm). The morphology was observed with S4800 Hitachi scanning electron microscope (SEM) and JEM1400 JEOL transmission electron microscopy (TEM). Energy-dispersive X-ray spectrum (EDS) was recorded on H7593 Horiba. The Fourier transform infrared (FT-IR) spectroscopy was measured on IR Affinity-1S spectrophotometer (Shimadzu). The specific surface area (BET) was determined by  $\text{N}_2$  adsorption–desorption isotherms at liquid nitrogen temperature (77 K) using Quantachrome TriStar 3000 V6.07A adsorption instruments. Magnetization measurements were carried out using a vibrating sample magnetometer (VSM) 7307, Lake Shore, USA. The UV–Vis spectrometry was recorded on Spectro UV-2650, Labomed, USA, at a wavelength of 664 nm. Residual As(V) was detected by Thermo Scientific iCAP Q ICP–MS. The point of zero charge ( $\text{pH}_{\text{PZC}}$ ) of CMC was investigated by the solid addition method.<sup>18</sup> A series of 45 mL of 0.5 M NaCl solutions were prepared in 100 mL flasks. The initial pH value ( $\text{pH}_i$ ) of the solution was adjusted from 2 to 12 using either 0.1 M NaOH or 0.1 M HCl solutions. The total volume of solution in each flask was precisely 50 mL by adding distilled water. Then, 0.1 g of CMC was added to each flask and kept on shaker at 180 rpm for 24 h. The final pH ( $\text{pH}_f$ ) of the solutions was recorded. The difference between the initial and final pH ( $\Delta\text{pH} = \text{pH}_i - \text{pH}_f$ ) was plotted against  $\text{pH}_i$ . The point of intersection of the curve with the abscissa, where  $\Delta\text{pH} = 0$ , presented  $\text{pH}_{\text{PZC}}$ .

### Adsorption experiment

Adsorption experiments were carried out using 0.1 g CMC in 100 mL of solution. Variable parameters including initial concentration, contact time, temperature, and pH of the medium were thoroughly investigated. The initial pH value of the solution was adjusted using either 0.1 M NaOH or 0.1 M HCl solutions. All adsorption experiments were carried out in duplicate. At predetermined time intervals, the adsorbent and solution were separated, and the residual MB and As(V) concentrations in the solution were measured using UV–Vis and ICP–MS, respectively.

The removal rate,  $R / \%$ , was calculated as:

$$R = 100(C_0 - C_e)/C_0 \quad (1)$$

where  $C_0$  and  $C_e$  are the initial and equilibrium concentrations of MB or As(V) solution. We listed different kinetic models, thermodynamic equations, and adsorption isotherms in Table S-I of the Supplementary material to this paper.

### Non-linear chi-square test

Optimization is indispensable in order to identify the suitable kinetic and isotherm models to the obtained experimental results. For the present study, apart from correlation coefficient ( $R^2$ ), a non-linear regression model is chi-square test was performed for data optimization process. The chi-square ( $\chi^2$ ) can be expressed as equation (2):

$$\chi^2 = \sum \frac{(q_{e,\text{exp}} - q_{e,\text{cal}})^2}{q_{e,\text{cal}}} \quad (2)$$

where  $q_{e,\text{exp}}$  is the experimental value of adsorption capacity and  $q_{e,\text{cal}}$  is the calculated value from the model. If experimental data is analogous to that from the model,  $\chi^2$  will be small, otherwise, it will be large.

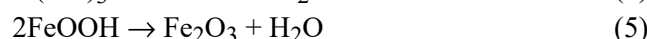
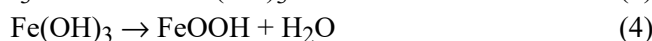
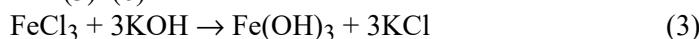
### Reusability

0.1 g CMC was added to 100 mL of a solution ( $120 \text{ mg L}^{-1}$  for MB and  $2.5 \text{ mg L}^{-1}$  for As(V) and stirred for 60 and 90 min, respectively, for saturated adsorption. Following the magnetic separation, the supernatant solution was discarded, and only adsorbed CMC was collected. The adsorbed CMC in the case of MB was then added to ethanol and a 0.1 M HCl solution in the case of As(V) for the desorption process.<sup>13,14</sup> The experiments were repeated 5 times in sequence to estimate the potentially regenerable property of CMC.

## RESULTS AND DISCUSSION

### Characterization of materials

As shown in Fig. 1a, regarding BS, the broad peak at  $2\theta = 22^\circ$  represented the characteristic reflection of carbon.<sup>19</sup> In CMC, the diffractions at  $2\theta$  30.46, 35.86, 43.58, 57.25 and  $62.65^\circ$  correspond to crystalline magnetite  $\text{Fe}_3\text{O}_4$  (JCPDS No. 19-0629), which agree with the literature data.<sup>20</sup> This demonstrated that Fe(III) is reduced into  $\text{Fe}_3\text{O}_4$  by carbon, which is formed under hydrothermal conditions by the reactions (3)–(6):<sup>2</sup>



In Fig. 1b, FT-IR spectra revealed that both BS and CMC contained functional groups at  $3413\text{--}3422 \text{ cm}^{-1}$  ( $-\text{OH}$  stretching vibrations),  $1627\text{--}1630 \text{ cm}^{-1}$  ( $\text{C}=\text{O}$  stretching vibration),  $1110\text{--}1114 \text{ cm}^{-1}$  ( $\text{C}-\text{O}$  stretching vibration),  $799\text{--}818 \text{ cm}^{-1}$  and  $450\text{--}474 \text{ cm}^{-1}$  ( $\text{Si}-\text{O}-\text{Si}$  stretching vibration) and  $1451\text{--}1456 \text{ cm}^{-1}$  ( $-\text{O}-\text{CH}_3$  deformation vibration).<sup>1,18,20</sup> In general, the intensity of all peaks in CMC is lower than that of BS and has a slight shift, indicating that chemical reactions occurred when  $\text{Fe}^{3+}$  was added to the solution. The peak near  $560 \text{ cm}^{-1}$ , assigned to the  $\text{Fe}-\text{O}$  stretching vibration, was only visible in CMC, which is consistent with XRD result.<sup>12</sup>

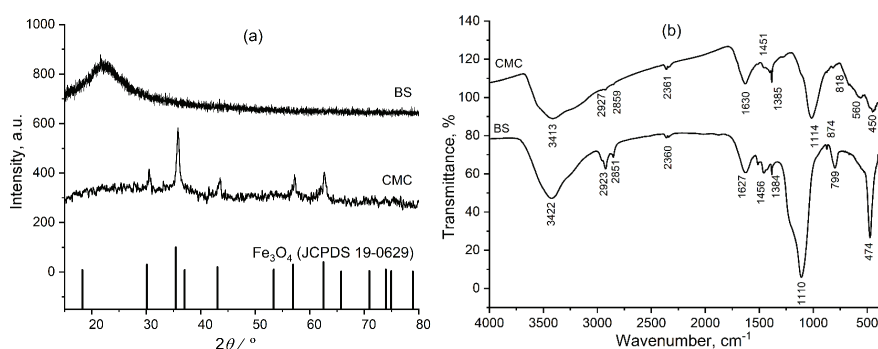


Fig. 1. a) XRD patterns of BS, CMC and standard  $\text{Fe}_3\text{O}_4$  (JCPDS No. 19-0629); b) FT-IR spectra of BS and CMC.

According to Figs. S-1 and S-2 of the Supplementary material, CMC is made up of C (19.21 %), O (34.38 %), Fe (42.24 %) and Si (4.16 %). In addition, EDS elemental mapping also shows that Fe is uniformly dispersed on the surface of the material, proving that iron oxide was formed in CMC. Fig. 2a and b depicts typical TEM and SEM images of CMC containing  $\text{Fe}_3\text{O}_4$  with sizes ranging from 50 to 120 nm and carbon as a shell with a thickness ranging from 30 to 50 nm. At room temperature, Fig. S-3 shows the saturation magnetisation value of  $33.7 \text{ emu g}^{-1}$ , which allows for the rapid separation and redistribution of CMC from aqueous solution and leads to cost-effective and reusable applications.<sup>21</sup> Table S-II compares the magnetization of CMC with various biochar.

Table S-III displayed specific surface area, total pore volume, and mean pore size for RS, BS, and CMC. The specific surface area of CMC ( $171.4 \text{ m}^2 \text{ g}^{-1}$ ) is significantly greater than that of BS ( $6.6 \text{ m}^2 \text{ g}^{-1}$ ) thanks to the combination of carbon and magnetic particles.<sup>22</sup> Furthermore, the mean pore size of CMC (6 nm) is smaller than that of BS (33 nm), attributed to the covered micropores in carbon.<sup>23</sup>

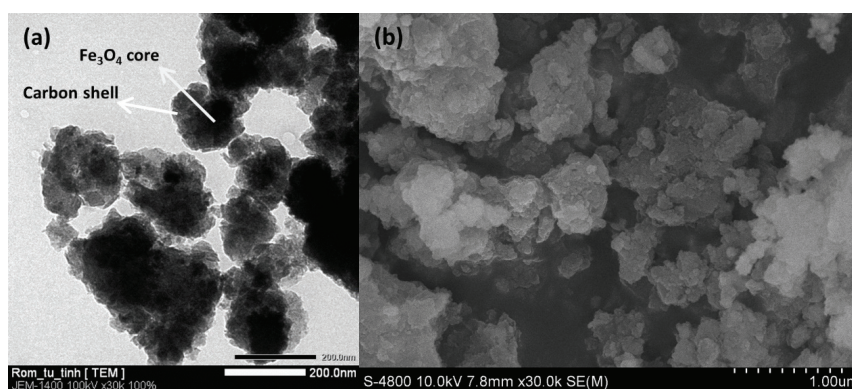


Fig. 2. TEM (a) and SEM (b) images of CMC.

#### *Effect of initial solution pH*

The pH of the solution plays an important role in the adsorption process, particularly in terms of adsorption capacity.<sup>24</sup> Because of the changing surface of CMC on MB and As(V), the pH value can alter its performance.<sup>25</sup> Investigation on the influence of initial pH solutions from 3 to 11 was carried out while keeping other parameters constant such as initial concentration ( $120$  and  $2.5 \text{ mg L}^{-1}$ ), equilibrium time (60 and 90 min at 303 K) for MB and As(V), respectively. The effect of pH on the adsorption of MB and As(V) on CMC is depicted in Fig. 3a and b.

The adsorption capacity of MB increases from 3 to 7 and changes slightly when solution pH exceeds 7. When  $\text{pH} < \text{pH}_{\text{PZC}}$ , the surface charge is positive,

and when  $\text{pH} > \text{pH}_{\text{pZC}}$ , the surface charge is negative. The  $\text{pH}_{\text{pZC}}$  of CMC is approximately 6.32 (Fig. S-4).

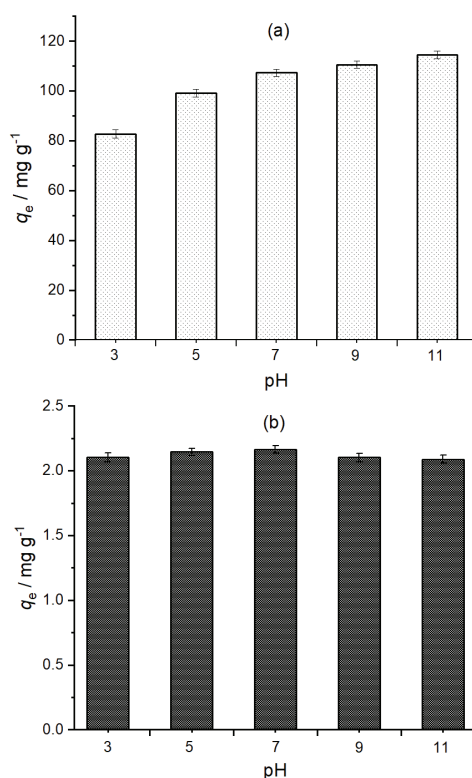


Fig. 3. Influence of pH value on the adsorption of: a) MB and b) As(V).

At low pH, low adsorption capacity resulted from electrostatic repulsion between the cationic ion MB and positively charged active sites on CMC. Electrostatic attraction occurs between negatively active sites on CMC and the cationic ion MB at higher pH levels, facilitating adsorption capacity. Arsenic acid exists in anionic forms ( $\text{H}_2\text{AsO}_4^-$ ,  $\text{HAsO}_4^{2-}$ ,  $\text{AsO}_4^{3-}$ ).<sup>26</sup> Moreover, CMC with positively charged active sites can attract arsenate ions, increasing adsorption capacity from 84.12 to 86.6 %. In contrast, at pH ranging 7 to 11, CMC with negatively charged active sites inhibited As(V) adsorption due to  $\text{OH}^-$  competing with arsenates, resulting in a decrease in yield to 83.54 %.<sup>27</sup> Hence, the initial pH solution for the following experiments is 7.

#### Adsorption thermodynamics

A linear van't Hoff plot (Fig. 4a and b) of  $\ln K_D$  versus  $1/T$  gives slope and intercept to determine the value of  $\Delta H^\circ$  and  $\Delta S^\circ$ , respectively. The calculated



thermodynamic parameters for MB and As(V) adsorption onto CMC are summarized in Table I at different temperatures. As temperature rises, the value of  $\Delta G^\circ$  becomes more negative, resulting in more spontaneous adsorption with high affinity of MB and As(V) to CMC. The value of  $\Delta H^\circ$  for absolute physical adsorption is typically less than  $20 \text{ kJ mol}^{-1}$ , whereas chemisorption is in the range of  $80$  to  $200 \text{ kJ mol}^{-1}$ .<sup>28,29</sup>

$\Delta H^\circ$  of MB on CMC is  $15.06 \text{ kJ mol}^{-1}$  indicates physical adsorption while the value of  $\Delta H^\circ$  ( $22.32 \text{ kJ mol}^{-1}$ ) for As(V) on CMC should be regarded as a mixture of physical adsorption and chemisorption, but dominated by physical adsorption, since the  $\Delta H^\circ$  was a slightly higher than  $20 \text{ kJ mol}^{-1}$ . With positive values of  $\Delta S^\circ$ , there is an affinity adsorbent for adsorbate.

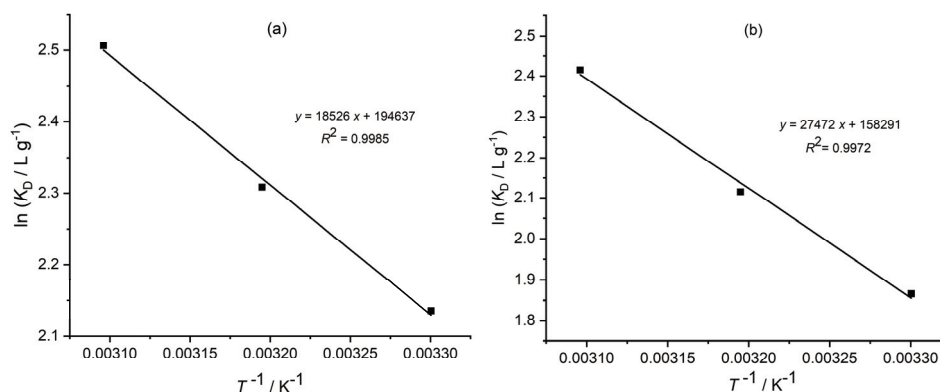


Fig. 4. The plot of  $\ln K_D$  vs.  $1/T$  for: a) MB and b) As(V) adsorption onto CMC.

TABLE I. Thermodynamic parameters for adsorption of adsorbates onto CMC

Adsorbate	Temperature, K	$\Delta S^\circ / \text{J mol}^{-1} \text{K}^{-1}$	$\Delta H^\circ / \text{kJ mol}^{-1}$	$\Delta G^\circ / \text{kJ mol}^{-1}$
MB	303	67.41	15.06	-5.38
	313			-6.01
	323			-6.73
As	303	89.10	22.32	-4.70
	313			-5.51
	323			-6.49

#### Effect of contact time and adsorption kinetics

For both MB and As(V), contact intervals of 0 to 105 min and 0 to 120 min are used to evaluate the adsorption process as a function of contact time, respectively. The adsorption of MB and As(V) occurs in three stages. Firstly, the adsorption rate for MB increases significantly in 10 and 30 min for As(V). The reason for this is that at the start, many vacant sites are available for adsorption. Then, it will gradually rise until it reaches the equilibrium value of 30 min for

MB and 75 min for As(V) (Fig. 5a and b), resulting from the fewer vacant sites and repulsive forces between the occupied sites and bulk phases.

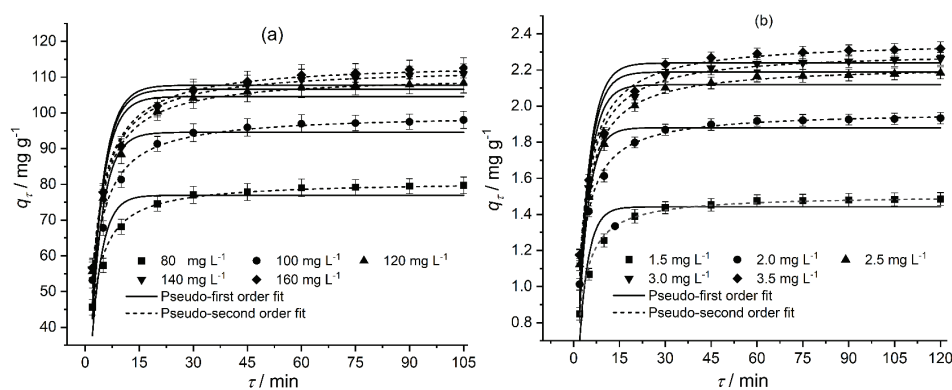


Fig. 5. Kinetic modeling for adsorption of: a) MB and b) As(V) onto CMC.

Therefore, we determined that the adsorption time for the next experiment will be 60 min for MB and 90 min for As(V). Adsorption of MB on the surface of CMC is physical, whereas adsorption of As(V) is both physical and chemical process, resulting in As(V) adsorption being slower than that of MB.<sup>30,31</sup>

To investigate the experimental data, different kinetic models including pseudo-first-order and pseudo-second-order were used to understand the adsorption process. The kinetic parameters, correlation coefficient ( $R^2$ ) and non-linear chi-square ( $\chi^2$ ) were listed in Table II.

TABLE II. Kinetic parameters for adsorption of a) MB; b) As(V) onto CMC at 303 K

Adsorbate	$C_0$ mg L <sup>-1</sup>	First-order kinetic model					Second-order kinetic model			
		$q_{e,exp}$ mg g <sup>-1</sup>	$k_1$ min <sup>-1</sup>	$q_{e,cal}$ mg g <sup>-1</sup>	$R^2$	$\chi^2$	$k_2$ g mg <sup>-1</sup> min <sup>-1</sup>	$q_{e,cal}$ mg g <sup>-1</sup>	$R^2$	$\chi^2$
MB	80	79.74	0.3357	76.94	0.864	3.043	0.0071	80.87	0.987	0.274
	100	98.03	0.2972	94.56	0.875	4.403	0.0050	99.72	0.986	0.459
	120	108.35	0.2870	104.55	0.900	3.950	0.0042	110.51	0.994	0.207
	140	110.91	0.2830	106.58	0.899	4.120	0.0041	112.78	0.995	0.193
	160	112.57	0.2796	107.75	0.893	4.473	0.0039	114.12	0.994	0.244
As(V)	1.5	1.482	0.3325	1.442	0.867	0.059	0.3774	1.507	0.987	0.006
	2.0	1.929	0.3084	1.880	0.915	0.053	0.2608	1.971	0.998	0.001
	2.5	2.179	0.2784	2.119	0.902	0.089	0.2049	2.227	0.993	0.006
	3.0	2.257	0.2752	2.189	0.888	0.104	0.1961	2.302	0.991	0.009
	3.5	2.312	0.2713	2.239	0.886	0.108	0.1855	2.362	0.989	0.010

The calculated  $q_e$  values ( $q_{e,cal}$ ) of both models are comparable to the experimental ones ( $q_{e,exp}$ ). However, the  $R^2$  of the pseudo-second-order kinetic model (approximately 0.99 for  $R^2$ ) is significantly higher than that of pseudo-

-first-order kinetic model (approximately 0.90 for  $R^2$ ), conversely, ( $\chi^2$ ) of the pseudo-second-order kinetic model is significantly lower than that of pseudo-first-order kinetic model, implying that the pseudo-second-order kinetic model is better for adsorption kinetics of MB and As(V) onto CMC.

#### Effect of initial concentration and adsorption isotherms

Fig. 6a and b indicated that the adsorption capacity of MB and As(V) onto CMC significantly increases with increasing ranges of 80 to 120 mg L<sup>-1</sup> and 1.5 to 2.5 mg L<sup>-1</sup>, respectively. When the concentrations of MB and As(V) exceed 120 and 2.5 mg L<sup>-1</sup>, the adsorption capacity increases insignificantly and reaches a maximum of 110.63 mg L<sup>-1</sup> ( $C_0 = 160$  mg L<sup>-1</sup>) and 2.312 mg L<sup>-1</sup> ( $C_0 = 3.5$  mg L<sup>-1</sup>), respectively. We can assume three main reasons to explain this phenomenon: 1) a large number of available active sites are used at higher concentrations of MB and As(V), 2) improved mass transfer and 3) the increased ability of MB and As(V) to collide with CMC.

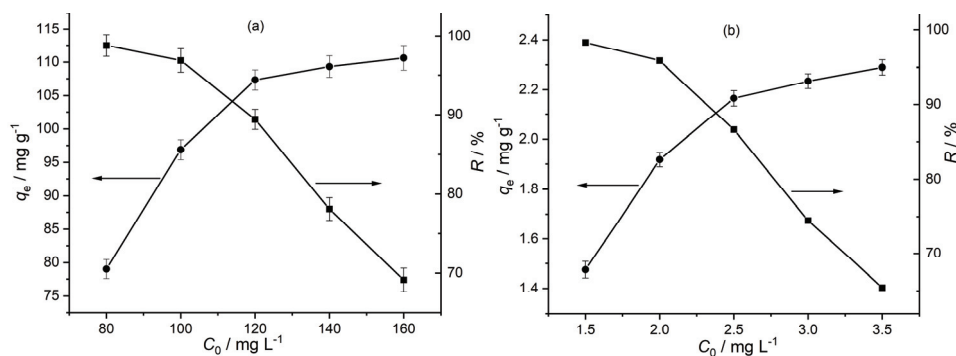


Fig. 6. Effect of initial concentration on adsorption capacity and removal efficiency of a) MB and b) As(V) onto CMC.

Furthermore, as the initial concentration increases from 80 to 160 mg L<sup>-1</sup> and from 1.5 to 3.5 mg L<sup>-1</sup>, the removal of MB and As(V) decreases from 98.79 to 69.14 % and from 98.60 to 65.97 %, respectively. When using higher concentrations of adsorbates with the same weight of CMC, the percentage removal of MB and As(V) is reduced because the number of active sites on CMC remains constant.

The Langmuir and Freundlich equations are the most used isotherms equation for modelling the adsorption data. The  $R^2$  obtained from Langmuir model is significantly higher than that obtained from Freundlich model, indicating that the Langmuir isotherm better fits the experimental data (Fig. 7a and b, Table III). Table S-IV compares the adsorption capacity of CMC with various adsorbents. The previously reported capacity of MB and As(V) onto CMC is greater than that

of many other previously reported adsorbents, implying that the as-prepared CMC has a high potential for use in wastewater treatment. A high  $K_L$  value indicates the high affinity of adsorbent for MB and As(V) adsorption.<sup>32,33</sup> The  $R_L$  values in the range of 0 and 1 indicate favourable adsorption.

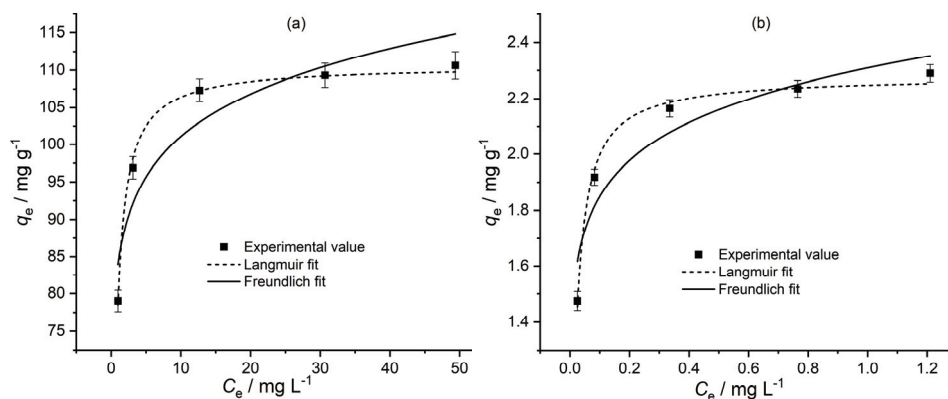


Fig. 7. Analyses of adsorption isotherm for: a) MB and b) As(V) onto CMC by Langmuir and Freundlich models at 303 K.

TABLE III. Isotherm parameters for adsorption of MB and As(V) onto CMC at different concentration

Adsorbate	$q_{e,exp}$ mg g <sup>-1</sup>	Langmuir isotherm model					Freundlich isotherm model			
		$q_{max}$ mg g <sup>-1</sup>	$K_L$ L mg <sup>-1</sup>	$R_L$	$R^2$	$\chi^2$	$K_F$ mg g (L/mg) <sup>1/n</sup>	$n_F$	$R^2$	$\chi^2$
MB	110.63	110.64	2.518	0.003	0.996	0.027	84.138	12.546	0.884	24.427
As(V)	2.31	2.285	81.919	0.003	0.985	0.003	2.325	10.950	0.904	0.608

### Reusability

CMC regeneration and recycling are critical for practical application. As shown in Fig. 8a and b, after five cycles, there is only a very slight decrease in

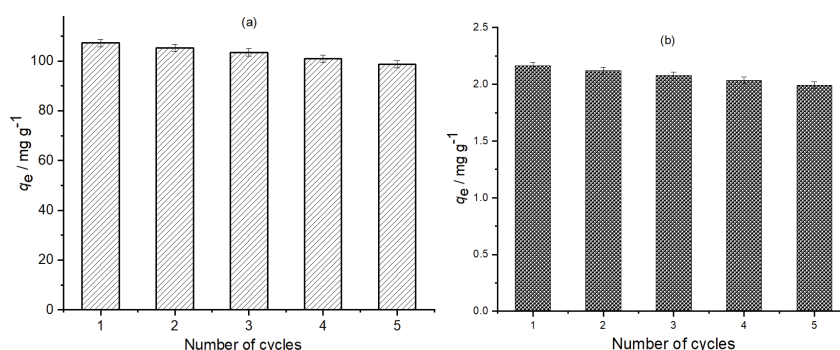


Fig. 8. Regeneration for: a) MB and b) As(V) adsorption onto CMC.

removal from 107.32 to 98.73 mg g<sup>-1</sup> for MB and from 2.165 to 1.992 mg g<sup>-1</sup> for As(V), indicating that CMC has excellent performance and application for MB and As (V) treatment.

#### CONCLUSION

CMC was prepared in a straightforward and efficient manner. They also have a fast adsorption rate, high adsorption efficiency, and fast magnetic separation from treated water, making them excellent materials for environmentally friendly water treatment. The maximum adsorption is 110.63 mg g<sup>-1</sup> for MB and 2.31 mg g<sup>-1</sup> for As(V). The kinetics of adsorption can be described using a pseudo-second-order equation, and the CMC adsorption isotherm agreed well with the Langmuir sorption equation. Furthermore, through the desorption process the product could be regenerated and reused multiple times.

#### SUPPLEMENTARY MATERIAL

Additional data and information are available electronically at the pages of journal website: <https://www.shd-pub.org.rs/index.php/JSCS/article/view/12026>, or from the corresponding author on request.

#### ИЗВОД

КАРАКТЕРИЗАЦИЈА МАГНЕТНОГ НАНОКОМПОЗИТА ПРЕВУЧЕНОГ УГЉЕНИКОМ ЗА УКЛАЊАЊЕ МЕТИЛЕНСКОГ ПЛАВОГ И АРСЕНАТА ИЗ ВОДЕНОГ РАСТВОРА

NGOC BICH NGUYEN<sup>1,2</sup>, THI QUE PHUONG PHAN<sup>3</sup>, CAO THANH TUNG PHAM<sup>1,4</sup>, HUU NGHI NGUYEN<sup>2</sup>, SY NGUYEN PHAM<sup>5</sup> и DINH THANH NGUYEN<sup>1,3</sup>

<sup>1</sup>Graduate University of Science and Technology, Viet Nam Academy of Science and Technology, Hanoi City, 100000, Vietnam, <sup>2</sup>Dong Thap University, Cao Lanh City, 870000, Vietnam, <sup>3</sup>Institute of Applied Materials Science, Viet Nam Academy of Science and Technology, Ho Chi Minh City, 700000, Vietnam, <sup>4</sup>Institute of Chemical Technology, Viet Nam Academy of Science and Technology, Ho Chi Minh City, 700000, Vietnam и <sup>5</sup>Ho Chi Minh City University of Natural Resources and Environment, Vietnam

Магнетни нанокомполит превучен угљеником произведен ниско-температурском хидротермалном методом је употребљен за уклањање метиленског плавог и арсената из воденог раствора. Лангмиров модел је добро описао експерименталне податке са израчунатим максималним адсорпционом капацитетом од 110,63 и 2,31 mg g<sup>-1</sup> за метиленско плаво и арсенат, редом. Такође, одређени адсорпциони механизми су физисорпција за метиленско плаво и комбинација физисорпције и хемисорпције за арсенат. Промена Гибсове енергије има негативне вредности што указује на то да се адсорпција метиленско плавог и арсената на магнетним материјалима дешава спонтано. Ово истраживање показује једноставну, ефикасну и поуздану методу за уклањање метиленско плавог и арсената.

(Примљено 2. августа, ревидирано 5. октобра, прихваћено 3. новембра 2022)

#### REFERENCES

1. S. Ji, C. Miao, H. Liu, L. Feng, X. Yang, H. Guo, *Nanoscale Res. Lett.* **13** (2018) 178 (<https://doi.org/10.1186/s11671-018-2580-8>)
2. W. J. Liu, K. Tian, H. Jiang, H. Q. Yu, *Sci Rep* **3** (2013) 2419 (<https://doi.org/10.1080/19443994.2015.1132476>)

3. T. H. Nguyen, T. H. Pham, H. T. N. Thi, T. N. Nguyen, M. V. Nguyen, T. T. Dinh, M. P. Nguyen, T. Q. Do, T. Phuong, T. T. Hoang, T. T. M. Hung, V. H. T. Thi, *J. Chem.* **2019** (2019) 1 (<https://doi.org/10.1155/2019/5295610>)
4. M. Inyang, B. Gao, P. Pullammanappallil, W. Ding, A. R. Zimmerman, *Bioresour. Technol.* **101** (2010) 8868 (<https://doi.org/10.1016/j.biortech.2010.06.088>)
5. N. Besharati, N. Alizadeh, S. Shariati, *J. Mex. Chem. Soc.* **62** (2018) 110 (<https://doi.org/10.29356/jmcs.v62i3.433>)
6. W. Chen, R. Parette, J. Zou, F. Cannon, B. Dempsey, *Water Res.* **41** (2007) 1851 (<https://doi.org/10.1016/j.watres.2007.01.052>)
7. M. Zhang, B. Gao, S. Varnoosfaderani, A. Hebard, Y. Yao, M. Inyang, *Bioresour. Technol.* **130** (2013) 457 (<https://doi.org/10.1016/j.biortech.2012.11.132>)
8. L. Huang, J. Cai, M. He, B. Chen, B. Hu, *Ind. Eng. Chem. Res.* **57** (2018) 6201 (<https://doi.org/10.1021/acs.iecr.7b05294>)
9. N. S. Pham, P. T. Q. Phan, B. N. Nguyen, V. X. Le, *J. Appl. Electrochem.* (2022) (<https://doi.org/10.1007/s10800-022-01747-1>)
10. N. S. Pham, V. X. Le, *J. Electroanal. Chem.* **921** (2022) 116507 (<https://doi.org/10.1016/j.jelechem.2022.116507>)
11. N. S. Pham, B. N. Nguyen, A. Q. K. Nguyen, *J. Appl. Electrochem.* (2022) (<https://doi.org/10.1007/s10800-022-01784-w>)
12. K. Dai, F. Wang, W. Jiang, Y. Chen, J. Mao, J. Bao, *Nanoscale Res. Lett.* **12** (2017) 528 (<https://doi.org/10.1186/s11671-017-2295-2>)
13. N. S. Pham, Y. H. Seo, E. Park, T. D. D. Nguyen, I.-S. Shin, *Data Br.* **31** (2020) 105891 (<https://doi.org/10.1016/j.dib.2020.105891>)
14. N. S. Pham, Y. H. Seo, E. Park, T. D. D. Nguyen, I.-S. Shin, *Electrochim. Acta* **353** (2020) 136446 (<https://doi.org/10.1016/j.electacta.2020.136446>)
15. V. X. Le, H. Lee, N. S. Pham, S. Bong, H. Oh, S.-H. Cho, I.-S. Shin, *Sensors Actuators, B* **346** (2021) 130552 (<https://doi.org/10.1016/j.snb.2021.130552>)
16. N. S. Pham, P. T. Q. Phan, V. X. Le, *J. Appl. Electrochem.* **52** (2022) 1343 (<https://doi.org/10.1007/s10800-022-01716-8>)
17. L. Zhu, F. Shen, R. L. Smith, L. Yan, L. Li, X. Qi, *Chem. Eng. J.* **316** (2017) 770 (<https://doi.org/10.1016/j.cej.2017.02.034>)
18. L. Ai, C. Zhang, Z. Chen, *J. Hazard Mater.* **192** (2011) 1515 (<https://doi.org/10.1016/j.jhazmat.2011.10.041>)
19. X. Bao, Z. Qiang, J.-H. Chang, W. Ben, J. Qu, *J. Environ. Sci.* **26** (2014) 962 ([https://doi.org/10.1016/S1001-0742\(13\)60485-4](https://doi.org/10.1016/S1001-0742(13)60485-4))
20. L. Verma, M. A. Siddique, J. Singh, R. N. Bharagava, *J. Environ. Manage.* **250** (2019) 109452 (<https://doi.org/10.1016/j.jenvman.2019.109452>)
21. J. Wang, J. Xu, N. Wu, *J. Exp. Nanosci.* **12** (2017) 297 (<https://doi.org/10.1080/17458080.2017.1325016>)
22. B. Qiu, H. Gu, X. Yan, J. Guo, Y. Wang, D. Sun, Q. Wang, M. Khan, X. Zhang, B. L. Weeks, D. P. Young, Z. Guo, S. Wei, *J. Mater. Chem. A* **2** (2014) 17454 (<https://doi.org/10.1039/C4TA04040F>)
23. H. Zeng, W. Qi, L. Zhai, F. Wang, J. Zhang, D. Li, *J. Environ. Chem. Eng.* **9** (2021) 105951 (<https://doi.org/10.1016/j.jece.2021.105951>)
24. Y. Bulut, H. Aydm, *Desalination* **194** (2006) 259 (<https://doi.org/10.1016/j.desal.2005.10.032>)
25. K. Y. Foo, B. H. Hameed, *Desalin. Water Treat.* **19** (2012) 255 (<https://doi.org/10.5004/dwt.2010.1214>)

26. A. Sharma, N. Verma, A. Sharma, D. Deva, N. Sankararamakrishnan, *Chem. Eng. Sci.* **65** (2010) 3591 (<https://doi.org/10.1016/j.ces.2010.02.052>)
27. X. Shi, C. Wang, Y. Ma, H. Liu, S. Wu, Q. Shao, Z. He, L. Guo, T. Ding, Z. Guo, *Powder Technol.* **356** (2019) 726 (<https://doi.org/10.1016/j.powtec.2019.09.002>)
28. B. Gu, J. Schmitt, Z. Chen, L. Llang, J. F. McCarthy, *Environ. Sci. Technol.* **28** (1994) 38 (<https://doi.org/10.1021/es00050a007>)
29. L. Ding, B. Zou, W. Gao, Q. Liu, Z. Wang, Y. Guo, X. Wang, Y. Liu, *Colloids Surfaces, A* **446** (2014) 1 (<https://doi.org/10.1016/j.colsurfa.2014.01.030>)
30. C. Li, Z. Xiong, J. Zhang, C. Wu, *J. Chem. Eng. Data* **60** (2015) 3414 (<https://doi.org/10.1021/acs.jced.5b00692>)
31. T. S. Anirudhan, J. Nima, S. Sandeep, V. R. N. Ratheesh, *Chem. Eng. J.* **209** (2012) 362 (<https://doi.org/10.1016/j.cej.2012.07.129>)
32. M. A. Ahmad, N. A. Ahmad Puad, O. S. Bello, *Water Resour. Ind.* **6** (2014) 18 (<https://doi.org/10.1016/j.wri.2014.06.002>)
33. X. Zhou, J. Zhou, Y. Liu, J. Guo, J. Ren, F. Zhou, *Fuel* **233** (2018) 469 (<https://doi.org/10.1016/j.fuel.2018.06.075>).

SUPPLEMENTARY MATERIAL TO

**Performance of carbon-coated magnetic nanocomposite in methylene blue and arsenate treatment from aqueous solution**

NGOC BICH NGUYEN<sup>1,2\*</sup>, THI QUE PHUONG PHAN<sup>3</sup>, CAO THANH TUNG PHAM<sup>1,4</sup>,  
 HUU NGHI NGUYEN<sup>2</sup>, SY NGUYEN PHAM<sup>5</sup>, QUOC KHUONG ANH NGUYEN<sup>6\*\*</sup>  
 and DINH THANH NGUYEN<sup>1,3\*\*\*</sup>

<sup>1</sup>Graduate University of Science and Technology, Viet Nam Academy of Science and Technology, Hanoi City, 100000, Vietnam, <sup>2</sup>Dong Thap University, Cao Lanh City, 870000, Vietnam, <sup>3</sup>Institute of Applied Materials Science, Viet Nam Academy of Science and Technology, Ho Chi Minh City, 700000, Vietnam, <sup>4</sup>Institute of Chemical Technology, Viet Nam Academy of Science and Technology, Ho Chi Minh City, 700000, Vietnam, <sup>5</sup>Ho Chi Minh City University of Natural Resources and Environment, Vietnam and <sup>6</sup>Institute of Applied Technology and Sustainable Development, Nguyen Tat Thanh University, Ho Chi Minh City, 70000, Vietnam

*J. Serb. Chem. Soc.* 88 (4) (2023) 423–435

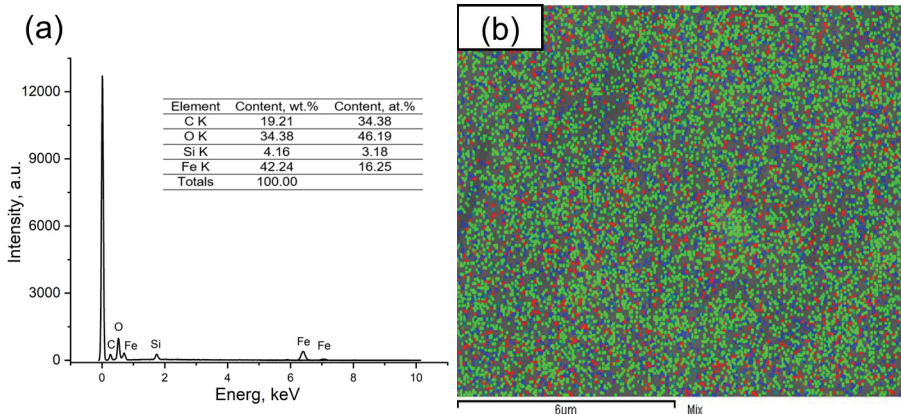


Fig. S-1. EDS analysis (a) and elemental map (b) of CMC.

\* Corresponding authors. E-mail: (\*)nmbich@dthu.edu.vn; (\*\*)nqkanh@ntt.edu.vn;  
 (\*\*\*)dinhthanhng53@gmail.com



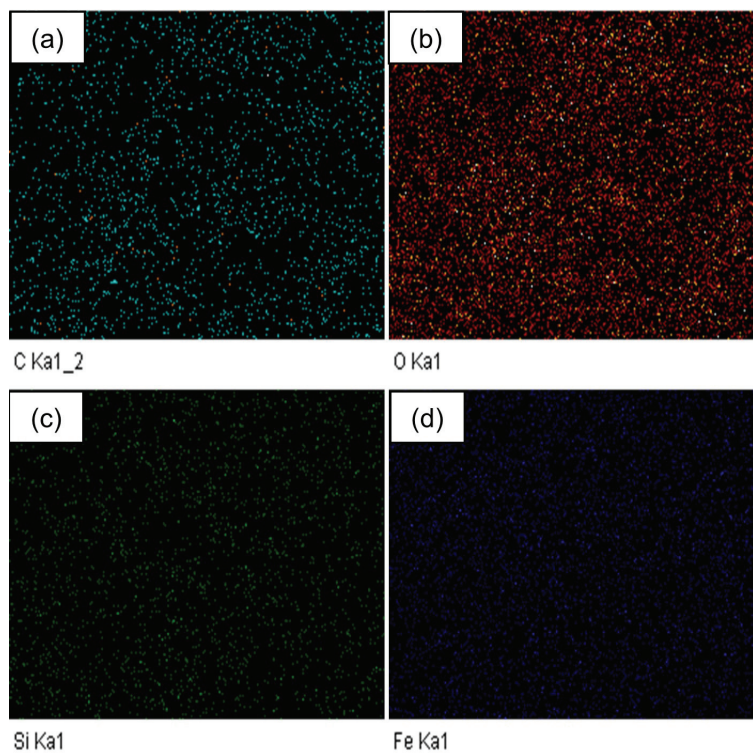


Fig. S-2. Elemental maps of C (a), O (b), Si (c) and Fe (d) of CMC.

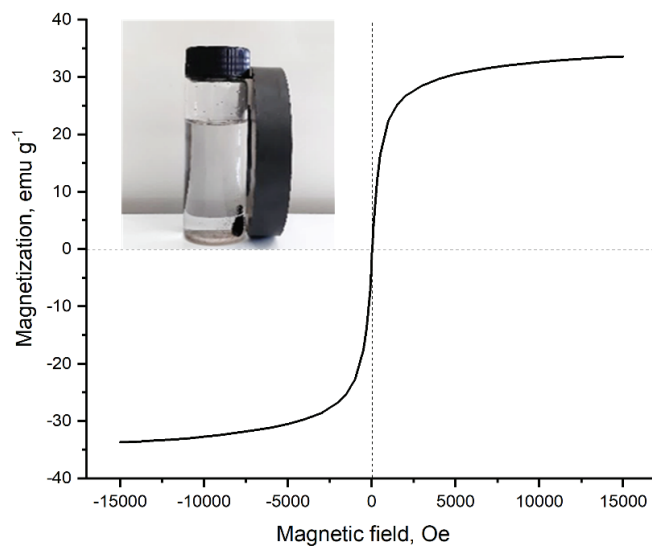


Fig. S-3. Magnetization curves and illustration of the magnetic separability of CMC.

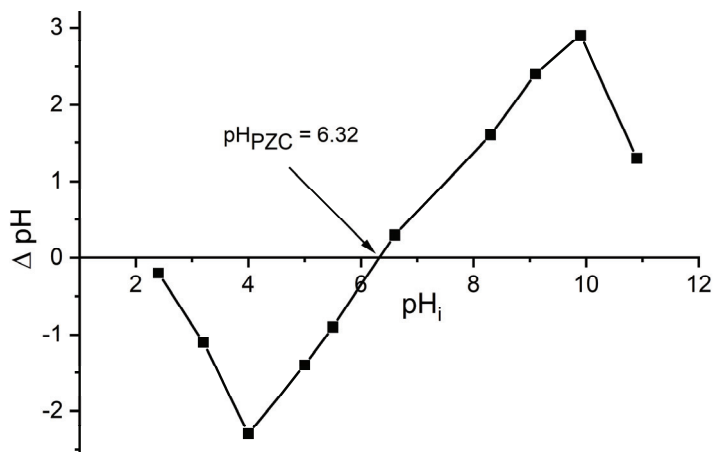


Fig. S-4. Plot of point of zero charge of CMC.

TABLE S-I. Different kinetic models, thermodynamic equations and adsorption isotherms

Model	Parameter	Equation
Adsorption kinetic models		
Pseudo first-order	$q_e / \text{mg g}^{-1}$ = equilibrium adsorption capacity	$q_t = q_e - q_e e^{-k_1 t}$ (1)
	$q_t / \text{mg g}^{-1}$ = adsorption capacity at time $t$	
	$k_1 / \text{min}^{-1}$ = rate constant	
Pseudo second-order	$k_2 / \text{g mg}^{-1} \text{min}^{-1}$ = rate constant	$q_t = \frac{k^2 q_e^2 t}{1 + k^2 q_e t}$ (2)
Thermodynamic equations		
	$\Delta S^\circ / \text{J mol}^{-1}$ = entropy change	$\ln K_D = \frac{\Delta H^\circ}{RT} + \frac{\Delta S^\circ}{R}$ (3)
Van't Hoff equation	$\Delta H^\circ / \text{J mol}^{-1}$ = enthalpy change	
	$R / \text{J mol}^{-1} \text{K}^{-1} = 8.314$ (universal gas constant)	
	$T / \text{K}$ = absolute temperature	
	$K_D / \text{L g}^{-1} = q_e / C_e$	
	thermodynamic equilibrium constant	
	$\Delta G^\circ / \text{J mol}^{-1}$ = Gibbs free energy change	$\square G^\circ = -RT \ln K_D$ (4)
Adsorption isotherms		
Langmuir	$q_m / \text{mg g}^{-1}$ = maximum monolayer adsorption capacity of the adsorbent	$\frac{C_e}{q_e} = \frac{1}{K_a q_m} + \frac{C_e}{q_m}$ (5)
	$K_a$ = energy constant	
	$R_L$ = separation factor which gives an idea about Langmuir isotherm	$R_L = \frac{1}{1 + K_a C_0}$ (6)
Freundlich	$K_F / \text{mg g}^{-1} \text{L}^{1/n} \text{mg}^{-1/n}$ = Freundlich constant $n$ = intensity of adsorption, $n > 1$ indicates a favourable and heterogeneous adsorption	$\ln q_e = \ln K_F + \frac{1}{n} \ln C_e$ (7)

TABLE S-II. The comparison of the magnetization of CMC with various biochar

Precursors of magnetic biochar	Method	Magnetization, $\text{emu g}^{-1}$	Reference
Rice straw, $\text{Fe}(\text{NO}_3)_3$ , KOH	Hydrothermal	33.7	This work
Coconut shells, $\text{FeCl}_3$	Pyrolysis, microwave	6.0	<sup>1</sup>
Corn stalk, $\text{FeSO}_4$ , $\text{Na}_2\text{S}_2\text{O}_3$ , NaOH	Hydrothermal	11.2	<sup>2</sup>
Corn stalk, $\text{FeSO}_4$ , $\text{Na}_2\text{S}_2\text{O}_3$ , NaOH	Pyrolysis	20.4	<sup>2</sup>
Palm fiber, $\text{FeSO}_4$ , $\text{FeCl}_3$ , $\text{NH}_3$	Pyrolysis	19.4	<sup>3</sup>
Firwood, $\alpha\text{-FeOOH}$	Pyrolysis	20.8	<sup>4</sup>
Oleyl amine, $\text{FeCl}_2$ , $\text{FeCl}_3$ , NaOH	Hydrothermal	21.7	<sup>5</sup>
Rice husk, $\text{Fe}(\text{NO}_3)_3$ , $\text{KMnO}_4$	Pyrolysis	27.5	<sup>6</sup>

TABLE S-III. The porous parameters of RS, BS, CMC samples

Sample	$S_{\text{BET}} / \text{m}^2 \text{g}^{-1}$	$V_{\text{T}} / \text{cm}^3 \text{g}^{-1}$	$D_{\text{p}} / \text{nm}$
RS	1.3	0.01	30.6
BS	6.6	0.04	33.0
CMC	171.4	0.15	6.0

TABLE S-IV. The comparison of the maximum adsorption capacity of MB and As(V) on CMC with various adsorbents.

Adsorbent	Capacity, $\text{mg g}^{-1}$		
	MB	As(V)	Ref.
CMC	110.63	2.31	This study
$\text{Fe}_2\text{O}_3\text{-ZrO}_2\text{/BC}$	38.1	1.01	<sup>7</sup>
M-MWCNTs	48.06	-	<sup>8</sup>
$\text{Fe}_3\text{O}_4\text{/MWCNT}$	74	-	<sup>9</sup>
$\text{Fe}_3\text{O}_4\text{@C NPs}$	117	-	<sup>10</sup>
HPB (hematite/biochar)	-	0.43	<sup>11</sup>
Ch-Rs (chitosan/red scoria)	-	0.72	<sup>12</sup>
OBC (Canola straw-based biochar)	-	0.95	<sup>13</sup>
TB 800 (biochar from waste)	-	1.25	<sup>14</sup>
PAC-500 (magnetic biosorbents)	-	2.00	<sup>15</sup>
MC-O/NC-L-MG (magnetite/ microcellulose)	-	18.5	<sup>16</sup>
ChM (Chitosan-Magnetite Hydrogel)	-	66.9	<sup>17</sup>

## REFERENCES

1. M. W. Yap, N. M. Mubarak, J. N. Sahu, E. C. Abdullah, *J. Ind. Eng. Chem.* **45** (2017) 287 (<https://doi.org/10.1016/j.jiec.2016.09.036>)
2. Y. Tu, Z. Peng, P. Xu, H. Lin, X. Wu, L. Yang, J. Huang, *Bioresources* **12** (2017) 1077 (<https://doi.org/10.15376/biores.12.1.1077-1089>)
3. X. Zhou, J. Zhou, Y. Liu, J. Guo, J. Ren, F. Zhou, *Fuel* **233** (2018) 469 (<https://doi.org/10.1016/j.fuel.2018.06.075>)
4. D. D. Sewu, H. N. Tran, G. Ohemeng-Boahen, S. H. Woo, *Sci. Total Environ.* **717** (2020) 137091 (<https://doi.org/10.1016/j.scitotenv.2020.137091>)
5. X. Bao, Z. Qiang, J.-H. Chang, W. Ben, J. Qu, *J. Environ. Sci.* **26** (2014) 962 ([https://doi.org/10.1016/S1001-0742\(13\)60485-4](https://doi.org/10.1016/S1001-0742(13)60485-4))

6. C. Sun, T. Chen, Q. Huang, J. Wang, S. Lu, J. Yan, *Environ. Sci. Pollut. Res. Int.* **26** (2019) 8902 (<https://doi.org/10.1007/s11356-019-04321-z>)
7. S. I. Siddiqui, S. A. Chaudhry, *J. Clean. Prod.* **223** (2019) 849 (<https://doi.org/10.1016/j.jclepro.2019.03.161>)
8. L. Ai, C. Zhang, F. Liao, Y. Wang, M. Li, L. Meng, J. Jiang, *J. Hazard. Mater.* **198** (2011) 282 (<https://doi.org/10.1016/j.jhazmat.2011.10.041>)
9. A. Suwattanamala, N. Bandis, K. Tedsree, C. Issro, *Mater. Today: Proc.* **4** (2017) 6567 (<https://doi.org/10.1016/j.matpr.2017.06.169>)
10. R. Wu, J.-H. Liu, L. Zhao, X. Zhang, J. Xie, B. Yu, X. Ma, S.-T. Yang, H. Wang, Y. Liu, *J. Environ. Chem. Eng.* **2** (2014) 907 (<https://doi.org/10.1016/j.jece.2014.02.005>)
11. S. Wang, B. Gao, A. R. Zimmerman, Y. Li, L. Ma, W. G. Harris, K. W. Migliaccio, *Bioresour. Technol.* **175** (2015) 391 (<https://doi.org/10.1016/j.biortech.2014.10.104>)
12. T. G. Asere, S. Mincke, J. De Clercq, K. Verbeken, D. A. Tessema, F. Fufa, C. V. Stevens, G. Du Laing, *Int. J. Environ. Res. Public Health* **14** (2017) 1 (<https://doi.org/10.3390/ijerph14080895>)
13. K. Zoroufchi Benis, J. Soltan, K. N. McPhedran, *Chem. Eng. J.* **423** (2021) 130061 (<https://doi.org/10.1016/j.cej.2021.130061>)
14. L. Verma, J. Singh, *J. Environ. Manage.* **248** (2019) 109235 (<https://doi.org/10.1016/j.jenvman.2019.07.006>)
15. L. Verma, M. A. Siddique, J. Singh, R. N. Bharagava, *J. Environ. Manage.* **250** (2019) 109452 (<https://doi.org/10.1016/j.jenvman.2019.109452>)
16. K. Taleb, J. Markovski, Z. Veličković, J. Rusmirović, M. Rančić, V. Pavlović, A. Marinković, *Arab. J. Chem.* **12** (2019) 4675 (<https://doi.org/10.1016/j.arabjc.2016.08.006>)
17. I. P. Verduzco-Navarro, E. Mendizabal, J. A. Rivera Mayorga, M. Renteria-Urquiza, A. Gonzalez-Alvarez, N. Rios-Donato, *Gels* **8** (2022) 1 (<https://doi.org/10.3390/gels8030186>).





*J. Serb. Chem. Soc.* 88 (4) 437–450 (2023)  
JSCS–5637

## Full factorial design methodology approach to optimize the elimination of gallic acid from water by coagulation using activated acorns barks as coagulant-aid

NADJIBA BOULAHIA<sup>1,2</sup>, DALILA HANK<sup>1,3\*</sup>, SAMIR MERIDJA<sup>1,2</sup>  
and ABDELMALEK CHERGUI<sup>3,4</sup>

<sup>1</sup>Ecole Nationale Supérieure Agronomique (ENSA), Hacen Badi, El Harrach Alger, Algérie,  
<sup>2</sup>Laboratoire de Maitrise de l'Eau en Agriculture, Ecole Nationale Supérieure Agronomique (ENSA), Hacen Badi, El Harrach Alger, Algérie, <sup>3</sup>Laboratoire des Sciences et Techniques de l'Environnement, Ecole Nationale Polytechnique, Hacen Badi, El Harrach Alger, Algérie and <sup>4</sup>Ecole Nationale Polytechnique, Hacen Badi, El Harrach Alger, Algérie

(Received 23 June, revised 20 November, accepted 9 December 2022)

**Abstract:** This study investigated the elimination of organic matter from water by the coagulation process using a biomaterial “acorns barks” as a coagulant-aid with the presence of aluminium sulphate in low concentration. The removal of gallic acid from water was first studied by two processes: the adsorption on activated acorns barks, and coagulation by aluminium sulphate, separately. The hybrid system was then studied, and the optimal operating conditions were determined. The performance of the hybrid system (coagulation/adsorption) mainly depends on the initial concentration of gallic acid, the coagulant dose and the mass of coagulant-aid. A full factorial design  $2^3$  was used to determine the optimum conditions for gallic acid removal. The maximum removal of gallic acid in water was 92.48 %, achieved at 20 mg L<sup>-1</sup> of initial gallic acid concentration, 50 mg L<sup>-1</sup> of aluminium sulphate coagulant concentration and 1.5 g of activated acorns barks adsorbent mass. The application of these optimal conditions on urban wastewater for the elimination of organic matter has shown the performance of this hybrid system treatment.

**Keywords:** adsorption; biomaterial; hybrid system; optimization; urban wastewater.

### INTRODUCTION

The increase of the quantity of wastewater containing various chemical substances and solid particles, caused by economic development, has become a serious threat to human health and sustainable development. Consequently, the treatment of polluted wastewaters remains a topic of global concern because

\* Corresponding author. E-mail: dalila.hank@g.enp.edu.dz  
<https://doi.org/10.2298/JSC220623084B>

wastewaters collected from municipalities, communities and industries must ultimately be returned to receiving waters or to the land.<sup>1</sup>

Wastewater contains a mixture of pollutants, among which phenols and their derivatives are the most common organic pollutants of wastewater that require careful treatment.<sup>2,3</sup> Phenols and its derivatives are toxic to humans, animals, and aquatic life, and they increase the oxygen demand of receiving water.<sup>4</sup> Phenolic compounds are very harmful to organisms even at low concentrations due to their high toxicity and carcinogenic properties.<sup>5</sup> Gallic acid is one of the most important phenolic components used in medical applications, food and the cosmetic industries.<sup>6</sup> Consequently, a great deal of wastewater containing gallic acid discharges into water bodies. Therefore, it is necessary to remove gallic acid from water. Several studies have been carried out for the elimination of gallic acid by different processes.<sup>7-10</sup> Moreover, it is difficult to remove gallic acid by the traditional water treatment processes due to its water solubility and small molecular weight.<sup>11</sup>

The selection of a particular treatment technique depends on the nature of the effluent, waste type and concentration, presence of other constituents, level of removal required and economics.<sup>12</sup> Traditionally, biological treatment, activated carbon adsorption and solvent extraction are the most widely used methods for the removal of phenols and its derivatives from wastewater.<sup>13</sup> Among them, adsorption is a well-established and powerful technique for treating domestic and industrial effluents.<sup>14</sup> The adsorption method is characterized by low initial cost, simple operation, insensitive to toxic substances, and high effectiveness.<sup>15</sup>

Activated carbon is the most widely and effectively used adsorbent because of its large surface area, micro-porous nature, and high adsorption capacity. However, due to its high price and its regeneration cost, activated carbon becomes inconvenient as an adsorbent.<sup>16</sup> Nowadays, one of the great challenges in the adsorption technologies is the exploring of new potential and low-cost adsorbents using biological material. These materials should be biodegradable and are presumed to be safe for human health.<sup>17</sup> Producing activated carbons usually entails carbonization, pyrolysis and activation (either chemical or physical).<sup>18,19</sup>

Coagulation flocculation technology has proved its advantages in separation processes. The process does not only separate suspended solids from water, but also remove colour and certain organic matters from diverse sources of wastewater.<sup>20</sup> Aluminium and iron salts are the most widely used coagulants in water treatment due to their high efficiency, as well as synthetic and natural organic polymers, which find application also.<sup>21</sup> However, Al-based coagulants are hazardous and can cause health problems, for example Alzheimer's disease.<sup>22</sup> In addition, it was reported that coagulation is not effective for some synthetic organic matters due to their physicochemical properties.<sup>23</sup> In recent years, there has been considerable interest in the development of biomaterial to become an alter-

native for conventional coagulants. Several studies referred to the use of alternative coagulants from recyclable materials, due to their cost effectiveness and good removal performance.<sup>24</sup>

The coagulation treatment process can be influenced by several factors, but the failure to consider the interaction of factors may lead to erroneous conclusions. The design of experiments methodology could be a meaningful method for modelling and optimizing the treatment process with a minimum number of experiments in order to identify the effective parameters and their interactions. Factorial design is a more practical technique than other traditional methods for modelling a multi-variable system. Several studies have referred to the use of factorial design to optimize adsorption treatments<sup>25–27</sup> and coagulation processes.<sup>28–30</sup>

In this study, acorns barks were used as a coagulant-aid for the elimination of a phenolic acid (gallic acid) from water with coagulation treatment. A factorial design was used to study the individual and interactive effects of three parameters that may affect the removal efficiency of gallic acid, followed by an application of the optimal conditions obtained on an urban wastewater.

## EXPERIMENTAL

### *Preparation of activated acorns barks*

For the preparation of carbon from acorns barks, the barks were washed with distilled water and then dried in an oven at 105 °C for 24 h. Ten g of the raw material was immersed in 100 mL of H<sub>2</sub>SO<sub>4</sub> solution (40 %) and kept at 105 °C for 2 h. The acid treated acorns barks was washed several times with distilled water and then dried at 105 °C for 24 h. The obtained sample was calcined at 500 °C for 2 h, crushed and sieved at a diameter ≤ 500 μm.<sup>31</sup>

### *Adsorption experiments*

Batch adsorption experiments were carried out in 1000 mL of Erlenmeyer flasks in which 500 mL of aqueous solution was mixing with a determined mass of activated acorns barks.

The mixture was shaken under ambient temperature at 150 rpm for 4 h to attain equilibrium. Samples were collected at predetermined time intervals, then filtered through a filter (0.45 μm) for the determination of gallic acid concentration.

### *Coagulation–flocculation experiments*

Coagulation experiments were conducted in jar-test apparatus by three steps: rapid mixing (200 rpm) for 3 min, slow mixing (60 rpm) for 30 min and 30 min sedimentation. The desired mass of activated acorns barks was added into 500 mL of organic compound solution in rapid mixing step, 30 s after adding the coagulant. Aluminium sulphate was used as a coagulant.

### *Gallic acid analysis*

The concentration of gallic acid in water was determined by measuring the absorbance on a UV–Vis spectrophotometer Shimadzu UVmini-1240, at a wavelength of 254 nm.

## RESULTS AND DISCUSSION

### *SEM and FTIR analysis*

*Scanning electron microscopy analysis (SEM).* The analysis of the pore structure of the raw acorns barks and the activated acorns barks is given in Fig. 1.



It's clear that no porous structure for the raw acorns barks in contrary to the activated acorns barks which possess a good porous structure.

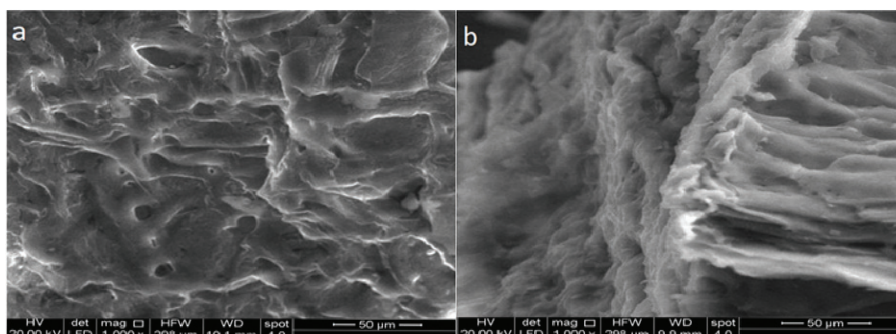


Fig. 1. SEM photographs of acorns barks raw (a) and activated (b).

For further study, the activated acorns barks were used as an adsorbent for the gallic acid elimination from water.

*Fourier transform infrared spectroscopy (FTIR).* FTIR is the best technique to analyse the chemical structural properties of natural materials.<sup>32</sup>

FTIR spectra are a useful tool to identify functional groups in a molecule, as each specific chemical bond often has a unique energy absorption band, and can obtain structural and bond information.<sup>33</sup> Fig. 2 shows the FTIR spectra of the activated acorns barks. A wide absorption band at  $3600\text{--}3050\text{ cm}^{-1}$  with a maximum at about  $3350\text{ cm}^{-1}$  is due to O–H and N–H stretching groups.<sup>34</sup> The band at  $1650\text{ cm}^{-1}$  characterizes the presence of carbonyl groups C=O.<sup>35</sup> Another band is observed at  $1050\text{ cm}^{-1}$  corresponds to C–C stretching.<sup>36</sup>

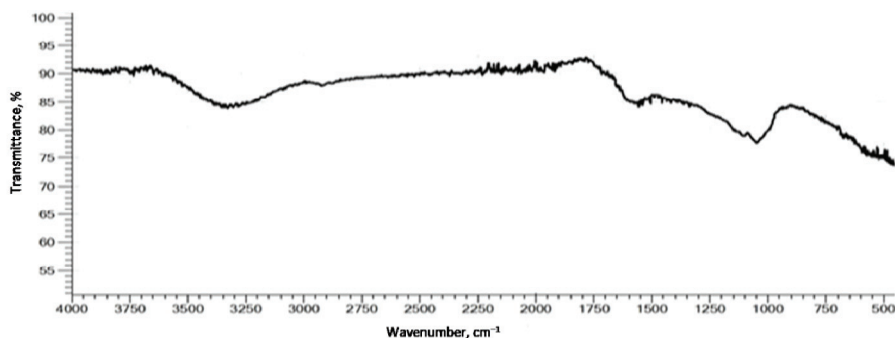


Fig. 2. FTIR of activated acorns barks.

### Adsorption

The adsorption experiments were performed out in batch system with different mass of the activated acorns barks for  $20\text{ mg L}^{-1}$  of gallic acid concentration.

The adsorption capacity is defined as the amount of gallic acid adsorbed per unit mass of adsorbent,  $q / \text{mg g}^{-1}$ :

$$q = (C_0 - C_t) \frac{V}{m} \quad (1)$$

where  $C_0 / \text{mg L}^{-1}$  is the initial gallic acid concentration.  $C_t / \text{mg L}^{-1}$  is the concentration at a defined time.  $V / \text{L}$  is the volume of solution, and  $m / \text{g}$  is the mass of the adsorbent.

Fig. 3 shows that that quantity of gallic acid can be eliminated by the activated acorns barks, and the adsorption equilibrium was 240 min. The adsorption capacity was found to be high at low doses, it decreased from 12.05 to 7.48  $\text{mg g}^{-1}$  with the activated acorns barks increasing from 1 to 2  $\text{g L}^{-1}$  at equilibrium time. This decrease in adsorption capacity with the increasing adsorbent dosage is due to the non-saturation of the adsorption sites.<sup>37</sup>

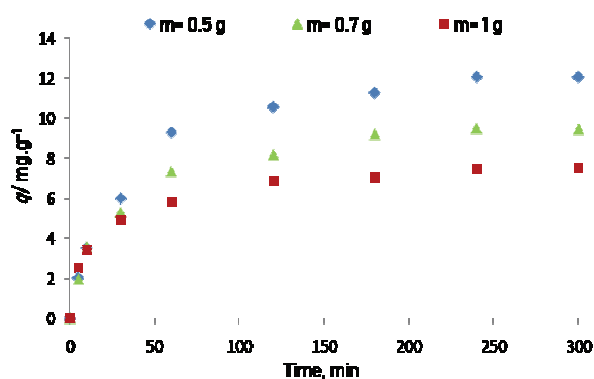


Fig. 3. The effect of adsorbent mass on the adsorption capacity of gallic acid.

#### Coagulation–flocculation

Different aluminium sulphate coagulant doses (10 to 100  $\text{mg L}^{-1}$ ) were used to remove gallic acid at a concentration of 20  $\text{mg L}^{-1}$ . The variation of the removal of gallic acid ( $R / \%$ ) was calculated as:

$$R / \% = 100 \left( \frac{C_0 - C_f}{C_0} \right) \quad (2)$$

where  $C_0$  and  $C_f$  are initial and final concentrations of gallic acid, respectively.

Fig. 4 shows that the removal of gallic acid increases with the coagulant dose due to the growth in the number of binding sites. The straight line after 50  $\text{mg L}^{-1}$  indicates that an optimum dose of 50  $\text{mg L}^{-1}$  was found at a removal of 50.20 %. The coagulant capacity was steady due to the screening effect between coagulant molecules.<sup>38</sup> However, higher coagulant dose can give charge

reversal and destabilization of colloids, and the colloidal products are rather difficult to be removed by precipitation or charge neutralization.<sup>24</sup>

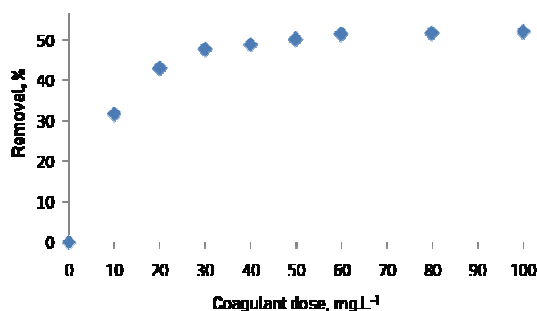


Fig. 4. Effect of coagulant dose on gallic acid removal by coagulation-flocculation.

*Aluminum sulphate/adsorbent combination in coagulation process.* Three masses of the adsorbent were used with the optimal dose of aluminium sulphate ( $50 \text{ mg L}^{-1}$ ) for the removal of gallic acid from water at a concentration of  $20 \text{ mg L}^{-1}$ . The intended mass of activated acorns barks was added into 500 mL of gallic acid solution in rapid mixing steps, 30 s after adding the coagulant in order to follow all the coagulation-flocculation steps.

The efficiency of hybrid system is well illustrated in Fig. 5. The removal of gallic acid from water by hybrid system is higher than the classical coagulation. Also, the removal of gallic acid increases with the activated acorns barks dose, in which the gallic acid removal increases from 64.32 % for 0.5 g to 91.35 % for 1.5 g. Thus, the activated acorns barks are an efficient coagulation-aid to enhance the coagulation performance with aluminium. This was consistent with previous studies in which better elimination performance was obtained when the coagulant-aid is used in combination with conventional coagulants.<sup>24,39,40</sup>

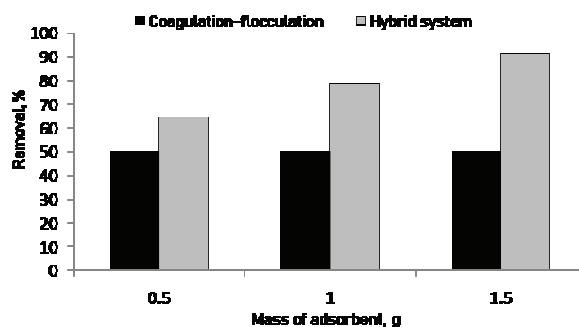


Fig. 5. Comparison of gallic acid removal by coagulation-flocculation and by hybrid system.

*Optimization of coagulation hybrid system treatment by full factorial design.* In this study, the full factorial design methodology was used to optimize the

treatment process and to establish the correlation between gallic acid removal and three input variables, the gallic acid concentration  $X_1$ , the aluminium sulphate concentration  $X_2$  and the mass of activated acorns barks  $X_3$ . The range and level of each variable are given in Table I.

TABLE I. Factors and levels used in the full factorial design

Factor	Low level (-1)	Hight level (+1)
$X_1$ – Gallic acid concentration, mg L <sup>-1</sup>	20	50
$X_2$ – Aluminum sulphate concentration, mg L <sup>-1</sup>	10	50
$X_3$ – Mass of activated acorns barks, g	0	1.5

The statistical analyses were applied to validate the model using JMP8. The mathematical model of the first-order polynomial can be given as:

$$Y = a_0 + a_1X_1 + a_2X_2 + a_3X_3 + a_{12}X_1X_2 + a_{13}X_1X_3 + a_{23}X_2X_3 + a_{123}X_1X_2X_3 \quad (3)$$

Where  $Y$  is the theoretical response function (removal of gallic acid),  $a_0$  is the constant,  $a_i$  is the linear effect and ( $a_{ij}$  and  $a_{ijk}$ ) are the interaction effects.

The real and coded values are in Table II.

TABLE II. Full factorial design matrix of three variables in coded and real values with the experimental responses

Run	Real values			Coded values			R / %
	Gallic acid concentration, mg L <sup>-1</sup>	Aluminum sulphate concentration, mg L <sup>-1</sup>	Mass of activated acorns barks, g	$X_1$	$X_2$	$X_3$	
1	20	10	0.00	-1	-1	-1	31.69
2	50	10	0.00	+1	-1	-1	12.48
3	20	50	0.00	-1	+1	-1	50.2
4	50	50	0.00	+1	+1	-1	41.42
5	20	10	1.50	-1	-1	+1	84.6
6	50	10	1.50	+1	-1	+1	70.23
7	20	50	1.50	-1	+1	+1	91.35
8	50	50	1.50	+1	+1	+1	77.48
9	35	30	0.75	0	0	0	64.82
10	35	30	0.75	0	0	0	61.37

By substituting the regression coefficients in Eq. (3), by their numerical values as given in Table III, we get:

$$Y = 58.564 - 7.02875X_1 + 7.68125X_2 + 23.48375X_3 + 1.36625X_1X_2 - 0.03125X_1X_3 - 4.18125X_2X_3 - 1.24125X_1X_2X_3 \quad (4)$$

Fig. 6 shows the predicted values versus the experimental values of the removal of gallic acid. The straight line in red colour represents the model, rectangles points are experimental points and the dotted lines represent the area of acceptable variation.

TABLE III. Estimated regression coefficients for the removal yield of gallic acid

Parameter	Estimate	Standard error	<i>t</i> -value	<i>P</i> -value
Constant	58.564	1.692279	34.61	0.0008
$X_1$	-7.02875	1.892025	-3.71	0.0654
$X_2$	7.68125	1.892025	4.06	0.0557
$X_3$	23.48375	1.892025	12.41	0.0064
$X_1 X_2$	1.36625	1.892025	0.72	0.5452
$X_1 X_3$	-0.03125	1.892025	-0.02	0.9883
$X_2 X_3$	-4.18125	1.892025	-2.21	0.1577
$X_1 X_2 X_3$	-1.24125	1.892025	-0.66	0.5792

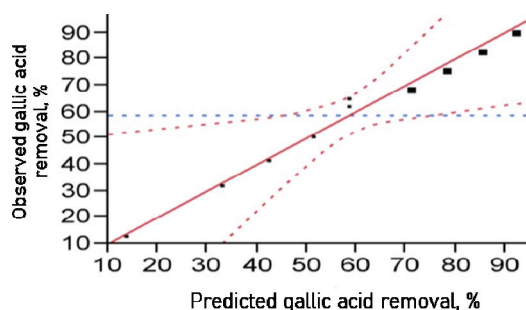


Fig. 6. Observed versus predicted response (removal of gallic acid).

The high value of  $R^2 = 0.989$  and  $R^2$  adjusted = 0.972 indicate that the model was successful in correlating the response to the studied parameters.

*Student's t-test.* The Student's test determines the significance of the regression coefficients of the different parameters. A large *t*-value associated with a low *P*-value ( $< 0.05$ ) of a variable indicates a high significance of the corresponding model term.

After eliminating the insignificant effects by step-by-step method, Table IV gives only the significant effects. The results suggest that the linear effects of gallic acid concentration, the aluminium sulphate concentration, the mass of adsorbent, and the interaction effect between the latter two are significant.

TABLE IV. Estimated regression significant coefficients for the removal yield of gallic acid

Parameter	Estimate	Standard error	<i>t</i> -value	<i>P</i> -value
Constant	58.564	1.300328	45.04	$<0.0001$
$X_1$	-7.02875	1.453811	-4.83	0.0047
$X_2$	7.68125	1.453811	5.28	0.0032
$X_3$	23.48375	1.453811	16.15	$<0.0001$
$X_2 X_3$	-4.18125	1.453811	-2.88	0.0347

The most significant effect is the activated acorns barks with a positive value. It means that the removal of gallic acid increases with the activated acorns bark dose.

The empirical model for the removal becomes:

$$Y = 58.568 - 7.02875X_1 + 7.68125X_2 + 23.48375X_3 - 4.18125X_2X_3 \quad (5)$$

*Interactions plot.* The interactions plot is given in Fig. 7. An effective interaction was observed between the concentration of aluminium sulphate and the mass of activated acorns barks with negative value ( $-4.18125$ ), It means that the effect of activated acorns barks dose is very high and positive on the removal of gallic acid when the sulphate concentration is low.

The other interactions seem to be insignificant, the lines representing the effects are parallels in the squares of the diagram.

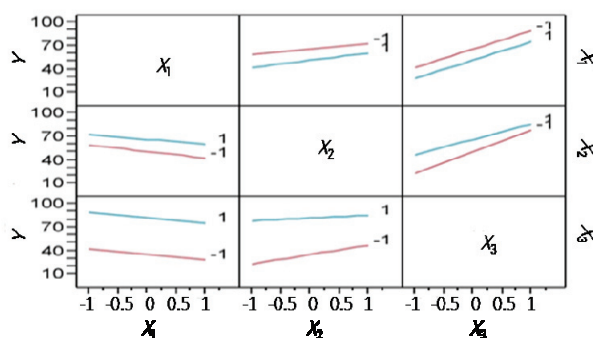


Fig. 7. Interaction effects.

*Analysis of variance (ANOVA).* The significance of the adjusted response was justified by ANOVA. The ANOVA summary is shown in Table V. The  $F$ -value obtained (80.12) and the  $P$ -value inferior to 0.05 indicate that the model is valid to predict the removal of gallic acid with the studied variables.

TABLE V. Analysis of variance (ANOVA);  $p$ : number of significant coefficients;  $N$ : total number of experiments

Source	Degrees of freedom	Sum of squares	Mean square	$F$ -ration	$P$ -value
Model	$(p-1) = 4$	5418.9944	1354.75	80.1222	0.0001
Residual	$(N-p) = 5$	84.5427	16.91		
Total	9	5503.5370			

*Optimization design using the desirability function.* The desirability function approach is the most current and strongly suggested method for the optimization of one or more responses.<sup>41</sup>

As shown in Fig. 8, the best combination of factor settings for achieving the optimum response was found to be: gallic acid concentration  $20 \text{ mg L}^{-1}$ , aluminium sulphate concentration  $50 \text{ mg L}^{-1}$  and activated acorns barks dose  $1.5 \text{ g}$ . These conditions lead to a removal of gallic acid of  $92.482 \%$  with a desirability of  $0.900$ .

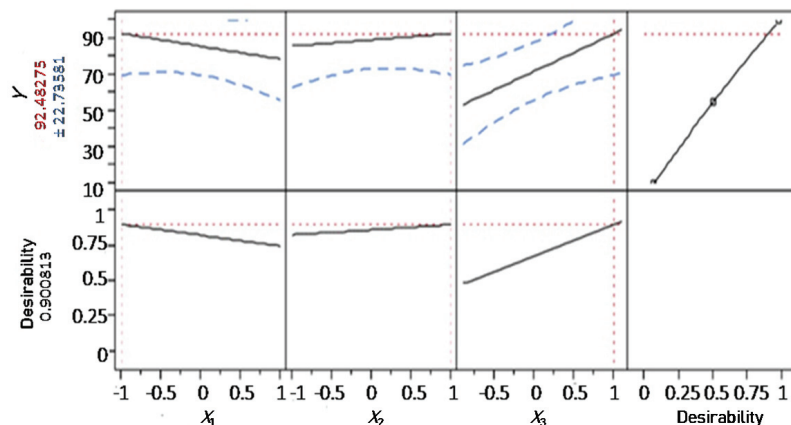


Fig. 8. Desirability function for removal of gallic acid.

#### *Application of the hybrid system treatment on urban wastewater*

Firstly, the hybrid system was used for treating a mixture of phenolic compounds: 20 mg L<sup>-1</sup> of gallic acid, 20 mg L<sup>-1</sup> of phenol and 10 mg L<sup>-1</sup> of humic substances under the optimal conditions found previously: 50 mg L<sup>-1</sup> of aluminium sulphate with 1.5 g of activated acorns barks.

Simple organic molecules with no functional group or only one non-ionized functional group (as phenol) are not (or very slightly) removed by coagulation, and molecules that have -COOH groups are easily eliminated.<sup>42</sup> Fig. 9 shows that the use of activated acorns barks as a coagulant-aid improved significantly the elimination of organic matter from water in comparison with the classical coagulation treatment. The high removal (96.72 %) is due to the contribution of the coagulant-aid to the elimination of organic matter by adsorption.

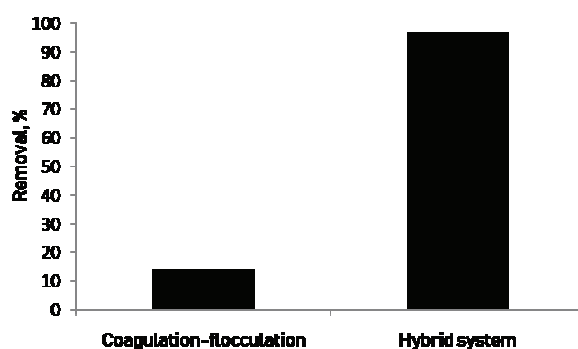


Fig. 9. Removal of organic matter by coagulation-flocculation and hybrid system.

Secondly, the optimal conditions of the hybrid system were applied to urban wastewater. The water sample was collected after pretreatment step at the waste-

water treatment plant which is situated in the Wilaya of Boumerdes (in the north of Algeria, 45 km from the capital Algiers). Its process chain consists of pretreatment, biological treatment and clarification. The treated wastewater is destined for irrigation.

At the treatment plant biological treatment is used for the elimination of organic pollution from water. In our study, organic pollution was eliminated from wastewater by the physicochemical treatment and compared with the biological treatment used.

Fig. 10 shows the organic pollution parameters in wastewater before secondary treatment, wastewater treated by hybrid system, and wastewater treated by biological treatment at the treatment plant.

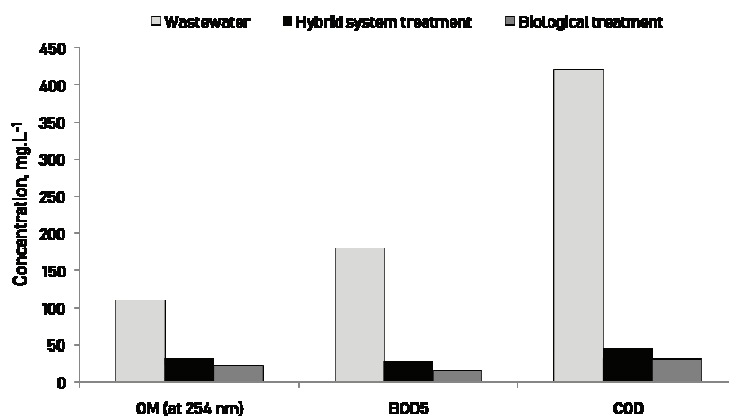


Fig. 10. Organic pollution parameters in wastewater before and after treatment.

With the hybrid system treatment, we observe an elimination of 72.41 % of organic matter (measured by measuring the absorbance at a wavelength of 254 nm), a reduction of 84.37 % for biological oxygen demand ( $BOD_5$ ) and 89.45 % for chemical oxygen demand ( $COD$ ). These results confirm the possibility of using acorns barks as a coagulant-aid for the elimination of organic matter in wastewater. The significant reduction of  $BOD_5$  and  $COD$  which represent cocktail of many organic compounds, confirm that the obtained model is valid for real wastewater and not only for one compound.

Thus, the efficiency of both hybrid system and biological treatments are very close; this shows that the treatment by combination coagulation/adsorption (physicochemical treatment) can be an alternative to biological treatment.

#### CONCLUSIONS

The present study analysed the feasibility of activated acorns barks using as coagulant-aid to improve the coagulation process for the elimination of gallic acid from water. The elimination of gallic acid by a classical coagulation was partial,



with a removal of 50.20 % for a concentration of 20 mg L<sup>-1</sup> gallic acid. This result was obtained using a maximum aluminium sulphate dose of 50 mg L<sup>-1</sup>.

The hybrid system of coagulation process for the removal of gallic acid from water using activated acorns barks as coagulant-aid was successfully modelled applying the full factorial design methodology. The optimal conditions for the hybrid system in which the removal of gallic acid reached 92.48 %, were achieved at the initial gallic acid concentration of 20 mg L<sup>-1</sup>, the aluminium sulphate dose of 50 mg L<sup>-1</sup> and the activated acorns barks mass 1.5 g.

The hybrid system has shown high efficiency in the elimination of organic matter in wastewater, the application of the optimal conditions removes 72.41 % of organic matter, 84.37 % of BOD<sub>5</sub> and 89.45 % of COD from urban wastewater. The performance of hybrid system in comparison with the secondary treatment applied in wastewater treatment plant gives the same results, which means that the hybrid system (combination coagulation/adsorption) can be an alternative to biological treatment.

#### ИЗВОД

#### МЕТОДОЛОГИЈА ПОТПУНОГ ФАКТОРИЈАЛНОГ ДИЗАЈНА У ОПТИМИЗАЦИЈИ ЕЛИМИНАЦИЈЕ ГАЛНЕ КИСЕЛИНЕ ИЗ ВОДЕ ПУТЕМ КОАГУЛАЦИЈЕ ПОМОЋУ АКТИВИРАНЕ КОРЕ ЖИРА КАО КОАГУЛАНТА

NADJIBA BOULAHIA<sup>1,2</sup>, DALILA HANK<sup>1,4</sup>, SAMIR MERIDJA<sup>1,2</sup> и ABDELMALEK CHERGUI<sup>3,4</sup>

<sup>1</sup>Ecole Nationale Supérieure Agronomique (ENSA), Hacén Badi, El Harrach Alger, Algérie, <sup>2</sup>Laboratoire de Maitrise de l'Eau en Agriculture, Ecole Nationale Supérieure Agronomique (ENSA), Hacén Badi, El Harrach Alger, Algérie, <sup>3</sup>Laboratoire des Sciences et Techniques de l'Environnement, Ecole Nationale Polytechnique, Hacén Badi, El Harrach Alger, Algérie u <sup>4</sup>Ecole Nationale Polytechnique, Hacén Badi, El Harrach Alger, Algérie

Ова студија је истраживала елиминацију органске материје из воде процесом коагулације коришћењем биоматеријала, коре жира, као помоћног коагуланта уз присуство алуминијум-сулфата у ниској концентрацији. Уклањање галне киселине из воде је прво проучавано применом два независна процеса: адсорпције на активираној кори жира и коагулације алуминијум-сулфатом. Затим је проучен хибридни систем (коагулација/адсорпција) и утврђени су оптимални услови рада. Перформансе хибридног система у највећој мери зависе од почетне концентрације галне киселине, дозе коагуланта и масе биоматеријала. За одређивање оптималних услова за уклањање галне киселине коришћен је потпун факторијални дизајн 2<sup>3</sup>. Максимално уклањање галне киселине у води износило је 92,48 %, а постигнуто је при 20 mg L<sup>-1</sup> почетне концентрације галне киселине, 50 mg L<sup>-1</sup> алуминијум-сулфата као коагуланта, и 1,5 g активиране масе адсорбента од коре жира. Примена ових оптималних услова на градске отпадне воде за елиминацију органских материја показала је добре особине овог хибридног система третмана.

(Примљено 23. јуна, ревидирано 20. новембра, прихваћено 9. децембра 2022)

#### REFERENCES

1. B. Khalfaoui, A. H. Meniai, R. Borja, *J. Chem. Technol. Biotechnol.* **64** (1995) 153 (<https://doi.org/10.1002/jctb.280640207>)

2. P. Schröder, B. Helmreich, B. Škrbić, M. Carballa, M. Papa, C. Pastore, Z. Emre, A. Oehmen, A. Langenhoff, M. Molinos, *Environ. Sci. Pollut. Res.* **23** (2016) 12835 (<https://doi.org/10.1007/s11356-016-6503-x>).
3. R. Pedrazzani, G. Bertanza, I. Brnardić, Z. Cetecioglu, J. Dries, J. Dvarionienė, A.J. García-Fernández, A. Langenhoff, G. Libralato, G. Lofrano, *Sci. Total Environ.* **651** (2019) 3202 (<https://doi.org/10.1016/j.scitotenv.2018.10.027>).
4. A. Ali, K. Saeed, *Desalin. Water Treat.* **57** (2016) 11242 (<https://doi.org/10.1080/19443994.2015.1041057>).
5. A. T. M. Din, B. Hameed, A. L. Ahmad, *J. Hazard. Mater.* **161** (2009) 1522 (<https://doi.org/10.1016/j.jhazmat.2008.05.009>).
6. A. E. Vilian, J. Y. Song, Y. S. Lee, S.-K. Hwang, H. J. Kim, Y.-S. Jun, Y. S. Huh, Y.-K. Han, *Biosens. Bioelectron.* **117** (2018) 597 (<https://doi.org/10.1016/j.bios.2018.06.064>).
7. J. Wang, A. Li, L. Xu, Y. Zhou, *J. Hazard. Mater.* **169** (2009) 794 (<https://doi.org/10.1016/j.jhazmat.2009.04.013>).
8. A. Gil, N. Taoufik, A. García, S. Korili, *Environ. Technol.* (2018) 3017 (<https://doi.org/10.1080/09593330.2018.1464066>).
9. Q. Zhou, L. Ding, Y. Zhu, M. Zhong, C. Yang, *Processes* **8** (2020) 273 (<https://doi.org/10.3390/pr8030273>).
10. X. Song, C. Li, Z. Chai, Y. Zhu, Y. Yang, M. Chen, R. Ma, X. Liang, J. Wu, *Sci. Total Environ.* **765** (2021) 142711 (<https://doi.org/10.1016/j.scitotenv.2020.142711>).
11. Z. Zhang, Q. Pang, M. Li, H. Zheng, H. Chen, K. Chen, *Environ. Sci. Pollut. Res.* **22** (2015) 1085 (<https://doi.org/10.1007/s11356-014-3409-3>).
12. I. Ghodbane, L. Nouri, O. Hamdaoui, M. Chiha, *J. Hazard. Mater.* **152** (2008) 148 (<https://doi.org/10.1016/j.jhazmat.2007.06.079>).
13. C. Brasquet, J. Roussy, E. Subrenat, P. L. Cloirec, *Environ. Technol.* **17** (1996) 1245 (<https://doi.org/10.1080/09593331708616494>).
14. Z. Aksu, J. Yener, *Waste Manage.* **21** (2001) 695 ([https://doi.org/10.1016/S0956-053X\(01\)00006-X](https://doi.org/10.1016/S0956-053X(01)00006-X)).
15. V. Srihari, A. Das, *Ecotoxicol. Environ. Saf.* **71** (2008) 274 (<https://doi.org/10.1016/j.ecoenv.2007.08.008>).
16. N. K. Amin, *J. Hazard. Mater.* **165** (2009) 52 (<https://doi.org/10.1016/j.jhazmat.2008.09.067>).
17. M. Šćiban, M. Klačnja, M. Antov, B. Škrbić, *Bioresour. Technol.* **100** (2009) 6639 (<https://doi.org/10.1016/j.biortech.2009.06.047>).
18. T. Zhang, W. P. Walawender, L. Fan, M. Fan, D. Daugaard, R. Brown, *Chem. Eng. J.* **105** (2004) 53 (<https://doi.org/10.1016/j.cej.2004.06.011>).
19. B. Škrbić, V. Marinković, S. Spaić, V. Milanko, S. Branovački, *Microchem. J.* **139** (2018) 9 (<https://doi.org/10.1016/j.microc.2018.02.007>).
20. A. K. Verma, R. R. Dash, P. Bhunia, *J. Environ. Manage.* **93** (2012) 154 (<https://doi.org/10.1016/j.jenvman.2011.09.012>).
21. C.-Y. Yin, *Process Biochem.* **45** (2010) 1437 (<https://doi.org/10.1016/j.procbio.2010.05.030>).
22. J. Li, S. Jiao, L. Zhong, J. Pan, Q. Ma, *Colloids Surfaces., A* **428** (2013) 100 (<https://doi.org/10.1016/j.colsurfa.2013.03.034>).
23. S. D. Kim, J. Cho, I. S. Kim, B. J. Vanderford, S. A. Snyder, *Water Res.* **41** (2007) 1013 (<https://doi.org/10.1016/j.watres.2006.06.034>).

24. H. Harfouchi, D. Hank, A. Hellal, *Process Saf. Environ. Prot.* **99** (2016) 216 (<https://doi.org/10.1016/j.psep.2015.10.019>)
25. G. Annadurai, R.-S. Juang, D.-J. Lee, *Adv Environ Res.* **6** (2002) 191 ([https://doi.org/10.1016/S1093-0191\(01\)00050-8](https://doi.org/10.1016/S1093-0191(01)00050-8))
26. S.A. Kordkandi, M. Forouzesh, *J. Taiwan Inst. Chem. Eng.* **45** (2014) 2597 (<https://doi.org/10.1016/j.jtice.2014.06.015>)
27. C. S. Araújo, I. L. Almeida, H. C. Rezende, S. M. Marcionilio, J. J. Léon, T. N. de Matos, *Microchem. J.* **137** (2018) 348 (<https://doi.org/10.1016/j.microc.2017.11.009>)
28. M. Franceschi, A. Girou, A. Carro-Diaz, M. Maurette, E. Puech-Costes, *Water Res.* **36** (2002) 3561 ([https://doi.org/10.1016/S0043-1354\(02\)00066-0](https://doi.org/10.1016/S0043-1354(02)00066-0))
29. M. Martin, I. González, M. Berrios, J. Siles, A. Martin, *Chem. Eng. J.* **172** (2011) 771 (<https://doi.org/10.1016/j.cej.2011.06.060>)
30. J. Dotto, M. R. Fagundes-Klen, M. T. Veit, S. M. Palacio, R. Bergamasco, *J. Clean. Prod.* **208** (2019) 656 (<https://doi.org/10.1016/j.jclepro.2018.10.112>)
31. S. Bouchareb, D. Hank, M.A. Salam, K. Ouddai, A. Hellal, *Desalin. Water Treat.* **137** (2019) 143 (<https://doi.org/10.5004/dwt.2019.23185>)
32. C.d.C.A. Lopes, P.H.J.O. Limirio, V.R. Novais, P. Dechichi, *Appl. Spectrosc. Rev.* **53** (2018) 747 (<https://doi.org/10.1080/05704928.2018.1431923>)
33. D. Zhou, L. Zhang, S. Guo, *Water Res.* **39** (2005) 3755 (<https://doi.org/10.1016/j.watres.2005.06.033>)
34. N. M. Mahmoodi, B. Hayati, M. Arami, C. Lan, *Desalination* **268** (2011) 117 (<https://doi.org/10.1016/j.desal.2010.10.007>)
35. P.D. Pathak, S.A. Mandavgane, *J. Environ. Chem. Eng.* **3** (2015) 2435 (<https://doi.org/10.1016/j.jece.2015.08.023>)
36. A. Ofomaja, E. Naidoo, *J. Chem. Eng.* **175** (2011) 260 (<https://doi.org/10.1016/j.cej.2011.09.103>)
37. N. N. Rudi, M. S. Muhamad, L. Te Chuan, J. Alipal, S. Omar, N. Hamidon, N. H. A. Hamid, N.M. Sunar, R. Ali, H. Harun, *Helvion* **6** (2020) 5049 (<https://doi.org/10.1016/j.helivon.2020.e05049>)
38. T.K. Hussein, N.A. Jasim, *Mater. Today Proc.* (2021) 1946 (<https://doi.org/10.1016/j.matpr.2020.12.240>)
39. Y. Zhao, Y. Wang, B. Gao, H. Shon, J.-H. Kim, Q. Yue, *Desalination* **299** (2012) 79 (<https://doi.org/10.1016/j.desal.2012.05.026>)
40. S. Zhao, B. Gao, Y. Wang, Z. Yang, *Colloids Surfaces., A* **417** (2013) 161 (<https://doi.org/10.1016/j.colsurfa.2012.10.062>)
41. M. Mourabet, A. El Rhilassi, H. El Boujaady, M. Bennani-Ziatni, R. El Hamri, A. Taitai, *Appl. Surf. Sci.* **258** (2012) 4402 (<https://doi.org/10.1016/j.apsusc.2011.12.125>)
42. F. Julien, B. Gueroux, M. Mazet, *Water Res.* **28** (1994) 2567 ([https://doi.org/10.1016/0043-1354\(94\)90075-2](https://doi.org/10.1016/0043-1354(94)90075-2)).



*J. Serb. Chem. Soc.* 88 (4) 451–465 (2023)  
JSCS–5638

## The effects of E-learning units on 13–14-year-old students' misconceptions regarding some elementary chemical concepts

INES NUIĆ<sup>1\*</sup> and SAŠA A. GLAŽAR<sup>2</sup>

<sup>1</sup>Faculty of Science, University of Sarajevo, Bosnia and Herzegovina and <sup>2</sup>Faculty of Education, University of Ljubljana, Slovenia

(Received 4 July, revised 26 December, accepted 30 December 2022)

**Abstract:** Students' misconceptions in science can lead to a range of learning difficulties if the teacher does not choose the appropriate teaching strategies to reduce their frequency. In this paper, 13–14-year-old students' misconceptions regarding structure and states of matter, pure substances, and mixtures are explored. The teaching strategy with E-learning material was applied to examine its effects on the frequency of misconceptions. The research was conducted in urban schools in Bosnia and Herzegovina with 7<sup>th</sup>- and 8<sup>th</sup>-grade students. Findings pointed to the misconceptions originating in transferring the macroscopic observations into the submicroscopic level and in misinterpretation of the size of particles. Students who used E-learning material at school mostly had lower percentages of misconceptions in comparison to students from the control group and students who accessed the same E-learning material from their home. This indicates that the E-learning strategy could have promising results if applied more extensively at schools. This study aims to direct teachers' attention toward applying E-learning in chemistry teaching, for students to gain scientifically accepted knowledge and to reduce the occurrence of misconceptions.

**Keywords:** structure of matter; pure substances; mixtures; misconceptions; E-learning material.

### INTRODUCTION

Four decades ago (in 1982), Johnstone presented his ideas about the three levels of representation of chemical concepts.<sup>1</sup> He suggested that chemical knowledge consists of “at least three levels”: macroscopic (visible), submicroscopic (particulate) and representative (symbolic), and represented them with a triangle. Chemistry teaching is not focused on a certain level of representation but placed inside the triangle, since teachers and students are expected to manage them simultaneously.<sup>1</sup> According to Johnstone, chemists were mainly thinking at the

\* Corresponding author. E-mail: [ividovic@pmf.unsa.ba](mailto:ividovic@pmf.unsa.ba)  
<https://doi.org/10.2298/JSC220704092N>

macroscopic and submicroscopic levels, but chemistry teachers taught students mainly from the perspective of the symbolic level. This meant that the students were not taught to “truly think like chemists”.<sup>2</sup>

Experiencing chemistry through demonstrations or laboratory work (macroscopic) and understanding it in terms of atomic and molecular interactions (submicroscopic) promotes the development of conceptual understanding. Among the main characteristics of students who demonstrate conceptual understanding, there is the ability to link macroscopic, submicroscopic, and symbolic levels of representation.<sup>3,4</sup> Therefore, chemistry instruction should emphasize this multilevel thinking.<sup>5</sup>

Many studies showed that students often develop an understanding of how nature is functioning,<sup>6</sup> which is not in line with the scientific meaning of concepts.<sup>6,7</sup> Students have beliefs about physical phenomena derived from prior learning or from interaction with physical and social world.<sup>8</sup> They obtain naive views about matter also through their experiences during childhood which lead them to incorrect ideas.<sup>9</sup> The consequences are incorrect understandings of science concepts and phenomena that affect the integration of new with the existing knowledge,<sup>10</sup> and may persist even after teaching, along with scientifically approved ones, or form a certain kind of synthetic model with them.<sup>11</sup> Misconceptions can be acquired both before and after teaching.<sup>6</sup> Misconceptions formed at school originate mainly from inadequate curricula, teaching material, textbooks<sup>6</sup>, ineffective instruction and textbook misrepresentation.<sup>12</sup>

#### *Misconceptions of some elementary chemical concepts – Literature review*

To understand states of matter, transitions between them, as well as pure substances and mixtures, the main prerequisite is the knowledge and understanding of the particle (particulate) theory of matter (PNM).<sup>13</sup> Misunderstanding of this theory may hinder learning of other topics such as states of matter.<sup>10</sup> The ability to understand the submicroscopic level is developed gradually with a careful teaching program over a time scale of years.<sup>14</sup>

A large proportion of students' difficulties encountered when moving from everyday thinking to scientific thinking is regarded as the projection of properties from the macroscopic world to the submicroscopic level of representation.<sup>15</sup> Students tend to generate a hybrid macroparticulate model in which particles possess macroscopic properties.<sup>16</sup>

Direct sensory experience leads students to a naive view of matter. They rely solely on sensory information when reasoning about matters up to the age of around 14 years.<sup>17</sup> One of the first published studies<sup>18</sup> on student's conceptions about changes in states of matter (melting, evaporation and condensation) uncovered many non-scientific conceptions among children aged 12–17 years old. Some of the detected misconceptions persisted even after teaching.<sup>18</sup> Students

often fail to understand the vibration of particles in the solid state, whereas a majority of them were able to indicate particle movement in liquid and gas states.<sup>19</sup> Students also experience specific difficulties with gases since those they know from everyday life (air) are invisible, which prevents them from forming the concept of gas spontaneously.<sup>17</sup> Research studies regarding the most common misconceptions about states of matter held by 12-, 14- and 16-year-old students suggest no significant difference between the misconceptions held by these different age groups.<sup>20</sup>

The concept of a pure substance is difficult for young learners, but 11–12 year-old students might understand the concept if the appropriate teaching methods were used. The characteristics of pure substances, such as having specific melting and boiling point as well as being composed of only one kind of particles, are too abstract for students at this age.<sup>14</sup> The term pure substance could be deceiving since “substances are just substances – they are not pure and impure substances”.<sup>21</sup> The term mixture is also simplified, “wood contains many substances; they are not simply mixed in a random way but built into a complex structure”.<sup>21</sup> One of the best ways to induce students’ thinking on the submicroscopic level (pure substances and mixtures) is to include particulate drawings into instruction.<sup>22</sup>

#### *E-learning*

The impact of E-learning on students’ achievement is complex and depends on many factors, but studies showed that students learn best with E-learning when they are interactively engaged in the content. Use of technology significantly improves their performance and shifts a teacher-centred classroom environment to a more learner-centred classroom environment.<sup>23</sup> Web-based educational software improved academic achievement of 7<sup>th</sup> grade students in Turkey in structure and properties of matter.<sup>24</sup> Findings of this study point to the benefits of these material: 1) web-assisted applications provide limitless time for the replaying option, and they are suitable for an individual’s learning speed, unlike the traditional learning environment; 2) rich audio–visual content has positive impact on students’ learning; 3) this material has been designed with meaningful learning that requires the connection of new with the previously acquired knowledge.<sup>24</sup>

Research findings confirm that the use of e-units created to connect the three levels of representation of chemical concepts results in improvement of students’ achievements.<sup>7</sup> The contents of E-units must also be relevant to the target group of students, and to contain appropriately designed multimedia elements. E-learning units are intended for both independent learning and repetition, as well as for work in the school under the guidance of a teacher.

Some research<sup>25,26</sup> examined the role of the virtual laboratory on 11–12-year-old students’ understanding of states of matter, pure substances and mix-

tures. This virtual laboratory contained all three levels of representation of a chemical concept and dynamic visualizations of the submicroscopic level. The results showed that students, to whom the virtual laboratory was displayed, scored higher in the achievement test than the students who were taught using the teacher-centred approach with static visualisations.<sup>25,26</sup>

## EXPERIMENTAL

### *Research problem*

This research was addressed to diagnosing misconceptions of selected science concepts (structure of matter, states of matter, pure substances and mixtures) held by 13–14-year-old students and exploring the effect of applying E-learning units on their frequency. According to the Curriculum Framework, the basics of states of matter are taught within the subject My environment in the 2<sup>nd</sup> grade (age 7–8). In the 5<sup>th</sup> grade (age 10–11) within *Science*, the states of matter are taught again, including phase changes. Within physics in the 7<sup>th</sup> grade (age 12–13), students are acquainted with the notion of atoms and molecules. Within chemistry in the 8<sup>th</sup> grade (age 13–14), students learn more deeply about the structure and states of matter, and then about pure substances and mixtures. After examining the corresponding literature, the following research questions are formulated:

1. What misconceptions about structure and states of matter do students have when entering the 8<sup>th</sup> grade and encountering chemistry as a school subject?
2. Does the teaching approach in 8<sup>th</sup> grade with E-learning units affect the occurrence of misconceptions about structure and states of matter?
3. Does the teaching approach in 8<sup>th</sup> grade with E-learning units affect the occurrence of misconceptions about pure substances and mixtures?

### *Educational material: E-learning units*

Two E-learning units (structure and states of matter – SSM and pure substances and mixtures – PSM) were designed, based on the E-learning units from the project E-kemija\*.<sup>27,28</sup> The tool for design and development of electronic textbooks eXecute was used. The content of the E-learning units was based on the Curriculum for Chemistry course in the 8<sup>th</sup> grade of primary school and applied in teaching relevant concepts. In E-learning units both macroscopic and submicroscopic levels of representation in chemistry were included. The symbolic level is not taught yet at this stage.

The E-learning units were composed of text, pictures, videos, animations, schemes, tables and tasks. The E-learning unit SSM contained seven sections (slides) with an average number of 157.4 words per slide; the E-learning unit PSM contained nine sections with an average number of 196.7 words per slide. In most cases, video clips and pictures represent the

---

\* <http://www.kii3.ntf.uni-lj.si/e-kemija/>. The result of E-kemija project are 125 E-units designed to enable the acquisition of basic knowledge of chemistry, deepening of knowledge and checking of understanding. E-units are mainly intended for independent learning, they are always available to students, so they can look at each one as many times as they want. The project was created with the financial support of the Ministry of Education and Sports of the Republic of Slovenia and the European Social Fund. Authors of the E-learning units: Bojana Boh, Iztok Devetak, Danica Dolničar, Saša A. Glažar, Andrej Godec, Samo Jamšek, Vida Mesec, Brane Pajk, Blaž Repe, Irena Sajovic, Matej Urbančič, Margareta Vrtačnik, Katarina Wissiak Grm, and Boris Zmazek.

observable (macroscopic) level. Simple animations and drawings were used for submicroscopic representations (*e.g.*, the representation of the arrangement and movement of the particles (SSM) and the difference between pure substances and mixtures (PSM)).

Tasks were incorporated into most sections and at the end of both E-learning units. Their role was to keep students' attention during learning and to give them feedback at the end of each section. No data were collected at this point.

#### *Design of the study*

The study was quasi-experimental by its design. Students were divided into one control (CG) and two experimental groups: experimental group 1 (EG1), where the teacher-centred approach at school was followed by working on E-learning material at home, and experimental group 2 (EG2), where the E-learning units were implemented at school only. Groups were equal in their previous knowledge of the relevant concepts; this fact was examined and confirmed with the pretest at the end of 7<sup>th</sup> grade. Two teaching units from the Curriculum for 8<sup>th</sup>-grade chemistry were selected: Structure and states of matter (SSM) and Pure substances and mixtures (PSM). When identifying answers as misconceptions, the following criterion<sup>29,30</sup> was used: Incorrect answers on multiple-choice items with the occurrence of 20 % and higher are defined as misconceptions.

#### *Participants*

Participants were students from four schools located in the urban area of Sarajevo, Bosnia and Herzegovina. Permission for research was granted by the principals, teachers and students' parents from every school.

The pre-test was administered in the first phase to a total number of 191 7<sup>th</sup> grade students. Some students dropped out from the sample for different reasons (change of school, inconsistency in writing their names/codes, absence from the classroom); therefore, in the second phase (next school year, 8<sup>th</sup> grade), 111 students participated (Table I).

TABLE I. Participants of the study

Group	Number of participants	
	Teaching unit SSM	Teaching unit PSM
CG	33	34
EG1	39	38
EG2	39	41

#### *Instruments and procedures*

The pre-test of knowledge was administered to students within physics class in the 7<sup>th</sup> grade. We were interested in students' knowledge of science content after the 7<sup>th</sup> grade, which is the basis for learning new content in the 8<sup>th</sup> grade.

Based on the results of the pretest, students were divided into three groups.

- The experimental group 1 (EG1) was formed to introduce E-learning units as homework material after the usual teaching (teacher-centred approach) at school. EG1 students received E-learning units as homework material on compact discs (CDs) to work on them at home. All students reported that they had personal computers or laptops at home.

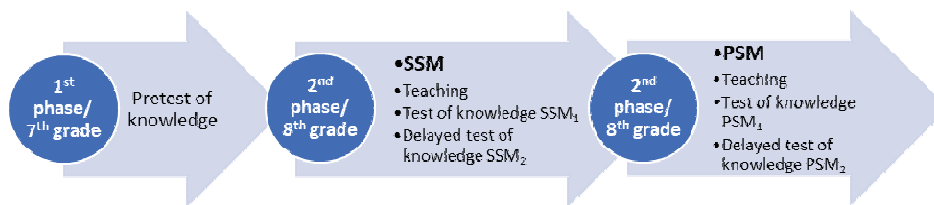
- In the experimental group 2 (EG2), students were learning using the E-learning units in the chemistry classroom under the supervision of a chemistry teacher and a researcher. Laptops were provided for each student in this group.



- The control group (CG) was taught traditionally, which in these schools implies teacher-centred approach. One of the researchers was present to ensure that the crucial concepts addressed in the E-learning units were also taught by the teacher in the control group.

The Levene's test of homogeneity of variances indicated that the variances are not homogeneous ( $F(2, 138) = 7.629, p = 0.001$ ), so the Welch test was chosen to test the difference between the groups. It did not result in a statistically significant difference between the control (CG) and experimental (EG1 and EG2) groups on the pretest of knowledge ( $F(2, 83.8) = 1.058, p = 0.352$ ). Cronbach's alpha for the pretest was  $\alpha = 0.596$  and it was considered as acceptable<sup>31</sup> for the purpose of this research\*.

After ensuring that students in all groups do not differ significantly with respect to their previous knowledge, the teaching strategies which include E-learning were applied in the experimental groups, and the teacher-centred approach was used in the control group. Teaching process was implemented at schools and lasted for one teaching hour (45 min) per teaching unit. After teaching, the students' knowledge was examined using the tests of knowledge, both applied as immediate and delayed post-tests (Scheme 1).



Scheme 1. Research methodology (1<sup>st</sup> phase: pre-test of knowledge; 2<sup>nd</sup> phase: Structure and states of matter (SSM) and pure substances and mixtures (PSM)).

One week after teaching structure and states of matter (SSM), the administration of the corresponding tests of knowledge (SSM<sub>1</sub>) followed in all three groups. Approximately three months after teaching, repeated post-tests of knowledge (SSM<sub>2</sub>) were administered to obtain insight into the retention of students' knowledge regarding the concepts taught. The same procedure was carried out with Pure substances and mixtures (PSM) teaching unit.

The reliability analysis resulted in Cronbach's alpha  $\alpha = 0.711$  for SSM<sub>1</sub> and 0.529 for SSM<sub>2</sub>, and it is considered as acceptable even though it is relatively low in the case of SSM<sub>2</sub>. Also, acceptable values of Cronbach's alpha were noted for PSM<sub>1</sub> ( $\alpha = 0.734$ ) and for PSM<sub>2</sub> ( $\alpha = 0.704$ ).

The sources for the construction of tests of knowledge included content of E-learning units (also taught in CG using teacher-centred approach). Incorrect options (distracters) in the items were derived from actual student alternative conceptions gathered from the literature. A pilot study was conducted one year earlier, and the tests were given to chemistry teachers prior to the application for a review, as well as to two university professors of Methodology of chemistry education.

In addition, validity was examined by conducting the analysis of correlation of each item with the total score on the test, and this resulted in statistically significant correlation for most of the items to the total score in each group of students.

\*Cronbach's alpha is recommended to be higher than or equal to 0.7 – some researchers accept 0.6 (van Griethuijsen, van Eijck & Haste, 2014) to satisfy the internal consistency of the test.

## RESULTS AND DISCUSSION

The pre-test of knowledge was administered after the corresponding teaching unit regarding atoms and molecules had been taught at the end of the 7<sup>th</sup> grade within physics class. Distractor analysis of the seven multiple-choice items was performed. Incorrect answers which indicate the existence of misconception,<sup>32</sup> sorted by frequency in decreasing order are presented in Table II.

TABLE II. Misconceptions – pre-test ( $N = 191$ )

No.	Misconception	Frequency, %
M1	Freezing/melting/evaporation can shrink water molecules.	45.1
M2	Bubbles that occur when water is heated are made of heat.	42.9
M3	When water evaporates, it splits into hydrogen and oxygen.	41.9
M4	We cannot obtain liquid water from water vapour since it has changed.	24.1
M5	Bubbles that occur when water is heated are made of gaseous hydrogen and oxygen.	22.0
M6	If a leaflet was made from a piece of gold, its atoms became straightened.	20.9
M7	We cannot obtain liquid water from water vapour since it disappeared.	20.4

The pre-test of knowledge revealed certain misconceptions regarding the structure and states of matter that students possessed prior to the instruction: 1) Misconceptions related to the changes in states of matter: M1, M2, M3, M4, M5, M7 and 2) misconceptions resulting from assigning the macroscopic properties to the particles: M6. Some misconceptions originate from students' everyday experiences to explain the changes surrounding them; some of them are formed long before students entered school. These concepts are more thoroughly taught later on in 8<sup>th</sup> grade within Chemistry.

The structure and states of matter (SSM) test of knowledge was administered one week after teaching (SSM<sub>1</sub>) and three months after teaching as a delayed test (SSM<sub>2</sub>). Incorrect answers on five multiple-choice and one completion items with a frequency ( $f$ ) of 20 % or higher in any of the groups on SSM<sub>1</sub> and/or SSM<sub>2</sub> are represented in Table S-I (Supplementary material to this paper), sorted by frequency in decreasing order. The proportions of students who have misconceptions as reported in Table S-I were examined using Pearson chi-square test.

Misconceptions regarding SSM can be classified as: 1) misconceptions about the arrangement and movement of particles in solids (M1 and M3); 2) the size of particles (M2, M4, M6 and M7); 3) the effect of freezing and condensation on the size of the molecule (M8, M10); 4) the existence of different particles in the same substance in different states of matter (M9); 5) the volume of a liquid can easily change (M5).

The most frequent misconceptions in all groups on both SSM<sub>1</sub> and SSM<sub>2</sub> were about the arrangement and movement of particles in solid substances (M1 and M3). The percentages of M1 and M3 for EG2 on both tests were lowest; on SSM<sub>2</sub>, the difference in favour of EG2 for M1 was statistically significant. The source of these misconceptions could be the attribution of macroscopic properties to the submicroscopic particles. It was evident from several animations in the E-learning unit SSM that the particles in ice vibrate, but students probably did not pay enough attention or did not transfer this knowledge to all substances in the solid state.

Misconceptions regarding the size of molecules (M2, M4 and M7) were also frequent on both immediate and delayed post-test, with the lowest percentages in EG2. On SSM<sub>2</sub> the difference in percentages in favor of EG1 and EG2 compared to CG for misconception M2 was statistically significant. Some studies also reported students' misconceptions regarding the size of atoms.<sup>12,32</sup> Research also showed that in comparison to the macroscopic level of representation, students' estimates of submicroscopic spatial sizes are less precise.<sup>33</sup> The unobservable nanoscale is hard to conceptualize even for older students,<sup>34</sup> which suggests that this concept should be addressed more thoroughly in the teaching process. There is the potential of E-learning units in teaching this concept, as the findings of this study showed that, even if the misconceptions regarding the size of the particles exist in EG2 and in EG1, the percentages are lower than in CG, and in one case (M2) the difference was statistically significant.

Misconceptions about freezing (M6, M8) and condensation (M10) affecting the size of the molecules did not reach the threshold of 20 % in EG2 either on SSM<sub>1</sub> or SSM<sub>2</sub>. In the case of CG, the threshold was reached for M6 on both SSM<sub>1</sub> and SSM<sub>2</sub>, and M10 on SSM<sub>2</sub>; in EG1 for M6 and M8 on SSM<sub>1</sub> and M10 on SSM<sub>2</sub>. Misconceptions related to macroscopic changes affecting the size or shape of the particles are reported in a significant body of research.<sup>15,16,35</sup>

Different states of the same substance contain different particles (M9) is a misconception found in EG1 on the immediate post-test and in CG on the delayed post-test. Some research studies also reported comparable findings<sup>17,18,36</sup> suggesting that teaching about mixtures, as well as about elements and compounds, needs to include particle representations.<sup>22</sup>

When considering the percentages of misconceptions on SSM<sub>1</sub>, the lower occurrences of misconceptions of EG2 students were noted, compared to CG and EG1, but the Pearson chi-square test did not indicate a statistically significant difference between the groups.

In the case of SSM<sub>2</sub>, statistical analysis confirmed that EG2 has a significantly lower percentage of two misconceptions: M6 (particles in water vapor are smaller than the particles in ice),  $p = 0.023$ ; M10 (freezing affects the size of a molecule),  $p = 0.037$ ). When considering CG, this group has a significantly

higher percentage for one misconception: M2 (the size of a plant cell is on the nano (1–100 nm) level),  $p = 0.048$ ). EG1 also has significantly higher percentage for one misconception: M1 (Particles in solids are equally distributed and do not move),  $p = 0.035$ )\*.<sup>6</sup>

Summarizing the above, the most common misconceptions on the structure of matter originate in transferring the macroscopic observations into the submicroscopic level and in misinterpretation of the size of particles. E-learning material can help in resolving these misconceptions by including animations of submicroscopic processes, but teachers' support is also required in explaining the processes and emphasizing the facts that distinguish submicroscopic processes from macroscopic observations.

#### *Students' misconceptions about pure substances and mixtures*

Indicators of the misconceptions about Pure substances and mixtures were also incorrect answers on seven multiple-choice and one completion items with a frequency of 20 % or higher in any of the groups. They are presented in Table S-II (Supplementary material), arranged by decreasing frequency. The test of knowledge was also administered twice: one week after teaching (PSM<sub>1</sub>) and three months after teaching (PSM<sub>2</sub>).

Misconceptions regarding PSM can be classified as:

Misconceptions about properties of pure substances in mixtures (M5, M10); they have also been reported in earlier research.<sup>22,38,39</sup>

Misconceptions about the differences between pure substances and mixtures from everyday life (M2, M4, M6, M8, M9 and M11) are also noted.<sup>38,40–42</sup> They originate in the everyday experience where some substances are referred to as pure (such as air, M8), and the perception of something natural (such as milk, M4) being pure. At the same time, some manufactured processed material is perceived as being a mixture.

Misconceptions about the composition of air and interchanging the notion of air with oxygen (M1, M2, M3, M8) were also reported in the literature.<sup>39,43–45</sup>

The Pearson chi-squared analysis for PSM<sub>1</sub> indicated that students in CG have significantly higher percentages for the misconception M1 ( $p = 0.010$ ), students in EG1 for the misconception M4 ( $p = 0.008$ ), while EG2 students have significantly lower percentages for misconceptions M1 ( $p = 0.010$ ), M6 ( $p = 0.003$ ) and M10 ( $p = 0.039$ ). The analysis of percentages of misconceptions noted on PSM<sub>2</sub> indicated that EG2 students have a statistically significant lower percentage of the misconception M3 (oxygen in the air and pure oxygen have different properties,  $p = 0.0001$ ), while EG1 students have a higher percentage than expected\*.<sup>37</sup>

\* According to the adjusted residuals generated in SPSS, higher than 1.96, which can be used to point to the groups that cause the differences.

The changes in percentages on the delayed tests (SSM<sub>2</sub> and PSM<sub>2</sub>) can be attributed to the teaching process and the role of the teacher. During the three months between the tests, teachers were teaching their usual way, which implies teacher-centred approach without E-learning or using multimedia-based teaching resources. The fact that misconceptions are noted in both experimental groups EG1 and EG2 on delayed test of knowledge could originate from the absence of E-learning resources. During this period, students were not exposed to E-learning material. Since SSM<sub>1</sub> and PSM<sub>1</sub> resulted in lower frequency of misconceptions of students in experimental groups, it is reasonable to hypothesize that more frequent use of E-learning material could result in better retention of knowledge and fewer misconceptions.

The incidence of misconceptions is higher regarding SSM than PSM in every group on both immediate and delayed tests of knowledge. The reason might be that students already possess certain knowledge (and misconceptions) regarding the states of matter (the effect of previously acquired misconceptions). Pure substances and mixtures (in the chemical terms) are new concepts for them.

#### CONCLUSIONS AND IMPLICATIONS

Two approaches to teaching the concepts of structure and states of matter, pure substances and mixtures using E-learning were applied. Effectiveness of E-learning approaches on the occurrence of misconceptions was explored, compared to the usual teacher-centred approach. One E-learning approach included the usual teacher-centred teaching in the classroom, supplemented by E-learning units as homework. The other E-learning approach was characterised by the application of E-learning units at school during chemistry classes, using laptop computers. The control group students were taught with teacher-centred teaching. With this in mind, the following research questions were examined:

1. What misconceptions about structure and states of matter do students have when entering the 8<sup>th</sup> grade and encountering chemistry as a school subject?

The insight into students' previous knowledge on the subject matter indicated that students have certain incorrect views. Misconceptions arising from assigning macroscopic properties to the submicroscopic particles were observed (physical changes affect the size of the particles, the lack of movement of particles in solids). The data gathered indicated that students have incorrect views about evaporation, believing that: 1) water splits into hydrogen and oxygen, 2) bubbles formed when water is heated are made of heat or 3) gaseous hydrogen and oxygen and 4) evaporation may shrink water molecules.

2. Does the teaching approach with E-learning units affect the frequency of misconceptions about structure and states of matter?

E-learning approach in school settings (EG2) resulted in fewer misconceptions on SSM<sub>1</sub> (6), compared to the control group – CG (7) and the application of

E-learning as homework material – EG1 (9). Findings pointed to the fact that the teaching applied in EG1 (teacher-centred approach at school and E-learning units at home) is less appropriate than E-learning at school (EG2) or teacher-centred approach at school only (CG). Also, the same misconceptions in EG2 (6) were noted on SSM<sub>2</sub>. The delayed test (SSM<sub>2</sub>) resulted in higher number of misconceptions in CG compared to SSM<sub>1</sub> (7 on SSM<sub>1</sub> and 9 on SSM<sub>2</sub>), and in lower number of misconceptions in EG1 (9 on SSM<sub>1</sub> and 7 on SSM<sub>2</sub>).

However, some misconceptions related to transferring the macroscopic properties to the submicroscopic level occur in every group (*e.g.*, particles do not move in a solid state, solidification causes particles to stop moving). These misconceptions result in lower percentages in EG2 compared to EG1 and CG, but the difference was not statistically significant. It is evident that they are rather resistant and are not significantly affected by the E-learning approaches (especially in EG1) compared to traditional teacher-centred approach. The reason might lie in the role of the teacher who moderated the learning process in EG2 at school, as the students paid too little attention to the animations of the distribution of particles in solids, which show that the particles vibrate.

Misconceptions regarding the perception of the size of particles also occur in every group (44–45 % of students in every group place plant cell on the nano level, but a lower percentage of EG2 students (26.8 %) place the particles in table salt at the micro (1–100  $\mu\text{m}$ ) level compared to EG1 (41.7 %) and CG (45.8 %). This fact points to the potential of representing the size of particles in E-units. It also suggests that the size of particles should be addressed more thoroughly in traditional teaching as well as in E-learning units. There was the positive effect of the particles representation in E-learning units, evident through the lower percentage of these misconceptions in EG2. However, this is not the fact for EG1. This points to the importance of the E-learning material moderated by the teacher, and the synergy of E-units with the teachers' explanation, since the size of the particles is abstract concept to the students if explained by the teacher only.

3. Does the teaching approach with E-learning units affect the frequency of misconceptions about pure substances and mixtures?

Misconceptions occurring in EG2 resulted in lower percentages for concepts of pure substances and mixtures: two misconceptions (M2 and M3) on PSM<sub>1</sub> and two misconceptions (M1 and M4) on PSM<sub>2</sub>, comparing to SSM teaching unit (six misconceptions (M1–M5, M7) on both SSM<sub>1</sub> and SSM<sub>2</sub>). The potential cause might be the fact that concepts of pure substances and mixtures are rather new for students from the chemical point of view, while they have certain knowledge (and pre-conceptions) on structure and states of matter from everyday life and earlier schooling and/or everyday life. It is evident that for these concepts, E-learning approaches have made significant difference as they resulted in fewer misconceptions than the traditional teaching approach. Moreover, the occurrence

of misconceptions regarding PSM in CG is higher (four on PSM<sub>1</sub>: M1, M2, M4, M10), three on PSM<sub>2</sub>: M1, M2, M3) than in the EG2 (two on PSM<sub>1</sub>: M2, M3, two on PSM<sub>2</sub>: M1, M4); in the case of EG1, the occurrence is also higher (nine on PSM<sub>1</sub>, four on PSM<sub>2</sub>). Rather high number of misconceptions occurring in EG1 points to the conclusion that the learning process with E-units needs to be moderated and monitored by the teacher. Here, four misconceptions rather resistant to the teaching approach could be selected: three of them (M1, M2, M3), appearing on PSM<sub>2</sub> in EG2 and on both PSM<sub>1</sub> and PSM<sub>2</sub> in EG1 and CG are related to the misconceptions related to the air (its composition, properties of oxygen in air, interchanging the notion of air and oxygen). M4 appears in all groups once, either on PSM<sub>1</sub> or on PSM<sub>2</sub>, and is related to the belief that milk is a pure substance. These findings favour the application of E-learning material in school settings compared to its application at home and with the teacher-centred approach.

The main prerequisite for E-learning in the educational process is adequate IT equipment, often limited to a few personal computers in the IT classroom. It might also require additional training for teachers, depending on their current knowledge about IT. Nevertheless, the cooperation between IT and chemistry teachers may result in the wider application of the E-learning units in school settings.

Results suggest that E-learning material that integrates macroscopic and sub-microscopic levels of representation has the potential to teach fundamental chemical concepts when applied in the classroom under the teachers' supervision (EG2 approach). It enables students to learn more comprehensively, to build conceptual understanding, and therefore to reduce the occurrence of misconceptions. The occurrence of misconceptions in EG1 (students who learned using E-learning material at home after the teacher-centred approach) is rather high, which indicates the need for the teacher to guide students during E-learning. This emphasizes the important role of the teacher in teaching fundamental chemical concepts that can be supported using E-learning material. Although EG1 students were taught by the teacher (teacher-centred approach), and the use of E-learning material followed at home, it is evident that teaching by the teacher should be combined with E-learning material, instead of applying the material later.

Further research could include a more thorough study on the application of E-learning units for learning at home, with online access to the E-learning units where the teacher could track students' activity and guide them through the learning process. This approach might have greater potential than the same material provided on a CD.

## SUPPLEMENTARY MATERIAL

Additional data and information are available electronically at the pages of journal website: <https://www.shd-pub.org.rs/index.php/JSCS/article/view/11965>, or from the corresponding author on request.

## ИЗВОД

## ЕФЕКТИ Е-УЧЕЊА НА ЗАБЛУДЕ УЧЕНИКА УЗРАСТА 13–14 ГОДИНА О НЕКИМ ОСНОВНИМ ХЕМИЈСКИМ ПОЈМОВИМА

INES NUIĆ<sup>1</sup> и SAŠA A. GLAŽAR<sup>2</sup>

<sup>1</sup>Faculty of Science, University of Sarajevo, Bosnia and Herzegovina и <sup>2</sup>Faculty of Education, University of Ljubljana, Slovenia

Заблуде ученика у области природних наука могу довести до низа тешкоћа у учењу ако наставник не изабере одговарајуће стратегије учења којима ће се смањити њихова учесталост. У овом раду истражене су заблуде ученика узраста 13–14 година о структури и агрегатном стању супстанци, о чистим супстанцама и смешама. Испитана је учесталост тих заблуда када се примени стратегија наставе са материјалом за Е-учење. Истраживање је изведено са ученицима 7. и 8. разреда у градским школама у Босни и Херцеговини. Добијени резултати су указали на заблуде ученика настале трансфером макроскопских посматрања на субмикроскопски ниво и погрешном интерпретацијом величине честица. Мањи проценат заблуда био је групи ученика који су користили Е-наставни материјал у школи у односу на контролну групу ученика и групу ученика који су истом материјалу за Е-учење приступали од куће. То указује да би стратегија Е-учења могла допринети бољим резултатима учења ако би се више примењивала у школама. Ова студија има за циљ да усмери пажњу наставника ка примени Е-учења у настави хемије како би ученици стекли научно прихватљива знања, а појава заблуда се смањила.

(Примљено 4. јула, ревидирано 26. децембра, прихваћено 30. децембра 2022)

## REFERENCES

1. A. H. Johnstone, *J. Comput. Assist. Learn.* **7** (1991) 75 (<http://dx.doi.org/10.1111/j.1365-2729.1991.tb00230.x>)
2. D. M. Bunce, in *Sputnik to Smartphones: A Half-Century of Chemistry Education; ACS Symposium Series*, M. V. Orna, Ed., American Chemical Society, New York, 2015, p. 107 (<http://dx.doi.org/10.1021/bk-2015-1208.ch007>)
3. D. D. Trivić, V. D. Milanović, *J. Serb. Chem. Soc.* **83** (2018) 1177 (<http://dx.doi.org/10.2298/JSC171220055T>)
4. T. A. Holme, C. J. Luxford, A. Brandriet, *J. Chem. Educ.* **92** (2015) 1477 (<http://dx.doi.org/10.1021/acs.jchemed.5b00218>)
5. S. M. Al-Balushi, I. S. Al-Harthy, *Chem. Educ. Res. Pract.* **16** (2015) 680 (<http://dx.doi.org/10.1039/c5rp00052a>)
6. H.-D. Barke, A. Hazari, S. Yitbarek, *Misconceptions in chemistry: Addressing perceptions in chemical education*, Springer-Verlag, Berlin, 2009
7. Y. J. Dori, J. Belcher, *J. Learn. Sci.* **14** (2005) 243 ([https://doi.org/10.1207/s15327809jls1402\\_3](https://doi.org/10.1207/s15327809jls1402_3))
8. J. P. Smith, A. A. di Sessa, J. Roschelle, *J. Learn. Sci.* **3** (1994) 115 ([http://dx.doi.org/10.1207/s15327809jls0302\\_1](http://dx.doi.org/10.1207/s15327809jls0302_1))
9. M. I. Stojanovska, B. T. Soptrajanov, V. M. Petrusovski, *Creat. Educ.* **03** (2012) 619 (<http://dx.doi.org/10.4236/ce.2012.35091>)



10. N. Azizoglu, M. Alkan, Ö. Geban, *J. Chem. Educ.* **83** (2006) 947 (<http://dx.doi.org/10.1021/ed083p947>)
11. D. F. Treagust, R. Duit, *Cult. Stud. Sci. Educ.* **3** (2008) 297 (<http://dx.doi.org/10.1007/s11422-008-9090-4>)
12. A. G. Harrison, D. F. Treagust, in *Chemical Education: Towards Research-Based Practice*, Kluwer Academic Publishers, Dordrecht, 2003, p. 189 ([http://dx.doi.org/10.1007/0-306-47977-X\\_9](http://dx.doi.org/10.1007/0-306-47977-X_9))
13. D. F. Treagust, A. L. Chandrasegaran, J. Crowley, B. H. W. Yung, I. P. A. Cheong, J. Othman, *Int. J. Sci. Math. Educ.* **8** (2010) 141 (<http://dx.doi.org/10.1007/s10763-009-9166-y>)
14. G. Papageorgiou, P. Johnson, *Int. J. Sci. Educ.* **27** (2005) 1299 (<http://dx.doi.org/10.1080/09500690500102698>)
15. B. Andersson, *Stud. Sci. Educ.* **18** (1990) 53 (<http://dx.doi.org/10.1080/03057269008559981>)
16. M. B. Nakhleh, A. Samarapungavan, Y. Saglam, *J. Res. Sci. Teach.* **42** (2005) 581 (<http://dx.doi.org/10.1002/tea.20065>)
17. V. Kind, *Beyond appearances: Students' misconceptions about basic chemical ideas*, University of Durham, School of Education, Durham, 2004 ([https://www.researchgate.net/publication/228799159\\_Beyond\\_Apearances\\_Students%27\\_Misconceptions\\_About\\_Basic\\_Chemical\\_Ideas](https://www.researchgate.net/publication/228799159_Beyond_Apearances_Students%27_Misconceptions_About_Basic_Chemical_Ideas))
18. R. J. Osborne, M. M. Cosgrove, *J. Res. Sci. Teach.* **20** (1983) 825 (<http://dx.doi.org/10.1002/tea.3660200905>)
19. K. Adbo, K. S. Taber, *Int. J. Sci. Educ.* **31** (2009) 757 (<http://dx.doi.org/10.1080/09500690701799383>)
20. M. Slapničar, I. Devetak, S. A. Glažar, J. Pavlin, *J. Balt. Sci. Educ.* **16** (2017) 308 (<http://dx.doi.org/10.33225/jbse/17.16.308>)
21. K. S. Taber, *Teaching Secondary Chemistry*, Hodder Education, London, 2012 (ISBN: 978-1444124323)
22. M. J. Sanger, *J. Chem. Educ.* **77** (2000) 1517 (<https://doi.org/10.1021/ed077p762>)
23. J. Olson, J. Codde, K. deMaagd, E. Tarkelson, J. Sinclair, S. Yook, R. Egidio, *An Analysis of E-Learning Impacts & Best Practices in Developing Countries with Reference to Secondary School Education in Tanzania*, The ICT4D Program, Michigan State University, East Lansing, MI, 2011. ([https://www.researchgate.net/publication/272682458\\_An\\_Analysis\\_of\\_e-Learning\\_Impacts\\_Best\\_Practices\\_in\\_Developing\\_Countries\\_With\\_Reference\\_to\\_Secondary\\_School\\_Education\\_in\\_Tanzania](https://www.researchgate.net/publication/272682458_An_Analysis_of_e-Learning_Impacts_Best_Practices_in_Developing_Countries_With_Reference_to_Secondary_School_Education_in_Tanzania))
24. E. Ural, O. Ercan, *J. Balt. Sci. Educ.* **14** (2015) 7 (<http://dx.doi.org/10.33225/jbse/15.14.07>)
25. N. Rizman Herga, B. Čagran, D. Dinevski, *Eurasia J. Math. Sci. Technol.* **12** (2016) (<http://dx.doi.org/10.12973/eurasia.2016.1224a>)
26. N. Rizman Herga, S. A. Glažar, D. Dinevski, *J. Balt. Sci. Educ.* **14** (2015) 351 (<http://dx.doi.org/10.33225/jbse/15.14.351>)
27. S. A. Glažar, *Snovi so iz delcev* ([http://www.kii3.ntf.uni-lj.si/e-kemija/uenota.php?a=sglazar&e=snovi\\_so\\_iz\\_delcev](http://www.kii3.ntf.uni-lj.si/e-kemija/uenota.php?a=sglazar&e=snovi_so_iz_delcev), accessed September 14, 2022) (in Slovenian)
28. S. A. Glažar, *Čiste snovi in zmesi* (<http://www.kii3.ntf.uni-lj.si/e-kemija/mod/resource/view.php?id=286>, accessed September 14, 2022) (in Slovenian)
29. H. S. Dhinsda, D. F. Treagust, *Brunei Int. J. Sci. Math. Educ.* **1** (2009) 33 (<https://shbiejournal.files.wordpress.com/2009/11/hsddavideditedpdf.pdf>)

30. D. D. Milenković, T. N. Hrin, M. D. Segedinac, S. Horvat, *J. Subj. Didact.* **1** (2016) 3 (<http://dx.doi.org/10.5281/zenodo.55468>)
31. K. S. Taber, *Res. Sci. Educ.* **48** (2018) 1273 (<http://dx.doi.org/10.1007/s11165-016-9602-2>)
32. J. K. Gilbert, *Res. Sci. Educ.* **7** (1977) 165 (<https://doi.org/10.1007/BF02643123>)
33. M. G. Jones, A. R. Taylor, *J. Res. Sci. Teach.* **46** (2009) 460 (<http://dx.doi.org/10.1002/tea.20288>)
34. T. R. Tretter, M. G. Jones, J. Minogue, *J. Res. Sci. Teach.* **43** (2006) 1061 (<http://dx.doi.org/10.1002/tea.20155>)
35. D. Özalp, A. Kahveci, *Chem. Educ. Res. Pract.* **16** (2015) 619 (<http://dx.doi.org/10.1039/c5rp00096c>)
36. G. M. Bodner, *J. Chem. Educ.* **68** (1991) 385 (<https://doi.org/10.1021/ed068p385>)
37. D. Sharpe, *Pract. Assess. Res. Evaluation* **20** (2015) 1 (<http://dx.doi.org/10.7275/tbfa-x148>)
38. F. Canada, R. Alvarez, M. J. Arevalo, M. V. Gill, J. Cubero, L. Ortega, in *Conference proceedings of the 5<sup>th</sup> International Conference on Education, Research and Innovation – ICERI2012* (2012), Madrid, Spain, International Academy of Technology, Education and Development (IATED), Valencia, 2012, p. 4598
39. B. Costu, S. Ünal, A. Ayas, *J. Balt. Sci. Educ.* **6** (2007) 35 (<http://oaji.net/articles/2014/987-1404286868.pdf>)
40. R. Martín del Pozo, P. Galán Martín, *Revista Eureka Sobre Enseñanza y Divulgación de Las Ciencias* **9** (2012) 213 (<https://revistas.uca.es/index.php/eureka/article/view/2768/2416>)
41. F. C. Cañada, D. Gonzalez-Gomez, L. V. Melo Niño, A. Acedo Dávila, *Int. Electron* **9** (2017) 499 <https://www.researchgate.net/publication/313986987>
42. G. Papageorgiou, D. Sakka, *Educ. Res. Pract. Eur.* **1** (2000) 237 (<http://dx.doi.org/10.1039/A9RP90025J>)
43. J. L. Kuethe, *Sci Educ* **47** (1963) 361 (<http://dx.doi.org/10.1002/sce.3730470410>)
44. G. I. Za'Rour, *J. Res. Sci. Teach.* **12** (1975) 385 (<http://dx.doi.org/10.1002/tea.3660120409>)
45. M. Stein, T. G. Larrabee, C. R. Barman, *J. Elem. Sci. Educ.* **20** (2008) 1 (<http://dx.doi.org/10.1007/BF03173666>).

SUPPLEMENTARY MATERIAL TO  
**The effects of E-learning units on 13–14-year-old students’  
misconceptions regarding some elementary chemical concepts**

INES NUIĆ<sup>1\*</sup> and SAŠA A. GLAŽAR<sup>2</sup>

<sup>1</sup>Faculty of Science, University of Sarajevo, Bosnia and Herzegovina and <sup>2</sup>Faculty of Education, University of Ljubljana, Slovenia

*J. Serb. Chem. Soc.* 88 (4) (2023) 451–465

TABLE S-I. Students’ misconceptions on the structure and states of matter

No.	Misconception	Group	SSM <sub>1</sub>			SSM <sub>2</sub>		
			<i>f</i> /%	$\chi^2$	<i>p</i>	<i>f</i> /%	$\chi^2$	<i>p</i>
M1	Particles in solids are equally distributed and do not move	CG	62.5			60.4		
		EG1	50.0	1.972	0.373	75.0	7.418	0.035
		EG2	48.8			41.5		
M2	The size of a plant cell is on the nano (1–100 nm) level	CG	43.8			52.1		
		EG1	45.8	0.031	0.984	29.2	6.065	0.048
		EG2	43.9			29.3		
M3	Water molecules stop moving if the water freezes	CG	45.8			41.7		
		EG1	41.7	3.557	0.169	45.8	2.224	0.329
		EG2	26.8			29.3		
M4	The size of the particles in table salt is on the micro (1–100 $\mu$ m) level	CG	45.8			47.9		
		EG1	41.7	3.557	0.169	33.3	5.409	0.067
		EG2	26.8			24.4		
M5	The volume of a substance in the liquid state can easily change	CG	22.9			20.8		
		EG1	41.7	3.125	0.210	37.5	3.404	0.182
		EG2	24.4			36.6		
M6	Particles in water vapour are smaller than the particles in ice	CG	33.3			31.3		
		EG1	33.3	2.458	0.293	8.3	7.531	0.023
		EG2	19.5			12.2		
M7	The size of the particles in ice is on the micro (1–100 $\mu$ m) level	CG	25.0			22.9		
		EG1	33.3	0.570	0.752	20.8	1.268	0.530
		EG2	26.8			31.7		
M8	Condensation affects the size of a molecule	CG	16.7			14.6		
		EG1	29.2	5.431	0.066	8.3	–*	
		EG2	7.3			9.8		
M9	Different states of the same substance contain different particles	CG	16.7			20.8		
		EG1	25.0	3.875	0.144	12.5	4.906	0.086
		EG2	7.3			4.9		
M10	Freezing affects the size of a molecule	CG	18.8			22.9		
		EG1	8.3	– <sup>a</sup>		25.0	6.604	0.037
		EG2	4.9			4.9		

<sup>a</sup>Pearson  $\chi^2$  analysis was not performed since the threshold of 20 % of answers was not reached in any of the groups

\* Corresponding author. E-mail: ividovic@pmf.unsa.ba

The  $p$  values lower than .05 that indicated the statistically significant difference in the proportion of students who had and who did not have the misconceptions, are in bold.

TABLE S-II. Students' misconceptions on pure substances and mixtures; The  $p$  values lower than .05 that indicated the statistically significant difference in the proportion of students who had and who did not have the misconceptions, are in bold

No.	Misconception	Group	SSM <sub>1</sub>			SSM <sub>2</sub>		
			f(%)	$\chi^2$	$p$	f(%)	$\chi^2$	$p$
M1	Particles in solids are equally distributed and do not move.	CG	62.5			60.4		
		EG1	50.0	1.972	.373	75.0	<b>7.418</b>	<b>.035</b>
		EG2	48.8			41.5		
M2	The size of a plant cell is on the nano (1–100 nm) level.	CG	43.8			52.1		
		EG1	45.8	.031	.984	29.2	<b>6.065</b>	<b>.048</b>
		EG2	43.9			29.3		
M3	Water molecules stop moving if the water freezes.	CG	45.8			41.7		
		EG1	41.7	3.557	.169	45.8	2.224	.329
		EG2	26.8			29.3		
M4	The size of the particles in table salt is on the micro (1–100 $\mu\text{m}$ ) level.	CG	45.8			47.9		
		EG1	41.7	3.557	.169	33.3	5.409	.067
		EG2	26.8			24.4		
M5	The volume of a substance in the liquid state can easily change.	CG	22.9			20.8		
		EG1	41.7	3.125	.210	37.5	3.404	.182
		EG2	24.4			36.6		
M6	Particles in water vapour are smaller than the particles in ice.	CG	33.3			31.3		
		EG1	33.3	2.458	.293	8.3	<b>7.531</b>	<b>.023</b>
		EG2	19.5			12.2		
M7	The size of the particles in ice is on the micro (1-100 $\mu\text{m}$ ) level.	CG	25.0			22.9		
		EG1	33.3	.570	.752	20.8	1.268	.530
		EG2	26.8			31.7		
M8	Condensation affects the size of a molecule.	CG	16.7			14.6		
		EG1	29.2	5.431	.066	8.3	-*	
		EG2	7.3			9.8		
M9	Different states of the same substance contain different particles	CG	16.7			20.8		
		EG1	25.0	3.875	.144	12.5	4.906	.086
		EG2	7.3			4.9		
M10	Freezing affects the size of a molecule.	CG	18.8			22.9		
		EG1	8.3	<b>-Error!</b>		25.0	<b>6.604</b>	<b>.037</b>
		EG2	4.9	<b>Bookmark not defined.</b>		4.9		

\*Pearson chi-square analysis was not performed since the threshold of 20% of answers was not reached in any of the groups.

**Examples of multiple-choice test items**

(Correct answers are marked in bold)

**A. Pretest****Item 2**

You accidentally spill some water to the floor, but you do not have time to wipe it off. A few hours later, the amount of spilled water decreased. What happened to the water?

- A. The amount of water decreased and now takes up less space.
- B. Water turned into gas and went into the air.**
- C. Water broke down to hydrogen and oxygen atoms, which are now in the air.

**Item 3**

What kind of particles is present in the water?

- A. Water molecules.**
- B. Water atoms.
- C. Atoms of hydrogen and oxygen.
- D. Molecules of hydrogen and oxygen.

**Item 4**

If you take a bottle of juice from the fridge and put it on the table in the warm room, on the outer side of the bottle appear drops. What are they?

- A. Juice drops from the bottle.
- B. Water drops from the steam from air.**
- C. Drops of water and juice from the bottle.
- D. Drops of water from the bottle.

**B) SSM<sub>1</sub> / SSM<sub>2</sub>****Item 1**

Which statement about water is **correct**?

- A. Water molecules will stop moving if the water freezes.
- B. Water molecules will stop moving if the water evaporates.
- C. Water molecules will stop moving if a glass with liquid water is not disturbed.
- D. Water molecules will not stop moving.**

**Item 2**

Which procedure can be used to **increase** the water molecule?

- A. Freezing.
- B. Melting.
- C. Evaporation.
- D. Condensation.
- E. None of the above.**

**Item 3**

Encircle the **correct** statements:

- a. Liquid substance can easily change its volume.
- b. The shape of the liquid depends on the container.**

- c. **Gases do not have a determined shape.**
- d. A substance cannot change its state from solid to gas.
- e. **The same substance can be found in several states of matter.**

### C) PSM<sub>1</sub> / PSM<sub>2</sub>

#### Item 1

Which of the following statements are **correct**?

- a. Milk is a pure substance.
- b. **Sugar is a pure substance.**
- c. **Blood is a mixture.**
- d. Air is a pure substance.

#### Item 2

Which of the following statements about air is **correct**?

- A. **Air is raw material for gases that air is composed of.**
- B. The major constituent of air is oxygen.
- C. Oxygen in air and pure oxygen have different properties.
- D. Nitrogen in the air is produced by photosynthesis.

#### Item 3

Which of the following statements are **correct**?

- a. **All particles in pure substances are equal.**
- b. Different parts of a pure substance have different properties.
- c. **Pure substances can be found in different states of matter, depending on a temperature.**
- d. Substances in nature are mostly found in pure form.
- e. **Properties of pure substances are the same in one gram and in 10 grams of those substances.**

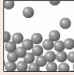
- Tvari se sastoje iz čestica
- Isparavanje broma
- Agregatna stanja tvari
- Agregatna stanja vode
- Sažetak
- Zadaci
- Zadaci

4. Koja tvrdnja je tačna za tvari u različitim agregatnim stanjima?

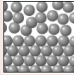
- U istim tvarima u različitim agregatnim stanjima nalaze se različite čestice.
- U čvrstim tvarima čestice se slobodno kreću.
- Čestice u plinovima su više udaljene jedna od druge nego u tekućinama.
- Brzina kretanja čestica iste tvari u svim agregatnim stanjima je jednaka.

5. Dopuni tekst.

Prikazane su sheme rasporeda čestica u vodi pri prijelazu među agregatnim stanjima. Koja shema prikazuje promjene pri topljenju leda, a koja pri isparavanju vode?



Raspored čestica na slici prikazuje \_\_\_\_\_ vode.

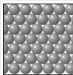


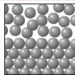
Raspored čestica na slici prikazuje \_\_\_\_\_ leda.

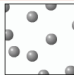
[Provjeri](#)

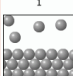
6. Dopuni tekst.

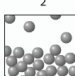
Prikazani su rasporedi čestica u različitim agregatnim stanjima. Kod svakog prikaza upiši broj agregatnog stanja, koje raspored predstavlja.

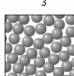
  
1

  
2

  
3

  
4

  
5

  
6

plin;  tekućina;  čvrsta tvar;  
 plin i tekućina;  
 čvrsta tvar i tekućina;  
 plin i čvrsta tvar

[Provjeri](#)

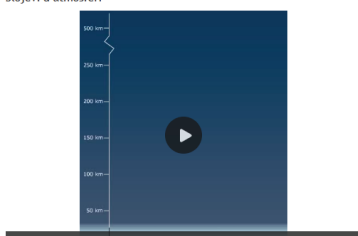
Fig. S-1. Illustration of one slide from the e-learning unit Structure and states of matter

Čiste tvari i smjese  
Smjese  
Zrak je smjesa plinova  
Plinovi u zraku  
Čiste tvari  
Čiste tvari  
Sažetak  
Zadaci  
Zadaci

**Zrak je smjesa plinova**

Oko Zemlje se nalazi atmosfera, koja predstavlja 1500 km deo stoji sloj plinova. Što se više udaljavamo od površine Zemlje, atmosfera je sve rjeđa.

Stojevi u atmosferi



Oko 80 % mase svih plinova u atmosferi je u najnižem sloju troposferi. To možemo osjetiti ako se penjemo na visoku planinu. Što se više penjemo, osjećamo se više umorno, jer je u zraku manje kisika nego na moru. U višim predjelima jednim udisajem dobitimo manje kisika nego u nižim i zato teže dišemo.

Zrak je smjesa plinova. Čestice plina u zraku.



Legenda

- dušik
- kisik
- argon
- ogljikov dioksid

Fig. S-2. Illustration of one slide from the e-learning unit Pure substances and mixtures.